UNIVERSITY OF CALIFORNIA SAN DIEGO

Active and Dynamical Information Acquisition with Applications in Communication Systems.

A dissertation submitted in partial satisfaction of the
requirements for the degree
Doctor of Philosophy

in

Electrical Engineering (Communication Theory and Systems)

by

Nancy Ronquillo

Committee in charge:

Professor Tara Javidi, Chair
Professor Todd Prentice Coleman
Professor Pamela C. Cosman
Professor Piya Pal
Professor Xinyu Zhang

2021

The dissertation of Nancy Ronquillo is approved, and it is acceptable in quality and form for publication on microfilm and electronically.

University of California San Diego

2021

DEDICATION

For my family.

EPIGRAPH

All our dreams can come true,

if we have the courage to pursue them.

—Walt Disney

TABLE OF CONTENTS

LIST OF FIGURES

LIST OF TABLES

ACKNOWLEDGEMENTS

I would like to acknowledge Professor Tara Javidi for her continuous support, which has helped me in an immeasurable way. Thank you for believing in me and trusting me from the beginning.

I want to thank my dissertation committee members Professor Pamela C. Cosman, Piya Pal, Todd Coleman, and Xinyu Zhang. I would also like to acknowledge my co-authors and lab mates Anusha Lalitha, Sun-En Chiu, and Shubhanshu Shekhar for their helpful advice, patience, and guidance through various research projects.

I wish to express my sincere appreciation to those that have served as mentors in my journey through graduate school. Thank you for listening, your mentorship is the greatest gift I could have. You inspire me to do the same for others.

I am very thankful to my partner Emmanuel for coming along with me on this adventure. Thank you for the hundreds of meals and many loads of laundry. Thank you for the warm hugs and words of encouragement when I've needed them. Thank you for believing in me, even when at times I didn't believe in myself. Thank you for your patience and your unconditional support.

I want to express my deepest gratitude to my family. To my sister Erica, thank you for showing me just how strong a person can be and thank you for always motivating me to keep going forward. To my sister Haidee, thank you for your selflessness in everything that you do, we are forever indebted to you. Thank you for always making things feel better, thank you for your support in every single way. To my nephews, Julio Cesar, D'Alessandro, and William thank you for always making me laugh and smile. To my parents, Sofia and Moises thank you for giving me my wings. I am in this position because of you, thank you for all of your hard work to provide for our family and for always believing and encouraging my dreams.

Chapter 2, in part, is a reprint of the material as it appears in the paper: Nancy Ronquillo and Tara Javidi, "Multiband Noisy Spectrum Sensing with Codebooks," in the proceedings of the Asilomar Conference on Signals, Systems, and Computers, Nov. 2016. The dissertation author was the primary investigator and author of this paper.

Chapter 2, in part, is a reprint of the material as it appears in the article: Anusha Lalitha, Nancy Ronquillo, and Tara Javidi, “Improved Target Acquisition Rates with Feedback Codes," IEEE Journal of Selected Topics in Signal Processing, Vol.12, no.5, pp. 871 - 885, Oct. 2018. The dissertation author was the secondary investigator and co-author of this paper.

Chapter 3, in full, is a reprint of the material as it appears in the article: Sung-En Chiu, Nancy Ronquillo, and Tara Javidi, “Active Learning and CSI Acquisition for mmWave Initial Alignment," IEEE Journal on Selected Areas in Communications, vol.37, issue 11, pp. 2474 - 2489,Dec. 2018.The dissertation author was the secondary investigator and co-author of this paper.

Chapter 4, in part, is a reprint of the material as it appears in the paper: Nancy Ronquillo and Tara Javidi, “Measurement Dependent Noisy Search with Stochastic Coefficients," IEEE International Symposium on Information Theory, 2020. The dissertation author was the primary investigator and author of this paper.

Chapter 4, in part, is a reprint of the material as it appears in the paper: Nancy Ronquillo, Sung-En Chiu, and Tara Javidi, “Sequential Learning of CSI for MmWave Initial Alignment," IEEE Asilomar Conference on Signals, Systems, and Computers, 2019. The dissertation author was the primary investigator and author of this paper.

Chapter 5, in full, is a reprint of the material as it appears in the paper: Nancy Ronquillo and Tara Javidi, “Active Beam Tracking Under Stochastic Mobility," IEEE International Conference on Communications, 2021. The dissertation author was the primary investigator and author of this paper.

Chapter 6, in full, is currently being prepared for submission for publication of the material. Nancy Ronquillo and Tara Javidi. The dissertation author was the primary investigator and author of this paper.

VITA

2015	Bachelor of Science in Aerospace Engineering, University of California, San Diego
2018	Master of Science in Electrical Engineering (Communication Theory and Systems), University of California, San Diego
2021	Doctor of Philosophy in Electrical Engineering (Communication Theory and Systems), University of California, San Diego

PUBLICATIONS

N. Ronquillo and T. Javidi, "Active and Dynamic Beam Tracking Under Stochastic Mobility," *in preparation*, 2021.

N. Ronquillo and T. Javidi, "Active Beam Tracking Under Stochastic Mobility," *IEEE International Conference on Communications*, 2021.

S. Karthikeyan, N. Ronquillo, P. Belda-Ferre, D. Alvarado, T. Javidi, C. A. Longhurst, and R. Knight, "High-Throughput Wastewater SARS-CoV-2 Detection Enables Forecasting of Community Infection Dynamics in San Diego County," *American Society for Microbiology Journals mSystems* Mar 2021.

N. Ronquillo and Tara Javidi, "Measurement Dependent Noisy Search with Stochastic Coefficients," *IEEE International Symposium on Information Theory*, 2020.

N. Ronquillo, SE. Chiu, and T. Javidi, "Sequential Learning of CSI for MmWave Initial Alignment," *IEEE Asilomar Conference on Signals, Systems, and Computers*, 2019.

SE. Chiu, N. Ronquillo, and T. Javidi, "Active Learning and CSI Acquisition for mmWave Initial Alignment," *IEEE Journal on Selected Areas in Communications*, vol.37, issue 11, pp. 2474 - 2489, Dec. 2018.

A.Lalitha, N. Ronquillo, and T. Javidi, "Improved Target Acquisition Rates with Feedback Codes," *IEEE Journal of Selected Topics in Signal Processing*, Vol.12, no.5, pp. 871 - 885, Oct. 2018.

A.Lalitha, N. Ronquillo, and T. Javidi, "Measurement Dependent Noisy Search: The Gaussian Case," *IEEE International Symposium on Information Theory*, June. 2017.

N. Ronquillo and T. Javidi, "Multiband Noisy Spectrum Sensing with Codebooks," *IEEE Asilomar Conference on Signals, Systems, and Computers*, Nov. 2016.

ABSTRACT OF THE DISSERTATION

Active and Dynamical Information Acquisition with Applications in Communication Systems.

by

Nancy Ronquillo

Doctor of Philosophy in Electrical Engineering (Communication Theory and Systems)

University of California San Diego, 2021

Professor Tara Javidi, Chair

This dissertation investigates the task of quickly and accurately learning possibly time-varying information about a system by making binary and noisy measurements that yield insight into its current state. This problem arises in beam alignment for millimeter-wave (mmWave) communication where the active learning of the location of a transmitter relative to the receiver is necessary to establish communication. In the problem of spectrum sensing for cognitive radio, active learning of the spectrum occupancy is used for opportunistic communication. These applications motivate our study of the problem of searching for a target(s) among a discrete set of locations by probing different locations with the caveat that probing larger areas leads to more incurred noise. The problem of binary search has been extensively studied and we are inspired by information-

theoretic principles to apply to practical problems in communication systems for enabling improved learning acquisition. Our methodology can be summarized by two central paradigms: active and sequential design of measurements, and dynamic tracking of a Bayesian posterior belief.

First, we cast the problem of searching for stationary, yet unknown, target locations as the problem of channel coding with state and feedback. We apply adaptive and sequential codes, i.e. measurement design, based on posterior matching to the problems of beam alignment and spectrum sensing to study these from a fundamental limit point of view. Our results characterize significant improvements in performance obtained by using adaptive measurements over non-adaptive ones, which is especially critical in the regimes of low signal-to-noise ratio. In the second half of this work, we generalize our work for learning time-varying measurement gains and dynamic target locations. We complement our strategies of active and sequential measurement design with simultaneous estimation of the measurement gains, which enables handling time-varying fading in mmWave beam alignment for example. Lastly, we enable handling stochastic mobility in mmWave beam alignment by incorporating predictive Bayesian filtering to dynamically evolve the posterior belief and by adaptively allocating pilots based on analysis of the mutual information and spectral efficiency. Combined, this dissertation moves towards solutions for the general and practical target search problem characterized by mobile and non-uniform targets.

Chapter 1

Introduction

Consider the general problem of recovering an unknown random vector $\mathbf{X}_t \in \mathbb{R}^{\frac{B}{\delta}}$ via a sequence of noisy binary observations. Mathematically, this is the problem of estimating $\mathbf{X}_t$ via observations Y_t, where an agent has control over the binary measurement vectors $\mathbf{A}_t \in \{0,1\}^{\frac{B}{\delta}}$, and all observations are impacted by an additive measurement-dependent noise. Specifically, the observations have the form

$$Y_t = \mathbf{A}_t^\intercal \mathbf{X}_t + N_t(\mathbf{A}_t) \tag{1.1}$$

An agent has the objective of finding a sequence of measurement vectors that minimize the probability of error in estimating $\mathbf{X}_t$ subject to a very low number of measurements available. Here we note two salient features of our formulation: 1) each observation is subject to additive noise $N_t(\mathbf{A}_t)$ that is affected by the choice of measurement $\mathbf{A}_t$, and 2) the measured signal is stochastic and potentially time-varying. Our problem formulation addresses the task of quickly and reliably learning potentially time-varying information about a system (summarized in $\mathbf{X}_t$) by making binary noisy measurements that yield insight into its current state. This set-up recovers the general problem of noisy binary search rooted in the work of [1] and extensively studied since in [2–5]. The feature of measurement dependent noise is studied from an information-theoretic perspective where many works have established a connection to the problem of channel coding over a binary input channel with [4–6] and without [7] feedback and the problem of joint-source channel coding

for dynamical systems [8]. Existing strategies propose to sequentially design measurements in response to accumulated belief, referred to as posterior matching, and have been shown to provide theoretical guarantees in performance [6, 9]. We draw on these works, leveraging the connection to channel coding, to develop our methodologies of active and sequential measurement design based on dynamically evolving our belief in response to observations or side information about the dynamic system. The following sections introduce two practical applications in communication systems that motivate this formulation.

1.1 Application to Beam Alignment in mmWave

Consider the problem of estimating channel state information (CSI) for establishing communications at millimeter-wave (mmWave) frequencies and above [10–12]. Prior to data transmission, the receiving base station and user equipment (UE) are tasked with aligning the transmitter and receiver antennas in the angular space through beamforming, which is enabled by acquiring an estimate of the CSI. The most general set-up of this problem may include deciphering the CSI for multiple potentially mobile UE's and subject to time-varying channel fading conditions. $\mathbf{X}_t$ can be thought of as the noiseless beam space representation of the channel, summarizing the UE path directionality and channel fading information. A measurement vector $\mathbf{A}_t$ can be interpreted as a particular beam pattern probing the angular space $B \subset (0, 360^\circ)$ with narrowest beam resolution δ. Furthermore, beam patterns with varying beam widths (in the angular domain) are associated with effects in perceived signal-to-noise ratio (SNR). That is, while narrow beams exploit antenna gains, wide beams with the same allocated power inherently achieve lower gains [13, 14] (where the gain is inversely proportional to the angular beam width). This effect results in lower perceived SNR for wider beams, and thus a higher probability of error in detecting a synchronization signal. This effect of beam width on the SNR motivates our model of measurement-dependent noise, where $N_t(\mathbf{A}_t)$. The problem of CSI acquisition is considered throughout this work, it is formally introduced in chapter 3 with details of the state of the art.

1.2 Application to Spectrum Sensing for Cognitive Radio

Consider the problem of spectrum sensing for cognitive radio [15], which aims to increase data transmission rates by allowing secondary users to monitor the occupancy of frequency bands in order to detect vacant subbands. Due to fluctuations in frequency subband occupancy by primary users, at a given time some frequency subbands may be left unused and eligible for unlicensed user transmissions. $\mathbf{X}_t$ can be thought of as a discrete representation of the spectrum occupancy over a total bandwidth of B with subbands of bandwidth δ. In this problem, a secondary user desires to locate vacant subbands quickly and reliably by making measurements about $\mathbf{X}_t$ through probing vectors $\mathbf{A}_t$ at every time t. We consider the energy-based detection [16] where joint multi-band detection is employed. Specifically, we are inspired by the group testing-based techniques for cognitive radio presented by [17] where a signal occupancy measurement is acquired by jointly deciding the occupancy of a group of subbands. Sequential measurements are made with a fixed sampling rate, i.e. a fixed power consumption. Due to noise folding effects caused by sub-Nyquist sampling [18] at each time instant t, the noise intensity depends on the number of subbands probed as dictated by a measurement vector $\mathbf{A}_t$. Thus, the noisy observation Y_t is a function of measurement dependent noise $N_t(\mathbf{A}_t)$. The resolution of the search, δ, can be limited by energy detection technology, while the accessible bandwidth space B is subject to change depending on the needs of the secondary user and is potentially unbounded. The problem of noisy spectrum sensing is considered in chapter 2 with details of the state of the art.

1.3 Overview

The following chapters are an exposition of our investigations that consider several cases of the unknown random vector $\mathbf{X}_t$. Combined, this work moves towards solving the most general problem (1.1). As our first step, in chapter 2 we consider the problem of recovering the unknown yet time-invariant support of a random vector $\mathbf{X}_t \in \mathbb{R}^{\frac{B}{\delta}}$. That is, an agent has the objective of finding a sequence of binary measurement vectors that minimize the probability of error in estimating

$\text{supp}(\mathbf{X}_t)$ subject to a very low number of measurements available and under the assumption of sparse $\mathbf{X}_t$. This problem arises in the example applications discussed above under stationary channel conditions for beam alignment for mmWave, and stationary vacant subbands with known magnitude for noisy spectrum sensing. This particular set-up is related to the problem of sparse Bayesian Learning and more closely to the problem of joint sparse support recovery, where the goal is to reconstruct a sparse common support vector via noisy compressed data [19–25]. We cast this problem as a target search problem under measurement-dependent noise and connect it to problems of channel coding with feedback. This connection to the problems of channel coding is crucial to our approaches and enables us to apply and analyze, from a fundamental limit point of view, existing codes or strategies with previously guaranteed performance. Under the additional condition of extreme sparsity $\|\text{supp}(\mathbf{X}_t)\|_0$, we characterize a gain in performance achieved by implementing adaptive measurement selection over non-adaptive or random methods, and we propose a scheme based on principles of posterior matching [6] for selecting measurements sequentially.

In chapter 3 we formally introduce the practical application of our work to the problem of initial alignment for mmWave communications. First, we formulate the CSI acquisition as active learning of the angle of arrival (AoA) of the UE signal subject to noisy measurements to propose a new adaptive and sequential beamforming strategy. This approach draws heavily from the results of our prior work in establishing a connection to channel coding with feedback of chapter 2, with the practical constraint of contiguous measurements. We develop an active and sequential algorithm for designing practically feasible measurements on the basis of posterior matching and analyze the proposed strategy to characterize fundamental limits and demonstrate the first possible work for standalone mmWave communication. In order to handle dynamic channel conditions, we propose a simple, yet mismatched solution for estimating the channel fading. While extremely successful under static or very well estimated channel conditions, our proposed scheme is shown to be sensitive to knowledge about the time-varying fading coefficients.

As a direct follow up, our work in chapter 4 continues our investigation into the problem (1.1) by studying the cases where the unknown random vector $\mathbf{X}_t$ can be decomposed into a

time-invariant common support, $\mathbf{W} = \text{ supp}(\mathbf{X}_t)$ and a vector of stochastic coefficients X_t, i.e. $\mathbf{X}_t = X_t\mathbf{W}$. As demonstrated in chapter 3, enabling learning of unknown channel gains (denoted by X_t) is crucial for handling dynamic channel conditions via sequential measurement selection. Our approach is to augment the learning of the AoA (denoted by $\mathbf{W}$) with a simultaneous online estimation of the channel fading coefficients X_t. We propose two algorithms for adaptively and sequentially selecting measurement vectors for jointly learning the common support and the unknown stochastic coefficients. For both the general formulation (1.1) and the application of mmWave beam alignment, we empirically show improvements over non-adaptive algorithms that design randomized measurements a priori.

The remainder of this dissertation is focused on the dynamic case of the unknown random vector $\mathbf{X}_t$ where the supp($\mathbf{X}_t$) changes in a stochastic fashion. We are influenced and motivated by the problem of mmWave beam alignment under the additional challenges of mobility, such as in cellular-enabled unmanned aerial vehicle (UAV) systems. We consider $\mathbf{X}_t$ to be a beam space representation of the CSI, thus UAV mobility can be thought of as a changing support in $\mathbf{X}_t$. More specifically, we assume that mobility translates into variations of the AoA, which we model as stochastic, thus the CSI (or equivalently supp($\mathbf{X}_t$) under no fading) must be constantly acquired or estimated online. In chapters 5 and 6 we propose a comprehensive communication scheme for enabling robust beam tracking under stochastic mobility. In chapter 5 we propose an active and sequential beam selection algorithm based on dynamically evolving the posterior in response to observed signals and mobility information. Numerically, we focus on a simplified channel model receiving pilots only to analyze the performance in terms of achievable beamforming gain. We show improvements in AoA estimation as well as significant increases in average beamforming gain compared to existing tracking strategies. In chapter 6 we propose a primarily computational method for adaptively allocating pilots to trade-off pilot enabled channel estimation and data transmission. We introduce a method for adaptively triggering pilots by maximizing an information reward which we define to consist of the mutual information and spectral efficiency terms of each communication phase. Our proposed dynamic tracking of the posterior, which enables simultaneous learning of the

AoA (both in the data transmission and pilot phases), is inspired by the reward optimization learning paradigm of reinforcement learning algorithms [26]. We empirically demonstrate our ability to maintain AoA alignment over time, which results in high average beamforming gains, as well as reduced pilot overhead compared to existing strategies.

1.4 Notations

We use boldface letters to represent vectors and matrices. $\|\mathbf{A}\|$ is the l_2 norm of $\mathbf{A}$. $\mathbf{A}(j)$ is the j^{th} element of a vector. $\|\mathbf{A}\|_0$ denotes the l_0 norm, i.e. sum of non-zero entries of $\mathbf{A}$. For a complex number $c = a + ib$, i.e. $c \in \mathbb{C}$, $|c| = \sqrt{a^2 + b^2}$ is the absolute value or complex modulus. $\mathfrak{R}(c)$ and $\mathfrak{I}(c)$ denote the real and imaginary parts of c. Let $\{0,1\}^M$ denote the set of all $M \times 1$ vectors made up of elements with values equal to 0 or 1. On the other hand, let $[0,1]^M$ denote the set of all $M \times 1$ vectors made up of elements with values between 0 and 1. $\{\mathbf{e}_1, \mathbf{e}_2, \ldots, \mathbf{e}_n\}$ is the set of basis vectors for $\mathbb{R}^n$, where $e_i(j) = 1$, if and only if $j = i$, and 0 otherwise. Let $[g]_a = g$ if $g \geq a$ otherwise $[g]_a = 0$. For any positive integer M, let $\mathsf{I}_M := \{\frac{1}{M}, \frac{2}{M}, \ldots, 1\}$ and let $[M] = \{1, 2, \ldots, M\}$. Let $\mathbb{1}_A$ denote the indicator function defined on set X indicating membership of an element in a subset A of X, with value 1 for all X in A and value 0 for all X not in A.

We denote the space of probability mass functions on set $\mathcal{X}$ as $P(x)$. Bern(q) is the Bernoulli distribution with parameter q. $\mathcal{N}(\mu, \sigma^2)$ is the Gaussian distribution with mean μ, and variance σ^2. Let $G(x; \mu, \sigma^2)$ denote the probability density function of a Gaussian random variable with mean μ and variance σ^2 at x. $\mathcal{CN}(\mu, \sigma^2)$ denotes circularly symmetric complex Gaussian distribution, where real and imaginary parts are Gaussian distributed with variance $\frac{\sigma^2}{2}$ and mean $\mathfrak{R}(\mu)$ and $\mathfrak{I}(\mu)$, respectively. $\mathcal{CN}(x; \mu, \sigma^2)$ is the $\mathcal{CN}(\mu, \sigma^2)$ probability density function evaluated at x. Logarithms are to the base 2. $h(p) = p \log \frac{1}{p} + (1-p) \log \frac{1}{(1-p)}$ denotes the entropy of a Bernoulli random variable with parameter p, and $D(p||(1-p)) = p \log \frac{p}{1-p} + (1-p) \log \frac{1-p}{p}$ denotes the Kullback-Leibler (KL) divergence between the distribution of two Bernoulli random variables with parameters p and $(1-p)$. The mutual information between random variable X and Y is defined as

$I(X,Y) = \sum_{x,y} p(x,y) \log \frac{p(x,y)}{p(x)p(y)}$, where $p(x,y)$ is the joint distribution and $p(x)$ and $p(y)$ are the marginals of X and Y.

In chapter 3 specifically, let $I(q;p)$ denote the mutual information of the input $X \sim \text{Bern}(q)$ and the output Y of a BSC channel with crossover probability p. $C_1(p) := D(\text{Bern}(p) \| \text{Bern}(1-p))$ denotes the error exponent of hypothesis testing of $\text{Bern}(p)$ versus $\text{Bern}(1-p)$. $\text{Rice}(\mu, \sigma^2)$ denotes and Rician distribution and $\text{Rice}(x; \mu, \sigma^2) := \frac{x}{\sigma^2} \exp\left(\frac{-(x^2+\mu^2)}{2\sigma^2}\right) J_0(\frac{x\mu}{\sigma^2})$ denotes its probability density function, where $J_0(\cdot)$ is the modified Bessel function of the first kind with order zero.

Chapter 2

Target Acquisition: An Information-Theoretic Perspective

In this chapter we introduce our first analysis of the general problem (1.1). We consider the special case when the random vector $\mathbf{X}_t$ has a known magnitude and a time invariant common support $\mathbf{W} = \text{supp}(\mathbf{X}_t)$. The goal is to recover the unknown support vector $\mathbf{W} \in \{0,1\}^{\frac{B}{\delta}}$ quickly and robustly under a limited number of measurements. In the first part of this chapter, we begin our study of practical communication systems applications under an information theoretic perspective. We cast the practical problem of spectrum sensing for cognitive radio (briefly introduced in chapter 1) as the task of searching for multiple targets under measurement dependent noise and formalize the connection to multiple access channel coding with feedback. As a main consequence, this approach allows for the characterization of fundamental limits on the speed and the reliability of optimal multiband spectrum sensing.

In the second part of this chapter, we consider the special case of extreme sparsity $\|\mathbf{W}\|_0 = 1$ and formalize the connection to the problem of binary input channel coding with state and feedback subject to codebook dependent Gaussian noise. Leveraging this connection to channel coding, we propose and investigate sequential acquisition methods for recovering $\mathbf{W}$ in an active manner (with feedback). Most notably, this work characterizes a lower bound on the adaptivity gain in expected

number of measurements required to acquire $\mathbf{W}$ for a desired probability of error. Our theoretical analysis reveals two distinct asymptotic regimes affecting the adaptivity gain based on the manner in which the number of locations $\frac{B}{\delta}$ grows.

2.1 Part I. Multiband Noisy Spectrum Sensing with Codebooks

In traditional wireless communication systems, licensed primary users are allocated portions of a spectrum. Due to fluctuations in frequency subband occupancy by primary users, at a given time, some frequency subbands may be left unused and eligible for unlicensed user transmissions. Cognitive radio [15] aims to increase data transmission rates by allowing secondary users to monitor the occupancy of frequency bands in order to detect vacant subbands. This work focuses specifically on the mulitiband sensing approach in which a secondary user searches across multiple narrow frequency subbands, searching for vacant subbands. In [27], multiband joint detection is introduced and shown to increase aggregate throughput and reliability in spectrum sensing for cognitive radio. Schemes such as [28] and [29] show further gains in performance by using adaptive algorithms. While heuristic strategies are proposed by [28] and [29], fundamental limits on the expected number of measurements required by adaptive strategies remain.

We cast the optimal and reliable multiband spectrum sensing problem as a target search problem with measurement dependent noise, and to show a direct connection to the problem of channel coding over a Multiple Access Channel (MAC) with feedback. In particular, we show that the locations of the vacant subbands can be thought of as individual senders and the choice of searching scheme can be viewed as a set of common codewords used by these "senders," with a caveat that the channel noise statistically depends on the codebook. Drawing on this connection to channel coding, non-adaptive and adaptive codes with previously guaranteed performance can be effectively used as sensing schemes under which bounds on the expected number of measurements can be obtained.

Here, we note that although this part of the chapter is focused on the practical application

of spectrum sensing for cognitive radio, beam alignment for mmWave can be similarly cast as a problem of searching for multiple target with measurement dependent noise (this application is studied in chapter 3). The deployment of mm-Wave links into a cellular or 802.11 network, the base station needs to to quickly switch between users and accommodate multiple mobile clients. In a dense network as such, a received signal at the base station will be corrupted by measurement dependent noise (due to channel properties) and by neighboring interfering users.

2.1.1 Problem Set-up

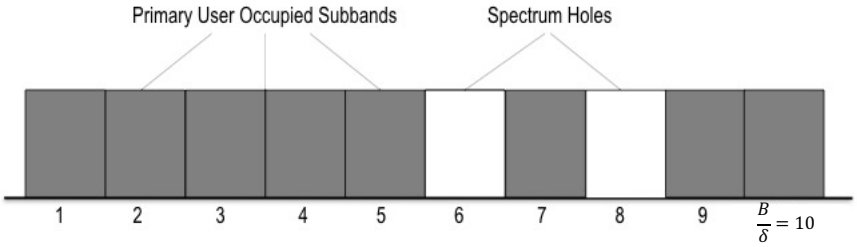

Figure 2.1: Schematic illustration of the occupancy of $\frac{B}{\delta}$ subbands [27]

Consider r vacant subbands among $\frac{B}{\delta}$ total subbands in a wireless spectrum (illustrated in Fig. 2.1 for $r = 2$). A user tasked with locating these r vacant subbands searches by conducting a sequence of noisy measurements, during which the occupancy of each subband remains fixed. At time t the user probes a group of subbands, denoted by the measurement vector $\mathbf{A}_t$, simultaneously and obtains a noisy observation Y_t. Let the locations of the r vacant subbands be denoted by a vector $\mathbf{W} \in \{0,1\}^{\frac{B}{\delta}}$, such that $\mathbf{W}(j) = 1$ if and only if subband j is vacant and $j = 1, 2, \ldots, \frac{B}{\delta}$.

Let the binary measurement vector $\mathbf{A}_t \in \{0,1\}^{\frac{B}{\delta}}$ denote the locations of the probed subbands at time t, where $\mathbf{A}_t(j) = 1$ if and only if subband j is searched at time t. Therefore, $\|\mathbf{A}_t\|_0$ denotes the number of subbands that are searched at time t. Let $\mathbf{n}_t$ be a vector of measurement noise, i.e. $\mathbf{n}_t(j)$ is assumed to be i.i.d across time t and subband j, for all t and j, with distribution $p_z(\cdot)$.

Then, the noisy observation is given as

$$\begin{aligned} Y_t &= \mathbf{A}_t^\intercal(\mathbf{W}+\mathbf{n}_t) \\ &= \mathbf{A}_t^\intercal\mathbf{W}+\mathbf{A}_t^\intercal\mathbf{n}_t \end{aligned} \tag{2.1}$$

The clean signal $\mathbf{A}_t^\intercal\mathbf{W}$ indicates the the number of targets present in the measurement vector $\mathbf{A}_t$. In other words, the vector of observations $\mathbf{Y}_{1:N} = [Y_1, ..., Y_N]$ contains noisy information about the location of targets, given as a result of search matrix $\mathbf{A}_{1:N} = [\mathbf{A}_1; ...; \mathbf{A}_N]$. The objective is to find the best estimate, $\hat{\mathbf{W}}$, of $\mathbf{W}$ and the best search matrix $\mathbf{A}_{1:N}$ in order to minimize the expected number of measurements subject to a small error probability $\mathrm{P}_e = \mathbb{P}(\hat{\mathbf{W}} \neq \mathbf{W}|\mathbf{Y}_{1:N}, \mathbf{A}_{1:N})$.

Here, we note that the search scheme, or search matrix $\mathbf{A}_{1:N}$, and the total number of measurements made, N, can be either be selected offline or sequentially as a function of past observations. More specifically, we say a searching scheme is of variable length if the number of measurements, N, is a random stopping time with respect to random sequence $[Y_1, Y_2, \ldots]$. Furthermore, if each column $\mathbf{A}_t$ is selected adaptively as a function of past observations, $[Y_1, \ldots, Y_{t-1}]$, then the search scheme, $\mathbf{A}_{1:N}$, is said to be adaptive. On the other hand, for a non-adaptive searching scheme $\mathbf{A}_{1:N}$ is populated (potentially randomly) independently of $\mathbf{Y}_{1:N}$. Note that, given the added complexity of adapting the choice of $\mathbf{A}_t$, it is very natural to introduce and analyze the effects of adaptivity, as it pertains to the design of $\mathbf{A}_{1:N}$.

We note that, assuming a uniform prior and a known search scheme $\mathbf{A}_{1:N}$, then upon a set of observations $\mathbf{Y}_{1:N}$ the best estimate, $\hat{\mathbf{W}}$, of $\mathbf{W}$ is easily derived via the maximum likelihood decoder over the set:

$$\mathcal{C} := \{\mathbf{C} : \mathbf{C} = \sum_{i=i_1}^{i_r} [\mathbf{A}_1(i), \mathbf{A}_2(i); \ldots; \mathbf{A}_N(i)]\}, \tag{2.2}$$

which is the set of all possible outputs in the absence of noise. Next, we utilize this formulation of the spectrum sensing problem, given by (2.1), to illustrate the connection to the problem of communications over a MAC.

2.1.2 An Information-Theoretic Perspective: Connection to MAC Coding

In the following section, we review channel coding over a MAC and formulate an equivalent model for comparison to (2.1). We highlight similarities and differences. After establishing a strong connection between the two problems, we propose a selection of non-adaptive and adaptive codebooks that, through this connection, may be used as sensing schemes. Finally, we specialize a maximum likelihood decoder for a general search with Gaussian noise.

Review of MAC

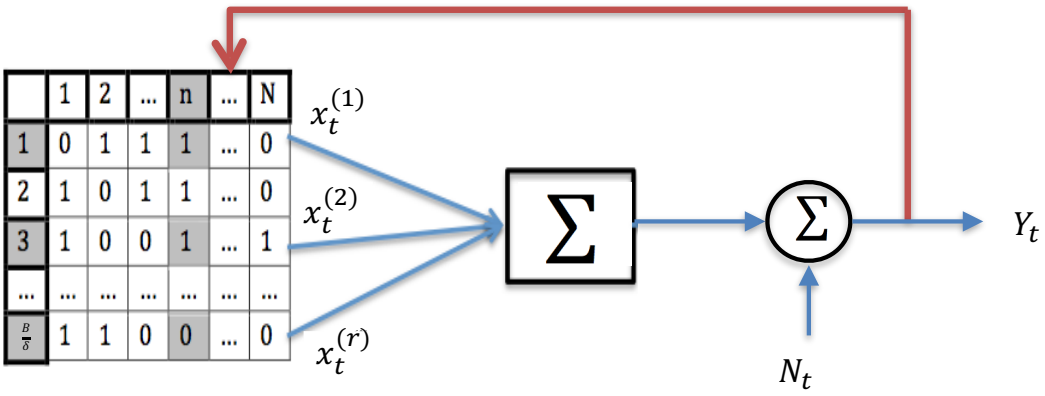

Figure 2.2: Diagram of multi-user communication over a multiple access channel (MAC) with r senders

We begin by reviewing a traditional r-sender MAC, illustrated in Fig. 2.2. The output of the MAC at for a time slot t is written as:

$$Y_t = \sum_{i=1}^{r} h^{(i)} x_t^{(i)} + N_t, \tag{2.3}$$

where $x_t^{(i)}$, for $i = 1, 2, \ldots, r$, represents the input symbol from the i^{th} sender at time t, $h^{(i)}$ is the channel gain associated with sender i, and N_t is the channel noise. It is often assumed that N_t, is an i.i.d, random variable. Equivalently, over N slots, $\mathbf{x}_{1:N}^{(i)} = [x_1^{(i)}, \ldots, x_N^{(i)}]$ represents the codeword for sender i. Given the availability of the codebooks of the senders at the receiver, and upon obtaining a set of observations, $\mathbf{Y}_{1:N}$, the receiver can detect the most likely codewords transmitted, i.e. decodes

all $\mathbf{x}_{1:N}^{(i)}$'s [30]. Define the probability of error $P_e = \mathbb{P}(\hat{\mathbf{x}}_{1:N}^{(i)} \neq \mathbf{x}_{1:N}^{(i)} | \mathbf{Y}_{1:N})$, for $i \in \{1, 2, \ldots, r\}$.

In this setting, the objective becomes to design a $\frac{B}{\delta} \times N$ codebook for each user $i = 1, 2, \ldots, r$ in the form:

$$\begin{bmatrix} \mathbf{x}_{1:N}^{(i_1)} \\ \mathbf{x}_{1:N}^{(i_2)} \\ \vdots \\ \mathbf{x}_{1:N}^{(i_{B/\delta})} \end{bmatrix}, \tag{2.4}$$

in order to minimize the expected number of measurements needed to decode all codewords while ensuring a desirable reliability $P_e \leq \epsilon$.

Spectrum Sensing as Coding over a MAC: Similarities and Differences

Recall the binary vector $\mathbf{W}$ contains r non-zero elements which indicate the locations of targets. In other words, we can write

$$\mathbf{W} = \sum_{i=1}^{r} \mathbf{W}_i, \tag{2.5}$$

where $\mathbf{W}_i \in \{\mathbf{e}_1, \mathbf{e}_2, \ldots, \mathbf{e}_M\}$ is in the set of basis vectors for $\mathbb{R}^M$, where $\mathbf{e}_i(j) = 1$, if and only if $j = i$, and 0 otherwise for all i. The output Y_t now can be written as :

$$Y_t = \sum_{i=1}^{r} \mathbf{A}_t^\intercal \mathbf{W}_i + \mathbf{A}_t^\intercal \mathbf{n}_t. \tag{2.6}$$

Setting $x_t^{(i)} = \mathbf{A}_t^\intercal \mathbf{W}_i$ for $i = 1, 2, \ldots, r$, and $N_t = \mathbf{A}_n^\intercal \mathbf{n}_t$, observation Y_t can be written as

$$Y_t = \sum_{i=1}^{r} x_t^{(i)} + N_t, \tag{2.7}$$

which, by comparing to (2.3), can be interpreted as the output of an r-user MAC with the following properties.

- **Channels have unit gain:** In (2.7), we note the missing gain elements, $h^{(i)}$, $i = 1, 2, \ldots, r$.

This establishes that all messages, $x_t^{(i)}$, in (2.7), have a fixed unit channel gain.

- **Matrix $\mathbf{A}_{1:N}$ is a common codebook:** By comparing the vector $[\mathbf{A}_1^\intercal \mathbf{W}_i, \ldots, \mathbf{A}_N^\intercal \mathbf{W}_i] = \mathbf{A}_{1:N}^\intercal \mathbf{W}_i$, from (2.6), to the codebook of a MAC user given in (2.4), we see that the rows in $\mathbf{A}_{1:N}$ can be viewed as the $\frac{B}{\delta}$ codewords of user i with a caveat that the codebook across targets $i = 1, 2, \ldots, r$ is constructed from a single search matrix, $\mathbf{A}_{1:N}$. Hence, when viewed as MAC encoding, all "transmitters" essentially share a single codebook. Further, the decoder need not label which transmitter sent which codeword so long as the right set of codewords are identified.

- **Additive noise depends on codebook:** Note that, N_t in (2.7), depends on vector $\mathbf{A}_t$, i.e. in contrast to (2.3), the measurement noise is dependent on the individual columns of the codebook. This dynamic codebook dependent noise model differs from a traditional MAC.

- **The MAC channel inputs are binary:** We note that both $\mathbf{W}_i$ and $\mathbf{A}_t$ are binary, and thus the shared codebook, $\mathbf{A}_{1:N}$, is restricted to binary codes.

Maximum Likelihood Detection for Gaussian Noise

In this subsection we derive the structure of the maximum likelihood decoder when the additive measurement noise is Gaussian, such that $\mathbf{n}_t(j) \sim \mathcal{N}(0, \sigma^2)$ is i.i.d accross time t and subband j and for all t and j. We note that, under i.i.d noise across subbands, the total additive noise $N_t = \mathbf{A}_t^\intercal \mathbf{n}_t \sim \mathcal{N}(0, \|\mathbf{A}|_0 \sigma^2)$, and thus measurement, i.e. codebook dependent. More specifically, we show that the optimal decoder can be reduced to finding an element in set $\mathcal{C}$, defined in (2.2), with the minimum weighted square distance to the observation vector $\mathbf{Y}_{1:N}$. Before formalizing this, we first remind the reader that $\mathcal{C}$ is a set of all possible outputs if the noise is absent. Hence, it is natural to require that our codebook (searching scheme), $\mathbf{A}_{1:N}$, be such that the sum of any r codewords is unique. Mathematically, this means that if

$$\sum_{i=i_1}^{i_r} [\mathbf{A}_1(i), \mathbf{A}_2(i), \ldots, \mathbf{A}_N(i)] = \sum_{i=j_1}^{j_r} [\mathbf{A}_1(i), \mathbf{A}_2(i), \ldots, \mathbf{A}_N(i)], \tag{2.8}$$

then for all $k = 1, 2, \ldots, r$, then

$$i_k = j_k. \tag{2.9}$$

Lemma 1. Let $\mathbf{n}_t(j) \sim \mathcal{N}(0, \sigma^2)$ across time t and subband j, for all t and j. Furthermore, let the codebook $\mathbf{A}_{1:N}$ satisfy the unique sum condition given by (2.8)-(2.9). The best estimate, $\hat{\mathbf{W}}$, of $\mathbf{W}$ is the unique vector $\hat{\mathbf{W}}$ such that $\hat{\mathbf{W}}^{\mathsf{T}}\mathbf{A}_{1:N} = \hat{\mathbf{C}}$ and

$$\hat{\mathbf{C}} = \arg\min_{[\mathbf{C}\in\mathcal{C}]} \sum_{t=1}^{N} \frac{|y_t - C(t)|^2}{\|\mathbf{A}_t\|_0 \sigma^2},$$

where recall $\|\mathbf{A}_t\|_0$ is the number of subbands sensed at time t.

2.1.3 Search with a Codebook

In this section, we discuss a variety of searching schemes, in the form of codebooks, that can be applied to the the sensing problem described by the model (2.1). This general approach of search using codebooks provides an efficient way to design and compare a slew of non-adaptive and adaptive codes. Before we proceed with the description of these example schemes, we remind the readers that the codebooks (hence searching schemes) can be classified based on the variability of the code-length (number of measurements conducted) as well as the adaptivity of the codebook to the observed output samples.

Variable Length Random Coding

A variable length random codebook is constructed by drawing the codebook, $\mathbf{A}_{1:N}$, randomly and without feedback information. In particular, $\mathbf{A}_t(j)$ is chosen according to i.i.d Bern(q) where parameter q describes the expected proportion of ones in $\mathbf{A}_t$, i.e. $\mathbb{E}[\frac{\|\mathbf{A}_t\|_0}{B/\delta}]$. Intuitively, due to our size dependent measurement noise model, as q is increased, $\|\mathbf{A}_t\|_0$ will be larger on average, thereby increasing the average size dependent measurement noise. However, if q is too small, for large $\frac{B}{\delta}$, the expected number of measurements needed to cover all subbands will increase. An optimal choice of q will trade-off search time and measurement noise.

Multi-phase adaptive algorithm

The multi-phase algorithm conducts a coarse search in its first phase by using the variable length non-adaptive code with a fixed parameter q. It resumes when a unique $\hat{\mathbf{W}}$ is found with high probability. Upon completion of the first phase, r smaller regions, each believed to contain a single target with high probability, are individually searched. The second phase has a zooming effect, which serves the two-fold purpose of reducing the multi-target search into r single target searches after the first phase, and of reducing measurement noise in each single target search.

Single-arget case with sorted posterior matching

In some instances, there may exist extreme sparsity in the vector $\mathbf{w}$. That is, a search is conducted to quickly and reliably locate a single vacant subband. In this single-target case we have a larger set of examples in the domain of point-to-point feedback codes. In particular, the remainder of this chapter is focused on applying and analyzing adaptive codebooks, from a fundamental limit stand point. We take inspiration from adaptive strategies based on the posterior matching scheme [31] which is a fully sequential point-to-point feedback code generalizing many special cases [1, 2, 32] in the literature. To handle the measurement dependent nature of the noise, we consider a slight modification of posterior matching under which the size of the search region is gradually shrunk. Under the adaptive search algorithm, termed *sort*PM by [9], the observations, $[Y_1, \ldots, Y_t]$, are used to first compute the posterior probability over possible single target messages $\mathbb{P}\{\mathbf{e}_i | Y_1, \ldots, Y_t\}$ where $\mathbf{e}_i$ is one out of $\frac{B}{\delta}$ possible single target messages. Search vectors are selected to "match" to the posterior, in an adaptive manner as uncertainty is reduced by updating the posterior over time as observations are received. Use of these posterior matching based codes enables analysis of the spectrum sensing problem from a fundamental limit point of view.

On the other hand, searching for multiple targets with measurement dependent noise is a significantly harder problem compared to a single target case and achievability strategies for this problem even in the absence of noise are far more complex [33, 34].

2.2 Part II: Improved Target Acquisition Rates with Feedback Codes

This part of the chapter is focused on the special case extreme sparsity of model (1.1), where $\|\mathbf{X}_t\|_0 = 1$. That is, the objective is to recover the unitary support time-invariant vector $\mathbf{W} \in \{0,1\}^{\frac{B}{\delta}}$ via a sequence of noisy linear measurements. Under the known magnitude and unitary support, this problem can be thought of as a single target acquisition over a search region of width B with a resolution up to width δ. Noisy linear measurements have the form

$$Y_t = \mathbf{A}_t^\intercal \mathbf{W} + N_t(\mathbf{A}_t), \tag{2.10}$$

where a binary measurement vector $\mathbf{A}_t \in \{0,1\}^{\frac{B}{\delta}}$ denotes the locations inspected and $N_t(\mathbf{A}_t)$ is a noise term whose statistics are a function of the measurement vector $\mathbf{A}_t$. The goal is to design a sequence of measurement vectors $\{\mathbf{A}_t\}_{t=1}^{\tau}$, such that the target location $\mathbf{W}$ is estimated with high reliability, while keeping the (expected) number of measurements τ as low as possible.

In this chapter, we first consider the linear model when the elements of noise per location searched are i.i.d Gaussian with zero mean and variance $\delta\sigma^2$. That is, $N_t(\mathbf{A}_t)$ in (2.10) are distributed as $\mathcal{N}(0, \|\mathbf{A}_t\|_0 \delta\sigma^2)$. For this case we show that the problem of searching for a target under measurement dependent Gaussian noise $N_t(\mathbf{A}_t)$ is equivalent to channel coding over a binary additive white Gaussian noise (BAWGN) channel with state and feedback (in Sect. 4.6 of [35]). This allows us not only to retrofit the known channel coding schemes based on sorted Posterior Matching (sortPM) [9] as adaptive search strategies, but also to obtain information theoretic converses to characterize fundamental limits on the target acquisition rate under both adaptive and non-adaptive strategies. Furthermore, by providing a non-asymptotic analysis of our two stage sorted Posterior-Matching-based adaptive strategy and our converse for non-adaptive strategy, we obtain a lower bound on the adaptivity gain.

2.2.1 Our Contributions

Our main results are inspired by the analogy between target acquisition under measurement dependent noise and channel coding with state and feedback. This connection was utilized in [36] under a Bernoulli noise model. In part of the chapter, in Proposition 1, we formalize the connection between our target acquisition problem with Gaussian measurement dependent noise and channel coding over a BAWGN channel with state. Here, the channel state denotes the measurement vector. The channel transition depends on the channel state as $\mathcal{N}(X_t, \|\mathbf{A}_t\|_0 \delta \sigma^2)$ for input codeword $X_t \in \{0, 1\}$. Adapting the codeword to the past channel outputs, i.e. using feedback codes is known to increase the capacity of a channel with state and feedback. This motivates us to use adaptivity when searching, i.e., to utilize past observations $Y_{1:t-1}$ when selecting the next measurement vector $\mathbf{A}_t$. Furthermore, this information theoretic perspective allows us to quantify the increase in the adaptive target acquisition rate. Our analysis of improvement in the target acquisition rate as well as the adaptivity gain, measured as the reduction in expected number of measurements, while using an adaptive strategy over a non-adaptive strategy has two components. Firstly, we utilize information theoretic converse for an optimal non-adaptive search strategy to obtain a non-asymptotic lower bound on the minimum expected number of measurements required while maintaining a desired reliability. As a consequence, this provides the best non-adaptive target acquisition rate. Secondly, we utilize a feedback code based on sorted Posterior Matching as a two-stage adaptive search strategy and obtain a non-asymptotic upper bound on the expected number of measurements while achieving a desired reliability. These two components of our analysis allow us to characterize a lower bound on the adaptivity gain.

Our non-asymptotic analysis of adaptivity gain reveals two qualitatively different asymptotic regimes. In particular, we show that adaptivity gain depends on the manner in which the number of locations grow. We show that the adaptivity grows logarithmically with the number of locations $\frac{B}{\delta}$, i.e., $O\left(\log \frac{B}{\delta}\right)$ when refining the search resolution δ (δ going to 0) and while keeping total search width B fixed. On the other hand, we show that as the search width B expands (B goes to ∞) while keeping search resolution δ fixed, the adaptivity gain grows with the number of locations as

$O\left(\frac{B}{\delta}\log\frac{B}{\delta}\right)$.

The problem of searching for a target under noisy observations has roots in [1]. Our problem setup is closely related to the problem of sequential estimation of the target location via the noisy 20 questions game studied by Jedynak et al. in [37] and collaborative 20 questions for target localization by Tsiligkaridis et al. in [38]. However, unlike these problem setups which focus on measurement independent noise we consider measurement dependent noise and hence focus on prior work considering the same. The problem of searching for a target under a binary measurement dependent noise, whose crossover probability increases with the weight of the measurement vector was studied by [36] and analyzed under sort PM strategy in [9]. In particular, [36] and [9] provide asymptotic analysis of the adaptivity gain for the case where $B = 1$ and δ approaches zero. Our prior work [39] by utilizing a (suboptimal) hard decoding of Gaussian observation Y_t, strengthens [36] and [9] by also accounting for the regime in which B grows. While the analysis in [39] strengthens the non-asymptotic bounds in [9] with Bernoulli noise it failed to provide tight analysis for our problem with Gaussian observations. In this part of the chapter, by strengthening our analysis in [39] we further extend the prior work. We provide the following detailed list of our main contributions in this part of the chapter:

1. We consider the problem of searching for a target (vacant) narrow band of width δ over a total bandwidth B via linear binary measurements subject to measurement dependent Gaussian noise (this model is referred to as noise folding in some literature). We establish the equivalence of this problem to the problem of binary-input channel coding over an additive Gaussian channel with state and feedback. This allows us to consider information theoretic techniques to characterize the fundamental limits of searching as well as construct feedback codes as effective search strategies (see Proposition 1 and Corollary 1).

2. We propose a simple intuitive two stage adaptive target search strategy inspired by known feedback codes. This strategy allows us to provide a tight non-asymptotic upper bound on the expected number of measurements needed by an optimal adaptive search strategy. The only known upper bound on the expected number of measurements needed by an optimal

adaptive search strategy in the use of Binary Symmetric Channel (BSC) [9, 36] provides an upper bound that is very loose in general and particularly loose for Gaussian observations. In this sense our upper bound significantly tightens the prior analysis (see Remark 3 and Fig. 2.8 and Fig. 2.9).

3. Obtaining tight non-asymptotic upper bounds on the expected number of measurements needed by an optimal adaptive search strategy allows us to provide better bound on adaptivity gain (see Theorem 1).

4. Our result extends and significantly improves the prior work in the asymptotic regime of B goes to ∞:

   - Our setup specializes to two practically relevant asymptotic problems given by the application to beam alignment in mmWave where resolution δ shrinks while search space width B remains fixed (noise variance shrinking to zero) and by the application to noisy spectrum sensing where resolution δ is fixed but search space width B grows (half bandwidth noise variance linearly growing).

   - Our two-stage strategy is shown to be asymptotically optimal in the regime where δ goes to zero and B is fixed. In this regime, our results extends prior work to on BSC [9, 36] to the Gaussian additive noise case with noise folding. Here we note that the BSC work in [9, 36] can be viewed as a pessimistic analysis of the Gaussian measurements with hard-decoding.

   - In the asymptotic regime where δ is fixed and B grows, our result significantly improves prior work [36] in incorporating an optimization of the proposed strategy in terms of a parameter α. Note that without such optimization, even if one accepts the hard decoding approximation, all known schemes and analysis fail to provide a non-trivial bound in the asymptotic regime (see Fig. 2.8).

Applications

This formulation address the practical applications of beam alignment in mmWave and noisy spectrum sensing described in chapter 1. Next, we discuss the state-of-the-art in these examples to highlight the impact of our contributions. Giordani et al. [13] compare the exhaustive search like the Sequential Beamspace Scanning considered by Barati et al. [40], where the base station sequentially searches through all angular sectors, against a two stage iterative hierarchical search strategy. In the first stage an exhaustive search identifies a coarse sector by repeatedly probing each coarse region for a predetermined SNR to be achieved. In the second stage an exhaustive search over all locations identifies the target. Giordani et al. show that in general the adaptive iterative strategy reduces the number of measurements over exhaustive search except when desired SNR is too high, forcing the number of measurements required at each stage to get too large. We show this through numerical results. In fact, as confirmed by our simulations random-coding-based non-adaptive strategies including the Agile-Link protocol [41], outperform the repetition based adaptive strategies.

Past literature on spectrum sensing for cognitive radio [27–29] and support vector recovery [42, 43] have focused on the problem where $\mathbf{A}_t$ can be real or complex, with measurement independent noise applying both exhaustive search and multiple adaptive search strategies. In contrast, our work considers a simple binary model, $\mathbf{A}_t \in \{0,1\}^{\frac{B}{\delta}}$, but captures the implications of measurement dependence of the noise, which is known in the spectrum sensing literature as noise folding. The problem of measurement dependent noise (known as noise folding) has been investigated in [18] where non-adaptive design of complex measurements matrix satisfying RIP condition has been investigated. Our work compliments this study by characterizing the gain associated with adaptively addressing the measurement dependent noise (noise folding), albeit for the simpler case of binary measurements. We note that the case of adaptively finding a subset of a sufficiently large vacant bandwidth with noise folding is considered in [17], where ideas from group testing and noisy binary search have been utilized. The solutions however depend strongly on the availability of sufficiently large consecutive vacant band and does not apply to our setting.

2.2.2 Problem Set-up

We consider a search agent interested in quickly and reliably finding the true location of a single stationary target by making measurements over time about the target's presence. In particular, we consider a total search region of width B that contains the target in a location of width δ. In other words, the search agent is searching for the target's location among $\frac{B}{\delta}$ total locations. Let $\mathbf{W} \in \{0,1\}^{\frac{B}{\delta}}$ denote the true location of the target, where $\mathbf{W}(j) = 1$ if and only if the target is located at location j. The target location $\mathbf{W}$ can take $\frac{B}{\delta}$ possible values uniformly at random whose value remains fixed during the search. A measurement at time n is given by a vector $\mathbf{A}_t \in \{0,1\}^{\frac{B}{\delta}}$, where $\mathbf{A}_t(j) = 1$ if and only if location j is probed. Each measurement can be imagined to result in a clean observation $X_t = \mathbf{W}^\intercal \mathbf{A}_t \in \{0,1\}$ indicating of the presence of the target in the measurement vector $\mathbf{A}_t$. However, only a noisy version of the clean observation X_t is available to the agent. The resulting noisy observation $Y_t \in \mathbb{R}$ is given by the following linear model with additive measurement dependent noise

$$Y_t = X_t + N_t(\mathbf{A}_t). \tag{2.11}$$

Here, we assume $N_t \sim \mathcal{N}(0, \|\mathbf{A}_t\|_0 \delta \sigma^2)$ which corresponds to the case of i.i.d white Gaussian noise with σ^2 denotes the noise variance per unit width. Conditioned on the measurement vector $\mathbf{A}_t$, the noise N_t is independent over time. Also define $\sigma^2_{\text{Total}} := \frac{B\sigma^2}{2}$, which denotes the noise intensity when the agent searches half of the search region $\frac{B}{2}$.

A search consisting of τ measurements can be represented by a sequence of measurement vectors $\mathbf{A}_{1:\tau} = \{\mathbf{A}_1, \mathbf{A}_2, \ldots, \mathbf{A}_\tau\}$ which yields a sequence of observations $Y_{1:\tau} = \{Y_1, Y_2, \ldots, Y_\tau\}$. At any time instant $n \in [\tau]$, the agent selects the measurement vector in general as a function of the past observations and measurements. Mathematically,

$$\mathbf{A}_t = g_t\left(\mathbf{Y}_{1:t-1}, \mathbf{A}_{1:t-1}\right), \tag{2.12}$$

for some causal (possibly random) function g_tAfter observing the noisy observations $Y_{1:\tau}$ and the

sequence of measurement vectors $\mathbf{A}_{1:\tau}$, the agent estimates the target location $\mathbf{W}$ as follows

$$\hat{\mathbf{W}} = d\left(Y_{1:\tau}, \mathbf{A}_{1:\tau}\right), \tag{2.13}$$

for some decision function d The probability of error for a search is given by $\mathsf{P}_e = \mathsf{P}(\hat{\mathbf{W}} \neq \mathbf{W} | \mathbf{Y}_{1:N}, \mathbf{A}_{1:N})$ and the average probability of error is given by $\overline{\mathsf{P}}_e = \mathsf{P}(\hat{\mathbf{W}} \neq \mathbf{W})$. Now we define the measurement strategy:

Definition 1 (ϵ-Reliable Search Strategy $\mathfrak{c}_\epsilon$)**.** For some $\epsilon \in (0,1)$, an *ϵ-reliable search strategy*, denoted by $\mathfrak{c}_\epsilon$, is defined as a sequence of τ (possibly random) number of causal functions $\{g_1, g_2, \ldots, g_\tau\}$, according to which the measurement matrix $\mathbf{A}_{1:\tau}$ is selected, and a decision function d which provides an estimate $\hat{\mathbf{W}}$ of $\mathbf{W}$, such that the average probability of error $\overline{\mathsf{P}}_e$ is at most ϵ.

Types of Search Strategies

Every measurement vector $\mathbf{A}_t$ and the number of total measurements τ can be selected either based on the past observations $\mathbf{Y}_{1:t-1}$, or independent of them. Based on these two choices, strategies can be divided into four types i) having fixed length versus variable length of sequence of measurement vectors $\mathbf{A}_{1:\tau}$, and ii) being adaptive versus non-adaptive. A *fixed length ϵ-reliable strategy* $\mathfrak{c}_\epsilon$ uses a fixed number of measurements τ predetermined offline independent of the observations, to obtain estimate $\hat{\mathbf{W}}$. On the other hand, a *variable length ϵ-reliable strategy* $\mathfrak{c}_\epsilon$ uses a random number of measurements τ (possibly determined as a function of the observation sequence $Y_{1:\tau}$) to obtain an estimate $\hat{\mathbf{W}}$. For example, τ can be selected such that agent achieves $\mathsf{P}_e \leq \epsilon$ in every search and hence τ is a random variable which is a function of the past noisy observations. Under an *adaptive strategy* $\mathfrak{c}_\epsilon$ the agent designs the measurement vector $\mathbf{A}_t$ as a function of the past observations $\mathbf{Y}_{1:t-1}$, i.e., g_t is a function of both $\mathbf{A}_{1:t-1}$ and $\mathbf{Y}_{1:t-1}$.

Definition 2. Let $\mathcal{C}_\epsilon^A$ be a class of all ϵ-reliable adaptive strategies.

Under a *non-adaptive strategy*, the agent designs the measurement vector $\mathbf{A}_t$ offline independent of past observations, i.e., g_t does not depend on $\mathbf{A}_{1:t-1}$ or $\mathbf{Y}_{1:t-1}$.

Definition 3. Let $\mathcal{C}_\epsilon^{NA}$ be a class of all ϵ-reliable non-adaptive strategies.

2.2.3 Preliminaries

In this section, we review fundamentals of channel coding with state and feedback and related the information theoretic concepts. The aim is to connect the problem of searching under measurement dependent Gaussian noise to the problem of channel coding with state and feedback. We then formulate an equivalent model of channel coding with state and feedback for comparison to (2.11).

Channel Coding with State and Feedback

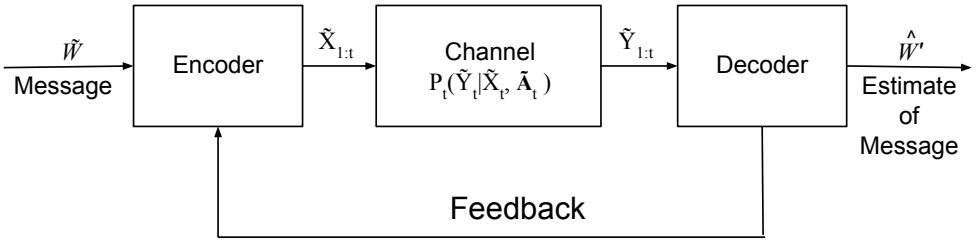

Figure 2.3: Transmission over a communication channel with state and feedback

A communication channel is specified by a set of inputs $\tilde{X} \in \tilde{\mathcal{X}}$, a set of outputs $\tilde{Y} \in \tilde{\mathcal{Y}}$, and a channel transition probability measure $\mathsf{P}(\tilde{y}|\tilde{x})$ for every $\tilde{x} \in \tilde{\mathcal{X}}$ and $\tilde{y} \in \tilde{\mathcal{Y}}$ that expresses the probability of observing a certain output $\tilde{y}$ given that an input $\tilde{x}$ was transmitted [44]. Throughout this work, we will concentrate on coding over a channel with state and feedback (in Sect. 4.6 in [35]). Formally, at time t the channel state, $\tilde{\mathbf{A}}_t$ belongs to a discrete and finite set $\tilde{\mathcal{A}}$. We assume that the channel state is known at both the encoder and the decoder. The transition probability at time t is specified by the conditional probability assignment

$$\mathsf{P}_t\left(\tilde{Y}_t\tilde{A}_{t+1}|\tilde{\mathbf{Y}}_{1:t-1}, \tilde{X}_{1:t}, \tilde{\mathbf{A}}_{1:t}\right) = \mathsf{P}_t\left(\tilde{A}_{t+1}|\tilde{\mathbf{Y}}_{1:t}, \tilde{X}_{1:t}, \tilde{\mathbf{A}}_{1:t}\right)\mathsf{P}\left(\tilde{Y}_t|\tilde{X}_t, \tilde{A}_t\right).$$

Transmission over such a channel is shown in Fig. 2.3. In general, the channel state $\tilde{\mathbf{A}}_t$ at time t evolves as a function of all past outputs, inputs, and states,

$$\tilde{\mathbf{A}}_t = \tilde{g}_t(\tilde{\mathbf{Y}}_{1:t-1}, \tilde{X}_{1:t-1}, \tilde{\mathbf{A}}_{1:t-1}). \tag{2.14}$$

The goal is to encode and transmit a uniformly distributed message $\tilde{\mathbf{W}} \in [M]$ over the channel. The encoding function ϕ_t at any time t depends on the message to be transmitted $\tilde{\mathbf{W}}$, all past states, and past outputs. Thus the next symbol to be transmitted is given by

$$\tilde{X}_t = \phi_t(\tilde{\mathbf{Y}}_{1:t-1}, \tilde{\mathbf{A}}_{1:t-1}, \tilde{\mathbf{W}}). \tag{2.15}$$

The encoder obtains the past outputs from the decoder due to the availability of a noiseless feedback channel from decoder to encoder. In this work, we assume that both encoder and decoder know the evolution of the channel state, i.e., the sequence $\tilde{\mathbf{A}}_{1:t}$. After τ channel uses, the decoder uses the noisy observations $\tilde{\mathbf{Y}}_{1:\tau}$ and state information $\tilde{\mathbf{A}}_{1:\tau}$ to find the best estimate $\tilde{\mathbf{W}}'$, of the message $\tilde{\mathbf{W}}$. The probability of error at the end of message transmission is given by $\mathsf{P}_e = \mathsf{P}(\tilde{\mathbf{W}}' \neq \tilde{\mathbf{W}} | \tilde{Y}_{1:\tau}, \tilde{\mathbf{A}}_{1:\tau})$ and the average probability of error is given by $\overline{\mathsf{P}}_e = \mathsf{P}(\tilde{\mathbf{W}}' \neq \tilde{\mathbf{W}})$.

Example 1 (Binary Additive White Gaussian Noise channel with State and feedback)**.** Consider a Binary Additive White Gaussian Noise (BAWGN) channel with noisy output $\tilde{Y}_t$ given as the sum of input $\tilde{X}_t \in \{0, 1\}$ and Gaussian random variable $\tilde{Z}_t \in \mathbb{R}$ whose distribution is a function of the channel state $\tilde{\mathbf{A}}_t$. Specifically, $\tilde{Z}_t$ is a Gaussian random variable with state dependent noise variance $\|\tilde{\mathbf{A}}_t\|_0 \delta\sigma^2$ for some $\delta > 0$. In other words, we have

$$\tilde{Y}_t = \tilde{X}_t + \tilde{Z}_t(\tilde{\mathbf{A}}_t), \tag{2.16}$$

where $\tilde{Z}_t \sim \mathcal{N}(0, \|\tilde{\mathbf{A}}_t\|_0 \delta\sigma^2)$, and the state evolves as $\tilde{\mathbf{A}}_t = \tilde{g}_t(\tilde{\mathbf{Y}}_{1:t-1}, \tilde{\mathbf{X}}_{1:t-1} \tilde{\mathbf{A}}_{1:t-1})$. Transmission over a BAWGN channel is illustrated in Fig. 2.4.

Proposition 1. *The problem of searching under measurement dependent Gaussian noise can be*

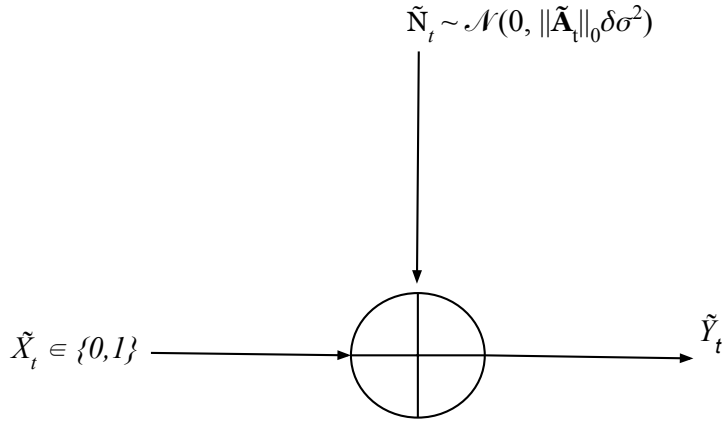

Figure 2.4: Transmission over a BAWGN channel with binary input $\tilde{X}_t$ and Gaussian noise $\tilde{Z}_t$.

cast as a problem of channel coding over a BAWGN channel with state and feedback. Specifically,

- *The true location vector* $\mathbf{W}$ *can be cast as a message* $\tilde{\mathbf{W}}$ *to be transmitted over the BAWGN. Therefore, by setting* $\tilde{\mathbf{W}} = \mathbf{W}$ *there are* $\frac{B}{\delta}$ *possible messages.*

- *The measurement vector fixes the probability* $\mathsf{P}(\tilde{Y}_t|\tilde{x}_t, \tilde{\boldsymbol{A}}_t) = \mathcal{N}(\tilde{x}_t, \|\boldsymbol{A}_t\|_0 \delta\sigma^2)$ *since noise distribution is* $\tilde{Z}_t \sim \mathcal{N}(0, \|\mathbf{A}_t\|_0 \delta\sigma^2)$ *for* $\tilde{x}_t \in \{0,1\}$*. In other words, by setting* $\tilde{\mathbf{A}}_t = \mathbf{A}_t$ *the measurement vector acts as the channel state and fixes the channel transition probability.*

- *An* ϵ*-reliable search strategy* $\mathfrak{c}_\epsilon$ *provides a sequence of* $\{g_1, g_2, \ldots, g_\tau\}$ *such that* $\mathsf{P}(\mathbf{W}' \neq \mathbf{W}) \leq \epsilon$*. Hence, by setting* $\tilde{g}_i = g_i$ *for all* $i \in \{1, 2, \ldots, \tau\}$*, the search strategy dictates the evolution of channel states* $\tilde{\mathbf{A}}_t$*.*

- *The sequence of measurement vectors* $\mathbf{A}_{1:t}$ *can be used as the codebook. Specifically, the codewords and the encoding strategy are obtained by setting*

$$\tilde{X}_t = \phi_t(\tilde{\mathbf{Y}}_{1:t-1}, \tilde{\mathbf{A}}_{1:t-1}, \tilde{\mathbf{W}}) = \mathbf{W}^\intercal \mathbf{A}_t. \tag{2.17}$$

In other words, ϵ*-reliable search strategy* $\mathfrak{c}_\epsilon$ *provides an encoding strategy with at most* ϵ *probability of error in decoding the true message.*

Corollary 1. *The problem of coding over BAWGN channel with codebook dependent state and feedback can be cast a problem of searching under measurement dependent Gaussian noise when the codebook dependent state is given as*

$$\tilde{\mathbf{A}}_t = [\phi_t(\tilde{\mathbf{Y}}_{1:t-1}, \tilde{\mathbf{A}}_{1:t-1}, \tilde{\mathbf{W}}(1)), \phi_t(\tilde{Y}_{1:t-1}, \tilde{\mathbf{A}}_{1:t-1}, \tilde{\mathbf{W}}(2)), \ldots, \phi_t(\tilde{\mathbf{Y}}_{1:t-1}, \tilde{\mathbf{A}}_{1:t-1}, \tilde{\mathbf{W}}(M))]^{\mathsf{T}}.$$

The measurement vector is obtained by setting $\mathbf{A}_t = \tilde{\mathbf{A}}_t$*. Therefore, a channel coding strategy with* $\mathsf{P}(\tilde{\mathbf{W}}' \neq \tilde{\mathbf{W}}) \leq \epsilon$ *provides an* ϵ*-reliable search strategy over* M *locations.*

The equivalence of problem of searching under measurement dependent noise and the problem of channel coding with state and feedback, implied by Proposition 1 and Corollary 1, provides an efficient way to design and compare non-adaptive and adaptive search strategies. Furthermore, it is known that feedback can improve the capacity of a channel with state [35]. In other words, adaptive coding strategies provide a gain in rate of transmission over non-adaptive coding strategies. This motivates our analysis of the gains to be seen when using an adaptive search strategy over a non-adaptive search strategy. Next we define appropriate figures merit to characterize the gain in using adaptive strategies for the problem of searching under measurement dependent noise.

Target Acquisition Rate and Adaptivity Gain

For any ϵ-reliable strategy $\mathfrak{c}_\epsilon$, the performance is measured by the expected number of measurements $\mathbb{E}_{\mathfrak{c}_\epsilon}[\tau]$. The following definition captures the growth of expected number of measurements as number of search locations grow.

Definition 4 (Achievable Target Acquisition Rate)**.** A target acquisition rate R is said to be ϵ-*achievable*, if for any $\xi > 0$ and t large enough, there is an ϵ-reliable search strategy $\mathfrak{c}_\epsilon$ which

satisfies the following

$$\mathbb{E}_{\mathfrak{c}_\epsilon}[\tau] \leq t, \tag{2.18}$$

$$\frac{B}{\delta} \geq 2^{t(R-\xi)}. \tag{2.19}$$

A targeting rate R is said to be *achievable target acquisition rate* if it is ϵ-achievable for all $\epsilon \in (0,1)$.

The above definition is motivated by information theoretic notion of transmission rate over a communication channel, which captures the exponential rate at which the number of messages grows with the number of channel uses while the receiver can decode with a small average error probability. Similarly, the target acquisition rate captures the exponential rate at which the number of target locations grow with the number of measurement vectors while a search strategy can still locate the target with a diminishing average error probability.

Definition 5. The BAWGN capacity with input distribution $\mathsf{Bern}(q)$ and noise variance σ^2 is defined as

$$C\left(q,\sigma^2\right) := -\int_{-\infty}^{\infty}\Big((1-q)G(y;0,\sigma^2)+qG(y;1,\sigma^2)\Big)\log\Big((1-q)G(y;0,\sigma^2)+qG(y;1,\sigma^2)\Big)\,dy$$
$$-\frac{1}{2}\log(2\pi e\sigma^2), \tag{2.20}$$

where $G(x;\mu,\sigma^2)$ denotes the pdf of Gaussian random variable with mean μ and variance σ^2 at x.

Corollary 2. *From channel coding over a BAWGN channel with state and feedback, we obtain that for any small $\xi > 0$ and t large enough, there exists an ϵ-reliable search strategy $\mathfrak{c}_\epsilon$ such the following holds*

$$\mathbb{E}_{\mathfrak{c}_\epsilon}[\tau] \leq t, \tag{2.21}$$

$$2^{t(C(\frac{1}{2},\sigma^2_{Total})-\xi)} \overset{(a)}{\leq} \frac{B}{\delta} \overset{(b)}{<} 2^{tC(\frac{1}{2},\delta\sigma^2)}, \tag{2.22}$$

where (a) follows by combining our Corollary 1 with Theorem 4.6.1 in [35], and (b) follows by

combining our Corollary 1 with the converse of the noisy channel coding theorem [44] and using the fact that the best channel is obtained when noise variance is the least, i.e., $\delta\sigma^2$.

Definition 6 (Target Acquisition Capacity under $\sigma^2_{\text{Total}} \geq \rho$)**.** The supremum of achievable target acquisition rates R under $\sigma^2_{\text{Total}} \geq \rho$ is called the target acquisition capacity C_ρ under $\sigma^2_{\text{Total}} \geq \rho$.

Remark 1. Let C_ρ^{NA} and C_ρ^{A} denote the target acquisition capacity under total noise variance $\sigma^2_{\text{Total}} \geq \rho$ over the class of non-adaptive and adaptive strategies respectively. From [9, 36], the gain in the target acquisition capacity when using adaptive strategies is given as

$$C_\rho^{\text{A}} - C_\rho^{\text{NA}} = 1 - \sup_q C(q, 2q\rho) > 0. \tag{2.23}$$

When the width of the search region B grows the noise intensity σ^2_{Total} grows unboundedly and the achievable rate goes to zero. Hence, we first characterize the following notion of adaptivity gain before we characterize the the improvement in target acquisition rate when using adaptive strategies over non-adaptive strategies.

Definition 7 (Adaptivity Gain)**.** The adaptivity gain is defined as the best reduction in the expected number of measurements when searching with an ϵ-reliable adaptive strategy $\mathfrak{c}'_\epsilon \in \mathcal{C}_\epsilon^A$, over an ϵ-reliable non-adaptive strategy $\mathfrak{c}_\epsilon \in \mathcal{C}_\epsilon^{NA}$. Mathematically, it is given as

$$\min_{\mathfrak{c}_\epsilon \in \mathcal{C}_\epsilon^{NA}} \mathbb{E}[\tau] - \min_{\mathfrak{c}'_\epsilon \in \mathcal{C}_\epsilon^{A}} \mathbb{E}[\tau']. \tag{2.24}$$

2.2.4 Main Results

In this section, we characterize a lower bound on the adaptivity gain $\min_{\mathfrak{c}_\epsilon \in \mathcal{C}_\epsilon^{NA}} \mathbb{E}[\tau] - \min_{\mathfrak{c}'_\epsilon \in \mathcal{C}_\epsilon^{A}} \mathbb{E}[\tau']$; the performance improvement measured in terms of reduction in the expected number of measurements for searching over a width B among $\frac{B}{\delta}$ locations under measurement dependent Gaussian noise. First we characterize a lower bound on $\min_{\mathfrak{c}_\epsilon \in \mathcal{C}_\epsilon^{NA}} \mathbb{E}[\tau]$.

Non-adaptive Strategies

Lemma 2. The minimum expected number of measurements required for any ϵ-reliable non-adaptive search strategy can be lower bounded as

$$\min_{\mathfrak{c}_\epsilon \in \mathcal{C}_\epsilon^{NA}} \mathbb{E}_{\mathfrak{c}_\epsilon}[\tau] \geq \frac{(1-\epsilon)\log\left(\frac{B}{\delta}\right) - h(\epsilon)}{C\left(q^*, q^* B\sigma^2\right)}. \tag{2.25}$$

Proof of the Lemma 2 is provided in Appendix A. The proof follows from the fact that clean signal X_i and noise N_i are independent over time and independent of past observations for $i \in [n]$, due to the non-adaptive nature of the search strategy. In the absence of information from past observation outcomes, the agent tries to maximize the mutual information $I(X_i, Y_i)$ at every measurement. Since $X_i \sim \mathsf{Bern}(q_i)$ and $N_i \sim \mathcal{N}(0, q_i B\sigma^2)$, the mutual information $I(X_i, Y_i) = C\left(q_i, q_i B\sigma^2\right)$ is maximized at $q_i = q^*$.

Fig. 2.5 shows the behavior of the maximum mutual information for a non-adaptive strategy $C\left(q^*, q^* B\sigma^2\right)$ as number of locations grow. When $B = 1$ and δ goes to zero, $C\left(q^*, q^* B\sigma^2\right)$ remains same for a given σ^2. On the other hand, when $\delta = 1$ and B grows, $C\left(q^*, q^* B\sigma^2\right)$ goes to zero. Furthermore, $C\left(q^*, q^* B\sigma^2\right)$ goes to zero faster when $\sigma^2 = 0.05$ than when $\sigma^2 = 0.001$. This implies non-adaptive strategies need a growing number of measurements as B grows. On the other hand, an adaptive strategy can reduce the number measurements as follows. Whenever the agent narrows down the target's location to some coarse fraction of the total search region (say a section of width αB) with high confidence, an adaptive strategy can zoom in and search only within αB section. This reduces the noise intensity in the measurements unlike a non adaptive strategy which still searches regions of width $q^* B$. Hence, non-adaptive strategies perform poorly in comparison to adaptive strategies that rapidly zoom in to smaller regions especially when $C\left(q^*, q^* B\sigma^2\right)$ close to zero (as shown in Fig. 2.5 for $\sigma^2 = 0.05$).

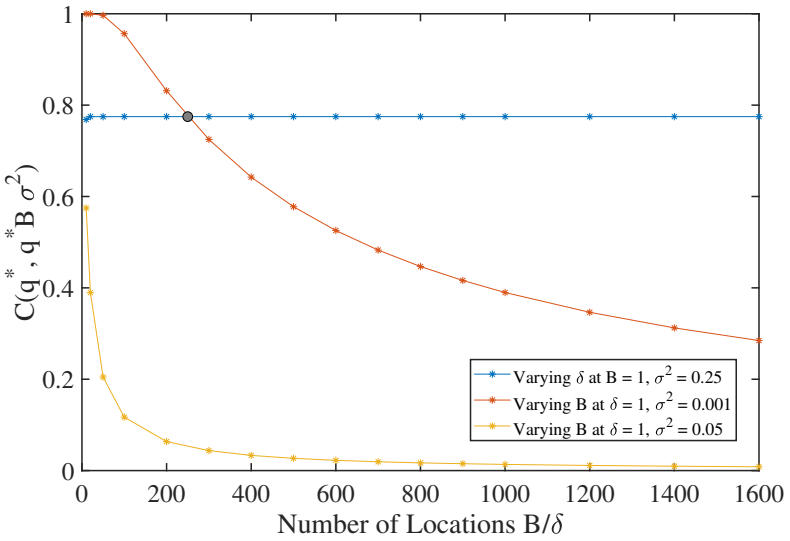

Figure 2.5: Non-adaptive capacity as number of locations grow for various values of σ^2.

Lower Bound on Adaptivity Gain

The expected number of measurements required to zoom in to a region of width αB with high confidence is larger when α is small. On the other hand, noise intensity reduces more significantly after zooming in to a region of width αB, for small α than for large α. This reduces the expected number of measurements needed to locate the target within the region αB upto a resolution δ with high confidence. For any adaptive strategy, there is a trade-off between how rapidly an adaptive strategy can zoom in to and the width of the region to which it zooms in. This trade-off is controlled by the value of parameter α. Since adaptive strategies observe less noisy measurements than non-adaptive strategies after zooming, parameter α also controls the adaptivity gain. This intuition is formalized by the following theorem.

Theorem 1. *Let $\epsilon \in (0,1)$. For any ϵ-reliable non-adaptive strategy $\mathfrak{c}_\epsilon \in \mathcal{C}_\epsilon^{NA}$ searching over a search region of width B among $\frac{B}{\delta}$ locations with τ number of measurements, there exists an ϵ-reliable adaptive strategy $\mathfrak{c}'_\epsilon \in \mathcal{C}_\epsilon^{A}$ with τ' number of measurements, such that for any $\eta > 0$ the following holds*

$$\min_{\mathfrak{c}_\epsilon \in \mathcal{C}_\epsilon^{NA}} \mathbb{E}_{\mathfrak{c}_\epsilon}[\tau] - \min_{\mathfrak{c}'_\epsilon \in \mathcal{C}_\epsilon^{A}} \mathbb{E}_{\mathfrak{c}'_\epsilon}[\tau'] \geq \max_{\alpha \in \mathsf{I}_{\frac{B}{\delta}}} \left\{ \frac{\log \frac{1}{\alpha}}{g^{(1)}_{\epsilon,\eta}(q^*, B\sigma^2)} + \frac{\log \frac{\alpha B}{\delta}}{g^{(2)}_{\epsilon,\eta}(\alpha, q^*, B\sigma^2)} - h_{\epsilon,\eta}(\delta, \alpha, B\sigma^2) \right\},$$

where

$$g^{(1)}_{\epsilon,\eta}(q^*, B\sigma^2) = \left(\frac{(1-\epsilon)}{C(q^*, q^* B\sigma^2)} - \frac{1}{C\left(q^*, q^* B\sigma^2\right) - \eta} \right)^{-1},$$
$$g^{(2)}_{\epsilon,\eta}(\alpha, q^*, B\sigma^2) = \left(\frac{(1-\epsilon)}{C(q^*, q^* B\sigma^2)} - \frac{1}{C\left(\frac{1}{2}, \frac{\alpha B\sigma^2}{2}\right) - \eta} \right)^{-1},$$

and

$$h_{\epsilon,\eta}(\delta, \alpha, B\sigma^2) = \frac{\log\left(\frac{2}{\epsilon}\right) + \log\log\left(\frac{1}{\alpha}\right) + a_\eta}{C\left(q^*, q^* B\sigma^2\right) - \eta} + \frac{\log\left(\frac{2}{\epsilon}\right) + \log\log\left(\frac{\alpha B}{\delta}\right) + a_\eta}{C\left(\frac{1}{2}, \frac{\alpha B\sigma^2}{2}\right) - \eta} + \frac{h(\epsilon)}{C(q^*, q^* B\sigma^2)},$$

$q^* = \mathrm{argmax}_{q \in \mathsf{I}_{\frac{B}{\delta}}} C(q, qB\sigma^2)$, *and* a_η *is the solution of the following equation*

$$\eta = \frac{a}{a-3} \max_{q \in \mathsf{I}_{\frac{B}{\delta}}} \int_{-\infty}^{\infty} \frac{e^{-\frac{y^2}{2Bq\sigma^2}}}{\sqrt{2\pi q B\sigma^2}} \left[\frac{2y-1}{2qB\sigma^2} \right]_{(a-3)} dy. \tag{2.26}$$

Proof of Theorem 1 is obtained by combining Lemma 2 and Lemma 3. Theorem 1 provides a non-asymptotic lower bound on adaptivity gain.The first two terms in the above lower bound can be viewed as corresponding to two stages. Intuitively, the first part corresponds to the initial stage of the search, where the agent narrows down the target's location to some coarse α fraction of the total search region, i.e., narrows to a section of width αB with high confidence. The second stage corresponds to refined the search within one of the coarse sections αB obtained from initial stage. For the first stage, our bound predicts negligible gains in using an adaptive strategy over a non-adaptive strategy and it is captured by the term $\frac{1}{g^{(1)}_{\epsilon,\eta}(q^*, B\sigma^2)}$. However, in the second stage where an adaptive strategy zooms in to a width of αB, a significant gain can be seen especially

as B grows and it is captured by the term $\frac{1}{g^{(2)}_{\epsilon,\eta}(\alpha,q^*,B\sigma^2)}$. The following corollary characterizes the adaptivity gain in the two asymptotic regimes δ going to zero and B growing.

Corollary 3. *Let $\epsilon \in (0,1)$. For any ϵ-reliable non-adaptive strategy $\mathfrak{c}_\epsilon \in \mathcal{C}_\epsilon^{NA}$ searching over a search region of width B among $\frac{B}{\delta}$ with τ number of measurements, there exists an ϵ-reliable adaptive strategy $\mathfrak{c}'_\epsilon \in \mathcal{C}_\epsilon^{A}$ with τ' number of measurements, such that for a fixed B the asymptotic adaptivity gain grows logarithmically with the total number of locations,*

$$\lim_{\delta\to 0} \frac{\mathbb{E}_{\mathfrak{c}_\epsilon}[\tau] - \mathbb{E}_{\mathfrak{c}'_\epsilon}[\tau']}{\log \frac{B}{\delta}} \geq \frac{1-\epsilon}{C(q^*, q^* B\sigma^2)} - 1. \tag{2.27}$$

For a fixed δ, the asymptotic adaptivity gain grows at least linearly with total number of locations,

$$\lim_{B\to\infty} \frac{\mathbb{E}_{\mathfrak{c}_\epsilon}[\tau] - \mathbb{E}_{\mathfrak{c}'_\epsilon}[\tau']}{\frac{B}{\delta}\log \frac{B}{\delta}} \geq \frac{(1-\epsilon)\delta\sigma^2}{\log e}. \tag{2.28}$$

Furthermore, we have

$$\lim_{B\to\infty} \frac{\min_{\mathfrak{c}_\epsilon\in\mathcal{C}_\epsilon^{NA}} \mathbb{E}_{\mathfrak{c}_\epsilon}[\tau]}{\frac{B}{\delta}\log \frac{B}{\delta}} \geq \frac{(1-\epsilon)\delta\sigma^2}{\log e}, \tag{2.29}$$

and

$$\lim_{B\to\infty} \frac{\min_{\mathfrak{c}_\epsilon\in\mathcal{C}_\epsilon^{A}} \mathbb{E}_{\mathfrak{c}'_\epsilon}[\tau']}{\frac{B}{\delta}} \leq 16\delta\sigma^2. \tag{2.30}$$

The proof of the above corollary is provided in Appendix-C.

Remark 2. The above corollary characterizes the two qualitatively different regimes discussed previously. For fixed B, as δ goes to zero the asymptotic adaptivity gain scales as only $\log \frac{B}{\delta}$, whereas for fixed δ, as B increases the asymptotic adaptivity gain scales as $\frac{B}{\delta}\log \frac{B}{\delta}$. In other words, adaptivity provides a larger reduction in the expected number of measurements for the regime where the total search width is growing than in the case where we fix the total width and shrink the location widths. In Sect. 2.2.6 we related this phenomenon to the diminishing capacity of BAWGN

channel when the total noise σ^2_{Total} grows.

Next we provide the main technical components of the proof of Theorem 1.

Adaptive Search Strategies

Consider the following two stage search strategy.

First Stage (Fixed Composition Strategy $\mathfrak{c}^1_{\frac{\epsilon}{2}}$)

We group the $\frac{B}{\delta}$ locations of width δ into $\frac{1}{\alpha}$ sections of width αB. Let $\mathbf{W}'$ denote the true location of the target among the sections of width αB. Now, we use a non-adaptive strategy to search for the target location among $\frac{1}{\alpha}$ sections of width αB. In particular, we use a fixed composition strategy where at every time instant t, the fraction of total locations probed is fixed to be q^*. In other words, the measurement vector $\mathbf{A}'_t$ at every instant t is picked uniformly randomly from the set of measurement vectors $\{\mathbf{A}' \in \{0,1\}^{\frac{1}{\alpha}} : \|\mathbf{A}'\|_0 = \lfloor \frac{q^*}{\alpha} \rfloor\}$. For the ease of exposition, we assume that $\frac{q^*}{\alpha}$ is an integer. Hence, for this strategy, at every t, $X_t \sim \mathsf{Bern}(q^*)$ and $N_t \sim \mathcal{N}(0, q^* B\sigma^2)$. For all $i \in \{1, 2, \ldots, \frac{1}{\alpha}\}$, let $\boldsymbol{\rho}'_t(i)$ be the posterior probability of the estimate $\hat{\mathbf{W}}'(i) = 1$ after reception of $\mathbf{Y}_{1:t-1}$, i.e., $\boldsymbol{\rho}'_t(i) := \mathsf{P}\left(\hat{\mathbf{W}}'(i) = 1 | \boldsymbol{Y}_{1:t-1}\right)$ and let $\boldsymbol{\rho}'_t := \left\{\boldsymbol{\rho}'_t(1), \boldsymbol{\rho}'_t(2), \ldots, \boldsymbol{\rho}'_t\left(\frac{1}{\alpha}\right)\right\}$. Assume that agent begins with a uniform probability over the $\frac{1}{\alpha}$ sections, i.e., $\boldsymbol{\rho}'_0 = \{\alpha, \alpha, \ldots, \alpha\}$. The posterior probability $\boldsymbol{\rho}'_{t+1}(i)$ at time $t+1$ when $Y_t = y$ is obtained by the following Bayesian update:

$$\boldsymbol{\rho}'_{t+1}(i) = \begin{cases} \frac{\boldsymbol{\rho}'_t(i) G(y;1,q^* B\sigma^2)}{\mathcal{D}'_t} & \text{if } \boldsymbol{A}'_t(i) = 1, \\ \frac{\boldsymbol{\rho}'_t(i) G(y;0,q^* B\sigma^2)}{\mathcal{D}'_t} & \text{if } \boldsymbol{A}'_t(i) = 0, \end{cases} \tag{2.31}$$

where

$$\mathcal{D}'_t = \sum_{j:\mathbf{1}_{\{\boldsymbol{A}_t(j)=1\}}} \boldsymbol{\rho}'_t(j) G(y;1,q^* B\sigma^2) + \sum_{j:\mathbf{1}_{\{\boldsymbol{A}_t(j)=0\}}} \boldsymbol{\rho}'_t(j) G(y;0,q^* B\sigma^2).$$

Let $\tau^1 := \inf\left\{n : \max_i \boldsymbol{\rho}'_t(i) \geq 1 - \frac{\epsilon}{2}\right\}$ be the number of measurements used under stage 1. Note that τ^1 is a random variable. Hence, first stage is a non-adaptive variable length strategy. Now,

the expected stopping time $\mathbb{E}_{\mathfrak{c}^1_{\frac{\epsilon}{2}}}[\tau^1]$ can be upper bounded using Lemma 7 from Appendix-B.

Second Stage (Sorted Posterior Matching Strategy $\mathfrak{c}^2_{\frac{\epsilon}{2}}$)

In the second stage, the agent zooms into the αB width section obtained from the first stage and uses an adaptive strategy to search only within this αB section. The agent searches for the target location of width δ among the remaining $\frac{\alpha B}{\delta}$ locations. In particular, we use the sorted posterior matching strategy proposed in [9] which we describe next. Let $\mathbf{W}''$ denote the true target location of width δ. For all $i \in \{1, 2, \ldots, \frac{\alpha B}{\delta}\}$, let $\boldsymbol{\rho}''_t(i)$ be the posterior probability of the estimate $\hat{\mathbf{W}}''(i) = 1$ after reception of $\mathbf{Y}_{1:t-1}$, i.e., $\boldsymbol{\rho}'_t(i) := \mathsf{P}\left(\hat{\mathbf{W}}''(i) = 1 | \mathbf{Y}_{1:t-1}\right)$ and let $\boldsymbol{\rho}''(n) := \{\boldsymbol{\rho}''_t(1), \boldsymbol{\rho}''_t(2), \ldots, \boldsymbol{\rho}''_t\left(\frac{\alpha B}{\delta}\right)\}$. Assume the agent begins with a uniform probability over the $\frac{\alpha B}{\delta}$ sections, i.e., $\boldsymbol{\rho}''_0 = \left\{\frac{\delta}{\alpha B}, \frac{\delta}{\alpha B}, \ldots, \frac{\delta}{\alpha B}\right\}$. At every time instant t, we sort the posterior values in descending order to obtain the sorted posterior vector $\boldsymbol{\rho}''^{\downarrow}_t$. Let vector I_t denote the corresponding ordering of the location indices in the new sorted posterior. Define

$$k^*_t := \underset{i}{\operatorname{argmin}} \left| \sum_{j=1}^{i} \boldsymbol{\rho}''^{\downarrow}_t(j) - \frac{1}{2} \right|. \tag{2.32}$$

We choose $\mathbf{A}''_t$ such that $\mathbf{A}''_t(j) = 1$ if and only if $j \in \{I_t(1), I_t(2), \ldots, I_t(k^*_t)\}$. Note that for this strategy, at every t, the noise is $N_t \sim \mathcal{N}(0, \|\mathbf{A}''_t\|_0 \delta \sigma^2)$ and the worst noise intensity is $\mathcal{N}(0, \frac{\alpha B \sigma^2}{2})$. The posterior probability $\boldsymbol{\rho}''_{t+1}(i)$ at time $t+1$ when $Y_t = y$ is obtained by the following Bayesian update:

$$\boldsymbol{\rho}''_{t+1}(i) = \begin{cases} \frac{\boldsymbol{\rho}''_t(i) G(y; 1, \|\mathbf{A}''_t\|_0 \delta \sigma^2)}{\mathcal{D}''_t} & \text{if } \boldsymbol{A}''_t(i) = 1, \\ \frac{\boldsymbol{\rho}''_t(i) G(y; 0, \|\mathbf{A}''_t\|_0 \delta \sigma^2)}{\mathcal{D}''_t} & \text{if } \boldsymbol{A}''_t(i) = 0, \end{cases} \tag{2.33}$$

where

$$\mathcal{D}''_t = \sum_{j : \mathbf{1}_{\{\boldsymbol{A}_t(j)=1\}}} \boldsymbol{\rho}''_t(j) G\left(y; 1, |\mathbf{A}''_t| \delta \sigma^2\right) + \sum_{j : \mathbf{1}_{\{\boldsymbol{A}_t(j)=0\}}} \boldsymbol{\rho}''_t(j) G\left(y; 0, |\mathbf{A}''_t| \delta \sigma^2\right).$$

Let $\tau^2 := \inf\left\{t : \max_i \boldsymbol{\rho}_t^2(i) \geq 1 - \frac{\epsilon}{2}\right\}$ be the number of measurements used under stage 2. Note that τ^2 is a random variable. Hence, the second stage is an adaptive variable length strategy. The expected number of measurements $\mathbb{E}_{\mathfrak{c}^2_{\frac{\epsilon}{2}}}[\tau'']$ can be upper bounded using Lemma 10 from Appendix-B.

Noting that the total probability of error of the two stage search strategy is less than ϵ and that the expected stopping time is $\mathbb{E}_{\mathfrak{c}'_\epsilon}[\tau'] = \mathbb{E}_{\mathfrak{c}^1_{\frac{\epsilon}{2}}}[\tau^1] + \mathbb{E}_{\mathfrak{c}^2_{\frac{\epsilon}{2}}}[\tau^2]$, we have the assertion of the following lemma.

Lemma 3. The minimum expected number of measurements required for the above ϵ-reliable adaptive search strategy $\mathfrak{c}'_\epsilon$ can be upper bounded as

$$\mathbb{E}_{\mathfrak{c}'_\epsilon}[\tau'] \leq \min_{\alpha \in \mathsf{I}_{\frac{B}{\delta}}} \left\{ \frac{\log\frac{1}{\alpha} + \log\frac{2}{\epsilon} + \log\log\frac{1}{\alpha} + a_\eta}{C\left(q^*, q^* B\sigma^2\right) - \eta} + \frac{\log\frac{\alpha B}{\delta} + \log\frac{2}{\epsilon} + \log\log\frac{\alpha B}{\delta} + a_\eta}{C\left(\frac{1}{2}, \frac{\alpha B\sigma^2}{2}\right) - \eta} \right\}.$$

Remark 3. Recall that $\min_{\mathfrak{c}'_\epsilon \in \mathcal{C}_\epsilon^A} \mathbb{E}_{\mathfrak{c}'_\epsilon}[\tau']$ denotes the minimum expected number of measurements required by the optimal adaptive strategy non-asymptotically. Lemma 3 provides an upper bound on $\min_{\mathfrak{c}'_\epsilon \in \mathcal{C}_\epsilon^A} \mathbb{E}_{\mathfrak{c}'_\epsilon}[\tau']$ using the two stage adaptive strategy. The sorted posterior matching strategy proposed in [9] provides another upper bound for $\min_{\mathfrak{c}'_\epsilon \in \mathcal{C}_\epsilon^A} \mathbb{E}_{\mathfrak{c}'_\epsilon}[\tau']$. However, this bound is very loose. In fact, sorted posterior matching strategy empirically performs significantly better than the bound predicted by the analysis in [9]. Lemma 3 using a possibly sub-optimal strategy than sorted posterior matching provides a significantly tighter bound on $\min_{\mathfrak{c}'_\epsilon \in \mathcal{C}_\epsilon^A} \mathbb{E}_{\mathfrak{c}'_\epsilon}[\tau']$ as illustrated in Fig. 2.8 and Fig. 2.9.

Remark 4. In the regime of fixed B and diminishing δ, Lemma 3 together with Corollary 2 establishes the asymptotic optimality of our proposed algorithm.

2.2.5 Generalization To Other Noise Models

The main results presented in this chapter so far consider the setup where the noise N_t is distributed as $\mathcal{N}(0, \|\mathbf{A}_t\|_0 \delta\sigma^2)$. In other words, the variance of the noise given by $(\|\mathbf{A}_t\|_0 \delta\sigma^2)$

is a linear function of the size of a measurement vector $\|\mathbf{A}_t\|_0$. This model assumption holds when each target location adds noise equally and independently of other locations when probed together. In general, due to correlation across locations the additive noise variance can be assumed to scale as a non-decreasing function $f(\cdot)$ of the measurement vector $\|\mathbf{A}_t\|_0$. In this section, we extend our model to a general formulation for the noise $N_t \sim \mathcal{N}(0, f(\|\mathbf{A}_t\|_0)\delta\sigma^2)$, where $f(\cdot)$ is a non-decreasing function of $\|\mathbf{A}_t\|_0$. For example, $f(\mathbf{A}_t) = \|\mathbf{A}_t\|_0^\gamma$ for some $\gamma > 0$. Fig. 2.6 shows that the effect of the noise function $f(\|\mathbf{A}_t\|_0)$ on the capacity. The following theorem is an extension of Theorem 1 to the general formulation of noise. We provide the theorem without a proof since it closely follows the proof of Theorem 1.

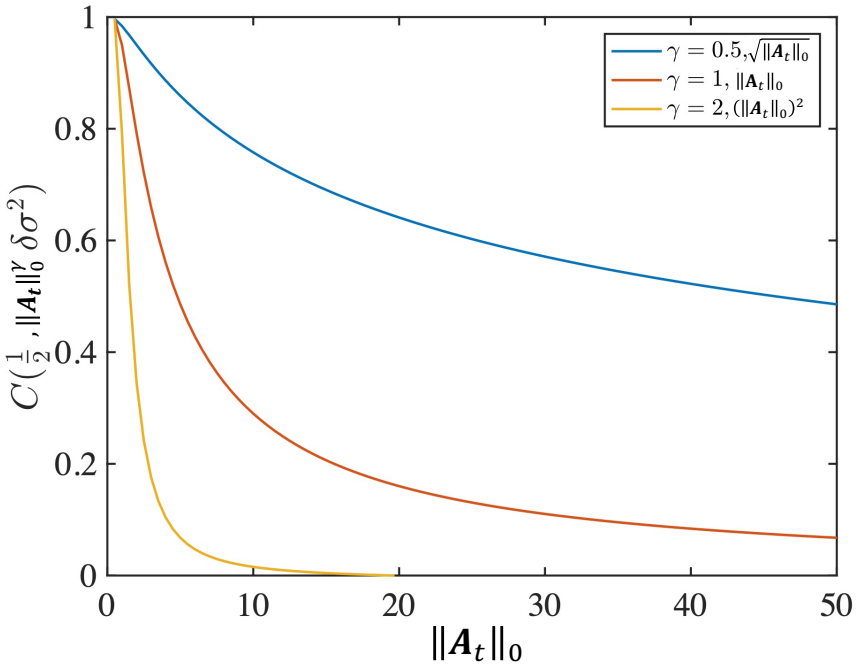

Figure 2.6: Behavior of capacity of BAWGN channel with $\sigma^2 = 0.25$ over a total search region of width $B = 10$, location width $\delta = 0.1$, as a function of the size of a measurement $\|\mathbf{A}_t\|_0$.

Theorem 2. *Let $\epsilon \in (0,1)$ and let $f(\cdot)$ be a non-decreasing function. For any ϵ-reliable non-adaptive strategy $\mathfrak{c}_\epsilon \in \mathcal{C}_\epsilon^{NA}$ searching over a search region of width B among $\frac{B}{\delta}$ locations with τ number of measurements, there exists an ϵ-reliable adaptive strategy $\mathfrak{c}'_\epsilon \in \mathcal{C}_\epsilon^{A}$ with τ' number of measurements, such that for any constant $\eta > 0$ the following holds*

$$\min_{\mathfrak{c}_\epsilon \in \mathcal{C}_\epsilon^{NA}} \mathbb{E}_{\mathfrak{c}_\epsilon}[\tau] - \min_{\mathfrak{c}'_\epsilon \in \mathcal{C}_\epsilon^{A}} \mathbb{E}_{\mathfrak{c}'_\epsilon}[\tau'] \geq \max_{\alpha \in \mathsf{I}_{\frac{B}{\delta}}} \left\{ \frac{\log \frac{1}{\alpha}}{g^{(1)}_{\epsilon,\eta}(q^*, B\sigma^2)} + \frac{\log \frac{\alpha B}{\delta}}{g^{(2)}_{\epsilon,\eta}(\alpha, q^*, B\sigma^2)} \right\} \times (1 + o(1)),$$

where

$$g^{(1)}_{\epsilon,\eta}(q^*, B\sigma^2) = \left(\frac{(1-\epsilon)}{C(q^*, f(\frac{q^*B}{\delta})\delta\sigma^2)} - \frac{1}{C\left(q^*, f(\frac{q^*B}{\delta})\delta\sigma^2\right) - \eta} \right)^{-1},$$

$$g^{(2)}_{\epsilon,\eta}(\alpha, q^*, B\sigma^2) \left(\frac{(1-\epsilon)}{C(q^*, f(\frac{q^*B}{\delta})\delta\sigma^2)} - \frac{1}{C\left(\frac{1}{2}, f(\frac{\alpha B}{2\delta})\sigma^2\right) - \eta} \right)^{-1},$$

and $q^* = \operatorname{argmax}_{q \in \mathsf{I}_{\frac{B}{\delta}}} C(q, f(\frac{qB}{\delta})\delta\sigma^2)$, *and* $o(1)$ *goes to 0 as* $\frac{B}{\delta} \to \infty$.

2.2.6 Numerical Results

In this section we provide numerical analysis.

Comparing Search Strategies

In this section, we empirically compare the performance in expected number of measurements $\mathbb{E}_{\mathfrak{c}_\epsilon}[\tau]$ required by four ϵ-reliable strategies proposed in the literature. In addition to the sortPM strategy $\mathfrak{c}^2_\epsilon$, and the optimal variable length non-adaptive strategy i.e., the fixed composition strategy $\mathfrak{c}^1_\epsilon$, we also consider two noisy variants of the binary search strategy. The noisy binary search applied to our search model selects the locations to be searched at time n, i.e. the search region $\mathbf{A}_t$, to be half the width of the previous search region $\mathbf{A}_{t-1}$. In particular, it zooms in to the half region of $\mathbf{A}_{t-1}$ which has accumulated higher posterior probability.

The first variant we consider is the fixed length noisy binary search, which resembles the adaptive iterative hierarchical search strategy [13]. In this strategy, each measurement is repeated $\alpha_\epsilon(\mathbf{A}_t)\|\mathbf{A}_t\|_0$ number of times, where $\alpha_\epsilon(\mathbf{A}_t)$ is a number chosen as a function of $\mathbf{A}_t$ such that all combined measurements result in an ϵ-reliable search strategy. That is, each measurement

vector $\mathbf{A}_t$ is used $\alpha_\epsilon(\mathbf{A}_t)\|\mathbf{A}_t\|_0$ number of times, before the strategy zooms into a region of half the size. The second variant is a variable length version of the similar noisy binary search where each measurement vector $\mathbf{A}_t$ is used until we obtain error probability less than $\epsilon_p := \frac{\epsilon}{\log B/\delta}$ either inside or outside of $\mathbf{A}_t$. Table 2.1 provides a quick summary of the search strategies. Note that Table 2.1 also includes a short summary of our two-stage strategy, although this strategy is studied in the next section (Sect. 2.2.6).

Table 2.1: Candidate Search Strategies

Strategies $\mathfrak{c}_\epsilon \in \mathcal{C}_\epsilon$	Description of $\mathbf{A}_t$ selection
Optimal non-adaptive	• Select $\mathbf{A}_t$ s.t. $\|\mathbf{A}_t\|_0 = \frac{q^* B}{\delta}$ as dictated by strategy $\mathfrak{c}_\epsilon^1$
Fixed Length Noisy Binary	• Select $\mathbf{A}_t$ as dictated by binary search strategy • Repeat $\alpha_\epsilon(\mathbf{A}_t)\|\mathbf{A}_t\|_0$ times
Variable Length Noisy Binary	• Select $\mathbf{A}_t$ as dictated by binary search strategy • Repeat τ times s.t. $\tau = \min\{t : \|\boldsymbol{\rho}_t\|_\infty \geq 1 - \epsilon_p\}$
Sorted Posterior Matching	• Select $\mathbf{A}_t$ as dictated by Sort PM strategy $\mathfrak{c}_\epsilon^2$
Two-stage Strategy	• Phase 1: Search among $(\frac{1}{\alpha})$ large subsets. Select $\mathbf{A}_t$ fixed composition s.t. $\|\mathbf{A}_t\|_0 = \frac{q^* B}{\delta}$ • Phase 2: Zoom into region of size αB, and select $\mathbf{A}_t$ with Sort PM strategy $\mathfrak{c}_\epsilon^2$

Fig. 2.7, shows the performance of each ϵ-reliable search strategy, when considering fixed parameters B, δ, and ϵ. We note that the fixed length noisy binary strategy performs poorly in comparison to the optimal non-adaptive strategy. This shows that randomized non-adaptive search strategies, similar to the one considered in [41] perform better than both the exhaustive search (as shown in [41]) and the iterative hierarchical search strategy. In particular, it performs better than the variable length noisy binary search since when the noise variance parameter σ^2 is large, this

higher noise intensity requires that each measurement is repeated far too many times in order to be ϵ-reliable. The performance of the optimal fully adaptive variable length strategies sort PM [9] is superior to all strategies even in the non-asymptotic regime.

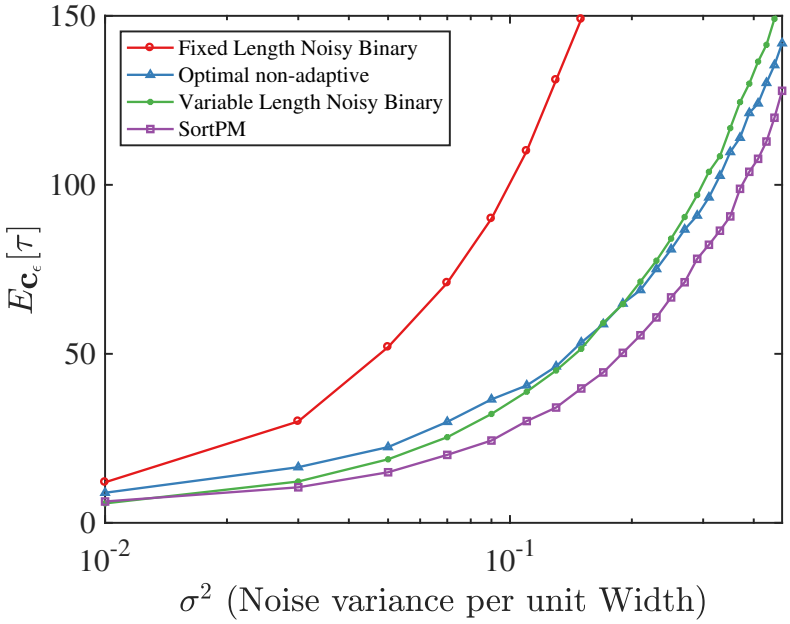

Figure 2.7: $\mathbb{E}_{\mathfrak{c}_\epsilon}[\tau]$ with $\epsilon = 10^{-4}$, $B = 16$, and $\delta = 1$, as a function of σ^2 for various strategies.

Two Distinct Regimes of Operation

In this section, for a fixed σ^2 we are interested in the expected number of measurements required $\mathbb{E}_{\mathfrak{c}_\epsilon}[\tau]$ by an ϵ-reliable strategy $\mathfrak{c}_\epsilon$, in the following two regimes: (1) varying δ while keeping B fixed, and (2) varying B while keeping δ fixed. Fig. 2.8 and Fig. 2.9 show the simulation results of $\mathbb{E}_{\mathfrak{c}_\epsilon}[\tau]$ as a function of width B, i.e. regime (1) and resolution δ, i.e. regime (2), respectively. The empirical performance is studied for the following: for the fixed composition non adaptive strategy $\mathfrak{c}_\epsilon \in \mathcal{C}_\epsilon^{NA}$, for the sort PM adaptive strategy $\mathfrak{c}_\epsilon \in \mathcal{C}_\epsilon^{A}$ and its respective upper bound (obtained from the analysis of [9]), for our proposed two-stage strategy along with dominant terms of the lower bound of Lemma 2, and the upper bound of Lemma 3.. In both regimes, we observe better performance using the sortPM strategy over our two-stage strategy. However, the upper bound of the sortPM strategy is extremely loose and fails to guarantee any adaptivity gain. In fact, in

Fig. 2.9 the sortPM upper bound is approximately 4 times larger in $\mathbb{E}_{\mathbf{c}_\epsilon}[\tau]$ than the sortPM strategy. On the other hand, under both regimes of operation, our tighter bounds empirically show positive adaptivity gain, albeit in distinctly different manners for each regime. For both regimes, we see that the adaptivity gain grows as the total number of locations increases; however in distinctly different manner as seen in Corollary 3.

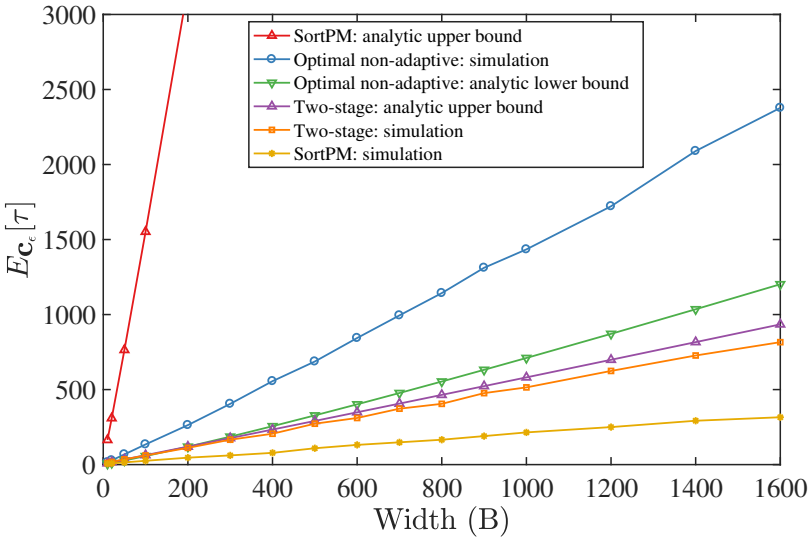

Figure 2.8: $\mathbb{E}_{\mathbf{c}_\epsilon}[\tau]$ with $\epsilon = 10^{-4}$, $\sigma^2 = 0.05$, and $\delta = 1$, as a function of B.

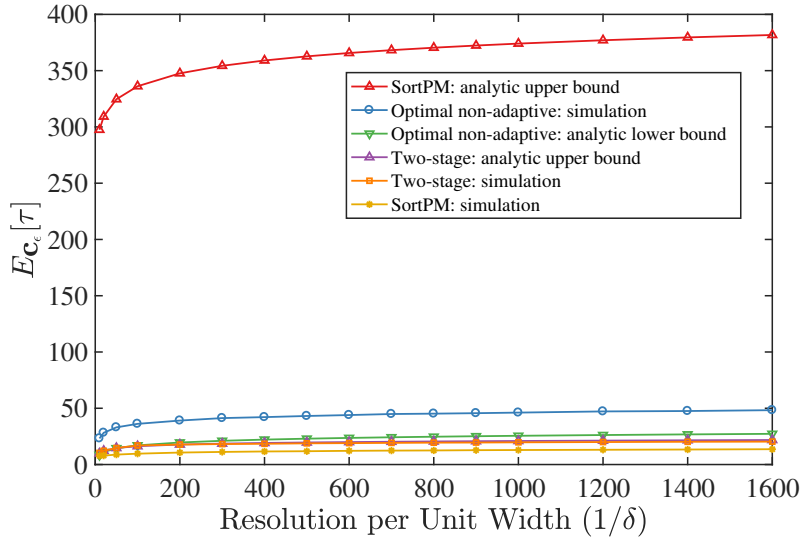

Figure 2.9: $\mathbb{E}_{\mathbf{c}_\epsilon}[\tau]$ with $\epsilon = 10^{-4}$, $\sigma^2 = 1$ and $B = 1$, as a function of δ.

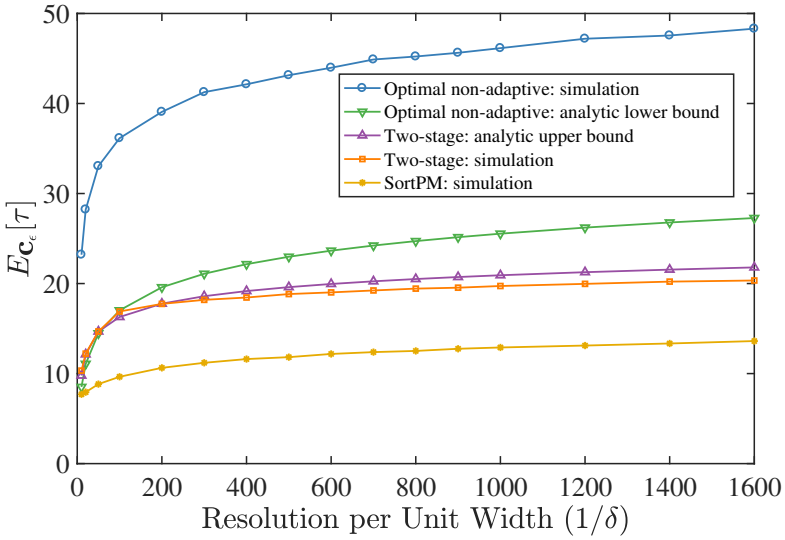

Figure 2.10: Close up of $\mathbb{E}_{\mathbf{c}_\epsilon}[\tau]$ with $\epsilon = 10^{-4}$, $\sigma^2 = 1$ and $B = 1$, as a function of δ.

Relating the Regimes of Operation to Capacity

In this section, we attempt to relate these two regimes of operation to the manner in which the capacity of a BAWGN channel varies. Let noise parameter $N_t \sim \mathcal{N}(0, 2q\sigma^2_{\text{Total}})$, where $q = \frac{\|\mathbf{A}_t\|_0 \delta}{B}$ is the fraction of the search region measured and $\sigma^2_{\text{Total}} = \frac{B\sigma^2}{2}$ is the half bandwidth variance. Fig. 2.11 shows the effects of the half bandwidth variance on the capacity of a search as a function of q. Intuitively, the target acquisition rate of the adaptive strategy relates to the time spent searching sets of size q as q varies from $\frac{1}{2}$ to $\frac{\delta}{B}$. This means for sufficiently small σ^2_{Total} (≤ 0.025 in this example), the adaptivity gain is negligible since $C(\frac{1}{2}, 2q\sigma^2_{\text{Total}})$ is about 1 for all q. For medium range σ^2_{Total} (for e.g., 0.25 in this example), the adaptivity effects the target acquisition rate from $C(\frac{1}{2}, 2q^*\sigma^2_{\text{Total}})$ to $C(\frac{1}{2}, 2\frac{\delta}{B}\sigma^2_{\text{Total}})$. When σ^2_{Total} grows significantly, however, the capacity drops rather quickly to zero, forcing the non-adaptive strategies to operate close to exhaustive search, whose measurement time increases linearly in $\frac{B}{\delta}$. This is the regime with most significant adaptivity gain as predicted by Corollary 3.

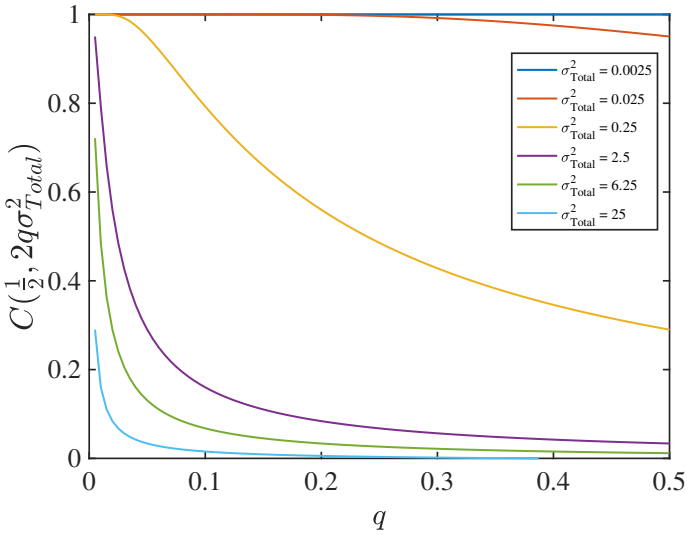

Figure 2.11: For arbitrary B and δ, and with $\epsilon = 10^{-4}$, $C(\frac{1}{2}, 2q\sigma^2_{Total})$ as a function of q for different values of total noise variance (σ^2_{Total})

Beyond a Linear Noise Model

In this section, we analyze $\mathbb{E}_{\mathfrak{c}_\epsilon}[\tau]$ under a general noise model, as presented in Sect. 2.2.5. Recall, $Y_t \sim \mathcal{N}(X_t, f(\|\mathbf{A}_t\|_0)\delta\sigma^2)$, where f is a non-decreasing function of the measurement vector $\|\mathbf{A}_t\|_0$. Fig. 2.6 shows that the behavior of the capacity range of a search with fixed parameters B, δ, $\mathbf{A}_t$ can be significantly affected by the function $f(\cdot)$. Let us consider the noise function $f(\cdot)$ to be of the form $\|\mathbf{A}_t\|_0^\gamma$. Fig. 2.12 shows the plot of dominant terms of the lower bound of Lemma 2, and the upper bound of Lemma 3 as a function of σ^2 for the values of $\gamma \in \{0.5, 1, 2\}$. The adaptivity gain is clearly more significant for larger values of gamma and hence, validates the need for generalizing the noise function.

2.3 Conclusion

We considered the problem of recovering the time-invariant support of a vector with known magnitude via a sequence of linear and measurement dependent noisy observations. Under these assumptions, the problem can be thought of as the task of searching for the unknown location of multiple targets under measurement dependent noise. In part I. of this chapter we considered

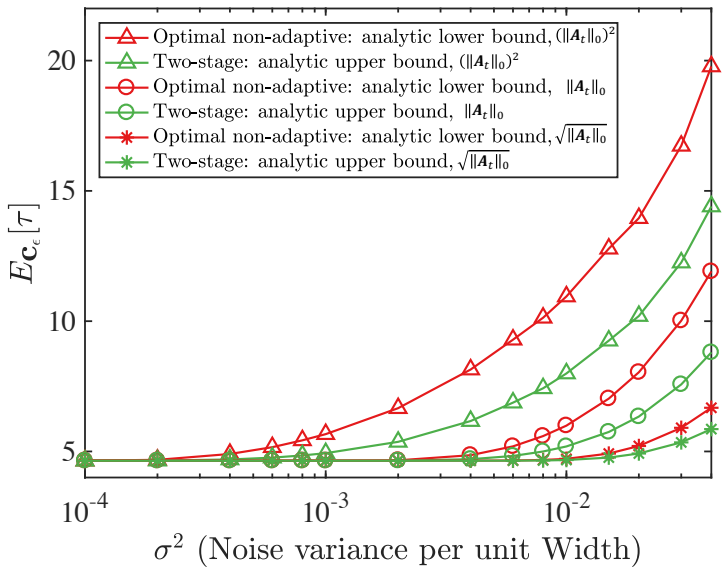

Figure 2.12: $\mathbb{E}_{\mathbf{c}_\epsilon}[\tau]$ with $\epsilon = 10^{-4}$, $\sigma^2 = 0.25$ and $B = 25$, $\delta = 1$, as a function of γ when $N_t \sim \mathcal{N}(0, \|\mathbf{A}_t\|_0^\gamma \delta\sigma^2)$.

the case of recovering r targets in as few measurements as possible. The problem was shown to be equivalent to MAC encoding with feedback. In the second part of this chapter we considered the special case of extreme sparsity, where we have the problem of searching for a single target's unknown location under measurement dependent Gaussian noise. We showed that this problem is equivalent to channel coding over a BAWGN channel with state and feedback. We used this connection to utilize feedback code based adaptive search strategies. We obtained information theoretic converses to characterize the fundamental limits on the target acquisition rate under both adaptive and non-adaptive strategies. As a corollary, we obtained a lower bound on the adaptivity gain. We identified two asymptotic regimes with practical applications where our analysis shows that adaptive strategies are far more critical when either noise intensity or the total search width is large. In contrast, in scenarios where neither the total width nor noise intensity is large, non-adaptive strategies might perform quite well. The immediate step is the extension of this work to a model with time-varying support, i.e. mobile targets, or with time-varying or unknown magnitudes.

Chapter 2, in part, is a reprint of the material as it appears in the paper: Nancy Ronquillo and Tara Javidi, "Multiband Noisy Spectrum Sensing with Codebooks," in the proceedings of the

Asilomar Conference on Signals, Systems, and Computers, Nov. 2016. The dissertation author was the primary investigator and author of this paper.

Chapter 2, in part, is a reprint of the material as it appears in the article: Anusha Lalitha, Nancy Ronquillo, and Tara Javidi, “Improved Target Acquisition Rates with Feedback Codes," IEEE Journal of Selected Topics in Signal Processing, Vol.12, no.5, pp. 871 - 885, Oct. 2018. The dissertation author was the secondary investigator and co-author of this paper.

Chapter 3

Active Learning and CSI Acquisition for mmWave Initial Alignment

In chapters 1 and 2 we have formulated the problem of target search with measurement dependent noise and studied the problem from information-theoretic perspective. In this chapter we formally introduce the practical application of our work to the problem of initial alignment for Millimeter-Wave (mmWave) communications and above. Specifically, we cast the problem of initial alignment as a target search problem under noisy linear measurements with the practical constraint of contiguous measurements. We develop an active and sequential algorithm for designing practically feasible measurements on the basis of posterior matching and analyze the proposed strategy to characterize fundamental limits.

3.1 Introduction

mmWave communication with massive antenna arrays is a promising technique that increases the data rate significantly, thanks to the large available bandwidth in mmWave frequency bands. While an inherent challenge for mmWave communication is extremely high pathloss [10]- [11], resulting in low SNR and high link outage, the small wavelength can be exploited to deploy an array with a very large number of antennas in a relatively small area. It has been shown [12] that

massive MIMO mmWave systems can be deployed to form highly directional beams to mitigate the pathloss and the associated low SNR and high link outage. However, it is important to note that the realization of highly directional beams requires a precise and reliable estimate of channel state information (CSI) [45] during the initial access phase. This chapter considers the problem of actively learning an optimal beamforming vector from a fundamental limit point of view.

With the scale of millimeter wavelength and the half wavelength spacing, a large number of antennas can be packed into a modest-sized device. For large antenna arrays, however, equipping each antenna with an RF chain is too hardware costly. This prevents per antenna digital processing. A hardware friendly proposal for practically implementing large array systems in mmWave bands deploys a single RF chain where CSI acquisition reduces to finding the optimal analog beamforming along the dominant direction of the signals between the base station (BS) and the user that is trying to establish the communication link. In this chapter we consider this practical scenario of mmWave communication with massive MIMO technology and the practically designed low complexity hierarchical beamforming codebook of [46] to propose an efficient and adaptive beamforming algorithm that quickly identifies the optimal beamforming direction under a single dominant path channel model. Furthermore, we obtain bounds on the performance of this algorithm to asymptotically match the fundamental information theoretic limits on the speed and reliability of active learning and CSI acquisition with the given hardware constraints.

The exhaustive linear search, which utilizes beams that scan over all possible directions to pick the best one, and is proposed in IEEE 802.15 and 5G standards, requires a relatively long initial access time that linearly grows with the angle resolution (highest resolution being the number of the antenna elements). On the theoretical front, in contrast, prior work which is based on simple measurement models noted that the problem of CSI acquisition in mmWave is closely related to that of noisy search, which itself has been shown to be closely related to the problem of channel coding over a binary input channel with [6, 47, 48] and without [7] feedback (see chapter 2 for a detailed description of the connection of initial alignment to channel coding). Under various noise models, it is shown that the number of measurements can be kept to grow only logarithmically with the

angular resolution and target error probability [6] and [48] (discussed in chapter 2)). While these early studies did not take the practical beam patterns into account, this logarithmic scaling was later also confirmed and reported in more practical systems with realistic and empirically precise beam patterns [46, 49, 50] with the caveat of a sufficiently large SNR model. In particular, [46] carefully developed a hierarchical beamforming codebook which in the noiseless setting allows for an (adaptive) binary search over the angular space; increasing transmission power and/or time is then used to combat the measurement noise. The authors in [49,50] showed that similar performance gains can also be achieved by a non-adaptive strategy. More specifically, the authors of [49] proposed random hash functions to generate a random beamforming codebook whose acquisition time, they showed, grows only logarithmically with target resolution/error probability. The logarithmic scaling (of search time with angular resolution) could also be obtained when viewing the problem as that of sparse estimation with compressive measurements (see [51] and references therein). Indeed, the authors of [50] recover the signal direction with a non-negative least square estimate from Compressive Sensing by measuring the received power via a random beamforming codebook which hashes the angular directions similarly to [49].

However, to guarantee coverage in low (< 5 dB)[1] raw SNR regimes (cell-edge users), these beamforming techniques (random direction and direct bisection) provide marginal advantage over the exhaustive linear search as noted in [47]. This limitation of prior work to operate in high raw SNR makes them unsuitable for cell-edge users in mmWave communication. This has major practical system design implications, namely the current 5G mmWave communication in 3GPP standards [52] supports mainly non-standalone mmWave in which the initial access phase is covered by legacy sub-6G infra-structure which provides higher SNR. This highlights the need for a strategy that can adaptively improve the measurement quality and is suitable for a low raw SNR regime.

[1] We note that while [50] provides a system working under -30 dB SNR_{BBF} (before beamforming), the system parameters used in their simulation were such that the SNR_{BBF} is defined differently than raw SNR in our set up. For a fair comparison we may interpret our raw SNR = $\frac{\text{SNR}_{\text{BBF}}}{c}$ where the scaling factor c is proportional to number of subcarriers and number of RF chains used in their simulation.

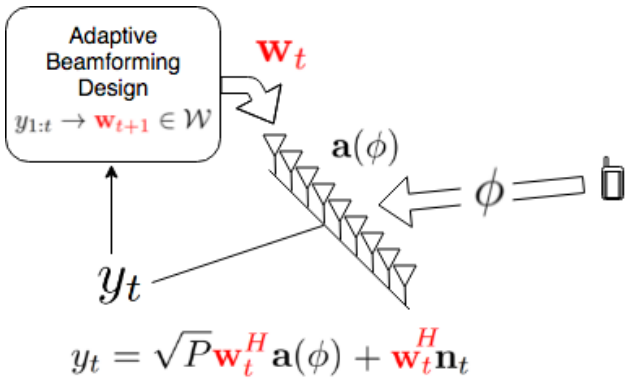

Figure 3.1: The active learning process of the AoA ϕ is to design the beams $\mathbf{w}_t \in \mathcal{W}^S$ adaptively for the sequential collection of the observations y_t, from which at the ending of the collection is to be used for the estimation of the AoA ϕ.

3.1.1 Contributions

In this paper, we consider the problem of CSI acquisition during the initial access phase for designing the analog beamforming in an environment with a single-path channel. We formulate the CSI acquisition as an active learning of the angle-of-arrival (AoA) at the base station (BS) side where the user's beamforming vector is assumed to be fixed, as illustrated in Fig. 3.1. We consider two measures of performance for the proposed search scheme: the (expected) resolved beam width (AoA resolution) and the (expected) error probability. Based on the nature of the initial access protocol, we consider two types of stopping criteria: fixed-length stopping, where a fixed amount of search time is allocated for the initial access phase, and variable-length stopping, where search is conducted over a random stopping time. The contributions of the chapter include:

- We formulate the initial beam alignment for massive MIMO as active learning of the AoA through multiple sequential and adaptive search beams. Our approach draws heavily from our prior work on algorithms for noisy search [9], active learning [53], and channel coding with feedback [48] (discussed in chapter 2).

- We propose a new adaptive beamforming strategy that utilizes the hierarchical beamforming codebook of [46]. The proposed adaptive strategy, hierarchical Posterior Matching ($hiePM$), accounts for the measurement noise and selects the beamforming vectors from the hierarchical

beamforming codebook based on the posterior of the AoA. The design and analysis of $hiePM$ extends our prior work of sorted posterior matching for noisy search [9] and [48] in that it restricts the search and the measurements to the practical and hierarchical beamforming patterns of [46].

- We analyze the proposed $hiePM$ strategy and give an upper bound on the expected acquisition time of a variable-length $hiePM$ search strategy required to reach a fixed (predetermined) target resolution and error probability in the AoA estimate. Even when the measurements are hard detected (1-bit quantized measurements), the achievable AoA acquisition rate and the error exponent of $hiePM$ are shown (Corollary 5) to be significantly better than those for the search methods of [46] and the random hashing of [49] in all raw SNR regimes.

- We show, via extensive simulations, that $hiePM$ is suitable for both fixed-length and variable-length initial access and significantly outperforms the state-of-art search strategies of [46] and [49]. The numerical simulations show that $hiePM$ is capable of reaching a good resolution and error probability even in a low (< 5dB) raw SNR regime with reasonable expected search time overhead, demonstrating the possibility of stand-alone mmWave communication for the first time

3.2 System Model

We consider a sectorized cellular communication system operating in EHF (30-300 GHz) bands, where a sector is formed by the BS serving users in a range of angles $[\theta_{\text{min}}, \theta_{\text{max}}]$ as depicted in Fig. 3.2. We focus on the model with one sector and a single user, where the interference from other sectors are assumed to be negligible. This assumption is justified due to high pathloss in the EHF bands [10], and the orthogonality (in time or code) of the transmissions from other users within the sector.

We consider a hardware architecture consisting of multiple antenna elements with a single RF chain [54] on both the BS and the user sides. Beamforming is applied on the antenna elements

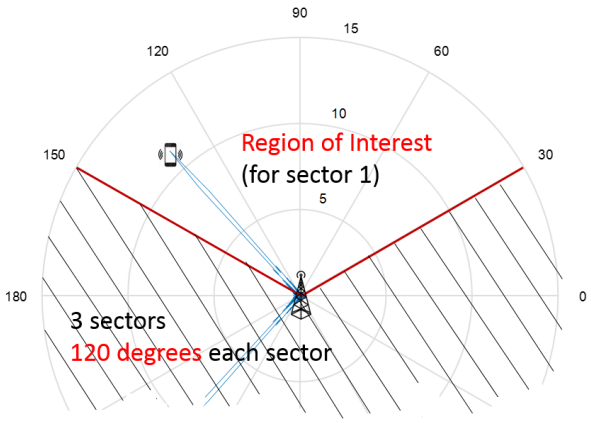

Figure 3.2: Base Station Serving sector $[30^o, 150^o]$ and a received beam at the BS formed by uniform linear array

such that the power gain due to beamforming may compensate the high pathloss in the mmWave communication system. We use a pilot-based procedure where the users send out pilots to the BS while the BS combines the signal from the antenna elements to the RF chain by the beamforming vector $\mathbf{w}_t \in \mathbb{C}^N$. We will focus on the procedure of obtaining a good beamforming vector at the BS, while assuming a fixed beamforming vector at the user which allows us to model the user's antennas as a single virtual antenna.

Let N be the number of antennas at the BS, $\sqrt{P}$ be the combined effect of the transmit power and the large-scale fading (pathloss and shadowing), and $\mathbf{h} \in \mathbb{C}^N$ be the small-scale frequency flat fading vector, i.e. h_i is the small-scale fading between the single virtual antenna of the user and the ith antenna element at the BS. For small-scale channel modelling, we use the stochastic multi-path modelling (see Ch.7 in [55]) assumption with a single dominant path. Furthermore, we assume that the user's mobility is negligible, i.e., the channel vector $\mathbf{h}$ is time invariant. In summary, we have the following assumption:

Assumption 1. *The small-scale channel can be described as:*

$$\mathbf{h} = \alpha \mathbf{a}(\phi), \tag{3.1}$$

where $\alpha \in \mathbb{C}$ is the fading coefficient and

$$\mathbf{a}(\phi) := [1, e^{j\frac{2\pi d}{\lambda}\sin\phi}, ..., e^{j(N-1)\frac{2\pi d}{\lambda}\sin\phi}] \tag{3.2}$$

is the array manifold created by the Angle-of-Arrival (AoA) $\phi \in [\theta_{min}, \theta_{max}]$ with antenna spacing d. Furthermore, we assume that the fading coefficient, α, and the AoA, ϕ, are static in time.

Let time index $t = 1, 2, ...$ be the time frame in which the BS can adapt the beamforming vector $\mathbf{w}_t$. Each beamforming slot consists of I samples of finer granularity either of time (e.g. CDMA) or of frequencies (e.g. OFDM subcarriers). Orthogonal spreading sequences $\mathbf{s}_k$ of length I are sent by each of the K users. In other words, we assume:

Assumption 2.

$$\mathbf{s}_k^H \mathbf{s}_{k'} = \begin{cases} 0 \textit{ for } k = k' \\ 1 \textit{ for } k \neq k' \end{cases} \tag{3.3}$$

With the assumption of orthogonality among users, correlating the pilot codes we can write the code-matched signal from a particular user as

$$\begin{aligned} y_t &= \sqrt{P}\mathbf{w}_t^H (\sum_{k'=1}^{K} \mathbf{h}_{k'} \mathbf{s}_{k'}^T)\mathbf{s}_k^* + \mathbf{w}_t^H \mathbf{N}_t \mathbf{s}_k^* \\ &\overset{(a)}{=} \alpha\sqrt{P}\mathbf{w}_t^H \mathbf{a}(\phi) + \mathbf{w}_t^H \mathbf{n}_t, \end{aligned} \tag{3.4}$$

where $\mathbf{N}_t$ is the $N \times I$ spatially uncorrelated AWGN noise matrix across the antenna elements (rows) and samples (columns). Note that in (a) we used single-path channel model (Assumption 1) and orthogonality of codes (Assumption 2) from different users as well as the static nature of the channel, $\mathbf{h}$, over the code resource I. Finally, $\mathbf{n}_t := \mathbf{N}_t \mathbf{s}_k^* \sim \mathcal{CN}(\mathbf{0}_{N\times 1}, \sigma^2 \mathbf{I})$ is the equivalent noise vector at the antenna array at the output of the code-matched filter, i.e., such that y_t has a raw SNR equal to P/σ^2 when no beamforming is applied.

In many practical scenarios only a partial information about y_t is available to the BS. As a

result, we consider the available signal to BS, z_t, to be of the form

$$z_t = q(y_t), \tag{3.5}$$

where $q(\cdot)$ represents a practically motivated partial information processing such as a quantization function. With the received signal model in (3.4) and (3.5), we are now ready to describe the sequential beam search problem which adaptively designs the beamforming vectors $\mathbf{w}_t$.

3.3 Active Learning and Hierarchical Posterior Matching

In this section we present our main result. In Sect. 3.3.1 we lay out the framework of active learning for sequential beam alignment. In Sect. 3.3.2 we describe the hierarchical beamforming codebook. In Sect. 3.3.3 we describe our proposed algorithm: Hierarchical Posterior Matching for sequentially selecting the beamforming vector from the beamforming codebook. Lastly, in Sect. 3.3.4 we describe the posterior update for various measurement models.

3.3.1 Sequential Beam Alignment via Active Learning

A sequential beam alignment problem in the initial access phase consists of a beamforming design strategy (possibly adaptive), a stopping time τ, and a final beamforming vector design. Specifically, we consider a stationary beamforming strategy as a causal (possibly random) mapping function from past observations to the beamforming vector: $\mathbf{w}_{t+1} = \gamma(z_{1:t}, \mathbf{w}_{1:t})$. Subsequently, the final beamforming vector selection $b(\cdot)$ is a (possibly random) mapping determining the final beamforming vector to be exploited for communication, $\hat{\mathbf{w}} = b(z_{1:\tau}, \mathbf{w}_{1:\tau})$, as a function of the sequence of the observations gathered during the initial access phase $[1:\tau]$. To reduce the reconfiguration time of the beamforming vector from $\mathbf{w}_t$ to $\mathbf{w}_{t+1}$, we use a pre-designed beamforming codebook:

Assumption 3. *The beamforming vector is chosen from a pre-designed beamforming codebook $\mathcal{W}^S$ with finite cardinality.*

Based on the nature of the protocol, we consider two criteria for selection of the length of the initial access phase:

Fixed-length stopping time: the user transmits a pre-determined number of frames during which the BS uses the beamforming vectors $\mathbf{w}_1, \mathbf{w}_2, ..., \mathbf{w}_T$. After the total pre-determined number of frames, n, the BS makes a prompt decision on the final beamforming vector $\hat{\mathbf{w}}$

Variable-length stopping time: the user sends out the initial access signal continually until a certain target link quality can be achieved by the final beamforming vector $\hat{\mathbf{w}}$ with high probability. Under a variable-length setup, the BS sends an ACK to the user which ends the initial access phase.

In Sect. 3.4, we propose an adaptive beam alignment algorithm with both types of the stopping rules, while our analysis in Sect. 3.4 focuses on the variable-length stopping time τ. Our numerical studies consider the performance under both stopping rules.

Since the best beamforming vector $\hat{\mathbf{w}} = \mathbf{a}(\phi)$ can boost the SNR by a factor of N, the fading coefficient α can also be estimated and equalized easily if the SNR at the RF chain (after antenna combining) is high enough. Therefore, under Assumption 1, one of the major goals of the initial access phase is to learn the AoA ϕ so that BS can form a good beam toward that direction. Therefore, we can treat the sequential beam alignment problem by the methods of active learning [53, 56] as shown in Fig. 3.1, where the beamforming vector $\mathbf{w}_t$ is equivalent to the query point and y_t is equivalent to the response in the learning problem. The adaptivity of $\mathbf{w}_t$ reflects that the query points are actively chosen as considered in active learning tasks.

The quality of the established link, under a single-path channel model $\mathbf{h} = \alpha\mathbf{a}(\phi)$, is determined by the accuracy of the final point estimate, $\hat{\phi}(y_{1:\tau}, \mathbf{w}_{1:\tau})$, of ϕ. In particular, a point estimate $\hat{\phi}$ together with a confidence interval δ provides robust beamforming with a certain outage probability. Hence, we measure the performance by the resolution and reliability of the final estimate $\hat{\mathbf{w}}$:

Definition 8. Under Assumption 1, a sequential beam search strategy with an adaptive beamforming design γ, stopping time τ, and final AoA estimate $\hat{\phi}$ is said to have resolution $\frac{1}{\delta}$ with error probability

ϵ if

$$\mathbb{P}|\hat{\phi} - \phi| > \delta \leq \epsilon. \tag{3.6}$$

We note that, given a sufficiently large number of antennas, one can increase the resolution $1/\delta$ and decrease the error probability ϵ by increasing the time of sample collection τ, or equivalently, by prolonging the initial access phase. In other words, the effectiveness of an initial access algorithm shall also be measured by the expected number of samples $\tau_{\epsilon,\delta}$ necessary to ensure a resolution $1/\delta$ and error probability ϵ. From an information theoretic viewpoint, one can think of a family of sequential adaptive initial access schemes that achieves acquisition rate R and reliability E:

Definition 9. Under Assumption 1, a family of sequential adaptive initial access schemes achieves acquisition rate-reliability (R,E) if and only if

$$R := \lim_{\delta \to 0} \frac{\log(\frac{1}{\delta})}{\mathbb{E}[\tau_{\epsilon,\delta}]}, \quad E := \lim_{\epsilon \to 0} \frac{\log(\frac{1}{\epsilon})}{\mathbb{E}[\tau_{\epsilon,\delta}]}. \tag{3.7}$$

Remark 1. The final beamforming vector (hence the quality of the established link) is determined by both the target resolution and the error (δ, ϵ), and is written as $\hat{\mathbf{w}}(z_{1:\tau}, \mathbf{w}_{1:\tau}, \epsilon, \delta)$. Given a total communication time frame T, the expected spectral efficiency, under the final beamforming vector $\hat{\mathbf{w}}$, is given as

$$\mathbb{E}\left[\frac{T-\tau}{T} \log\left(1 + \frac{P \mid \alpha \hat{\mathbf{w}}(z_{1:\tau}, \mathbf{w}_{1:\tau}, \epsilon, \delta)^H \mathbf{a}(\phi) \mid^2}{\sigma^2}\right)\right], \tag{3.8}$$

and is an important performance metric from a system point of view. This performance metric, however, requires a further system optimization over the length of the initial access phase, τ, and the length of the communication phase, T, which is outside the scope of this paper. Therefore, in our analysis we focus on the parameters ϵ and δ. For a comparison of different initial beam search algorithms, the system performance of (3.8) is also evaluated in the numerical simulations for some nominal choice of τ and T.

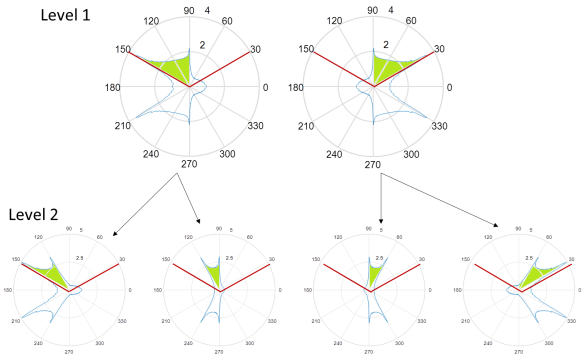

Figure 3.3: The first 2 levels of hierarchical beamforming codebook with practical beam pattern formed by 64 antenna elements

3.3.2 Hierarchical Beamforming Codebook

We adopt the hierarchical beamforming codebook $\mathcal{W}^S$ proposed in [46] with S levels of beam patterns. The beams divide the space dyadically in a hierarchical manner such that the disjoint union of the beams in each level is the whole region of interest. The codebook is the set $\mathcal{W}^S = \cup_{l=1}^{S} \mathcal{W}_l$, where $\mathcal{W}_l$ is all the beam patterns in level l whose main beam has a width $\frac{|\theta_{\max} - \theta_{\min}|}{2^l}$. More specifically, for each level l, $\mathcal{W}_l$ contains 2^l beamforming vectors which divide the sector $[\theta_{\max}, \theta_{\min}]$ into 2^l directions, i.e.

$$[\theta_{\max}, \theta_{\min}] = \bigcup_{k=1}^{2^l} D_l^k, \tag{3.9}$$

each associated with a certain range of AoA D_l^k. The beamforming vector $\mathbf{w}$ covering the angular range D_l^k is designed such that the beamforming gain $|\mathbf{w}^H \mathbf{a}(\phi)|$ is almost constant for an AoA $\phi \in D_l^k$ and almost zero for $\phi \notin D_l^k$.

Note that $\mathcal{W}^S$ can be represented as a binary hierarchical tree, where each level-l beam has two descendants in level $l+1$ such that each level-l beam is the union of two disjoint beams, i.e., $D_l^k = D_{l+1}^{2k} \cup D_{l+1}^{2k-1}$. This binary tree hierarchy is illustrated in Fig. 3.3 with the beam patterns of the first two levels of the codebook. Note that without loss of generality, the beamforming vectors in the codebook are assumed to have unit norm $\|\mathbf{w}\|^2 = 1$.

3.3.3 Hierarchical Posterior Matching

In this section we propose a search mechanism based on the connection between initial access beamforming, noisy search [9], active learning [53], and channel coding with feedback as discussed in chapter 2, with the caveat that the beamforming vector is constrained to the practically feasible beamforming codebook of [46] as in set $\mathcal{W}^S$. Instead of using all past observations $\mathbf{w}_{t+1} = \gamma(z_{1:t}, \mathbf{w}_{1:t})$, $hiePM$ selects $\mathbf{w}_{t+1}$ based on the posterior of the AoA ϕ at time t, which is a sufficient statistic. We discretize the problem by assuming that the resolution $\frac{1}{\delta}$ is an integer and that the AoA ϕ is from

$$\phi \in \{\theta_1, ..., \theta_{1/\delta}\},\ \theta_i = \theta_{\text{min}} + (i-1) \times \delta \times (\theta_{\text{max}} - \theta_{\text{min}}). \tag{3.10}$$

Such discretization approaches the original problem of initial access as $\delta \to 0$. Under such discretization, we define $\tilde{\mathbf{w}}_{[l,k]} \in \{0,1\}^{\frac{1}{\delta}}$ to be the angular space binary vector representation of the beamforming vector $\mathbf{w}$ of level l and k, where $\tilde{\mathbf{w}}_{[l,k]}(i) = 1$ if and only if $\theta_i \in D_l^k$. To support resolution $1/\delta$, the corresponding size of the hierarchical beamforming codebook

$$S = \log_2(1/\delta) \tag{3.11}$$

is used. With this discretization, the posterior probability distribution can be written as a $\frac{1}{\delta}$-dimensional vector $\boldsymbol{\pi}(t)$, where the i^{th} component is of the form

$$\pi_i(t) := \mathbb{P}\phi = \theta_i | z_{1:t}, \mathbf{w}_{1:t},\ i = 1, 2, ..., \frac{1}{\delta}. \tag{3.12}$$

The posterior probability of the AoA ϕ being within a range covered by the beamforming vector $\mathbf{w}$ of level l and k, can be computed as

$$\pi_{\tilde{\mathbf{w}}_{[l,k]}}(t) := \sum_{i=1}^{1/\delta} \tilde{\mathbf{w}}_{[l,k]}(i) \pi_i(t). \tag{3.13}$$

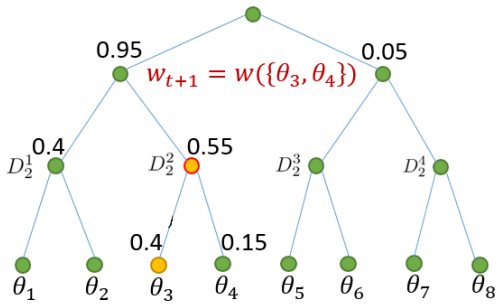

Figure 3.4: Illustration of the hierarchical posterior matching algorithm. In this example, we search down the tree hierarchy to levels 2 and 3, where level 3 has the first codeword that contains posterior lesser than half. Between level 2 and level 3, the codeword in level 2 of posterior 0.55 is selected since it's closer to half (0.55 v.s. 0.4).

Now we are ready to present the proposed $hiePM$ algorithm. The proposed adaptive beamforming strategy, $hiePM$, chooses a beamforming vector at each time t from the hierarchical beamforming codebook $\mathcal{W}^S$. The main idea of $hiePM$ is to select $\mathbf{w}_{t+1} \in \mathcal{W}^S$ by examining the posterior probability $\pi_{\tilde{\mathbf{w}}_{[l,k]}}(t)$ of all beams, i.e. for all $l = 1, 2, ..., S$ and $k = 1, 2, ..., 2^l$. Specifically, let

$$l_t^* = \underset{l}{\operatorname{argmax}} \left\{ \max_k \pi_{\tilde{\mathbf{w}}_{[l,k]}} \geq \frac{1}{2} \right\}, \tag{3.14}$$

the proposed $hiePM$ algorithm selects a codeword at either level l_t^* or $l_t^* + 1$ according to Alg. 1 below. Given a snapshot of the posterior at time t, the selection rule is illustrated in Fig. 3.4. The algorithm runs for a fixed length of time (fixed-length stopping) or until a certain error probability ϵ for resolution $1/\delta$ is achieved (variable-length stopping). The final choice of beamforming vector is determined by ϵ and δ. The details of $hiePM$ are summarized in Alg. 1 below.

Algorithm 1: Hierarchical Posterior Matching for Beamforming

Input: target resolution $\frac{1}{\delta}$, target error probability ϵ, codebook $\mathcal{W}^S$ $(S = \log_2(1/\delta))$, *stopping-criterion* (with stopping time n if fixed-length), *algorithm-type*

Output: Estimate of the AoA $\hat{\phi}$

Initialization: $\pi_i(0) = \delta$ for all $i = 1, 2, ..., 1/\delta$, $k = 0$

for $t = 1, 2, ...$ **do**

  # Select codeword from $\mathcal{W}^S$:

  for $l = 1, 2, ..., S$ **do**

    if $\pi_{\tilde{\mathbf{w}}_{[l,k]}}(t) > 1/2$ **then**

      # select the larger descendant: $l_t^* = l$; $k \leftarrow \text{argmax}_{k' \in \{2k-1, 2k\}} \boldsymbol{\pi}_{\tilde{\mathbf{w}}_{[l+1,k']}}(t)$;

    else $(l_{t+1}, k_{t+1}) = \text{argmin}_{(l',k') \in \{(l_t^*, \lceil \frac{k}{2} \rceil), (l_t^*+1, k)\}} \left| \pi_{\tilde{\mathbf{w}}_{[l',k']}}(t) - \frac{1}{2} \right|$

  # Selected codeword: $\mathbf{w}_{t+1}$ corresponding to $\tilde{\mathbf{w}}_{[l_{t+1}, k_{t+1}]}$

  # Receive next measurement:

$$y_{t+1} = \alpha \sqrt{P} \mathbf{w}_{t+1}^H \mathbf{a}(\phi) + \mathbf{w}_{t+1}^H \mathbf{n}_{t+1}, \; z_{t+1} = q(y_{t+1}) \tag{3.15}$$

  # Posterior update by Bayes' Rule (Sect. 3.3.4) :

$$\boldsymbol{\pi}(t+1) \leftarrow z_{t+1}, \boldsymbol{\pi}(t) \tag{3.16}$$

  case: stopping-criterion = fixed length (FL)

  if $t + 1 = n$ **then**

    break (to final beamforming);

  case: stopping-criterion = variable length (VL)

  if $\max_i \pi_i(t+1) > 1 - \epsilon$ **then**

    break (to final beamforming);

Final beamforming vector design: $\tau = t + 1$ (length of the initial access phase)

case: algorithm-type = fixed resolution (FR)

$$[\hat{l}, \hat{k}] = (S, \underset{k}{\text{argmax}}\, \pi_{\tilde{\mathbf{w}}_{[S,k]}}(\tau)) \tag{3.17}$$

case: algorithm-type = variable resolution (VR)

$$\hat{l} = \begin{cases} 1, \; \max_k \pi_{\tilde{\mathbf{w}}_{[1,\hat{k}]}}(\tau) < 1 - \epsilon \\ \max\{l : \max_k \pi_{\tilde{\mathbf{w}}_{[l,\hat{k}]}}(\tau) \geq 1 - \epsilon\}, \; o.w. \end{cases}, \; \hat{k} = \underset{k}{\text{argmax}}\, \pi_{\tilde{\mathbf{w}}_{[\hat{l},k]}}(\tau) \tag{3.18}$$

$\hat{\mathbf{w}}$ corresponding to $\tilde{\mathbf{w}}_{[\hat{l},\hat{k}]}$

Remark 2. The $hiePM$ algorithm can be thought of as a noisy generalization of a bisection search where the posterior is used to create almost equally-probable search subsets subject to the codebook $\mathcal{W}^S$. Compared with the vanilla bisection method proposed in [46], $hiePM$ allows for significantly lower SNR search outcomes whose reliability are dealt with over time. This can also be viewed as water-filling in angular domain.

Remark 3. See chapter 2 for a detailed description of the connection between our beam search problem and a channel coding problem in data transmission. In this light, the vanilla noise-compensated bisection method of [46] can be viewed as a repetition coding strategy which is known to have zero rate, while $hiePM$ can be viewed as a constrained (subject to hierarchical codebook $\mathcal{W}^S$) approximation to the capacity achieving posterior matching feedback coding scheme of [31].

3.3.4 Posterior Update

Let $\gamma_h : \boldsymbol{\pi}(t) \to \mathcal{W}^S$ be the $hiePM$ sequential beamforming design given in Alg. 1, i.e. let $\mathbf{w}_{t+1} = \gamma_h(\boldsymbol{\pi}(t))$. By the measurement model in (3.15), the posterior update in Alg. 1 in general can be written as

$$\pi_i(t+1) = \frac{\pi_i(t) f(z_{t+1}|\phi = \theta_i, \mathbf{w}_{t+1} = \gamma_h(\boldsymbol{\pi}(t)))}{\sum_{j=1}^{1/\delta} \pi_j(t) f(z_{t+1}|\phi = \theta_j, \mathbf{w}_{t+1} = \gamma_h(\boldsymbol{\pi}(t)))}, \tag{3.19}$$

where $f(z_{t+1}|\phi = \theta_i, \mathbf{w}_{t+1} = \gamma_h(\boldsymbol{\pi}(t)))$ is the conditional distribution of z_{t+1} and depends on the function $q(\cdot)$ as well as the channel state information (e.g. the fading coefficient α) known to the BS. Here, we give a few examples:

- *Full measurement* $z_t = y_t$:

  In the case of static channel (zero mobility), we may assume that the fading coefficient α is known to the BS. With a full measurement $z_t = y_t$, the conditional distribution of z_t is a complex Gaussian, written as

$$f(z_{t+1}|\phi = \theta_i, \mathbf{w}_{t+1} = \gamma_h(\boldsymbol{\pi}(t))) = \mathcal{CN}(z_{t+1}; \alpha\sqrt{P}\mathbf{w}_{t+1}^H \mathbf{a}(\theta_i), \sigma^2). \tag{3.20}$$

In the case where α is not known, the algorithm is assumed to use an estimate $\hat{\alpha}$:

$$f(z_{t+1}|\phi=\theta_i, \mathbf{w}_{t+1}=\gamma_h(\boldsymbol{\pi}(t))) \approx \mathcal{CN}(z_{t+1}; \hat{\alpha}\sqrt{P}\mathbf{w}_{t+1}^H \mathbf{a}(\theta_i), \sigma^2) \tag{3.21}$$

for the posterior update.

- *1-bit measurement* $z_t = \mathbb{1}(|y_t| > v_t)$:

  For practical high speed ADC implementation, we consider an extreme quantization function of a 1-bit [51, 57, 58] measurement model $z_t = \mathbb{1}(|y_t| > v_t)$, where at each time instance t the BS only has 1-bit of information indicating whether or not the received power passes the threshold v_t. Equivalently, we can write the measurement model as

$$z_t = \mathbb{1}(\phi \in D_{l_t}^{k_t}) \oplus u_t(\phi), \;\; u_t(\phi) \sim \text{Bern}(p_t(\phi)), \tag{3.22}$$

  where $u_t(\phi)$ is the equivalent Bernoulli noise with flipping probability $p_t(\phi)$, and $\oplus$ denotes the exclusive OR operator. The setting of the threshold v_t and the corresponding flipping probability $p_t(\phi)$ is given in Lemma 11. In this case, the conditional distribution of z_t can therefore be written as

$$f(z_{t+1}|\phi=\theta_i, \mathbf{w}_{t+1}=\gamma_h(\boldsymbol{\pi}(t))) = \text{Bern}(z_{t+1} \oplus \mathbb{1}(\theta_i \in D_{l_t}^{k_t}); p_{t+1}(\theta_i)). \tag{3.23}$$

3.4 Analysis

Our analysis for $hiePM$ focuses on the variable-length stopping criteria with fixed resolution $\frac{1}{\delta}$ and a fixed target error probability ϵ, where by Alg. 1 the variable-length stopping time $\tau_{\epsilon,\delta}$ can be written as

$$\tau_{\epsilon,\delta} = \min\{t : 1 - \max_i \pi_i(t) \leq \epsilon\}. \tag{3.24}$$

We will also focus on the 1-bit measurement model described in Sect. 3.3.4. Furthermore, we make the assumption of an ideal hierarchical beamforming codebook for the analysis:

Assumption 4. *The beam formed by the beamforming vector* $\mathbf{w} \in \mathcal{W}^S$ *corresponding to* $\tilde{\mathbf{w}}_{[l,k]}$ *has constant beamforming power gain for any signal of AoA* $\phi \in D_l^k$ *and rejects any signal outside of* D_l^k*, i.e.*

$$|\mathbf{w}^H \mathbf{a}(\phi)| = \begin{cases} G_l, & \text{if } \phi \in D_l^k \\ 0, & \text{if } \phi \notin D_l^k \end{cases}. \tag{3.25}$$

Remark 4. Assumption 4 is mainly for better presentation. This assumption is approximately true when we have massive number of antennas $N \gg \frac{1}{\delta}$. The deterioration of performance due to the imperfect beamforming, such as that resulting from sidelobe leakage, is not the focus of our analysis. In our numerical simulations, however, we will remove this assumption by investigating the performance of the algorithms under the actual beamforming pattern with finite number of antennas.

Under the 1-bit measurement $z_t = \mathbb{1}(|y_t| > v_t)$ with Assumption 4 and the optimal choice of the threshold v_t in Lemma 11, the flipping probability $p_t(\phi)$ of the Bernoulli noise in (3.22) is independent of the AoA ϕ and only depends on the beamforming codeword level l_t selected at time t. In particular, we have

$$p_t(\phi) = p[l_t] := \int_0^{v_t} \text{Rice}(x; PG_l^2, \sigma^2)\, dx, \tag{3.26}$$

where $p[l] > p[l+1]$ and $p[l] \to 0$ since $G_l < G_{l+1}$ and $G_l \to \infty$ as $l \to \infty$ (assuming unlimited number of antenna) by the design of the codebook. Furthermore, we assume that $\log_2(1/\delta)$ is an integer. Now we are ready to give an upper bound of the expected stopping time $\tau_{\epsilon,\delta}$ with resolution $\frac{1}{\delta}$ and outage probability ϵ of the proposed $hiePM$ sequential beam search algorithm:

Theorem 3. *By using codebook* $\mathcal{W}^S$ *with* $S = \log_2(1/\delta)$ *levels and assuming the perfect beamforming assumption (Assumption 4) and the 1-bit measurement model* $z_t = \mathbb{1}(|y_t| > v_t)$ *with the*

optimal choice of v_t in Lemma 11, the expected stopping time of $hiePM$, of resolution $\frac{1}{\delta}$ and error probability ϵ, can be upper bounded by

$$\mathbb{E}[\tau_{\epsilon,\delta}] \leq \frac{\log(1/\delta)}{R_h} + \frac{\log(1/\epsilon)}{E_h} + o(\log(\frac{1}{\delta\epsilon})), \tag{3.27}$$

where $E_h = C_1(p[\log_2(1/\delta)])$, $R_h = I(1/3; p[l'])$ with $l' = \left\lfloor \frac{K_0 \lceil \log\log \frac{1}{\delta} \rceil}{\log 2} - 1 \right\rfloor$ and K_0 is a constant defined in Lemma 14.

Proof. See Appendix B.3 □

Corollary 4. *Let, $\mathbb{E}[\tau_{\epsilon,\delta}] = n$. For all values of δ such that $\delta \leq 2^{-nR_h}$, the error probability of $hiePM$ can be approximately upper bounded by*

$$\mathbb{P}|\hat{\phi} - \phi| > \delta \lessapprox \exp\left(-nE_h\left(1 - \frac{\log(1/\delta)}{nR_h}\right)\right) \tag{3.28}$$

when δ is small enough.

Corollary 5. *Under the same conditions and by Theorem 3, $hiePM$ achieves acquisition rate*

$$\begin{aligned} \lim_{\delta\to 0} \frac{\log(1/\delta)}{\mathbb{E}[\tau_{\epsilon,\delta}]} &\geq \lim_{\delta\to 0} R_h \\ &= \lim_{\delta\to 0} I(1/3; p^*(\delta,\epsilon)) = 1 \end{aligned} \tag{3.29}$$

for arbitrarily small error $\epsilon > 0$, and error exponent

$$\lim_{\epsilon\to 0} \frac{\log(1/\epsilon)}{\mathbb{E}[\tau_{\epsilon,\delta}]} \geq \lim_{\epsilon\to 0} E_h = C_1(p[\log_2(1/\delta)]) \tag{3.30}$$

for any $\delta > 0$.

Remark 5. The integer assumption of $\log_2(1/\delta)$ is for notational simplicity. If the desired resolution $1/\delta$ is not of power of 2, one can simply take a higher resolution $1/\delta' = 2^{\lceil \log_2(1/\delta) \rceil}$. The corresponding upper bound in Theorem 3 can be written accordingly and the conclusion in Corollary 5 remains true.

Remark 6. The rate of one in equation (3.29) implies that $hiePM$ performs asymptotically ($\delta \to 0$) in the same manner as a *noiseless* bisection search which is the optimal usage of the hierarchical beamforming codebook $\mathcal{W}^S$. The asymptotically noiseless behavior is due to the facts that $hiePM$ shrinks the angular region of the search $\|\tilde{\mathbf{w}}\|_0$ quickly, and that together with Assumption 4 an unlimited number of antennas allow the beamforming gain $|\mathbf{w}^H\mathbf{a}(\phi)|^2 = \frac{\pi}{|D_l^k|} \to \infty$ as $l \to \infty$. Compared with other beam alignment algorithms, non-adaptive random coding based strategies [49] are not able to shrink the region of the search beam. Therefore, the corresponding acquisition rate of [49] rate is strictly lesser than 1. On the other hand, the adaptive noisy vanilla bisection algorithm in [46] has rate zero even though the region of the search beam shrinks over time. This is due to the fact that the noisy bisection of [46], in effect, employs repetition coding which has rate zero even with feedback (adaptivity).

Remark 7. To further compare our theoretical result of $hiePM$ with prior works, we plot Corollary 5 together with error probability upper bounds of [46] and [49] in Fig. 3.5 with $\mathbb{E}[\tau] = 28$, $1/\delta = 128$ and $|\theta_{\text{max}} - \theta_{\text{min}}| = 120^o$ and the ideal beamforming assumption (Assumption 4). For the bisection algorithm of [46], we take the upper bound from the author's analysis for equal power allocation with fixed fading coefficient $\alpha = 1$. While for the random hashing of [49], we take an optimization of the number of directions over Gallager's random coding bound of BSC as

$$P_e \leq \min_q \exp\left(-28 \times E_{RC}(q)\right), \tag{3.31}$$

where $E_{RC}(q) = \max_{0\leq\rho\leq 1}\left(E_0(\rho, q) - \rho \times \frac{\log_2(128)}{28}\right)$ and

$$\begin{aligned} E_0(\rho, q) = -\log\Bigg(&\left(q(p_q)^{\frac{1}{1+\rho}}(1-q)(1-p_q)^{\frac{1}{1+\rho}}\right)^{1+\rho} \\ &+ \left(q(1-p_q)^{\frac{1}{1+\rho}} + (1-q)(p_q)^{\frac{1}{1+\rho}})\right)^{1+\rho}\Bigg) \end{aligned} \tag{3.32}$$

with

$$p(q) := \int_0^{v_t} \text{Rice}(x; P\frac{3}{2q}, \sigma^2)\, dx, \tag{3.33}$$

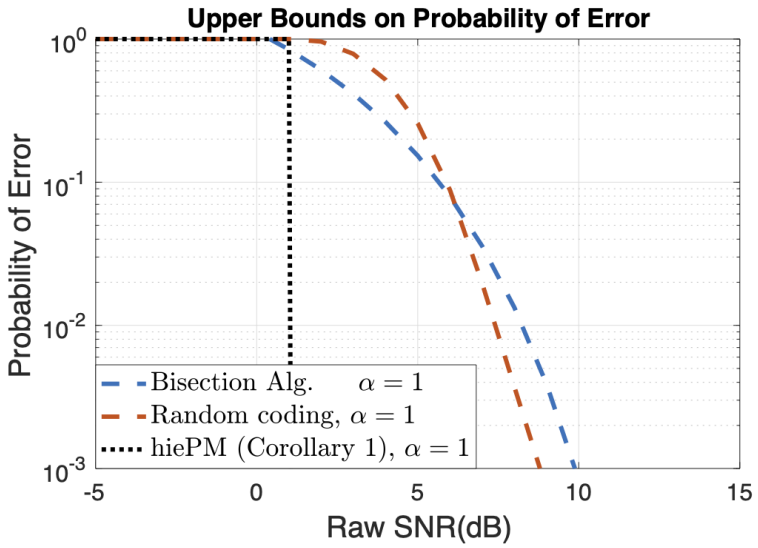

Figure 3.5: Comparison of the theoretical upper bounds on error probability between $hiePM$, random coding, and the bisection algorithm of [46] as a function of raw SNR P/σ^2. The upper bound on $hiePM$ is given by Corollary 4. While the upper bound on random coding is given by Gallager's bound as in (3.31), and the upper bound on the bisection algorithm is provided by [46].

where again v_t is optimally chosen according to Lemma 11. The illustration of Corollary 5 in Fig. 3.5 predicts the superior performance of $hiePM$ over the prior works [46] and [49]. We note that for these upper bounds, $hiePM$ and random hashing of [49] assume a 1-bit quantizer, whereas the bisection method of [46] is favorably given the unquantized amplitude information. We will further show in numerical simulation (Fig. 3.7) that with practical beam patterns and unquantized measurements, the actual performance of $hiePM$ is not only indeed better than the prior works, but in fact achieves a significantly smaller error probability than our theoretical upper bound. Furthermore, we will see that the non-adaptive random hashing based method in [49] in fact outperforms the adaptive bisection in [46] due to the lack of good coding in [46].

3.5 Numerical Results

In this section, we compare the performance of our proposed *hiePM* algorithms against the bisection algorithm of [46] and an optimized random-code-based strategy, which is taken as an upper bound on the performance of the random hash-based solution of [49]. Before we proceed

with this performance analysis, however, we first provide a summary of the simulation setup and parameters.

3.5.1 Simulation Setup and Parameters

We use the hybrid analog/digital system architecture described in Sect. 3.2, where the BS has $N = 64$ antenna elements in a uniform linear array with antenna spacing $\frac{\lambda}{2}$, and the user has a single (virtual) antenna. Furthermore, due to the use of orthogonal spreading sequences, we focus on the single user case $K = 1$. The channel consists of a single path with fast fading coefficient α. The rule-of-thumb [59] estimate of channel coherence time given by

$$T_c \approx \frac{0.432}{f_m} = \frac{0.432c}{f_c v}, \tag{3.34}$$

where c is the speed light, f_c is the carrier frequency, and v is the user speed. So even for mmWave communication with 73GHz, at walking speed (< 3 km/hour) the coherence time is

$$T_c = \frac{0.432 \times 3 \times 10^9 \text{ (m/s)}}{73 \times 10^9 \text{ (Hz)} \times 3 \text{ (km/hour)}} \approx 8.127 \text{ milliseconds}. \tag{3.35}$$

Note that, additionally, narrow beamforming and the existence of a dominant sub-path (e.g. Line-of-Sight) can both increase the coherence time significantly [60]. Therefore, in Sect. 3.5.3 we assume that the fading coefficient α is static during the entire initial access duration of 2 milliseconds (ms). We consider both the case when the fading coefficient α is known exactly $\hat{\alpha} = \alpha$, and the case when it is estimated with the estimation inaccuracy modeled as $\hat{\alpha} \sim \mathcal{CN}(\alpha, \sigma_\alpha^2)$. In Sect. 3.5.4 we further study the robustness of $hiePM$ with a static estimate of the time varying fading coefficient α_t of a Rician AR-1 model with a coherence time corresponding to higher user mobility. Finally, we consider learning the AoA with an angular resolution of $1/\delta = 128$, and an (expected) stopping time of $E[\tau] = 28$, i.e., with $E[\tau]$ selections of beamforming vectors, hence, samples.

To provide a sense for the above normalized parameters, let us consider some candidate PHY layer solutions. In particular, when using the 5G new radio Physical Random Access Channel

(PRACH) format B4 [61], the $E[\tau] = 28$ samples translate to less than 2 ms acquisition time for sub-1-degree angular resolution within a $[0°, 120°]$ sector. We present our results as a function of raw SNR $\frac{P}{\sigma^2}$ to get a sense for reasonable values of SNR. In Fig. 3.6 we compute and illustrate the expected distance at which a target raw SNR is obtained. We consider a case under the 3GPP TR 38.901 UMi LOS pathloss channel model (summarized in [62]), with 23 dBm maximum user power, -174 dBm/Hz thermal noise density, 5 dB receiver noise figure at BS, with a bandwidth of 100 MHz. As seen in Fig. 3.6, one can argue that given our selection of this PHY layer and parameters, the practical raw SNR regime of interest is within -15 dB to 10 dB.

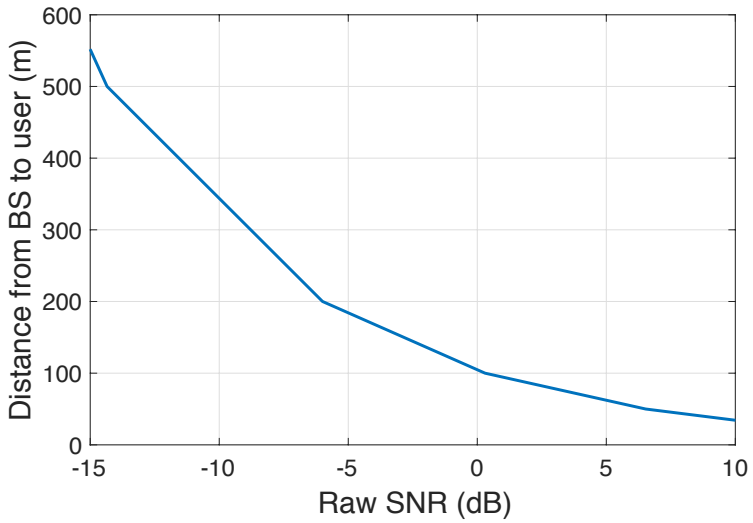

Figure 3.6: Relationship between raw SNR P/σ^2 and distance from BS to user, under the 3GPP TR 38.901 UMi LOS pathloss channel model (summarized in [62]), with 73GHz carrier frequency, 23 dBm maximum user power, -174 dBm/Hz thermal noise density, 5 dB receiver noise figure at BS, and a bandwidth of 100 MHz.

3.5.2 Algorithm Details and Parameters

Like the the bisection algorithm of [46], our proposed algorithm *hiePM* is based on sequential beam refinement, but implements additional coding techniques. Thus, we focus our comparison to the bisection refinement of [46] to highlight that the use of this coding strategy differentiates *hiePM* from existing beam refinement strategies. For the bisection algorithm of [46], the number of beamforming vectors in each level is 2, and the power is allocated according to the equal power

distribution strategy.

For both $hiePM$ and the bisection algorithm of [46], the finite set of beamforming vectors $\mathcal{W}^S$ are designed with a hierarchical structure, where individual beamforming vectors $\mathbf{w}$ with corresponding $\tilde{\mathbf{w}}_{[l,k]}$ are designed with the objective of near constant gain for signal directions with AoA $\phi \in \mathcal{D}_l^k$ and zero otherwise (Assumption 4). In other words, each beamforming vector solves

$$\mathbf{A}_{BS}^H \mathbf{w} = C_s \tilde{\mathbf{w}}_{[l,k]}, \tag{3.36}$$

where $\mathbf{A}_{BS}$ is the $N \times (1/\delta)$ matrix of array manifolds

$$\mathbf{A}_{BS} = [\mathbf{a}(\phi_1); \mathbf{a}(\phi_2); \ldots; \mathbf{a}(\phi_{1/\delta})] \tag{3.37}$$

and C_s is a normalization constant. An approximate solution to (3.36), obtained using the pseudo inverse, is

$$\mathbf{w}^* = C_s (\mathbf{A}_{BS} \mathbf{A}_{BS}^H)^{-1} \mathbf{A}_{BS} \tilde{\mathbf{w}}_{[l,k]}. \tag{3.38}$$

The resulting beamforming weight vectors, applied with phase and gain control at each element, produce beam patterns with improved sidelobe suppression, and near constant gain in the intended probing directions. We can use these vectors in our simulations to ensure that our analytic Assumption 4 is a matter of analytic simplicity but is not consequential in a practical setting.

To represent non-adaptive algorithms that are a variation of random coding, such as the random hashing algorithm of [49], we compare to the random search algorithm that randomly scans the region of interest. The random search algorithm uses a codebook $\mathcal{W}^{\frac{q}{n}}$ with finite cardinality, i.e. size $\binom{n}{q}$, which consists of all possible beam patterns with total width $\frac{q}{n}|\theta_{\text{max}} - \theta_{\text{min}}|$, where the region of interest $|\theta_{\text{max}} - \theta_{\text{min}}|$ has been divided into n non-overlapping directions, and q directions are probed in each beam pattern. At any time instant t, the random search algorithm randomly selects a beamforming vector $\mathbf{w}_{t+1}$ from the pre-designed codebook $\mathcal{W}^{\frac{q}{n}}$. A fixed number of measurements τ are taken according to (3.15) and the final beamforming vector is selected according to (3.16) and (3.17). The discretization parameter is set to $n = 1/\delta = 128$, we set $\tau = 28$, and we plot various

values of q. The performance of $hiePM$ over the optimized choice of q is important as it provides a first order insight into "adaptivity gain."

3.5.3 Simulation Results

In this section, we provide a comparative analysis of our proposed *hiePM* algorithm against prior work [46] and [49]. In particular, Fig. 3.7 plots the error probability as a function of raw SNR. In summary, Fig. 3.7 shows that both fixed-length and variable-length stopping variations of *hiePM* outperform the bisection algorithm of [46] as well as random coding, or random-hash based solutions of [49]. We also note that random beamforming codebooks outperform the bisection algorithm of [46], as expected by our analysis in Remark 6. By optimizing the coding rate q, and comparing against *hiePM*, one can also fully characterize the adaptivity gain. Finally, we note that our analytic upper bound (in Fig. 3.5) is rather loose and $hiePM$ performs significantly better than our analysis predicted.

Probability of Error versus Raw SNR

For the system and channel described above, we conduct the simulation scenario where the average error probability as a function of raw SNR is analyzed. We take the error probability of the AoA estimation to be the probability of selecting an erroneous final beamforming vector $\text{Prob}\{\hat{\mathbf{w}}(z_{1:\tau}, \mathbf{w}_{1:\tau}, \epsilon, \delta) \neq \mathbf{w}(\{\phi\})\}$.

For clarity, from now on we use the naming convention *hiePM(stopping-criterion, resolution-criterion)* to specify the case selections of stopping criteria and resolution-criteria in the proposed *hiePM* algorithm (detailed in Alg. 1). To ensure a reasonable comparison, we first discuss *hiePM*(FL, FR) which is most comparable to the bisection algorithm of [46] and the random search algorithm described above. Fig. 3.7 shows the superior performance of *hiePM*(FL, FR) with fixed and known fading coefficient $\alpha = 1$ over both the bisection algorithm of [46] and the random search algorithm. We also notice that under reasonable tuning of parameter q, even the non-adaptive random search algorithm achieves better performance than the adaptive bisection algorithm of [46]. As we expected

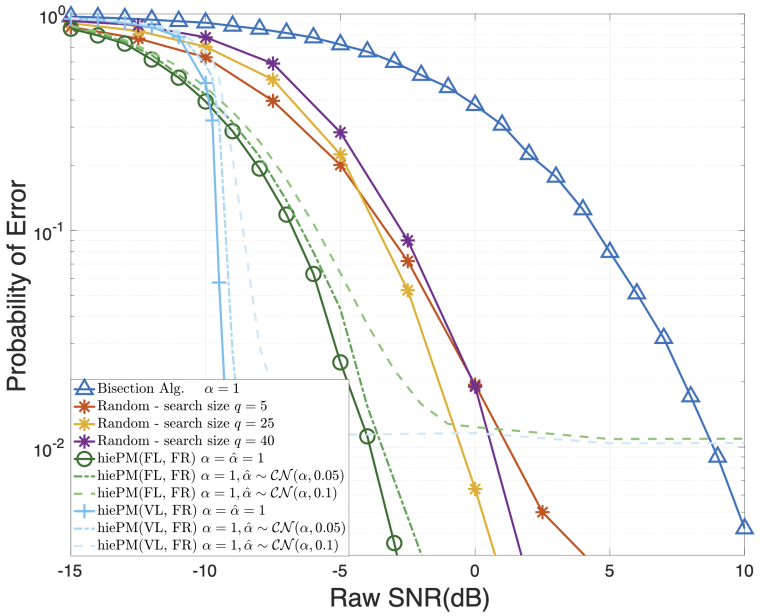

Figure 3.7: Comparison of the error probability between *hiePM*, the random search algorithm, and the vanilla bisection algorithm of [46] as a function of raw SNR P/σ^2. Initial access length $\tau = 28$, achieved under 2 ms using the 5G NR PRACH format B4 [61] ($E[\tau] = 28$ for variable-length stopping type), is used for acquiring the AoA with resolution $1/\delta = 128$.

from Remark 6, the best performance is achieved by *hiePM* due to its sequential coding strategy, while the performance of the bisection algorithm of [46] suffers as it resembles a repetition code.

Improvements in the probability of error are further demonstrated by *hiePM*(VL, FR) with targeted error probability ϵ selected such that $\mathbb{E}[\tau] = 28$, i.e., the parameter ϵ is strategically chosen (usually ϵ is large), such that *hiePM*(VL, FR) has an expected duration of the initial access phase equal to the duration of the fixed-length variations, this ensures a fair comparison. Of course, ϵ may be selected to be close to zero, thereby ensuring the best error probability and aquisition rate at the cost of a longer initial access phase duration. The benefit of allowing a variable stopping time is evident in that it causes a sharp drop in the error probability at approximately -10 dB raw SNR. The error probability upper bound (Corollary 4) on *hiePM*(VL, FR) is also plotted. We see in Fig. 3.7 that this upper bound predicts the sharp slope of *hiePM*(VL, FR), theoretically guaranteeing a significant performance improvement in error probability for *hiePM*(VL, FR) over the bisection algorithm of [46] and the random search algorithm for large SNR. A further exploration of this sharp transition in the low (< 0 dB) raw SNR regime is beyond the scope of this paper.

Investigating effects of imperfect channel knowledge

The bisection algorithm of [46] learns the AoA without any knowledge of the channel. It combines the procedures of AoA estimation and channel estimation. On the other hand our proposed algorithm *hiePM*, requires knowledge of the fading coefficient α in the posterior update of Alg. 1 (3.16). While a channel estimation procedure can be used to learn α preceding *hiePM*, perhaps in a short preliminary phase, we explore the performance achieved using an estimate for the fading coefficient $\hat{\alpha}$ instead. We find that the improved performance by *hiePM* over the bisection algorithm of [46] and the random search algorithm holds even without full knowledge of the fading coefficient α. To see this we consider the case of a mismatched update rule (3.16) with an estimate for the fading coefficient $\hat{\alpha} = \mathcal{CN}(\alpha, \sigma_\alpha^2)$. We see that even under a reasonably mismatched estimate of the fading coefficient ($\sigma_\alpha^2 = 0.05$), all *hiePM* based algorithms still achieve a lower probability of error than the bisection algorithm of [46]. In other words, the degradation due to estimation error is far less significant, saturating in error probability only at very large SNR (> 5 dB). As we can see in Fig. 3.7 using a mismatched estimate of the fading coefficient α causes the performance of probability of error to saturate at large SNR (> 0 dB). This reflects the times when the estimate of the fading coefficient α is very inaccurate, which will occur with a constant probability regardless of the SNR value, due to our modeling of $\hat{\alpha}$. In practice, the accuracy of the estimate $\hat{\alpha}$ will improve as SNR increases. However, this is beyond the scope of this chapter and we refrain from investigating such effects.

Spectral efficiency versus Raw SNR

Practically speaking, a more efficient AoA learning algorithm is advantageous in that it both reduces communication overhead and increases the accuracy of the final beamforming vector. Next, we empirically analyze the overall performance of a communication link established by the proposed algorithm *hiePM* in terms of the data spectral efficiency. The spectral efficiency is evaluated according to equation (3.8), using the final beamforming vector $\hat{\mathbf{w}}(z_{1:\tau}, \mathbf{w}_{1:\tau}, \epsilon, \delta)$ resulting from each algorithm. Due to its dependence on the final beamforming vector $\hat{\mathbf{w}}$, the

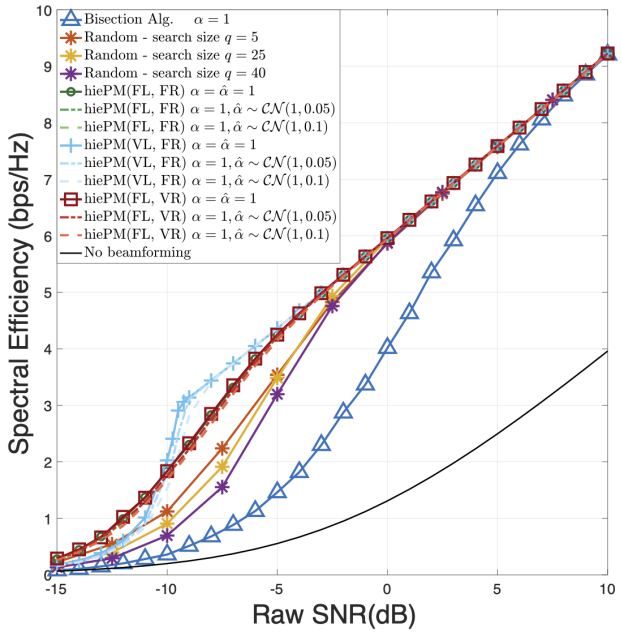

Figure 3.8: Comparison of the spectral efficiency, given by (3.8), obtained by *hiePM*, the random search algorithm, and the vanilla bisection algorithm of [46] as a function of raw SNR P/σ^2. Initial access time $\tau = 28$, achieved under 2 ms using the 5G NR PRACH format B4 [61] ($E[\tau] = 28$ for variable-length stopping).

spectral efficiency encompasses both the design parameters ϵ and δ, which have been the focus of our analysis, while still providing an intuitive practical measure. We set the total communication time frame to $T = 100 \times \mathbb{E}[\tau]$ (further optimization of this parameter beyond the scope of this paper).

Fig. 3.8 shows the gain in spectral efficiency obtained by various implementations of the proposed algorithm *hiePM* over both the bisection algorithm of [46] and the random search algorithm for the system and channel described above as a function of raw SNR. The spectral efficiency when no beamforming is used is provided for reference. Fig. 3.8 shows that all variants of *hiePM* outperform the bisection algorithm of [46] significantly in the raw SNR regime of (-5dB to 5dB). On the other hand, the performance of the bisection algorithm of [46] approaches the performance of *hiePM* as raw SNR grows beyond 7dB or so. Fig. 3.8 also shows the benefits of opportunistically selecting the resolution of the final beam as is done under *hiePM*(FL, VR) according to (3.18). This is particularly important in very low raw SNR models (-15dB to -7dB) where *hiePM*(FL, VR) adapts the final beamforming vector to the final posterior distribution at

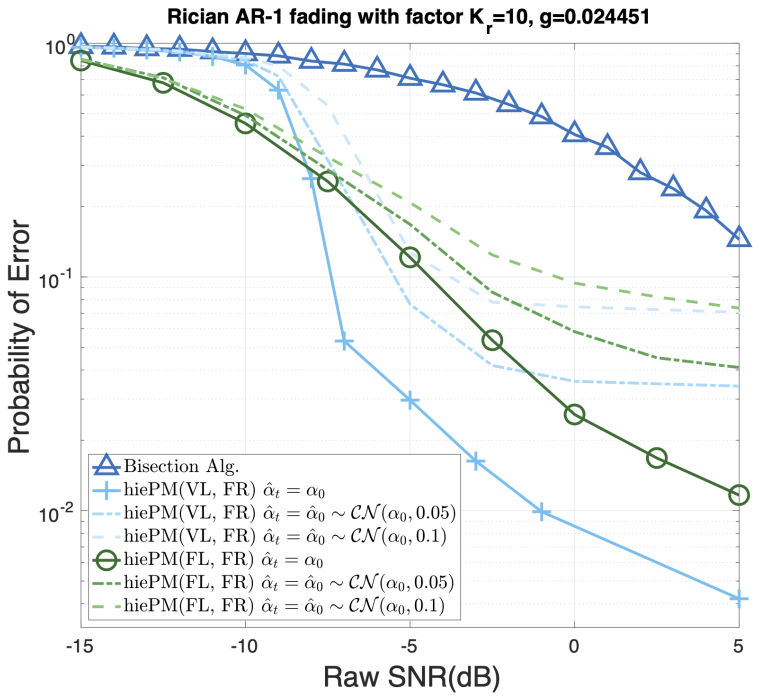

Figure 3.9: Comparison of the error probability as a function of raw SNR P/σ^2 under Rician AR-1 fading with factor $K_r = 10$, and $g = 0.024451$ (i.e. $T_c = 2$). Initial access length $\tau = 28$, achieved under 2 ms using the 5G NR PRACH format B4 [61] ($E[\tau] = 28$ for variable-length stopping type), is used for acquiring the AoA with resolution $1/\delta = 128$.

time τ, hence setting the angular resolution of the communication beam in an opportunistic manner. Even more importantly, this significant performance improvement is robust to channel estimation error and mismatched estimate of the fading coefficient $\hat{\alpha}$. To understand this phenomenon we refer to Fig. 3.7, where the error probability of finding the correct beam with resolution $1/\delta$, when SNR is less than -5dB, is non-negligible under *hiePM*(FL, FR), and *hiePM*(VL, FR).

3.5.4 Time varying channel

In this subsection, we will discuss the channel coherence time and how our initial beam alignment algorithm works in a time-varying channel scenario. We verify our framework by extending our algorithms to be adapted to a simple Rician AR-1 model. Let us consider a Rician AR-1 fading channel of factor K_r with perfect knowledge of the operating SNR (large-scale fading)

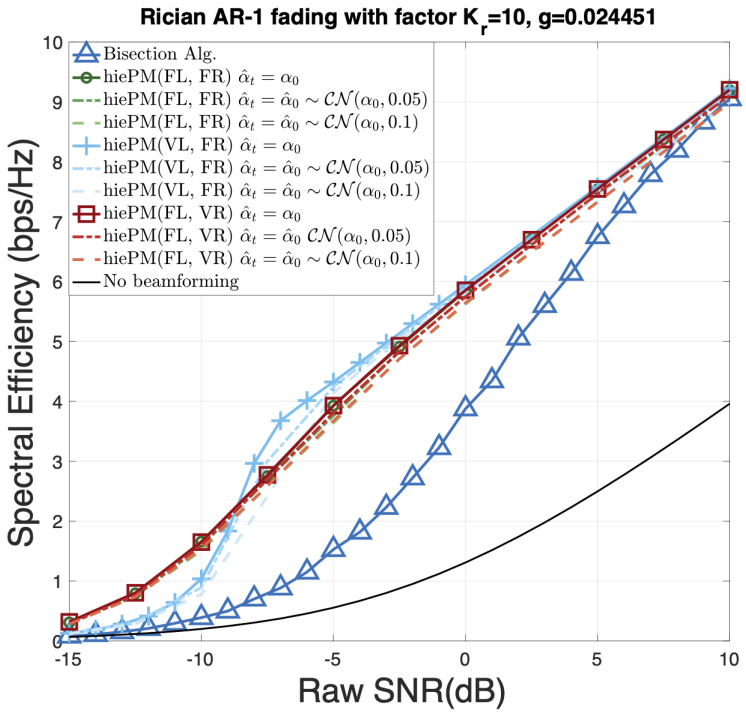

Figure 3.10: Comparison of the spectral efficiency, given by (3.8), obtained by *hiePM* and the vanilla bisection algorithm of [46] as a function of raw SNR P/σ^2 under Rician AR-1 fading with factor $K_r = 10$, and $g = 0.024451$, (i.e. $T_c = 2$). Initial access time $\tau = 28$, achieved under 2 ms using the 5G NR PRACH format B4 [61] ($E[\tau] = 28$ for variable-length stopping).

as well as perfect frequency/phase synchronization, i.e. the fading coefficient is given as

$$\alpha_t = \sqrt{\frac{K_r}{1+K_r}}\mu + \sqrt{\frac{1}{1+K_r}}\beta_t,\ t = 0,1,2,...,\tau, \tag{3.39}$$

where $\mu = 1$ and $\beta_t \sim CN(0,1)$ is the complex Gaussian diffusion AR process given as

$$\beta_{t+1} = \beta_t\sqrt{1-g} + e_t\sqrt{g},\ \ t = 0,1,2,...,\tau, \tag{3.40}$$

where $e_t \sim \mathcal{CN}(0,1)$ is the independent noise term. The correlation parameter g is set such that

$$1-(1-g)^{14T_c} = 0.5, \tag{3.41}$$

where T_c is the 50% time of the diffusion β_t in ms (recall that we assume a system with 14 beam slots in 1 ms). Combining (3.39) and (3.40), the Rician AR-1 model can be written as

$$\alpha_{t+1} = \sqrt{\frac{K_r}{1+K_r}}\mu + \left(\alpha_t - \sqrt{\frac{K_r}{1+K_r}}\mu\right)\sqrt{1-g} + e_t\sqrt{\frac{g}{1+K_r}},\ \ t = 0,1,2,...,\tau. \tag{3.42}$$

Fig. 3.9 demonstrates the robustness of $hiePM$ to the Rician AR-1 fading channel model described above with coherence time $T_c = 2$ ms of the AR process β_t, and a Rician factor $K_r = 10$ (this is a reasonable value, e.g. indoor mmWave channel models [63]). We again use an erroneous/mismatched and fixed estimate of the fading coefficient $\hat{\alpha}_t = \hat{\alpha}_0 \sim \mathcal{CN}(\alpha_0, \sigma_\alpha^2)$ for $t = 1,2,\ldots,\tau$. In particular, we compare the performance achieved by our $hiePM$ algorithms with different degrees of knowledge of the fading estimate (i.e. $\sigma_\alpha^2 = 0, 0.05, 0.1$) against the performance obtained by the bisection algorithm of [46]. As expected, the performance of the probability of error worsens for both algorithms in a time-varying fading, as compared to the static model $\alpha = 1$ in Fig. 3.7. However, even under a mismatched and fixed estimate of the fading coefficient $\hat{\alpha}_t$, our main conclusions still hold. In particular, the performance degradation in spectral efficiency due to the time-varying channel is almost negligible, as we show in Fig. 3.10. Note that, this is the

effect of the time-varying channel during the initial access phase, whereas in the communication phase the spectral efficiency is calculated by (3.8) because our focus is the impact of a time-varying channel on the initial beam alignment. Our variable resolution algorithm $hiePM$(FL,VR) (with opportunistic choice of final beamwidth) is unaffected in terms of spectral efficiency, while the $hiePM$(FL,FR) and $hiePM$(VL,FR) cases incur a small loss of spectral efficiency due to the degree of the mismatched estimate (correlated to the severity of σ_α^2).

3.6 Conclusion

In this paper, we addressed the initial access problem for mmWave communication with beamforming techniques. With a single-path channel model, the proposed sequential beam search algorithm $hiePM$ demonstrates a systematic way of actively learning an optimal beamforming vector from the hierarchical beamforming codebook of [46].

Using a single-path channel model, we characterize the performance of the proposed learning algorithm $hiePM$ by the resolution and the error probability of learning the AoA, which are closely related to the link quality established by the final beamforming vector. We analyze $hiePM$ by giving an upper bound on the expected search time $\tau_{\epsilon,\delta}$ required to achieve a resolution $\frac{1}{\delta}$ and error probability ϵ in Theorem 3. As a corollary, we provide an upper bound on the error probability achieved with a search time $\mathbb{E}[\tau_{\epsilon,\delta}]$, and resolution $\frac{1}{\delta}$ for $hiePM$ in Corollary 4. We also specialize our analysis and compare the error exponent obtained by $hiePM$ and the bisection algorithm of [46]. A higher error exponent is shown across a wide range of raw SNR even when only 1-bit of information about the measurement is available to $hiePM$. The numerical simulations show a significant improvement on the spectral efficiency over the previous vanilla bisection algorithm of [46] and the random search algorithm modeled as a best case of [49, 50], demonstrating a first work of possible standalone mmWave communication.

Future directions of this work include generalizing the channel model and considering multiple paths, as well as learning the fading coefficient together with the direction during beam

search. On the theoretical end, closing the gap between the upper bound of error probability and its actual performance (demonstrated in Fig. 3.7) is worth pursuing for theoretical interest. On the practical side, reducing the computation complexity of the posterior calculations and required statistics will be helpful for implementation purposes.

Chapter 3, in full, is a reprint of the material as it appears in the article: Sung-En Chiu, Nancy Ronquillo, and Tara Javidi, “Active Learning and CSI Acquisition for mmWave Initial Alignment," IEEE Journal on Selected Areas in Communications, vol.37, issue 11, pp. 2474 - 2489,Dec. 2018.The dissertation author was the secondary investigator and co-author of this paper.

Chapter 4

Measurement Dependent Noisy Search with Stochastic Coefficients

4.1 Introduction

Recall the general problem of recovering the unknown time-invariant support of the random vector $\mathbf{X}_t \in \mathbb{R}^M$ via a sequence of noisy linear observations (1.1) discussed in chapter 1. In this chapter, we consider one step towards solving the more general problem (1.1) by considering a special case where $\mathbf{X}_t$ can be written as $X_t\mathbf{W}$, i.e. the product of a stochastic coefficient X_t and an unknown unit common support vector $\mathbf{W} = \text{supp}(\mathbf{X}_t)$. This model is related to the problem of sparse Bayesian Learning and more closely to the problem of joint sparse support recovery [19, 24], where the goal is to reconstruct a sparse common support vector via noisy compressed data, with the additional caveat of measurement dependent noise. With sufficiently high signal to noise ratio (SNR), existing sparse recovery methods successfully recover $\text{supp}(\mathbf{X}_t)$ with no prior information (see [20–25] and references therein) assuming sufficiently large SNR. These methods focus largely on the reconstruction of $\text{supp}(\mathbf{X}_t)$ only while the acquisition measurement vectors $\mathbf{A}_t$ are selected in an off-line manner, i.e. measurement strategies are not adapted to the observations. However, under the condition of measurement dependent noise the performance of these methods significantly

drops with a drop in SNR. Thus, the measurement dependency phenomenon makes sequential acquisition methods interesting solutions to investigate.

This setup lies at the intersection of sparse recovery, group-testing, and measurement-dependent noisy search.Common support recovery is addressed by the group testing with noise literature as in [64, 65]. The recovery of $\mathbf{W} = \text{supp}(\mathbf{X}_t)$ under measurement dependent noise is cast as problem of channel coding over a Multiple Access Channel (MAC) with feedback by considering a practical target localization problem in multiband spectrum sensing. The special case of extreme sparsity, i.e. $\|\text{supp}(\mathbf{X}_t)\|_0 = 1$, this becomes equivalent to the problem of single target search with measurement dependent noise where the target is the location of the non-zero element of $\mathbf{X}_t$ [6, 66], we cast this problem as a binary input and Gaussian noise channel with state and feedback in Sect. 2.2. We propose two algorithms for sequentially designing measurement vectors $\mathbf{A}_t$, which augment the learning of $\mathbf{W}$ to include simultaneous estimation of X_t in order to mitigate the effects of unknown stochastic coefficients. The first is a posterior matching-based scheme applied to the discrete marginal probability estimate of $\mathbf{W}$. In light of excessive computations required to compute the Bayesian posterior, we develop a heuristic approximation with lower memory complexity. This second strategy complements the sequential design of the measurement vectors with an estimate of X_t via a Kalman Filter. Numerically, we show improvements over randomized algorithms that design (randomized) measurements a priori. This demonstrates the advantage of the sequential (proposed) strategies in critically small SNR ($\frac{1}{\sigma^2} < 20$) when the budget of observations is small. In the second part of this chapter we pose the mmWave initial alignment problem discussed in chapter 3 as equivalent to the probelm of measurement dependent noise with stochastic coefficients and extend the proposed algorithms to this context for handling stochastic channel fading, which consist of two schemes for sequentially selecting beamforming vectors in order to lear the dynamic channel state information in an active manner.

4.2 Part I: General Formulation

4.2.1 Problem Set-up

Let $\mathbf{W} = \{0,1\}^M$ denote an unknown support vector, and $X_t \in \mathbb{R}$ denote a stochastic multiplicative coefficient. Y_t is the observation at time t given by

$$Y_t = X_t \mathbf{A}_t^\intercal \mathbf{W} + N_t(\mathbf{A}_t). \tag{4.1}$$

Binary measurement vectors $\mathbf{A}_t \in \mathcal{A} = \{0,1\}^M$ are applied to observations, however they do not affect $\mathbf{W}$ or X_t. In this work we consider a linear model for the measurement dependent noise, i.e., observations are subject to i.i.d. $N_t(\mathbf{A}_t) \sim \mathcal{N}(0, \|\mathbf{A}_t\|_0 \sigma^2)$, where perfect knowledge of the variance σ^2 is assumed. The observation vector $Y_{1:\tau} = [Y_1, Y_2, \ldots, Y_\tau]$ contains noisy information about the unknown sparse vector $\mathbf{W}$. An agent has the objective of finding a sequence of measurement vectors $\mathbf{A}_{1:\tau} = [\mathbf{A}_1, \mathbf{A}_2, \ldots, \mathbf{A}_\tau]$ that minimize the distortion, as measured by a bivariate distortion function $D(\cdot,\cdot)$, in estimating $\mathbf{W}$ subject to a fixed number of measurements, i.e.,

$$\text{minimize } \mathbb{E}[D(\hat{\mathbf{W}}, \mathbf{W}) | Y_{1:\tau}, \mathbf{A}_{1:\tau}] \tag{4.2}$$

subject to $\tau = T$. In this chapter, we restrict our attention to a $0/1$ distortion for the accuracy of the final estimate $\hat{\mathbf{W}}$, i.e. we aim to minimize the probability of error

$$P_e = \mathbb{P}(\hat{\mathbf{W}} \neq \mathbf{W} | Y_{1:\tau}, \mathbf{A}_{1:\tau}). \tag{4.3}$$

In sparse problem formulations, $\mathbf{W}$ is assumed to be sparse with at most k non-zero entries. In this work we consider the special case where $k = 1$, which is equivalent to the problem of searching for the true location of single 1 in $\mathbf{W}$. Thus, we can write more simply $\mathbf{W} \in \{\mathbf{e}_1, \mathbf{e}_2, \ldots, \mathbf{e}_M\}$.

Sequential Policy

For the set-up described above, a sequential noisy search procedure consists of selecting the best measurement vectors $\mathbf{A}_t(Y_{1:t-1}, \mathbf{A}_{1:t-1})$ at each time slot $t = 1, 2, \ldots, \tau$, possibly sequentially in an adaptive manner as function of prior observations. Observations Y_t in (4.1) can be thought of as the probing of certain locations (indicated by $\mathbf{A}_t$), which give information about the presence or absence of the target 1 element of $\mathbf{W}$ in these locations. After τ measurements, an estimate $\hat{\mathbf{W}}$ about the location of the single target 1 is made. In this chapter, we focus on strategies with sequential refinement of the search space. More specifically, at time t a measurement vector $\mathbf{A}_t(Y_{1:t-1}, \mathbf{A}_{1:t-1})$ is selected sequentially with the aim of probing a fewer number of locations over time.

(Marginal) Posterior Belief

Let us model $\mathbf{W}$ and X_t as a random vector with joint probability distribution $f_{\mathbf{W},\mathbf{X}_t}(\mathbf{e}_i, x)$. The marginal probability belief of $\mathbf{W}$ after reception of $Y_{1:t}$ is $\boldsymbol{\pi}^{\mathbf{W}}(t) \in [0,1]^M$, where each element is:

$$\pi_i(t) := \mathbb{P}(\mathbf{W} = \mathbf{e}_i | y_{1:t}) = \int_{-\infty}^{\infty} f_{\mathbf{W},X_t|Y_{1:t}}(\mathbf{e}_i, x | y_{1:t}) dx \tag{4.4}$$

for $i = 1, 2, ..., M$. We write an update for the posterior probability $\boldsymbol{\pi}^{\mathbf{W}}(t)$, upon receiving y_t, using Bayes' Rule:

$$\pi_i(t) = \frac{f_{Y_t|\mathbf{W},Y_{1:t-1}}(y_t|\mathbf{e}_i, y_{1:t-1})\pi_i(t-1)}{\sum_{i'=1}^{M} f_{Y_t|\mathbf{W},Y_{1:t-1}}(y_t|\mathbf{e}_{i'}, y_{1:t-1})\pi_{i'}(t-1)}. \tag{4.5}$$

The conditional distribution is:

$$
\begin{aligned}
& f_{Y_t|\mathbf{W},Y_{1:t-1}}(y_t|\mathbf{e}_i, y_{1:t-1}) \\
& \approx \int_{-\infty}^{\infty} \frac{1}{G_i} f_{X_t|\mathbf{W},Y_{1:t-1}}\Big(\frac{y_t - n}{G_i}|\mathbf{e}_i, y_{1:t-1}\Big) f_{N_t}(n) dn \\
& \overset{(a)}{=} - \int_{-\infty}^{\infty} f_{X_t|\mathbf{W},Y_{1:t-1}}(x|\mathbf{e}_i, y_{1:t-1}) f_{N_t}(y_t - xG_i) dx \\
& \overset{(b)}{=} - \int_{-\infty}^{\infty} f_{X_t|\mathbf{W},Y_{1:t-1}}(x|\mathbf{e}_i, y_{1:t-1}) g\left(\frac{y_t - xG_i}{\sigma_t}\right) dx
\end{aligned}
\tag{4.6}
$$

where recall $N_t(\mathbf{A}_t) \sim \mathcal{N}(0, |\mathbf{A}_t|\sigma^2)$, and where

$$
G_i = \mathbf{A}_t^{\intercal}\mathbf{e}_i, \quad \sigma_t^2 = \|\mathbf{A}_t\|_0 \sigma^2, \tag{4.7}
$$

(a) is by a change of variables, (b) follows by assumption of i.i.d Gaussian noise, and $g(\frac{y-\mu}{\sigma})$ is the density $\mathcal{N}(0,1)$ evaluated at $(\frac{y-\mu}{\sigma})$.

Marginal Posterior Matching

Next, we describe a sequential policy based on marginal sorted posterior matching (*marginalPM*) adapted from [67], where sequential $\mathbf{A}_t(\boldsymbol{\pi}^{\mathbf{W}}(t-1))$ are selected based on the marginal posterior probability of $\mathbf{W}$. Upon reception of a new observation Y_t, $marginalPM$ updates the marginal posterior probability $\boldsymbol{\pi}^{\mathbf{W}}(t)$ according to (4.5) and sorts the values in descending order to obtain $\boldsymbol{\pi}^{\mathbf{W}\downarrow}(t)$. Let $\mathbf{I}_t$ denote the ordered location indices corresponding to $\boldsymbol{\pi}^{\mathbf{W}\downarrow}(t)$. $MarginalPM$ selects the measurement vector such that locations with accumulated probability closest to $\frac{1}{2}$ are probed, selecting

$$
k_t^* \coloneqq \underset{k}{\operatorname{argmin}} \left| \sum_{i=1}^{k} \pi_i^{\mathbf{W}\downarrow}(t) - \frac{1}{2} \right|, \tag{4.8}
$$

and setting the next $\mathbf{A}_{t+1}(j) = 1$ if and only if $j \in \{\mathbf{I}_t(1), \mathbf{I}_t(2), \ldots, \mathbf{I}_t(k_t^*)\}$. The effect is a sequential probing of the possible locations $\{1, 2, \ldots, M\}$, where the number of probed locations, i.e. $\|\mathbf{A}_t\|_0$, decreases over time corresponding to the accumulated belief about $\mathbf{W}$.

Prior Work

The computation of $\boldsymbol{\pi}^{\mathbf{W}}(t)$ depends on the one-step prediction $f_{X_t|\mathbf{W},Y_{1:t-1}}(x|\mathbf{e}_i, y_{1:t-1})$ which itself depends on filtering equation $f_{X_{t-1}|\mathbf{W},Y_{1:t-1}}(x|\mathbf{e}_i, y_{1:t-1})$. In other words, while the main objective is to estimate $\mathbf{W}$, $marginalPM$ and corresponding sequential measurement strategies depend on the designer's ability to predict the dynamics of the coefficient X_t, hence are reminiscent of the general problem of information acquisition and utilization formulated in [66].

The simpler case of known and time-invariant $X_t = x^*$, which can be written as

$$f_{X_t|\mathbf{W},Y_{1:t-1}}(x|\mathbf{e}_i, y_{1:t-1}) = \begin{cases} 1, & \text{if } x = x^* \\ 0, & \text{otherwise,} \end{cases} \tag{4.9}$$

recovers the formulation of our prior work [48] on the problem of noisy search with measurement dependent noise, where $x^* = 1$, discussed in chapter 2. The problem of noisy search with measurement dependent noise has been studied from an information-theoretic perspective where many works have established a connection to the problem of channel coding over a binary input channel with [6, 9, 39, 47, 48, 68] and without [7] feedback. Existing strategies based on posterior matching have been shown to provide theoretical guarantees in performance [6, 9]. Chapter 2 characterizes a lower bound on the gain in performance achieved by an optimal adaptive strategy over non-adaptive ones. We draw on these works, leveraging the connection to channel coding, to develop our adaptive algorithms based on posterior matching expecting a similar adaptivity gain in performance over non-adaptive strategies [20, 21, 23, 69].

4.2.2 Proposed Algorithms

Discrete $marginalPM$

The Bayes' posterior probability update (4.5) may be formulated for any continuous probability density function, however, this may be computationally infeasible. In Alg. 2 we approach the computation of $\boldsymbol{\pi}^{\mathbf{W}}(t)$ by first discretizing X_t over a finite set. First, let $X_t = x_j$ for $j = \{1, 2, \ldots, \frac{1}{\triangle_X}\}$ denote

$$X_t \in [x_j - \frac{\triangle_X}{2}, x_j + \frac{\triangle_X}{2}], \tag{4.10}$$

where $x_j = x_{\text{min}} + \frac{\triangle_X}{2} + (j-1) \times \triangle_X \times (x_{\text{max}} - x_{\text{min}})$ for the total range $X_t \in [x_{\text{min}}, x_{\text{max}}]$. We note that this discretization becomes tight as $\triangle_X \to 0$. A coarser choice of $\triangle_X$ reduces complexity and memory requirements (see Sect. 4.2.4 for a discussion of practical values for these resolution parameters).

Next, $marginalPM$ is applied to select measurement vectors $\mathbf{A}_t(\boldsymbol{\pi}^{\mathbf{W}}(t-1))$ sequentially as a function of the discrete marginal posterior belief on $\mathbf{W}$. For a received observation y_t, each element of the discrete marginal posterior update $\boldsymbol{\pi}^{\mathbf{W}}(t)$ can be obtained by plugging (4.6) into (4.5)

$$\pi_i(t) = \frac{\sum_{j=1}^{1/\triangle_X} g\Big(\frac{y_t - x_j G_i}{\sigma_t}\Big) \mathbb{P}(x_j | \mathbf{e}_i, y_{1:t-1}) \pi_i(t-1)}{\sum_{j'=1}^{1/\triangle_X} \sum_{i'=1}^{M} g\Big(\frac{y_t - x_{j'} G_{i'}}{\sigma_t}\Big) \mathbb{P}(x_{j'} | \mathbf{e}_{i'}, y_{1:t-1}) \pi_{i'}(t-1)}. \tag{4.11}$$

Note, this is equivalent to marginalizing the joint probability $\boldsymbol{\pi}^{\mathbf{W}, X_t}(t-1) \in [0,1]^{M \times \frac{1}{\triangle_X}}$ over X_t, with knowledge of a one-step prediction from X_{t-1} to X_t, where $\boldsymbol{\pi}^{\mathbf{W}, X_t}(t-1)$ has elements:

$$\pi_{i,j}(t-1) = \mathbb{P}(X_t = x_j | \mathbf{e}_i, y_{1:t-1}) \pi_i(t-1). \tag{4.12}$$

Alg. 2 requires, at worst, $(\frac{1}{\triangle_X} \times M)$ computations per iteration to update the posterior (4.11), and the number of iterations (duration) is fixed to τ. Here, we note that approximations for the computing the posterior, such as by variational Bayesian inference [70], may be implemented

in order to further reduce computational requirements. however this lies beyond the scope of this chapter.

Algorithm 2: Discrete Marginal Posterior Matching

Input: Resolution $(M, \triangle_X)$, noise variance σ^2, set of possible measurement vectors $\mathcal{A}$, duration τ

Output: Estimate $\hat{\mathbf{W}}$

Initialization: prior $\boldsymbol{\pi}^{\mathbf{W},X_1}(0)$

for $t = 1, 2, ..., \tau$ **do**

Select measurement by $marginalPM$ Eq. (4.8)

$$\mathbf{A}_t(\boldsymbol{\pi}^{\mathbf{W}}(t-1)) \in \mathcal{A}$$

Observation with measurement-dependent noise

$$Y_t = X_t \mathbf{A}_t^{\intercal} \mathbf{W} + N_t(\mathbf{A}_t)$$

Marginal posterior update Eq. (4.11)

$$\boldsymbol{\pi}^{\mathbf{W}}(t) \leftarrow y_t, \boldsymbol{\pi}^{\mathbf{W},X_t}(t-1)$$

Final estimate

$$i^* = \underset{i}{\operatorname{argmax}}\, \pi_i(\tau) \tag{4.13}$$

$\hat{\mathbf{W}} = \mathbf{e}_{i^*}$

$MarginalPM$ with a Kalman Filter

We propose an alternative method in Alg. 3 which reduces the worst-case arithmetic computations per iteration for the updates to $(M+2)$ by supplementing $marginalPM$ with the Kalman Filter [71]. Specifically, Alg. 3 selects measurement vectors $\mathbf{A}_t(\boldsymbol{\pi}^{\mathbf{W}}(t-1))$ sequentially according to $marginalPM$, where the update of $\boldsymbol{\pi}^{\mathbf{W}}(t)$ incorporates the Kalman filter estimate of X_t. For this approach, we assume the conditional probability density is Gaussian with a known prior $(\mu_{X_1}(0), \sigma^2_{X_1}(0))$

$$f_{X_t|\mathbf{W},Y_{1:t-1}}(x|\mathbf{e}_i, y_{1:t-1}) \sim \mathcal{N}(\mu_{X_t}(t-1), \sigma^2_{X_t}(t-1)). \tag{4.15}$$

Algorithm 3: Kalman Filter for Marginal Posterior Matching

Input: Resolution M, noise variance σ^2, set of possible measurement vectors $\mathcal{A}$, duration τ

Output: Estimate $\hat{\mathbf{W}}$

Initialization: priors $\boldsymbol{\pi}^{\mathbf{W}}(0)$ and $(\mu_{X_1}(0), \sigma^2_{X_1}(0))$

for $t = 1, 2, ..., \tau$ **do**

Select measurement by $marginalPM$ Eq. (4.8)

$$\mathbf{A}_t(\boldsymbol{\pi}^{\mathbf{W}}(t-1)) \in \mathcal{A}$$

Observation with measurement-dependent noise

$$Y_t = X_t \mathbf{A}_t^\intercal \mathbf{W} + N_t(\mathbf{A}_t)$$

Marginal posterior update Eq. (4.11)

$$\boldsymbol{\pi}^{\mathbf{W}}(t) \leftarrow y_t, \boldsymbol{\pi}^{\mathbf{W}}(t-1), \mu_{X_t}(t-1), \sigma^2_{X_t}(t-1)$$

Update and predict by Kalman Filter Eq. (4.17)

$$\mu_{X_{t+1}}(t), \sigma^2_{X_{t+1}}(t) \leftarrow y_t, \mu_{X_t}(t-1), \sigma^2_{X_t}(t-1)$$

Final estimate

$$i^* = \underset{i}{\operatorname{argmax}}\, \pi_i(\tau) \tag{4.14}$$

$\hat{\mathbf{W}} = \mathbf{e}_{i^*}$

Recall, observations are a linear combination of X_t, i.e. $Y_t = X_t \mathbf{A}_t^\intercal \mathbf{W} + N_t$, thus we can derive the Kalman filter to estimate the unknown state X_t and update it sequentially. Upon receiving a new observation y_t, Alg. 3 uses the one-step prediction estimate of X_t (4.17) to obtain the marginal

posterior update $\boldsymbol{\pi}^{\mathbf{W}}(t)$ by plugging (4.6) and (4.15) into (4.5)

$$\begin{aligned}\pi_i(t) &= \frac{\left(\int_{-\infty}^{\infty} g\left(\frac{x-\mu_{X_t}(t-1)}{\sigma_{X_t}(t-1)}\right) g\left(\frac{y_t - xG_i}{\sigma_t}\right)\right) dx\ \pi_i(t-1)}{\sum_{i'=1}^{M}\left(\int_{-\infty}^{\infty} g\left(\frac{x-\mu_{X_t}(t-1)}{\sigma_{X_t}(t-1)}\right) g\left(\frac{y_t - xG_{i'}}{\sigma_t}\right)\right) dx\ \pi_{i'}(t-1)} \\ &= \frac{g\left(\frac{y_t - \mu_{X_t}(t-1)G_i}{\sqrt{\sigma^2_{X_t}(t-1)|G_i|^2 + \sigma_t^2}}\right)\pi_i(t-1)}{\sum_{i'=1}^{M} g\left(\frac{y_t - \mu_{X_t}(t-1)G_{i'}}{\sqrt{\sigma^2_{X_t}(t-1)|G_{i'}|^2 + \sigma_t^2}}\right)\pi_{i'}(t-1)}.\end{aligned} \tag{4.16}$$

Next, the moments of X_t are updated via the Kalman Filter.

$$\begin{aligned}\mu_{X_t}(t) &= \mu_{X_t}(t-1) + \frac{\sigma^2_{X_t}(t-1)\hat{G}}{\sigma^2_{X_t}(t-1)\left|\hat{G}\right|^2 + \sigma_t^2}(y_t - \mu_{X_t}(t-1)\hat{G}) \\ \sigma^2_{X_t}(t) &= \sigma^2_{X_t}(t-1)\frac{\sigma_t^2}{\sigma^2_{X_t}(t-1)\left|\hat{G}\right|^2 + \sigma_t^2},\end{aligned} \tag{4.17}$$

where $\hat{G} = \mathbf{A}_t^{\intercal}\boldsymbol{\pi}^{\mathbf{W}}(t)$ is the estimate of the gain $(\mathbf{A}_t^{\intercal}\mathbf{W})$.

4.2.3 Specializing Bayes Updates

Even though Alg. 2 and Alg. 3 can be implemented for any X_t, in this section we develop specifics for the Bayes' update in Alg. 2 and for the Kalman Filter in Alg. 3 under two density cases of X_t.

4.2.4 Static Coefficient $X_t = X$ with Gaussian Prior

Here we assume the coefficient X is a random variable that is static over t. In other words, we have the simplification

$$\begin{aligned}&f_{X_t|\mathbf{W},Y_{1:t-1}}(x|\mathbf{e}_i, y_{1:t-1}) = \\ &f_{X|\mathbf{W},Y_{1:t-1}}(x|\mathbf{e}_i, y_{1:t-1}) \sim \mathcal{N}(\mu_X(t-1), \sigma_X^2(t-1))\end{aligned} \tag{4.18}$$

with prior $(\mu_X(0), \sigma_X^2(0))$.

Apply to Alg. 2

Consider a conservative range for X:

$$[x_{\min}, x_{\max}] = [\mu_X(0) - 3\sigma_X(0), \mu_X(0) + 3\sigma_X(0)], \tag{4.19}$$

with corresponding resolution parameter $\triangle_X$, which densely covers the Gaussian prior[3]. To discretize the prior into $\frac{1}{\triangle_X}$ bins, let

$$\mathbb{P}(X = x_j | \mathbf{e}_i, y^0) \propto g(\frac{x_j - \mu_X(0)}{\sigma_X(0)}),\ j = \{1, \ldots, \frac{1}{\triangle_X}\}, \tag{4.20}$$

and normalize by c such that $\sum_{j=1}^{M} \mathbb{P}(X = x_j | \mathbf{e}_i, y^0) c = 1$. The discrete prior update is made without need for prediction step from X_t to X_t using (4.11), (line 7 of Alg. 2).

Apply to Alg. 3

Under the Gaussian prior (4.18), the mean and variance are updated by the Kalman Filter:

$$\begin{aligned} \mu_X(t) &= \mu_X(t-1) + \frac{\sigma_X^2(t-1)\hat{G}}{\sigma_X^2(t-1)|\hat{G}|^2 + \sigma_t^2}(y_t - \mu_X(t-1)\hat{G}) \\ \sigma_X^2(t) &= \sigma_X^2(t-1)\frac{\sigma^2}{\sigma_X^2(t-1)|\hat{G}|^2 + \sigma_t^2}, \end{aligned} \tag{4.21}$$

and the one-step prediction is not required due to static X. In other words, $\mu_{X_t}(t-1) = \mu_X(t-1)$ and $\sigma_{X_t}^2(t-1) = \sigma_X^2(t-1)$ are used in the Bayes' update (4.16). (4.21) is used in lieu of (4.17) to update moments (line 8 Alg. 3).

[3] A very coarse resolution parameter will reduce complexity but may impact performance, a further investigation is outside the scope of this chapter.

4.2.5 i.i.d. Coefficients X_t with Gaussian Prior

Next, we consider an i.i.d. time-varying model for X_t, where we have the simplification

$$f_{X_t|\mathbf{W},Y_{1:t-1}}(x|\mathbf{e}_i, y_{1:t-1}) = f_{X_t}(x) \sim \mathcal{N}(\mu_{\tilde{X}}, \sigma^2_{\tilde{X}}) \tag{4.22}$$

is i.i.d for all t with prior $(\mu_{\tilde{X}}, \sigma^2_{\tilde{X}})$.

Apply to Alg. 2

Again, we utilize a binned Gaussian prior, as in (4.20), and the added simplification $\mathbb{P}(X_t = x_j|\mathbf{e}_i, y_{1:t-1}) = \mathbb{P}(X_t = x_j)$ by assumption of i.i.d. coefficients. Plugging into (4.11), the marginal posterior update reduces to

$$\pi_i(t) = \frac{\sum_{j=1}^{1/\triangle_X} g\left(\frac{y_t - x_j G_i}{\sigma_t}\right) g(\frac{x_j - \mu_{\tilde{X}}}{\sigma_{\tilde{X}}}) c\, \pi_i(t-1)}{\sum_{j'=1}^{1/\triangle_X} \sum_{i'=1}^{M} g\left(\frac{y_t - x_{j'} G_{i'}}{\sigma_t}\right) g(\frac{x_{j'} - \mu_{\tilde{X}}}{\sigma_{\tilde{X}}}) c\, \pi_{i'}(t-1)} \tag{4.23}$$

for all t (line 7 of Alg. 2).

Apply to Alg. 3

For i.i.d $X_t \sim \mathcal{N}(\mu_{\tilde{X}}, \sigma^2_{\tilde{X}})$, the one-step prediction of the moments is eliminated by $\mu_{X_t}(t-1) = \mu_{\tilde{X}}$ and $\sigma^2_{X_t}(t-1) = \sigma^2_{\tilde{X}}$. These moments are plugged directly into the marginal posterior update (4.16) (line 7 Alg. 3). Here we note that under these conditions for Alg. 3, the conditional probability (4.15) is not an approximation, due to the i.i.d. and Gaussian nature of X_t. Thus, should result in performance of Alg. 3 comparable to Alg. 2.

4.2.6 Numerical Results

Next, we analyze the performance in terms of the probability of error (4.3) for the proposed algorithms under the special cases of static and of i.i.d X_t as a function of the SNR $1/\sigma^2$. We focus

on the scenario of low overhead time, and limit total the number of observations to $\tau = \{10, 30\}$ and set the dimensions of $\mathbf{W}$ to $M = 25$, where recall $|\mathbf{W}| = 1$. Many reconstruction algorithms, implementing compressive sensing and/or greedy techniques [20–25] exist in the literature. However, for ease of exposition we restrict our comparisons to two random-coding-based strategies, which we believe to be representative of the performance of these random-based schemes. The extensive study of existing strategies is ongoing and we refer the reader to our future work. The random strategies we consider build $\mathbf{A}_{1:t}$ randomly a priori from a finite codebook $\mathcal{A}^q$. Specifically, $\mathcal{A}^q$ is the finite set of binary vectors $\{0, 1\}^M$ probing qM number of locations, resulting in $|\mathcal{A}^q| = \binom{M}{qM}$. We plot solutions for $q = 0.25$, probing $(0.25 \times M)$ locations in each measurement, which is on par with the parameters used in the practical setting of [50] although we note this parameter can be optimized further. The first scheme considered utilizes the maximum likelihood (ML) decoder [30] for reconstructing $\mathbf{W}$. The second scheme utilizes a non-negative constrained least squares (NNLS) solution [25, 50] on the quadratic measurements Y_t^2 for reconstructing $X_t^2\mathbf{W}$ which has the benefit of not requiring knowledge of σ^2 or any prior on X_t.

Probability of error: static $X_t = X$

First, we analyze the performance under a static coefficient $X_t = X$ with Gaussian prior (Sect. 4.2.4) in Fig. 4.1. Our proposed Alg. 2 outperforms the random schemes significantly, achieving greater reliability in less time. That is, Alg. 2 can achieve almost the same performance of the NNLS scheme in $1/3$ of the duration ($\tau = 10$, versus $\tau = 30$). The lower-complexity solution of Alg. 3 similarly achieves improved performance over the random algorithms for a short duration $\tau = 10$, although less so than Alg. 2 for a long duration $\tau = 30$ due to the assumptions made in order to reduce complexity. This suggests that Alg. 2 and Alg. 3 are successful in learning X and $\mathbf{W}$ with sequential measurement vectors, especially with a low overhead duration τ. This demonstrates evidence of an adaptivity gain, i.e. a gain in performance due to sequentially selecting $\mathbf{A}_t$, achieved by our adaptive strategies over the non-adaptive random strategies.

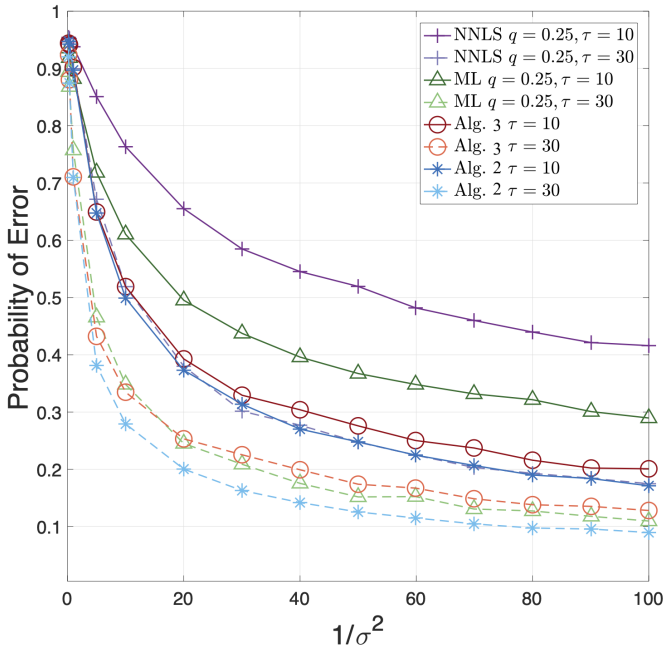

Figure 4.1: Comparison of the probability of error (given by (4.3)) performance between our proposed algorithms and random algorithms as a function of $1/\sigma^2$ under a static $X_t = (X \sim \mathcal{N}(1,1))$, and resolution $\triangle_X = 0.01$.

Probability of error: i.i.d X_t

Next, we study the performance under a time-varying i.i.d. $X_t \sim \mathcal{N}(\mu_{\tilde{X}}, \sigma^2_{\tilde{X}})$ with Gaussian prior (Sect. 4.2.5). At first thought, any attempt to learn X_t over time may seem fruitless due to the i.i.d. nature of X_t, however, Alg. 2 and Alg. 3 yield some improvements over the random algorithms in terms of probability of error as illustrated in Fig. 4.2. Under this i.i.d. condition, Alg. 2 and Alg. 3 incorporate the prior on X_t as an account of the extra uncertainty in the Bayes' update of $\boldsymbol{\pi}^{\mathbf{W}}(t)$ which has the effect of selecting $\mathbf{A}_t$ more conservatively. These conservative adaptive selections achieve again an adaptivity gain in performance over the random algorithms which do adapt to the observations, especially in the high noise range $(1/\sigma^2 < 20)$. Under significantly improved noise $(1/\sigma^2 > 20)$ and longer time $\tau = 30$, even the random schemes are robust in this i.i.d. setting, however, at a significantly lesser rate than Alg. 2 and Alg. 3.

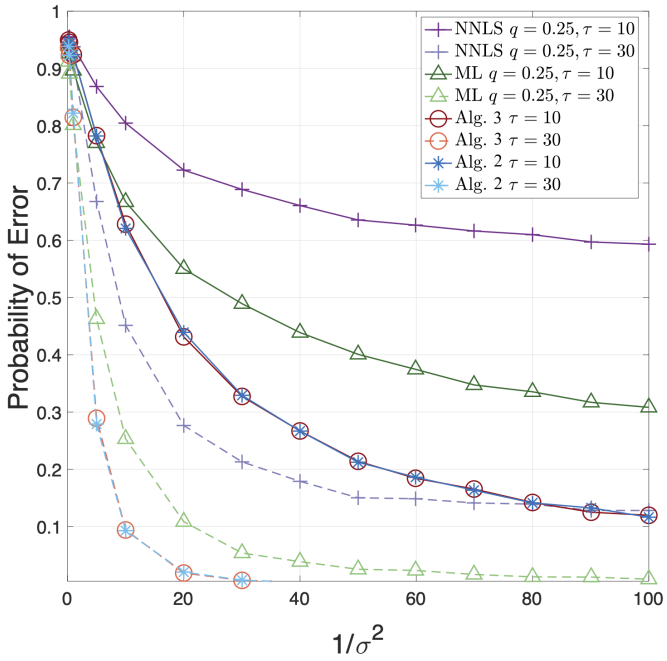

Figure 4.2: Comparison of the probability of error (given by (4.3)) performance between our proposed algorithms and random algorithms as a function of $1/\sigma^2$ under a time-varying i.i.d. $X_t \sim \mathcal{N}(1,1)$, and resolution $\triangle_X = 0.01$.

4.3 Part II: Millimeter-wave Communications with Unknown Fading

Next, we revisit the problem of initial alignment discussed in chapter 3. We are particularly concerned with enabling robustness to variations of the channel dynamics. For a fixed power allocation and fixed very low overhead setting existing approaches [49, 72, 73] can handle alignment with no prior CSI despite a time-varying fading model with the caveat a sufficiently large SNR, or custom codebooks for improving SNR. In chapter 3 a fully adaptive initial alignment method based on posterior matching was proposed, which theoretically characterizes an upper-bound on the probability of error in the AoA acquisition under a known static fading coefficient α. A significant improvement over [46] and random beamforming method of [49] in the system communication rate is shown. For a slightly mismatched estimate of the fading coefficient α (i.e. a very good estimate) these improvements hold even under a time-varying channel. However, the performance is highly

dependent on the quality of the channel knowledge. In fact, in the absence of a good estimate of α and under a time-varying fading model the performance is quite poor.

In this part of the chapter we aim to mitigate the effects of imperfect channel knowledge under a dynamical channel by augmenting the detection of the AoA to include simultaneous estimation of α for a given user. We extend the algorithms proposed in part I of this chapter specifically to the context of mmWave Initial Alignment. The resulting methods simultaneously and adaptively learn the fading coefficient as well as the AoA. The proposed algorithms are compared to our prior work [74], included in chapter 3, and the bisection algorithm of [46] using the performance measures of outage probability and expected spectral efficiency. Numerically, we show improvements over [46] and [74], which suggests promising performance by our strategies for combining the learning of the AoA of the fading coefficients in the relevant regime of low (-10dB to $+5$dB) raw SNR.

In this chapter, we extend our prior work by proposing two methods that simultaneously and adaptively learn the fading coefficient as well as the AoA. The idea is to mitigate the effects of imperfect channel knowledge under a dynamic channel by augmenting the detection of the AoA to include simultaneous estimation of α for a given user. We propose two algorithms that work with the searching methods of prior work [74] in order to fully learn the CSI (AoA and α). Specifically, the contributions of the chapter are as follows:

- First, we propose a direct extension of our prior work [74] to be robust to a time-varying fading model by adapting the posterior matching based strategy to include estimation of α.
- In light of excessive computations required to compute a Baysian posterior, we develop a heuristic approximation with low memory complexity. This strategy compliments the sequential detection of AoA with estimation of the fading coefficient via a Kalman filter.
- The proposed algorithms are compared to our prior work [74] and the bisection algorithm of [46] using the performance measures of outage probability and expected spectral efficiency. Numerically, we show improvements over [46] and [74], which suggests promising perfor-

mance by our strategies for combining the learning of the AoA of the fading coefficients in the relevant regime of low (-10dB to $+5$dB) raw SNR.

4.3.1 Problem Set-up

The system model is identical to Sect. 3.2 of chapter 3. We consider a base Station (BS) equipped with N antennas serving k users (UE), each with a fixed beamforming acting as single virtual antenna. The active alignment process is summarized in Fig. 4.3. Recall, the code-matched signal from a particular user is given by

$$y_t = \alpha_t \sqrt{P} \mathbf{w}_t^H \mathbf{a}(\phi) + \mathbf{w}_t^H \mathbf{n}_t, \tag{4.24}$$

where $\mathbf{w_t}$ is the receive beam vector, $\alpha_t \in \mathbb{C}$ is the time-varying fading coefficient, $\mathbf{a}(\phi)$ is the array manifold created by the Angle-of-Arrival (AoA) ϕ, $\sqrt{P}$ is the combined transmit power and large scale fading. Without loss of generality, the beamforming vectors in the codebook are assumed to have unit norm $\|\mathbf{w}\|^2 = 1$. Thus, the complex additive noise $\underline{\eta}_t = \mathbf{w}_t^H \mathbf{n}_t \sim \mathcal{CN}(0, \sigma^2)$. In this work we focus on relative performance in terms of the raw SNR $\frac{P}{\sigma^2}$, although the physical properties corresponding to this range of raw SNR (like cell size, and bandwidth) can be defined as in Fig. 3.6 of chapter 3.

Sequential Initial Alignment

For the setup considered above, the initial alignment problem consists of finding the best directional beamforming vector at the receiver in order to establish a link to a given user, it does so via the process of initial alignment (described in detail in Sect. 3.3.1 of chapter 3). As in part I of this chapter, we focus on strategies with sequential refinement of measurement vectors. In the context of mmWave initial alignment, this is equivalent to sequential refinement of the beamforming vectors, which we achieve by using the hierarchical codebook $\mathcal{W}^S$ of [46] with practically feasible beams and finite cardinality (described in Sect. 3.3.2 of chapter 3). More specifically, at any given

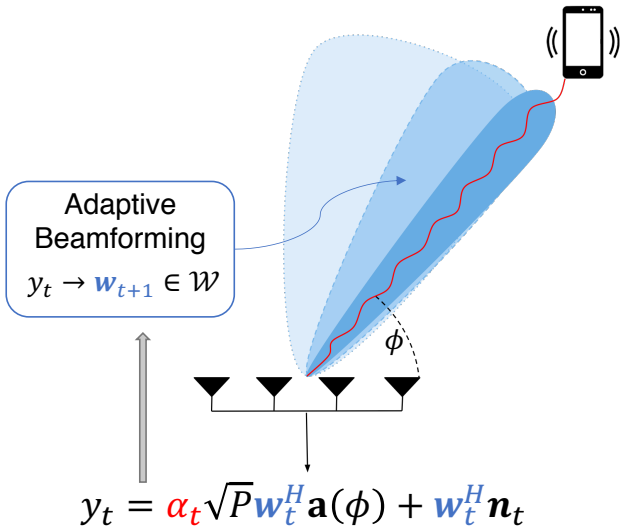

Figure 4.3: Active initial alignment is the process of sequentially selecting the beamforming vectors $\mathbf{w_t}(y_t)$, for a pilot-based procedure, based on prior observations y_t, after which the best directional beamforming vector for transmission is selected.

time t, a beamforming vector $\mathbf{w_t} \in \mathcal{W}^S$ is selected sequentially as a function of previously observed signals $(y_{1:t-1})$. We extend our proposed algorithms in part I of this chapter to the setting of initial alignment problem with unknown and dynamic channel fading. Our approach is to sequentially select beamforming vectors based on prior observations in an active manner, to simultaneously learn the CSI consisting of the AoA ϕ, and the time-varying fading coefficient α_t. We utilize the hierarchical posterior matching ($hiePM$) Alg. 1 of chapter 3 (summarized below in Sect. 4.3.1), where the choice of $\mathbf{w_t}$ is such that the probability of ϕ lying in the area covered by $\mathbf{w_t}$ is closest to $\frac{1}{2}$. The effect is a sequential scanning of the angular space, where the practically feasible contiguous beamforming vectors become refined over time. First, we briefly review the $hiePM$ scheme of chapter 3.

Brief Review of hiePM (Alg. 1)

$HiePM$ is a method of sequentially selecting beamforming vectors $\mathbf{w}_{t+1}$ from the codebook $\mathcal{W}^S$ based on the posterior probability vector for active learning of the AoA ϕ. We resolve the AoA with a resolution $1/\delta$ from a range of angles $[\theta_{\text{min}}, \theta_{\text{max}}]$. For ease of exposition, we restrict the AoA to the discretized set $\phi \in \{\theta_1, ..., \theta_{1/\delta}\}$, $\theta_i = \theta_{\text{min}} + (i-1) \times \delta \times (\theta_{\text{max}} - \theta_{\text{min}})$. The prior

probability vector of ϕ, is defined as $\boldsymbol{\pi}^{\phi}(t) \in [0,1]^{1/\delta}$, where each element is:

$$\pi_i(t) := \mathbb{P}(\phi = \theta_i | \mathbf{y}_{1:t}),\ i = 1, 2, ..., \frac{1}{\delta}. \tag{4.25}$$

$HiePM$ selects $\mathbf{w}_{t+1}(\boldsymbol{\pi}^{\phi}(t)) \in \mathcal{W}^S$ in a manner that sequentially refines the width of the beamforming vectors over time corresponding to the accumulated belief around the correct AoA ϕ as described by probability vector $\boldsymbol{\pi}^{\phi}(t)$, which is a sufficient statistic. $HiePM$ selects a codeword at either level l^* or l^*+1 based on which codeword has probability closest to $\frac{1}{2}$.

Computing marginal posterior belief $\boldsymbol{\pi}^{\phi}(t)$

In this section, we define the marginal posterior update (4.5) in the context of the mmWave communications model (4.24). This definition is an extension to our prior work [74], included in chapter 3, which accounts for the random yet time-varying fading coefficient α_t. Let us model the channel state at time t as a random vector $(\phi, \underline{\alpha}_t) \in [\theta_{\text{min}}, \theta_{\text{max}}] \times \mathbb{C}$ with joint distribution $f_{\phi,\underline{\alpha}_t}(\theta, \alpha)$, such that

$$\sum_{i=1}^{1/\delta} \int_{-\infty}^{\infty} \int_{-\infty}^{\infty} f_{\phi,\underline{\alpha}_t}(\theta_i, \alpha) d\Re\alpha d\Im\alpha = \sum_{i=1}^{1/\delta} \mathbb{P}(\phi = \theta_i) = 1. \tag{4.26}$$

The belief vector $\boldsymbol{\pi}^{\phi}(t)$ can be computed sequentially:

$$\mathbb{P}(\phi = \theta_i | y_{1:t}) = \frac{f_{Y_t|\phi,Y_{1:t-1}}(y_t|\theta_i, y_{1:t-1})\mathbb{P}(\theta_i|y_{1:t-1})}{\sum_{i'=1}^{1/\delta} f_{Y_t|\phi,Y_{1:t-1}}(y_t|\theta_i, y_{1:t-1})\mathbb{P}(\theta_{i'}|y_{1:t-1})} \tag{4.27}$$

where

$$Y_t = \underline{\alpha}_t \sqrt{P} \mathbf{w}_t^H \mathbf{a}(\phi) + \underline{\eta}_t. \tag{4.28}$$

where recall $(\underline{\eta}_t = \mathbf{w}_t^H \mathbf{n}_t) \sim \mathcal{CN}(0, \sigma^2)$. The conditional distribution is:

$$
\begin{aligned}
f_{Y_t|\phi,Y_{1:t-1}}(y_t|\theta_i, y_{1:t-1}) &\approx \int_{-\infty}^{\infty}\int_{-\infty}^{\infty} \frac{1}{G_i} f_{\underline{\alpha}_t|\phi,Y_{1:t-1}}\Big(\frac{y_t-\eta}{G_i}|\theta_i, y_{1:t-1}\Big) f_{\underline{\eta}_t}(\eta) d\eta \\
&\overset{(a)}{=} -\int_{-\infty}^{\infty}\int_{-\infty}^{\infty} f_{\underline{\alpha}_t|\phi,Y_{1:t-1}}(\alpha|\theta_i, y_{1:t-1}) f_{\underline{\eta}_t}(y_t - \alpha G_i) d\alpha \\
&\overset{(b)}{=} -\int_{-\infty}^{\infty}\int_{-\infty}^{\infty} f_{\underline{\alpha}_t|\phi,Y_{1:t-1}}(\alpha|\theta_i, y_{1:t-1}) g\Big(\frac{y_t-\alpha G_i}{\sigma}\Big) d\alpha
\end{aligned}
\tag{4.29}
$$

where $d\eta = d\Re\eta d\Im\eta, d\alpha = d\Re\alpha d\Im\alpha$,

$$
G_i = \sqrt{P}\mathbf{w_t}^H \mathbf{a}(\theta_i), \tag{4.30}
$$

and (a) is by a change of variables, (b) follows by assumption of i.i.d noise, and where $g(\frac{y-\mu}{\sigma})$ is $\mathcal{CN}(0,1)$ evaluated at $(\frac{y-\mu}{\sigma})$. $f_{\underline{\alpha}_t|\phi,Y_{1:t-1}}(\alpha|\theta_i, y_{1:t-1})$ can be obtained as a one-step prediction from $f_{\underline{\alpha}_{t-1}|\phi,Y_{1:t-1}}(\alpha|\theta_i, y_{1:t-1})$.

It follows that computation of $\boldsymbol{\pi}^{\phi}(t)$ depends on knowledge of $f_{\underline{\alpha}_t|\phi,Y_{1:t}}(\alpha|\theta_i, y_{1:t})$, a one-step prediction formulation for each time t, and may require infinite precision. We approach this computation by considering some special cases discussed in the next section.

4.3.2 Proposed Algorithms for Beamforming

Earlier in this chapter we proposed two strategies for sequentially and jointly learning stochastic coefficients and a common support vector (Alg. 2 and Alg. 3). In this section we apply these algorithms to the context of mmWave initial alignment for dealing with channel fading. First, we discuss some special density cases to consider for the fading coefficient $\underline{\alpha}_t$.

Known and static fading coefficient $\underline{\alpha}_t = \alpha^*$:

For the case that the fading coefficient is static and known to the BS, we can write

$$f_{\underline{\alpha}_t|\phi,Y_{1:t-1}}(\alpha|\theta_i, y_{1:t}) = \begin{cases} 1, & \text{if } \alpha = \alpha^* \\ 0, & \text{otherwise.} \end{cases} \tag{4.31}$$

Plugging into Eq. (4.27) gives $\boldsymbol{\pi}^{\phi}(t)$ as:

$$\mathbb{P}(\phi = \theta_i|y_{1:t}) = \frac{g\left(\frac{y_t - \alpha^* G_i}{\sigma}\right)\mathbb{P}(\theta_i|y_{1:t-1})}{\sum\limits_{i'=1}^{1/\delta} g\left(\frac{y_t - \alpha^* G_{i'}}{\sigma}\right)\mathbb{P}(\theta_i|y_{1:t-1})}, \tag{4.32}$$

which is finite, and does not require a one-step prediction of the conditional density of α. This is recovers the formulation of our prior work [74], discussed in chapter 3.

i.i.d. complex Gaussian fading coefficient with mean $\mu_{\tilde{\alpha}}$ and variance $\sigma^2_{\tilde{\alpha}}$.

In this case:

$$f_{\underline{\alpha}_t|\phi,Y_{1:t-1}}(\alpha|\theta_i, y_{1:t-1}) = f_{\underline{\alpha}_t}(\alpha) \sim \mathcal{CN}(\mu_{\tilde{\alpha}}, \sigma^2_{\tilde{\alpha}}) \tag{4.33}$$

is i.i.d for all t. Plugging into Eq. (4.27) gives the update $\boldsymbol{\pi}^{\phi}(t)$:

$$\begin{aligned} \mathbb{P}(\phi = \theta_i|y_{1:t}) &= \frac{\left(\int\limits_{-\infty}^{\infty}\int\limits_{-\infty}^{\infty} g\left(\frac{\alpha - \mu_{\tilde{\alpha}}}{\sigma_{\tilde{\alpha}}}\right) g\left(\frac{y_t - \alpha G_i}{\sigma}\right) d\alpha\right)\mathbb{P}(\theta_i|y_{1:t-1})}{\sum\limits_{i'=1}^{1/\delta}\left(\int\limits_{-\infty}^{\infty}\int\limits_{-\infty}^{\infty} g\left(\frac{\alpha - \mu_{\tilde{\alpha}}}{\sigma_{\tilde{\alpha}}}\right) g\left(\frac{y_t - \alpha G_{i'}}{\sigma}\right) d\alpha\right)\mathbb{P}(\theta_i|y_{1:t-1})} \\ &= \frac{g\left(\frac{y_t - \mu_{\tilde{\alpha}} G_i}{\sqrt{\sigma^2_{\tilde{\alpha}}|G_i|^2 + \sigma^2}}\right)\mathbb{P}(\theta_i|y_{1:t-1})}{\sum\limits_{i'=1}^{1/\delta} g\left(\frac{y_t - \mu_{\tilde{\alpha}} G_{i'}}{\sqrt{\sigma^2_{\tilde{\alpha}}|G_{i'}|^2 + \sigma^2}}\right)\mathbb{P}(\theta_{i'}|y_{1:t-1})}. \end{aligned} \tag{4.34}$$

Note that E.q. (4.34) differs from the perfect knowledge scenario E.q. (4.32) only in $f_{Y_t|\phi,Y_{1:t-1}}(y_t|\theta_i, y_{1:t-1})$. E.q. (4.34) accounts for the uncertainty on the knowledge of the fading coefficient by increasing the variance by $(\sigma^2_{\tilde{\alpha}}|G_i|^2)$, where the effect is a more conservative update.

Static fading coefficient $\underline{\alpha}_t = \underline{\alpha}$

Here we make the simplification that the fading coefficient is static for a period of time, this is a typical assumption for a duration less than the channel coherence time:

$$f_{\underline{\alpha}_{t+1}|\phi,Y_{1:t}}(\alpha|\theta_i, y_{1:t}) = f_{\underline{\alpha}|\phi,Y_{1:t}}(\alpha|\theta_i, y_{1:t}). \tag{4.35}$$

Of course the Bayes' joint posterior probability update, detailed in Eq. (4.27), may be computed directly for a continuous density $f_{\underline{\alpha}|\phi,Y_{1:t}}(\alpha|\theta_i, y_{1:t})$, however, this may be computationally infeasible. In our first proposed Alg. 2 for a general formulation we approach the computation of $\boldsymbol{\pi}^{\phi}(t)$ by first discretizing $\underline{\alpha}$ over a finite number of sets. To do this for the application to beam selection, let us make the simplification that $\underline{\alpha} = r_j + \mathrm{i}z_k$ for $j = \{1, 2, \ldots, \frac{1}{\triangle_r}\}$ and $k = \{1, 2, \ldots, \frac{1}{\triangle_z}\}$ denotes that

$$\begin{aligned} \Re\underline{\alpha} &\in [r_j - \triangle_r/2, r_j + \triangle_r/2] \\ \Im\underline{\alpha} &\in [z_k - \triangle_z/2, z_k + \triangle_z/2], \end{aligned} \tag{4.36}$$

where

$$\begin{aligned} r_j &= r_{\min} + (j-1) \times \triangle_r \times (r_{\max} - r_{\min}) \\ z_j &= z_{\min} + (z-1) \times \triangle_z \times (z_{\max} - z_{\min}), \end{aligned} \tag{4.37}$$

for $\Re\underline{\alpha} \in [r_{\min}, r_{\max}]$, and $\Im\underline{\alpha} \in [z_{\min}, z_{\max}]$. Under this discretization, the probability is:

$$\mathbb{P}(\underline{\alpha} = r_j + \mathrm{i}z_k|\theta_i y_{1:t}) = f_{\underline{\alpha}}(r_j + \mathrm{i}z_k)\triangle_r\triangle_z \tag{4.38}$$

We note that this discretization becomes tight as $\triangle_r, \triangle_z \to 0$. Coarser choices of ($\triangle_r$, $\triangle_z$) reduce complexity and memory requirements. (see Sect. 4.3.3 for a discussion of practical values for these resolution parameters used in our simulations).

Discrete $marginalPM$ for Beam Alignment

Using the practical case of a static fading, i.e. $\underline{\alpha}_t = \underline{\alpha}$ we develop the proposed algorithms for beamforming under channel fading. In Alg. 4, we propose beamforming vectors to be sequentially selected according to $hiePM$, where the posterior belief on ϕ, $\boldsymbol{\pi}^{\phi}(t)$, is used to make the beam selection from $\mathcal{W}^S$. For a received observation y_t each element of the posterior update on the belief on ϕ, $\boldsymbol{\pi}^{\phi}(t)$, can be obtained by Eq. (4.27) and (4.38):

$$\mathbb{P}(\phi = \theta_i | y_{1:t}) = \frac{\sum_{j=1}^{1/\triangle_r} \sum_{k=1}^{1/\triangle_z} g\left(\frac{y_t - (r_j + \mathrm{i} z_k) G_i}{\sigma}\right) \mathbb{P}(r_j, z_k | \theta_i, y_{1:t-1}) \mathbb{P}(\theta_i | y_{1:t-1})}{\sum_{j'=1}^{1/\triangle_r} \sum_{k'=1}^{1/\triangle_z} \sum_{i'=1}^{1/\delta} g\left(\frac{y_t - (r_j + \mathrm{i} z_k) G_{i'}}{\sigma}\right) \mathbb{P}(r_{j'}, z_{k'} | \theta_i, y_{1:t-1}) \mathbb{P}(\theta_{i'} | y_{1:t-1})} \tag{4.39}$$

Note, here we write the marginal posterior probability in two steps, first with an update to get the joint probability $\boldsymbol{\pi}^{\phi,\underline{\alpha}}(t)$, and then a marginalization to get $\boldsymbol{\pi}^{\phi}(t)$. The joint probability $\boldsymbol{\pi}^{\phi,\underline{\alpha}}(t) \in [0,1]^{\frac{1}{\delta} \times \frac{1}{\triangle_r} \times \frac{1}{\triangle_z}}$ at all times t, defined as:

$$\pi_{i,j,k}(t) = \mathbb{P}(r_j, z_k | \theta_i, y_{1:t}) \mathbb{P}(\theta_i | y_{1:t}). \tag{4.40}$$

Thus Alg. 4 has a computational cost on the order of $O(\frac{1}{\triangle_r} \times \frac{1}{\triangle_z} \times \log(\frac{1}{\delta}))$. We also specialize Alg. 3 for the application of beam selection in order to reduce the computational cost to $O(\frac{1}{\delta} \times \log(\frac{1}{\delta}))$ by implementing the Kalman filter [71]. First, we assume the conditional probability density Eq.(4.35) is complex Gaussian:

$$f_{\underline{\alpha}|\phi,Y_{1:t}}(\alpha | \theta_i, y_{1:t}) \sim \mathcal{CN}(\mu_{\alpha,i}(t), \sigma^2_{\alpha,i}(t)), \tag{4.43}$$

with known prior $(\mu_{\underline{\alpha},i}(0), \sigma^2_{\underline{\alpha},i}(0))$ for all i.

The proposed algorithm (summarized in Alg. 5) selects beamforming vectors sequentially according to $hiePM$, where a marginalized probability over ϕ, $\boldsymbol{\pi}^{\phi}(t)$, is used to make the beam selection from $\mathcal{W}^S$. Upon receiving a new observation y_{t+1}, the mean and variance of this conditional

Algorithm 4: Marginal Posterior Matching for Beam Alignment

Input: target resolution $(\delta, \triangle_r, \triangle_z)$, codebook $\mathcal{W}^S$ $(S = \log_2(1/\delta))$, τ (length of the initial access phase)

Output: Estimate of the AoA $\hat{\phi}$

Initialization: $\boldsymbol{\pi}^{\phi,\underline{\alpha}}(0) : \pi_{i,j,k}(0) = \delta\triangle_r\triangle_z \; \forall i,j,k$

for $t = 1, 2, ..., \tau$ **do**

  # Marginal posterior of ϕ, $\boldsymbol{\pi}^{\phi}(t)$:

$$\pi_i(t+1) = \sum_{j=1}^{1/\triangle_r} \sum_{k=1}^{1/\triangle_z} \pi_{i,j,k}(t+1). \tag{4.41}$$

  # Beam selection according to $hiePM$ Alg. 1:

$$\mathbf{w}_{t+1}(\boldsymbol{\pi}^{\phi}(t)) \in \mathcal{W}^S$$

  # Take next measurement

$$y_{t+1} = \underline{\alpha}_{t+1}\sqrt{P}\mathbf{w}_{t+1}^H\mathbf{a}(\phi) + \mathbf{w}_{t+1}^H\mathbf{n}_{t+1}$$

  # Joint posterior update by Bayes' Rule Eq. (4.39)

$$\boldsymbol{\pi}^{\phi,\underline{\alpha}}(t+1) \leftarrow y_{t+1}, \boldsymbol{\pi}^{\phi,\underline{\alpha}}(t)$$

Final beamforming vector design

$$\hat{\phi} = \underset{\theta_i}{\operatorname{argmax}}\, \pi_i(\tau) \tag{4.42}$$

$\hat{\mathbf{w}} = \mathbf{w}(\hat{\phi})$

probability are updated by the Kalman filter:

$$\begin{aligned} \mu_{\underline{\alpha},i}(t+1) &= \mu_{\underline{\alpha},i}(t) + \frac{\sigma^2_{\underline{\alpha},i}(t)\overline{G_i}}{\sigma^2_{\underline{\alpha},i}(t)|G_i|^2 + \sigma^2}(y_{t+1} - \mu_{\underline{\alpha},i}(t)G_i) \\ \sigma^2_{\underline{\alpha},i}(t+1) &= \sigma^2_{\underline{\alpha},i}(t)\frac{\sigma^2}{\sigma^2_{\underline{\alpha},i}(t)|G_i|^2 + \sigma^2}. \end{aligned} \tag{4.44}$$

Next, Alg.4 uses the estimate of the fading coefficient to obtain $\boldsymbol{\pi}^{\phi}(t)$ by Eq. (4.27) and (4.44):

$$\begin{aligned}\mathbb{P}(\theta_i|y_{1:t}) =& \frac{\left(\int_{-\infty}^{\infty}\int_{-\infty}^{\infty} g\left(\frac{\alpha-\mu_{\underline{\alpha},i}(t)}{\sigma_{\underline{\alpha},i}(t)}\right)g\left(\frac{y_t-\alpha G_i}{\sigma}\right)\right)d\alpha\mathbb{P}(\theta_i|y_{1:t-1})}{\sum_{i'=1}^{1/\delta}\left(\int_{-\infty}^{\infty}\int_{-\infty}^{\infty} g\left(\frac{\alpha-\mu_{\underline{\alpha},i'}(t)}{\sigma_{\underline{\alpha},i'}(t)}\right)g\left(\frac{y_t-\alpha G_{i'}}{\sigma}\right)\right)d\alpha\mathbb{P}(\theta_i|y_{1:t-1})} \\ =& \frac{g\left(\frac{y_t-\mu_{\underline{\alpha},i}(t)G_i}{\sqrt{\sigma^2_{\underline{\alpha},i}(t)|G_i|^2+\sigma^2}}\right)\mathbb{P}(\theta_i|y_{1:t-1})}{\sum_{i'=1}^{1/\delta} g\left(\frac{y_t-\mu_{\underline{\alpha},i'}(t)G_{i'}}{\sqrt{\sigma^2_{\underline{\alpha},i'}(t)|G_{i'}|^2+\sigma^2}}\right)\mathbb{P}(\theta_i|y_{1:t-1})}.\end{aligned} \tag{4.45}$$

Algorithm 5: Kalman Filter for Marginal Posterior Matching - Beam Alignment

Input: target resolution δ, codebook $\mathcal{W}^S$ $(S = \log_2(1/\delta))$, τ (length of the initial access phase)

Output: Estimate of the AoA $\hat{\phi}$

Initialization:$\boldsymbol{\pi}^{\phi}(0) : \pi_i(0) = \delta \ \forall i$, $(\boldsymbol{\mu}_{\underline{\alpha}}(0), \boldsymbol{\sigma}^2_{\underline{\alpha}}(0))$

for $t = 1, 2, ..., \tau$ **do**

Beam selection according to $hiePM$ Alg. 1:

$$\mathbf{w}_{t+1}(\boldsymbol{\pi}^{\phi}(t)) \in \mathcal{W}^S$$

Take next measurement

$$y_{t+1} = \underline{\alpha}_{t+1}\sqrt{P}\mathbf{w}^H_{t+1}\mathbf{a}(\phi) + \mathbf{w}^H_{t+1}\mathbf{n}_{t+1}$$

Update moments by Kalman Filter Eq. (4.44)

$$(\boldsymbol{\mu}_{\underline{\alpha}}(t+1), \boldsymbol{\sigma}^2_{\underline{\alpha}}(t+1)) \leftarrow y_{t+1}, \boldsymbol{\mu}_{\underline{\alpha}}(t), \boldsymbol{\sigma}^2_{\underline{\alpha}}(t)$$

Posterior update by Bayes' Rule Eq. (4.45)

$$\boldsymbol{\pi}^{\phi}(t+1) \leftarrow y_{t+1}, \boldsymbol{\pi}^{\phi}(t), \boldsymbol{\mu}_{\underline{\alpha}}(t), \boldsymbol{\sigma}^2_{\underline{\alpha}}(t)$$

Final beamforming vector design

$$\hat{\phi} = \underset{\theta_i}{\operatorname{argmax}}\, \pi_i(\tau) \tag{4.46}$$

$\hat{\mathbf{w}} = \mathbf{w}(\hat{\phi})$

4.3.3 Numerical Results

Our numerical simulations analyze the proposed algorithms using the performance measures of outage probability and achieved spectral efficiency in the the relevant regime of low (-10dB to +5dB) raw SNR.

Simulation Scenario

We consider a scenario where the BS is equipped with a uniform linear array with $N = 64$ antenna elements with spacing $\frac{\lambda}{2}$. We focus on the single user case, where the UE has fixed beamforming acting as a single virtual antenna. We aim to learn the AoA with resolution $1/\delta = 128$.

Even though Alg. 4 and Alg. 5 are developed for the case of static fading in Sect. 4.3.2, we test their performance under a more practical AR-1 time correlated model, described below. Under perfect knowledge of the operating SNR (large-scale fading) as well as perfect frequency/phase synchronization, the fading coefficient is given as:

$$\alpha_{t+1} = \alpha_t\sqrt{1-g} + \sqrt{\frac{k_r}{1+k_r}}\gamma\left(1-\sqrt{1-g}\right) + e_t\sqrt{\frac{g}{1+k_r}},$$

where $\gamma = 1$, k_r is the Rician fading factor, g is the correlation parameter, and $e_t \sim \mathcal{CN}(0,1)$ is the independent noise term.

The correlation parameter g is set such that coherence time $T_c = 2$ ms (equivalent to $\tau = 28$ total slots using the 5G NR PRACH format B4 [61]), and a Rician factor $k_r = 10$ (this is a reasonable value, e.g. indoor mmWave channel models [63]). For these parameters, we assume a conservative range for $\underline{\alpha}_t$ to be: $[r_{\text{min}}, r_{\text{max}}] = [0, 2],\ [z_{\text{min}}, z_{\text{max}}] = [-0.7, 0.7]$, with resolution parameters $\frac{1}{\triangle_r} = \frac{1}{\triangle_z} = 50$ Very low resolution parameters will reduce complexity but may impact performance, a further investigation is outside the scope of this chapter.

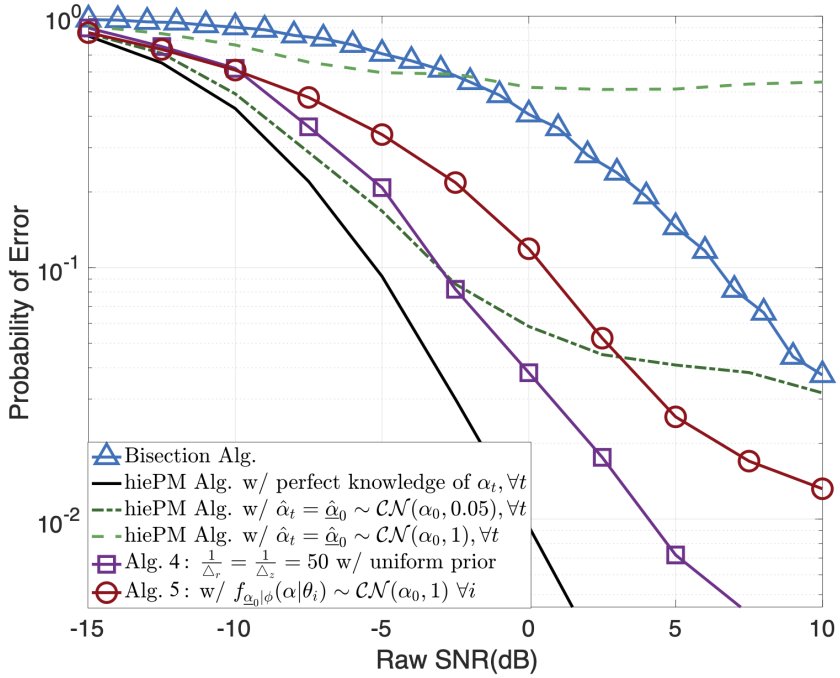

Figure 4.4: Comparison of the error probability performance between our proposed algorithms and prior works as a function of raw SNR P/σ^2 under Rician AR-1 fading. The probability of error in selecting the correct final beamforming is given by Eq. (4.47).

Probability of error

First, we analyze the performance of our proposed algorithms in terms of the probability of error in choosing the correct final beamforming vector, defined as:

$$\text{Prob}\{\mathbf{w}(\hat{\phi}) \neq \mathbf{w}(\phi)\}. \tag{4.47}$$

In Fig. 4.4 we compare performance to the Bisection algorithm of [46], which utilizes no prior knowledge of of the fading coefficient, and to our prior work $hiePM$ of chapter 3 which utilizes the mismatched guess $\hat{\alpha} = (\underline{\alpha}_0 \sim \mathcal{CN}(\alpha_0, \sigma_\alpha^2))$ for all t. First, we note that while $hiePM$ with mismatch can be robust to the time-varying fading, this performance is highly dependent on the quality of the estimate. Our proposed Alg. 4 closely approaches the performance of perfect knowledge $\hat{\alpha}_t = \alpha_t$ and outperforms the mismatched estimates of [74] and the bisection algorithm of [46]. This suggests that Alg. 4 is in fact learning $\underline{\alpha}$ while simultaneously beamforming to detect ϕ in the duration τ. Similarly, Alg. 5 also improves on [74] and [46]. However, as expected the performance is not

a good as Alg. 4 due to the assumption we make about shape of the estimate $f_{\underline{\alpha}|\phi,Y_{1:t}}(\alpha|\theta_i, y_{1:t})$ in order to reduce the computation complexity. As a result, the proposed algorithms highlight a trade-off between computational complexity and performance in terms of probability of error.

Spectral Efficiency

Next, we analyze the practical metric of spectral efficiency. Given a total communication time frame T (τ and T may require further system optimization, however, this is outside the scope of this work), the expected spectral efficiency achieved using the final beamforming vector $\mathbf{w}(\hat{\phi})$ is:

$$\mathbb{E}\left[\frac{T-\tau}{T}\log\left(1+\frac{P \mid \mathbf{w}(\hat{\phi})^H \mathbf{a}(\phi) \mid^2}{\sigma^2}\right)\right]. \tag{4.48}$$

In Fig. 4.5 we plot the performance in spectral efficiency Eq. (4.48) of our proposed algorithms compared to $hiePM$ with mismatch estimates of [74] and the Bisection algorithm of [46]. The results mimic closely the results we observed in performance of probability of error. Our proposed Alg. 4 and Alg. 5 achieve improvements spectral efficiency over [74] and [46] due to the mistakes that these make in the selection of the correct final beamforming vector. We see how critical these mistakes are in the regime low (-10dB to $+5$dB) raw SNR where correct selection of the beamforming vector enables much higher spectral efficiency.

4.4 Conclusion

This work considers the problem of recovering a unit common support vector $\mathbf{W}$ with unknown stochastic coefficients. In part I. we present a scheme, $marginalPM$, for sequentially selecting measurement vectors and two corresponding algorithms for recovering $\mathbf{W}$. As a first step to demonstrate an adaptivity gain over a non-adaptive algorithms, we demonstrate an adaptivity gain for the case with correlations between measurements with a static $X_t = X$, and with uncorrelated i.i.d. X_t. Our ongoing work considers development of a Kalman prediction step for complexity reduction in Alg. 5 and a prediction formulation in the posterior for Alg. 4 for even better performance under

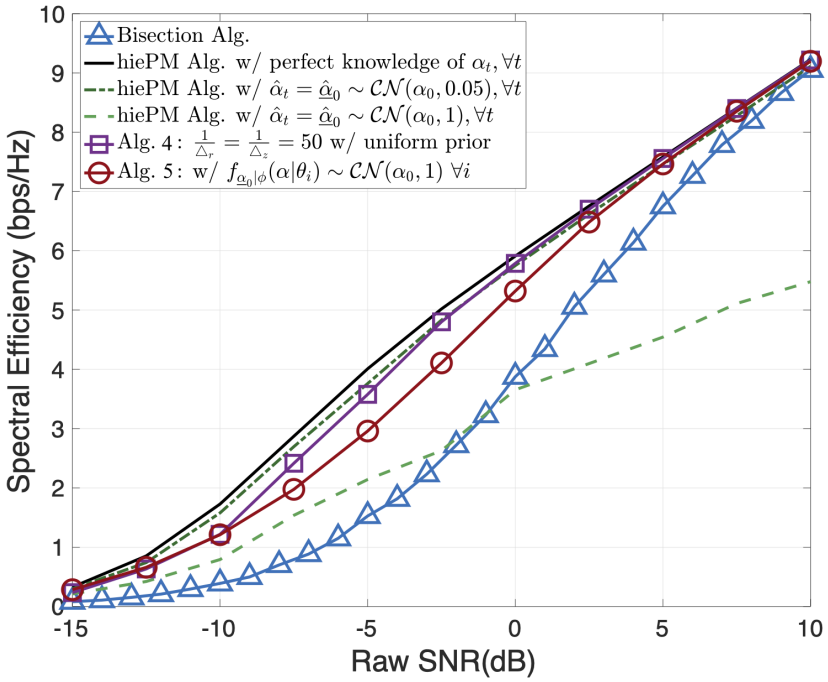

Figure 4.5: Comparison of the spectral efficiency between our proposed algorithms and prior works as a function of raw SNR P/σ^2 under Rician AR-1 fading. The spectral efficiency is given by Eq. (4.48).

other dynamic models. Comparison to existing strategies that utilize non-binary measurement vectors, or carefully designed recovery techniques is left as a future work. Analysis of the more complicated model with $\|\mathbf{W}\|_0 > 1$ is also of practical interest. In part II. of this chapter we revisit the problem of sequential beamforming design for mmWave initial alignment, with the added challenge of dynamic channel conditions. We extend the proposed algorithms for learning the CSI made up of the fading coefficient and AoA. As a first step to demonstrate robustness under a practical time-varying fading model, our numerical results show that under a practical hierarchical codebook the proposed algorithms outperform our prior work, $hiePM$ with mismatched estimate of α, and a strategy for sequential beam refinement in the literature (the Bisection algorithm of [46]). Comparison to strategies that utilize larger, user specific, or carefully designed codebooks is left as a future work. Analysis under other types of fading with more complicated models like multi-path fading, and mobile users is also of practical interest.

Chapter 4, in part, is a reprint of the material as it appears in the paper: Nancy Ronquillo and Tara Javidi, “Measurement Dependent Noisy Search with Stochastic Coefficients," IEEE

International Symposium on Information Theory, 2020. The dissertation author was the primary investigator and author of this paper.

Chapter 4, in part, is a reprint of the material as it appears in the paper: Nancy Ronquillo, Sung-En Chiu, and Tara Javidi, “Sequential Learning of CSI for MmWave Initial Alignment," IEEE Asilomar Conference on Signals, Systems, and Computers, 2019. The dissertation author was the primary investigator and author of this paper.

Chapter 5

Active Beam Tracking Under Stochastic Mobility

This chapter includes our final step towards solving the more general problem of recovering the random vector $\mathbf{X}_t$ (1.1). We consider the case where $\mathbf{X}_t$ is extremely sparse, i.e. $\|\mathbf{W}\|_0 = 1$, but the location of the non-zero element changes over time. In terms of the mmWave beam alignment problem, we can think of this as the very practical scenario where the transmitter is moving over time relative to the receiver. In this chapter we propose a novel method of active and sequential beam tracking at mmWave frequencies and above. We focus on the dynamic scenario of UAV to UAV communications where the problem is equivalent to tracking an optimal beam vector along the line-of-sight path. We propose an algorithm for actively and sequentially selecting beamforming vectors based on a Bayesian posterior with a prediction step to account for the mobility.

5.1 Introduction

Communication at mmWave frequencies and above utilizing antenna arrays with a small footprint has been been proposed as part of next generation wireless systems, enabling significantly higher data rates. Numerous yet small antenna arrays can overcome propagation and atmospheric losses by concentrating power through directional beamforming. In scenarios with

static or quasi-static channel conditions, many innovative solutions have been proposed to obtain robust beamforming for communication, even at a low SNR regime (< 5 dB) [47, 72, 74], as discussed in chapter 3.

However, we note that these solutions rely on the static or quasi-static nature of the channel to ensure a robust directional beamforming based on near real-time acquisition of channel state information. The problem is far more challenging under dynamic channel conditions such as a cellular enabled unmanned aerial vehicle (UAV) systems. This work proposes an active beam tracking solution for mobile scenarios where channel state information can vary significantly and in an unpredictable stochastic fashion. Our work generalizes earlier work on beam tracking under predictable movement [75], as well as Kalman-based estimation strategies [76–78] for small angle variations.

Our proposed algorithm utilizes a hierarchical codebook with beams of various widths and variable achievable gains to sequentially select beamforming vectors. Drawing on a connection between dynamic measurement dependent noisy search, which we introduced in chapter 2 (see also [6, 9, 48, 68]), and joint-source channel coding for dynamical systems [8] to account for stochastic movements. The proposed methodology relies on the key elements of posterior matching [6] for sequentially selecting beamforming vectors, a corresponding posterior update, and a one-step prediction of the posterior for beam tracking. We provide closed form solutions of the posterior update and prediction equations for select Markov movement models, which as a special case can recover prior work on predictable mobility [75] as well as the Extended Kalman filter [76]. Numerically, we demonstrate the superior performance of our proposed tracking algorithm over prior work in terms of normalized beamforming gain under various stochastic mobility models.

5.2 Problem Set-up

Consider a UAV to UAV communication system. We consider the general problem of adaptive processing for a receiving UAV (RX) with a Uniform Planar Array equipped with $N \times M$

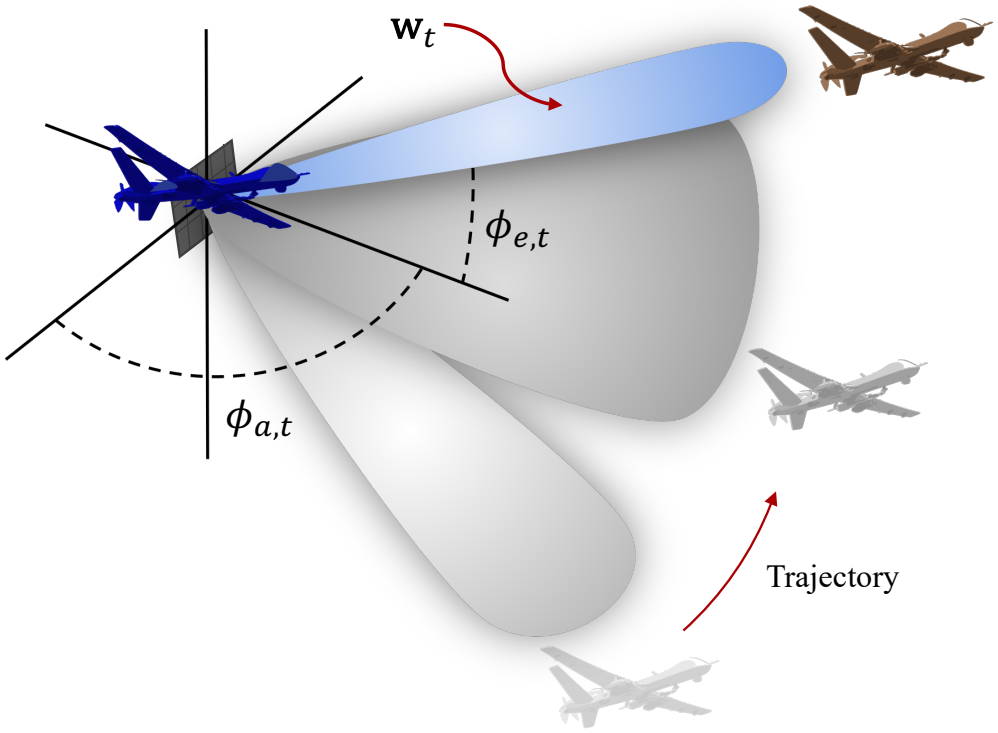

Figure 5.1: UAV beamforming setup for AoA $\Phi_t = (\phi_{a,t}, \phi_{e,t})$.
87

antennas and 3-D angular range. However, we note that the proposed algorithm is also suitable for a 2-D set up with a Uniform Linear Array and N antennas, which is discussed in Sect. 5.4.

Each transmitting UAV (TX) has fixed beamforming acting as single virtual antenna. We consider a low-power set-up where all UAV use a single RF Chain. The RX combines the signal from the antenna elements to the RF chain by the directional beamforming vector $\mathbf{w_t}$ at time $t = 1, 2, \ldots, \tau$, where t represents a beamforming slot. Fig. 5.1 illustrates the beamforming setup for an RX tracking a mobile TX across its movement trajectory. In this work we focus on the pilot training in order to analyze strategies for selecting beamforming vectors $\mathbf{w}_t$ at each time slot. When different UAV are simultaneously transmitting, the code-matched signal from a given UAV, $k \in K$, can be written as

$$y_t^k = \sqrt{P}\mathbf{w}_t^H (\sum_{k'=1}^{K} \mathbf{h}_{k'} \mathbf{s}_{k'}^T)\mathbf{s}_k^* + \mathbf{w}_t^H \mathbf{N}_t \mathbf{s}_k^*. \tag{5.1}$$

We use the stochastic multi-path modelling assumption with a single dominant path.

Assumption 5. *The small-scale channel can be described as:*

$$\mathbf{h} = \alpha_t \mathbf{a}(\Phi_t), \tag{5.2}$$

where $\alpha_t \in \mathbb{C}$ is the complex path gain, $\Phi_t = (\phi_{a,t}, \phi_{e,t})$ is the AoA in azimuth and elevation for $\phi_{a,t}$ and $\phi_{e,t} \in [\theta_{min}, \theta_{max}]$,

$$\begin{aligned}\mathbf{a}(\Phi_t) := \sqrt{\frac{1}{NM}}\Big[1, e^{j\frac{2\pi d}{\lambda}[\sin\phi_{a,t}\sin\phi_{e,t}+\cos\phi_{e,t}]}, \\ \ldots, e^{j\frac{2\pi d}{\lambda}[(N-1)\sin\phi_{a,t}\sin\phi_{e,t}+(M-1)\cos\phi_{e,t}]}\Big]\end{aligned} \tag{5.3}$$

is the array manifold created by the Angle-of-Arrival (AoA) with antenna spacing d.

Furthermore, we assume orthogonal sequences where a given TX $k \in K$, sends pilot sequence s_k such that:

Assumption 6.

$$\mathbf{s}_k^H \mathbf{s}_{k'} = \begin{cases} 1 \textit{ for } k = k' \\ 0 \textit{ for } k \neq k' \end{cases}. \tag{5.4}$$

Under Assumptions 5 and 6, the received signal for a given UAV is simplified to:

$$y_t = \sqrt{P}\alpha_t \mathbf{w}_t^H \mathbf{a}(\Phi_t) + \mathbf{w}_t^H \mathbf{n}_t, \tag{5.5}$$

where the additive noise vector $\mathbf{n}_t := \mathbf{N}_t \mathbf{s}_k^* \sim \mathcal{CN}(0_{N\times 1}, \sigma^2 \mathbf{I})$, under the assumption of normalized beams $\|\mathbf{w}_t\| = 1$, without loss of generality. We consider perfect knowledge of the operating SNR, defined as $\frac{P}{\sigma^2}$ which is the SNR that would be received with narrowest aligned beamforming. In this chapter we focus on the adaptive selection of beamforming vectors although the specific communication protocol is discussed in chapter 6.

5.2.1 Mobility Model

We consider a UAV mobility model where the AoA trajectory changes according to an independent increment process consisting of predictable and unpredictable (random) elements. That is, the AoA Φ_t evolves as

$$\Phi_{t+1} = \Phi_t + V + \mathbf{r}, \tag{5.6}$$

where the known vector, V, models predictable elements of mobility, for example an AoA position changing with constant speed. The zero mean random vector $\mathbf{r} \in \mathbb{R}$ models the unpredictable components, such as a sudden jump.

5.2.2 Beamforming with a Codebook

We are interested in the selection of beamforming vectors to use at each slot t in order to track the AoA. Specifically, we consider a stationary beamforming design policy as a causal (possibly random) mapping function from past observations to the beamforming vector: $\mathbf{w}_{t+1} = \gamma(y_{1:t}, \mathbf{w}_{1:t})$. Under Assumption 5, the quality of the established communication link depends on the estimate of channel state information $\hat{\mathbf{h}}_t$, which is determined by a current estimate $\hat{\Phi}_t$. In particular, each estimate provides beamforming $\mathbf{w}_t$ which results in normalized beamforming gain:

$$G_{BF} = \mathbb{E}\Big(\frac{|\mathbf{w}_t^H \alpha_t \mathbf{a}(\Phi_t)|^2}{|\alpha_t \mathbf{a}(\Phi_t)|^2}\Big). \tag{5.7}$$

In other words, the quality of the established communication link over a period of time $t = [1:T]$ strongly depends on a method to robustly and continuously detect and track the AoA Φ_t for $t = [1:T]$. To reduce complexity, it is common to limit $\mathbf{w}_t$ to a pre-designed beamforming codebook $\mathcal{W}^S$ with finite cardinality and hierarchical structure. Such hierarchical codebooks are investigated for UAV communications in [79] and in [80] for small angle variations. We assume the codebook, $\mathcal{W}^S$, has S levels with k_l vectors in each level $l \in S$ that partition the angular search space into contiguous sectors with increasing resolution $k_l < k_{l+1}$ and finest resolution $k_S = \frac{1}{\delta_a} \times \frac{1}{\delta_e}$ in azimuth and

elevation. Let the matrix $\tilde{\mathbf{w}}_t \in \{0,1\}^{\frac{1}{\delta_a}\times\frac{1}{\delta_e}}$ be a binary angular space matrix representation of $\mathbf{w}_t$. Beamforming vectors are assumed to be designed with the objective of near constant gain for intended directions (i.e. the non zero entries of $\tilde{\mathbf{w}}_t$) and almost zero otherwise.

5.3 Proposed Algorithm

Observations y_t given in (5.5) can be thought of as the probing of certain angular locations, indicated by $\tilde{\mathbf{w}}_t$, which give information about the presence or absence of the AoA in the angular space spanned by $\mathbf{w}_t$. This allows us to sequentially select beamforming vectors whose angular width $\|\tilde{\mathbf{w}}_t\|_0$ matches the accumulated belief about Φ_t.

We propose Alg. 6 which implements an active beamforming policy γ based on Bayesian posterior updates and predictions, and which achieves sequential refinement of uncertainty on the time-varying AoA Φ_t. Specifically, we implement $hiePM$ (Alg. 1 of chapter 3) to actively select each $\mathbf{w}_t$ based on posterior matching. We build on this algorithm and extend the evolution of the posterior to incorporate an update and prediction step which enables tracking for handling mobile UAV. We restrict the AoA point estimate $\hat{\Phi}_t = (\hat{\phi}_{a,t}, \hat{\phi}_{e,t})$ to the discrete set where $\hat{\phi}_{(a,t)} = \{\theta_1, \theta_2, \ldots \theta_{1/\delta_a}\}$, and $\theta_i = \theta_{\text{min}} + (i - \frac{1}{2}) \times \delta_a \times (\theta_{\text{max}} - \theta_{\text{min}})$. $\hat{\phi}_{e,t}$ is discretized similarly. Let the probability vector over Φ_t with resolution (δ_a, δ_e) be defined as $\boldsymbol{\pi}(t|t) \in [0,1]^{\frac{1}{\delta_a}\times\frac{1}{\delta_e}}$, where each element is:

$$\pi_{i,j}(t|t) := \mathbb{P}(\Phi_t = (\theta_i, \theta_j)|\mathbf{y}_{1:t}),\ i = 1, ..., 1/\delta_a, j = 1, ..., 1/\delta_e \tag{5.8}$$

and the probability of Φ_t being in the angular range covered by a beamforming vector $\mathbf{w}_t$ (with angular span $\tilde{\mathbf{w}}_t$) is the sum of the posterior entries corresponding to the non-zero entries of $\tilde{\mathbf{w}}_t$:

$$\pi_{\tilde{\mathbf{w}}_t}(t|t) := \sum_{i,j} \tilde{w}_{t,i,j} \pi_{i,j}(t|t). \tag{5.9}$$

Upon receiving a new observation y_t, the posterior probability is updated and followed by a

prediction step:

$$\boldsymbol{\pi}(t+1|t) \leftarrow \boldsymbol{\pi}(t|t) \leftarrow y_t, \boldsymbol{\pi}(t|t-1). \tag{5.10}$$

A beamforming vector at either level l^* or l^*+1 is selected for the next beamforming slot based on the accumulated belief around Φ_{t+1} as described by the prediction posterior probability $\boldsymbol{\pi}(t+1|t)$, which is a sufficient statistic. In other words, $\mathbf{w}_{t+1}(\boldsymbol{\pi}(t+1|t))$ is chosen as the k_{t+1}^{th} codeword in level l_{t+1} covering $\tilde{\mathbf{w}}_{[l_{t+1},k_{t+1}]}$ where:

$$[l_{t+1}, k_{t+1}] = \underset{[l',k']}{\operatorname{argmin}} \left| \pi_{\tilde{\mathbf{w}}_{[l',k']}}(t) - \frac{1}{2} \right|. \tag{5.11}$$

The first step in (5.10) is a Bayesian posterior update:

$$\begin{aligned} &\pi_{i,j}(t|t) = \mathbb{P}(\Phi_t = (\theta_i, \theta_j) | y_{1:t}) \\ &= \frac{f(z_t|\Phi_t = (\theta_i, \theta_j), \mathbf{w}_t)\pi_{i,j}(t|t-1)}{\sum_{i'=1}^{1/\delta_a} \sum_{j'=1}^{1/\delta_e} f(z_t|\Phi_t = (\theta_{i'}, \theta_{j'}), \mathbf{w}_t)\pi_{i',j'}(t|t-1)}. \end{aligned} \tag{5.12}$$

where $f(z_t|\Phi_t = (\theta_i, \theta_j), \mathbf{w}_t)$ is the conditional distribution of $z_t = q(y_t)$ and depends on the function $q(\cdot)$ of available information. For a pilot slot with received signal y_t (5.5), the full measurement $z_t = y_t$ is known to be:

$$f(z_t|\Phi_t = (\theta_i, \theta_j), \mathbf{w}_t) = g\Big(y_t - G_{i,j}\Big), \tag{5.13}$$

where $G_{i,j} = \mathbf{w}_t^H \mathbf{a}(\theta_i, \theta_j)$ is the gain conditioned on $\Phi_t = (\theta_i, \theta_j)$ and $g(x)$ is the circularly symmetric complex normal distribution with variance σ^2 and assumption of known $\alpha = 1$, $P = 1$. We note that our approach, and specifically the extensions detailed in chapter 4, can handle stochastic and time varying complex gain through simultaneous estimation of α_t. However, in this chapter we focus only on the performance in terms of recovering and tracking Φ_t by fixing the gain.

It follows that the computational requirements of sequentially designing $\mathbf{w}_{t+1} = \gamma(\boldsymbol{\pi}(t+1|t))$ at every beamforming slot will include the selection policy γ (5.11), the Bayesian posterior

update (5.12), and the one-step prediction update. While the first steps of Alg. 6 can be generalized as above, the one-step posterior update from $\boldsymbol{\pi}(t|t)$ to $\boldsymbol{\pi}(t+1|t)$ will depend on the formulation for a particular movement model (5.6). The computation complexity is dominated by the cost of the posterior update (5.12) at each beamforming slot t. The worst case cost is $O(\frac{1}{\delta_a} \times \frac{1}{\delta_e})$ if each element is updated individually. However, this can be reduced to $O(log(\frac{1}{\delta_a} \times \frac{1}{\delta_e}))$ by considering the geometric constraints on the hierarchical contiguous codebook elements [81].

Algorithm 6: Active beam tracking for mobile AoA

Input: target resolution (δ_a, δ_e), codebook $\mathcal{W}^S$, T (last beamforming slot), Markov mobility model (5.6)

Output: Beamforming vector $\mathbf{w}_t$ and estimate of the AoA $\hat{\Phi}_t$ up to a resolution δ for each slot t

Initialization: uniform $\boldsymbol{\pi}(1|0)$

while $t \leq T$ **do**

  # Beam selection based on hierarchical posterior matching with variable width beams (5.11):

$$\mathbf{w}_t(\boldsymbol{\pi}(t|t-1)) \in \mathcal{W}^S$$

  # Received output: $y_t = \sqrt{P}\alpha_t \mathbf{w}_t^H \mathbf{a}(\Phi_t) + \mathbf{w}_t^H \mathbf{n}_t$

  # Posterior update by Bayes' Rule (5.12)

$$\boldsymbol{\pi}(t|t) \leftarrow y_t, \boldsymbol{\pi}(t|t-1)$$

  # Posterior one-step prediction

$$\boldsymbol{\pi}(t+1|t) \leftarrow \boldsymbol{\pi}(t|t)$$

  # Estimate of AoA: $\hat{\Phi}_t = \text{argmax}_{(\theta_i,\theta_j)}\, \pi_{i,j}(t|t)$

5.4 Example Scenarios

In this section, we illustrate the proposed tracking scheme by considering a special case where we reduce the AoA point estimates to the 2-D angular domain, to study select examples of Markov mobility in the form (5.6). Assuming the point estimates $\hat{\Phi}_t = \hat{\phi}_t \in \{\theta_1, \theta_2, \ldots \theta_{1/\delta}\}$ and $\theta_i = \theta_{\text{min}} + (i - \frac{1}{2}) \times \delta \times (\theta_{\text{max}} - \theta_{\text{min}})$. We utilize the hierarchical beamforming codebook, $\mathcal{W}^S$,

of [46] where vectors in level $l \in S = log_2(1/\delta)$ have angular width $\|\tilde{\mathbf{w}}_t\|_0 = \frac{1/\delta}{2^l}$ that is half the size of the prior level. This is approximately achieved via a pseudo inverse approximation. The resulting beams are slightly imperfect with reduced gain in angles further from the center beam directions, however, these effects are fully accounted for in our numerical simulations.

We consider three movement models that fall into two broad categories: predictable and unpredictable mobility. Predictable mobility consists of fixed and known angular movements, like a constant velocity, where ϕ_{t+1} can be calculated from ϕ_t. We consider unpredictable mobility to be modeled by stochastic processes and we look at two examples: Gaussian angular movements and Bernoulli angular jumps. We show that predictable mobility is equivalent to no movement when the predictable mobility can be accounted for. On the other hand, stochastic mobility is much harder to handle, but can be tracked by incorporating side information into the prediction step of (5.10).

For brevity, we only provide the one-step prediction formulation of (5.10) and numerical results for three example UAV movements. However, the one-step prediction can be similarly formulated and analyzed for any other stochastic model in the form of (5.6), we leave an in depth analysis of any other mobility models as potential future work.

5.4.1 Predictable Movement

Fixed Angular Movement

Consider the AoA to change according to a fixed angular velocity:

$$\phi_{t+1} = \phi_t + V \tag{5.14}$$

where $V = \nu\delta\pi$ summarizes the constant velocity $\nu\delta\pi$ radians per time slot. In this work we assume that V is known, however, a small preamble to determine an unknown angular velocity is easily implemented as in [75]. Intuitively, for integer values of ν the corresponding one-step prediction in (5.10) is:

$$\pi_i(t+1|t) = \pi_{i-\nu}(t|t), \tag{5.15}$$

and for $|\nu| < 1$

$$\pi_i(t+1|t) = (1-\nu)\pi_i(t|t) + \nu\pi_{i+sign(\nu)}(t|t). \tag{5.16}$$

Remark 8. The one-step posterior prediction $\boldsymbol{\pi}(t+1|t)$ is a shifted version of the posterior update $\boldsymbol{\pi}(t|t)$, this is easiest to see for integers ν, where this is a simple horizontal translation. For any predictable mobility the one-step prediction will result in a shifting or deterministic rearranging of the posterior $\boldsymbol{\pi}(t|t)$. As a result, we can apply the same fundamental limits as in Sect. 3.4 of chapter 3 in terms of estimation error probability and time required to obtain a robust initial estimate of $\hat{\phi}_t$.

5.4.2 Stochastic Movement

Gaussian Angular Movement

Consider the mobility scenario where the AoA changes with Gaussian angular movements due to small intractable position changes on the UAV such as with small drones. That is, the AoA evolves as:

$$\phi_{t+1} = \phi_t + \mathbf{z}_t \tag{5.17}$$

where $\mathbf{z}_t$ is an i.i.d. zero mean Gaussian with variance σ_ϕ^2. Intuitively, this is a good model for small uncertainties about direction or vibrations. Note that in case of a misalignment event, the cumulative movement results in a linear growth in uncertainty. The corresponding one-step prediction of (5.10) is:

$$\pi_i(t+1|t) = \langle \boldsymbol{\pi}(t|t), \mathbf{g}_{[\theta_i, \sigma_\phi^2]} \rangle, \tag{5.18}$$

where $\mathbf{g}_{[\theta_i,\sigma_\phi^2]} \in [0,1]^{1/\delta}$ is a probability mass function obtained from a quantized and truncated Gaussian random variable $x \sim \mathcal{N}(\theta_i, \sigma_\phi^2)$ with resolution δ. Equivalently, each element is given as:

$$g_{[\theta_i,\sigma_\phi^2]}(n) \propto \mathbb{P}[\theta_n - \frac{\delta\pi}{2} \leq x < \theta_n + \frac{\delta\pi}{2}], \tag{5.19}$$

for $n = \{1, \ldots, 1/\delta\}$, and normalized such that $\sum \mathbf{g}_{[\theta_i,\sigma_\phi^2]} = 1$.

Bernoulli Angular Jumps

Next, consider the case where the AoA can incur a large random jump from one beamforming slot to another. We assume the AoA moves according to

$$\phi_{t+1} = \phi_t + b\mathbf{q} \tag{5.20}$$

where $b = \beta\delta\pi$ is a known probable jump size and $\mathbf{q}$ is a Bernoulli random variable with parameter (p), where p is the probability of a jump. This can occur for example in the cases of blockage or sudden changes in velocity. This is difficult to handle because the random movement almost certainly will cause an outage if the beamforming is not updated quickly. As a result of such jumps, existing tracking methods will likely trigger a reset or re-estimation protocol due to invalid tracking (i.e. not meeting a minimum tracking quality). If the jump is small enough, a Kalman filtering strategy may try to update the estimate on the state ϕ_t based on observations y_t and catch up. In contrast, our approach is to conservatively account for the uncertainty about ϕ_t preemptively, by widening the posterior in the prediction step. That is, the proposed algorithm accounts for the likelihood of jumps by increasing the posterior probability in probable jump locations. For integer estimates of the jump size β, the one-step prediction in (5.10) can be specified as:

$$\pi_i(t+1|t) = \Big[(1-p)\ \pi_i(t|t) + p\pi_{i-\beta}(t|t)\Big]. \tag{5.21}$$

In general, the mobility model for a target AoA may differ from the ones considered here. The aim of this work is to introduce the idea of incorporating mobility information into the the selection of

beamforming vectors for tracking, especially for the cases where the movement may be stochastic, in order to robustly handle outage scenarios. The main idea is to use prior information and adapt to the uncertainty by widening and shrinking the beam width $\|\tilde{\mathbf{w}}_t\|_0$ corresponding to probable movements or a misalignment rather than forcing a reset protocol. We summarize the one-step predictions for the models discussed in Table 5.1.

Table 5.1: One-Step Posterior Prediction - Markov Movements

	Movement $\phi_{t+1} =$	One-step Predict $\pi_i(t+1\|t) =$
Static	ϕ_t	$\pi_i(t\|t)$
Constant	$\phi_t + \nu\delta\pi$	$\pi_{i-\nu}(t\|t),\ \nu$ integer $(1-\nu)\pi_i(t\|t) + \nu\pi_{i\pm1}(t\|t),\ \|\nu\| < 1$
Gaussian	$\phi_t + \mathbf{z}$, $\mathbf{z} \sim \mathcal{N}(0, \sigma_\phi^2)$	$\langle \boldsymbol{\pi}(t\|t), \mathbf{g}_{[\theta_i, \sigma_\phi^2]} \rangle$
Jumps	$\phi_t + b\mathbf{q}$, $\mathbf{q} \sim$ Bern(p)	$(1-p)\pi_i(t\|t) + p\pi_{i-\beta}(t\|t)$

5.5 Numerical Results

Next, we analyze the performance of the proposed beamforming algorithm under the mobility examples discussed above. We focus on comparisons to beamforming selections by the the extended Kalman filtering (EKF) algorithm of [76] and the dynamic pilot insertion algorithm of [75]. Our proposed algorithm provides a methodology for including mobility information when it is available in an adaptive manner, which incurs a computational and memory cost dominated by the cost of computing the posterior updates $O(log(\frac{1}{\delta}))$. However, we note that the strategies of [75, 76] do not require any prior knowledge of the mobility model. Instead, these strategies [75, 76] operate under the assumption of unknown quasi static AoA, where reset phases are used for dealing with severe misalignment which are less computationally intensive but may require larger downtime to recover an estimate. We compare performance in terms of the normalized beamforming gain (5.7) to assess the validity of our sequential beam selection algorithm and illustrate the gains achievable by adaptively responding to mobility information.

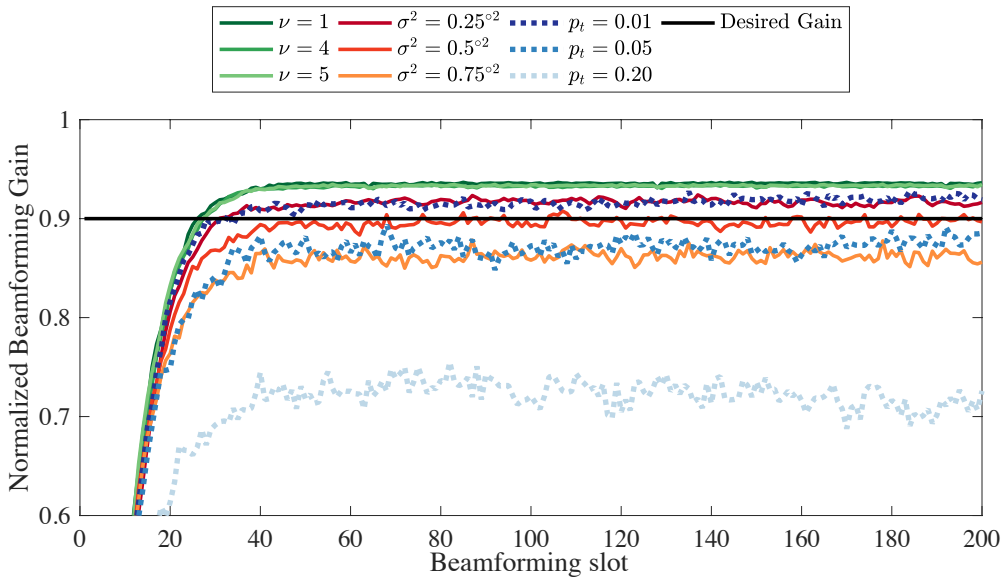

Figure 5.2: Average normalized beamforming gain (5.7) obtained by the proposed algorithm for the various mobility models considered in Table 5.1 at 10dB SNR.

5.5.1 Fixed Angular Movement

The EKF and dynamic pilot algorithms [75, 76] switch between estimation of the AoA (via exhaustive search) and active tracking. After an exhaustive search over the $1/\delta$ possible beams, an initial estimate $\hat{\phi}_{1/\delta}$ is obtained. The next step for the EKF algorithm [76] is to choose beams based on tracking estimates of the state $\hat{\phi}_t$ with extended Kalman filter updates. In the dynamic pilot algorithm [75] beams are chosen based on tracking updates that geometrically account for a constant angular velocity. For both strategies [75, 76], the tracking duration is determined by a threshold on the quality of tracking. When tracking is no longer valid, a reset is triggered and the exhaustive beams are used again in order to obtain another estimate of the AoA. The EKF algorithm [76], imposes a minimum MSE threshold ($\sqrt{MSE} = \frac{BW}{2}$ half beam width), while the dynamic pilot algorithm [75] uses a threshold on the receive power (P_{min}). We note that these tracking thresholds require optimization, thus in the following simulations we generously assume perfect exhaustive search estimates and try to optimize the tracking parameters empirically in order to compare performance.

The following simulations consider an RX with N=32 antennas and an angular discretization

with $1/\delta = 64$. We consider $\phi_t \in [-\pi, 0]$ and randomize the starting point ϕ_0 to fully account for cases on the edges of the angular space. We focus on relative comparisons, although physical properties corresponding to the considered SNR values (like cell size and bandwidth) can be defined as in Fig. 3.6 of chapter 3.

Fig. 5.2 shows the expected normalized beamforming gain over time achieved by the proposed algorithm at 10 dB SNR for each of the mobility models considered. We average the results over $1,000$ iterations. We begin by looking at the model of fixed angular mobility (5.14) with $V = \nu\delta\pi$, $\nu = \{1, 4, 5\}$, which is made up entirely of predictable movements. The number of beamforming slots required by the proposed algorithm to reach a stable gain is a lot fewer than those required by the exhaustive search (requiring $1/\delta$ beamforming slots). Note that Fig. 5.2 verifies Remark 8 by showing that the performance is invariant to the velocity and thus can be handled by our algorithm as efficiently as detecting a static AoA $(\nu = 0)$ without compromising beamforming gain. To get a sense of performance compared to existing approaches in terms of tracking quality, in Fig. 5.3 we show an AoA trajectory for one instance over time and the corresponding AoA estimates and beamforming gains achieved by the algorithms considered. The extended Kalman filter and the dynamic pilot strategy adjust estimates $\hat{\phi}_t$ based on a given to be known speed and can successfully account for this predictable movement as well as the proposed algorithm. None of the algorithms are significantly affected by this constant velocity in terms of achievable beamforming gain, other than slight dips in the gain which are caused when the AoA lies near the edge of a selected beam.

5.5.2 Gaussian Angular Movement

Next, we analyze Gaussian angular movements (5.17) for $\sigma_\phi^2 = \{0.25^{\circ 2}, 0.5^{\circ 2}, 0.75^{\circ 2}\}$. Fig. 5.2 shows that the proposed algorithm can achieve a high and stable beamforming gain quickly and can maintain this robustly in the long term for up to $\sigma_\phi^2 = 0.5^{\circ 2}$. Even for mobility with larger entropy $\sigma_\phi^2 = 0.75^{\circ 2}$, the achievable gain remains stable, albeit slightly decreased. This suggests that beams are being selected potentially with larger widths slightly more frequently to ensure tracking under such high mobility and to prevent and recover from outages. For comparisons to the strategies

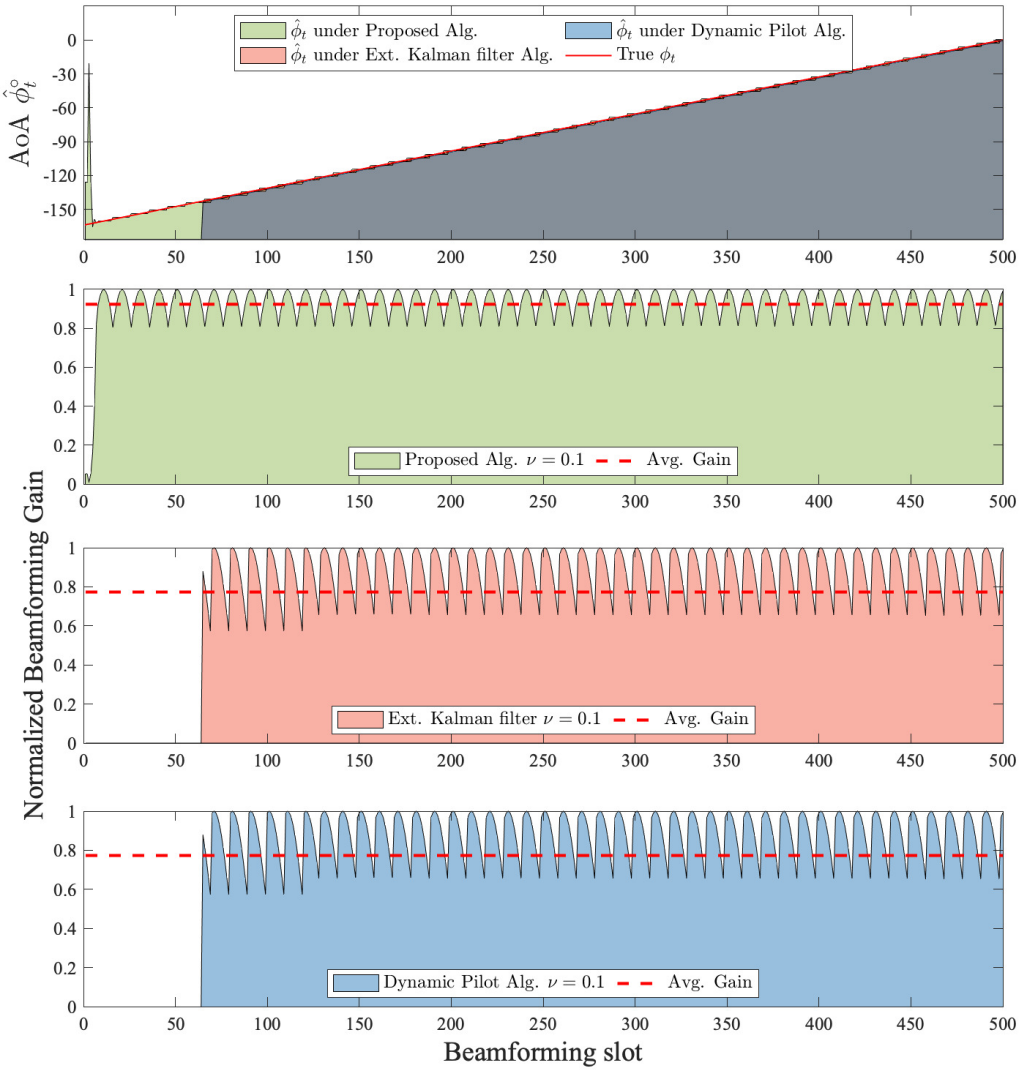

Figure 5.3: Example - Normalized beamforming gain (5.7) at 10dB SNR for constant angular movement (5.14) with $\nu = 0.1$.

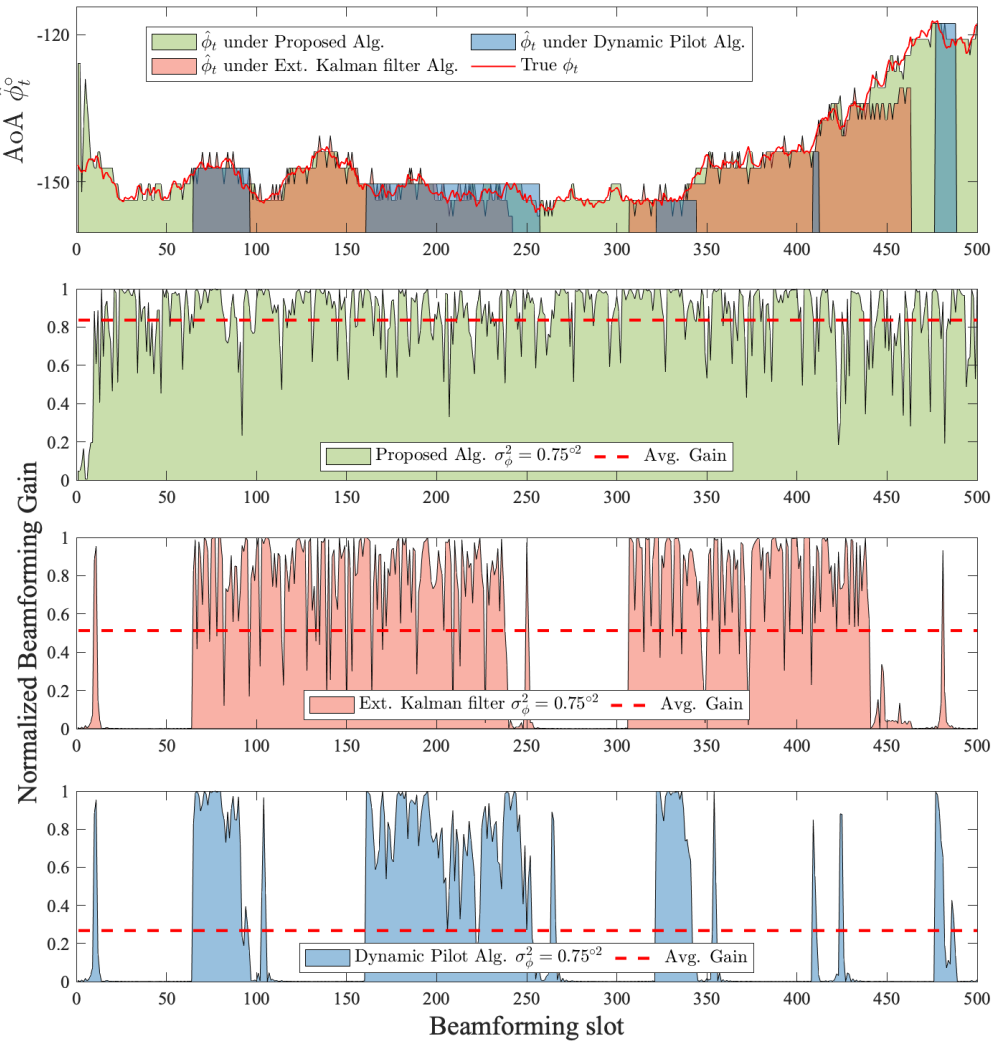

Figure 5.4: Example - Normalized beamforming gain (5.7) at 10dB SNR for Gaussian Movement (5.17) with $\sigma_\phi^2 = 0.75^{\circ 2}$.

of [75, 76] in terms of tracking performance, in Fig. 5.4 we look specifically at the most difficult case of $\sigma_\phi^2 = 0.75^{\circ 2}$.The proposed algorithm is best able to maintain high beamforming gains with occasional but quick recoveries, while the other algorithms must resort to the reset protocols when severe outages occur.

5.5.3 Bernoulli Angular Jumps

Lastly, we analyze occasional Bernoulli jumps (5.20) with jump size $b = 5^\circ$ and probabilities $p = \{0.01, 0.05, 0.20\}$. Such random jumps are very difficult to handle because alignment schemes (including exhaustive search) will struggle to obtain correct initial estimates if a jumps occurs in this phase since they operate under the assumption quasi-static AoA. Even if a good beam estimate is obtained successfully, the duration of following tracking phase will largely depend on the frequency of the jumps (the entropy), since each jump is likely to cause an outage. Fig. 5.2 shows that the performance of the proposed algorithm is affected by the entropy of such jumps, where the achievable gain begins to drop for higher probability of a jump p. However, it maintains stable beamforming gain for all values of p under the caveat of less than ideal gain for high p values. In Fig. 5.5 we plot performance comparisons to the strategies of [75, 76], however we note that the algorithms we compare to are not specifically designed for such mobility. Thus as expected, the algorithms of [75, 76] respond to sudden jumps by triggering a reset and re-estimation of the AoA. On the other hand, the proposed algorithm recovers quickly after a jump due to the embedding of mobility information in the selection of beams following a jump.

5.6 Conclusion

We consider the problem of active and sequential tracking of the CSI for robust beamforming at mmWave frequencies and above. We are interested in tracking stochastic movements, which may be especially critical in systems of communication between mobile UAV. Existing beamforming methods implement approaches which require a reset step in response to outages or low tracking

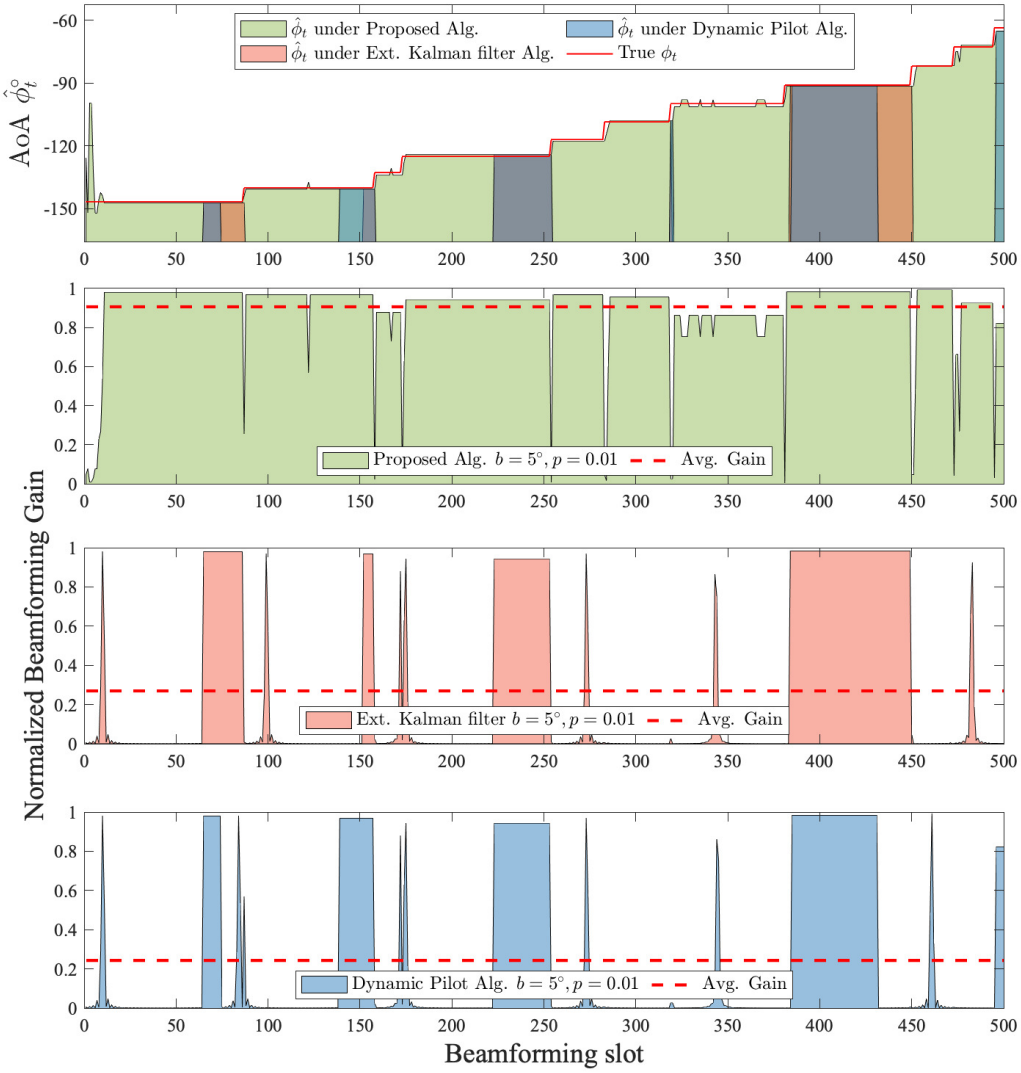

Figure 5.5: Example - Normalized beamforming gain (5.7) at 10dB SNR for Bernoulli jumps (5.20) with jump size $b = 5\circ$ and probability $p = 0.01$.

quality. We propose an active beamforming algorithm that incorporates mobility information into the sequential selection of beamforming vectors based on prior observations. We provide closed form equations for posterior updates and predictions for a selection of 2-D Markov mobility models. Our Numerical results show improved performance over the reset-type approaches and appear to have fewer sensitivities to movements with larger entropy.

Chapter 5, in full, is a reprint of the material as it appears in the paper: Nancy Ronquillo and Tara Javidi, “Active Beam Tracking Under Stochastic Mobility," IEEE International Conference on Communications, 2021. The dissertation author was the primary investigator and author of this paper.

Chapter 6

Active and Dynamical Beam Tracking Under Stochastic Mobility

In our presentation of active beam alignment up to chapter 5 we have thus far focused only on the beamforming selection process and the alignment performance in terms of probability or error and corresponding beamforming gain. To build a communication scheme, we envision the proposed algorithm for sequentially selecting beam vectors is suitable for adaptive pilot allocation as presented in this chapter. We formulate the communication signaling model and highlight the exploration exploitation dilemma brought on by mobility when aiming for beam alignment and desiring high data throughput. Our proposed adaptive piloting scheme is based on analysis of the mutual information and maximum achievable spectral efficiency. We observe bust beamforming and reduced overhead due to our analysis of the receive power in the data communication phase which enables power only Bayesian updates.

6.1 Introduction

CSI acquisition for maintaining beam alignment over time in the scenarios of high mobility, commonly referred to as beam tracking, has been extensively studied in [75–80, 82–86] We restrict our attention to the cases of beamforming under the practical implementation constraints of a

beamforming codebook, where the challenge can be thought of as effective beam selection or management. Existing approaches for handling very high mobility heavily rely on schemes of pilot allocation, switching between data transmission and pilot phases. More specifically, the pilot phase is used generally used for CSI and/or mobility estimation, for example by leveraging compressive sensing or least squares techniques [84]. In the data transmission phase, channel and/or mobility estimates are used to exploit the best predicted beam.

Some solutions focus on tracking predictable movements, such as a UAV moving at a known or estimated velocity, or where the AoA or UAV trajectory and position can otherwise be inferred or predicted according to a model geometry after estimation in the pilot phase [75, 82, 87]. If the transmitters mobility is unpredictable with random AoA variations, for example movements close to Gaussian noise with small variance, Kalman filtering based strategies for estimating the AoA can support tracking [76, 77] - possibly supplemented with geometric calculations for predicting the position of the transmitter instead [78]. However, for largely unpredictable movements such as large jumps or changes in trajectory, these solutions operate model-agnostic and handle sudden changes by implementing a form of adaptive switching between estimation and tracking based on either recurringly allocating pilots or by constantly evaluating the quality of tracking. Recent works have studied the benefits of using beams covering wider angular regions, rather than exclusively using narrow beams, in order to capture fast angle variations and reduce the pilot overhead [80, 86]. The pilot overhead can be reduced further by focusing on local beams according to current estimates, the caveat is reduced link quality due to the wider beam width.

We propose a method for actively and dynamically learning the AoA throughout the data transmission phase as well as adaptively allocating pilots. Specifically, our method actively selects beamforming vectors based on evolving a Bayesian probability belief dynamically. In the absence of excess uncertainty and with moderate SNR, posterior updates rely on the signal energy (which allows the update to be agnostic to the knowledge about the data sequence). When the belief displays a large variance, in contrast, our algorithm deploys a pre-designed pilot sequence to speed up learning.

6.1.1 Contributions

We consider the practical implementation with a single RF chain, and small scale channel dominated by the line-of-sight (LoS) single path, where CSI acquisition reduces to the problem of estimation and tracking of the dynamical angle of arrival (AoA). In particular, we view this problem as an active search for the AoA under the caveat of noisy measurements, whose noise intensity in dictated by the type of measurement. The problem of noisy search with measurement dependent noise has been studied from an information theoretic perspective where many works have established a connection to the problem of channel coding over a binary input channel [6,9,47,48,68], and to joint-source channel coding for dynamical systems in [8]. Existing adaptive strategies for measurement selection based on posterior matching have been shown to provide theoretical guarantees in performance [6, 48, 74]. We draw on these works, leveraging the connection to channel coding, to develop our adaptive beamforming algorithm based on posterior matching using a beamforming codebook. Our work generalizes earlier work on beam tracking under predictable movement [75], as well as filter-based estimation strategies [76–78] for small angle variations. Our contributions are as follows:

1. **Active and Sequential beam selection** We propose a method for sequentially selecting beamforming vectors in an active manner from a practically feasible hierarchical codebook, with beams of various widths and variable achievable gains based on posterior matching [6]. Our methodology consists of evolving the posterior via Bayesian updates and predictive filtering in order to incorporate mobility information in a dynamical manner. Our proposed active and sequential beam selection is restated from chapter 5.

2. **Adaptive Pilot Allocation** We propose an adaptive pilot allocation strategy to complete the communication scheme. Specifically, we propose to trade-off the pilot and data transmission phases by analyzing the mutual information and maximum achievable spectral efficiency terms. Combined with our active and sequential beam selection and dynamic tracking of the posterior, our approach trades off the pure exploration of pilot transmission against

exploitation in the data transmission. Our proposed tracking of the posterior, which enables simultaneous learning of the AoA (both in the data transmission and pilot phases), is inspired by the reward optimization learning paradigm of reinforcement learning algorithms [26].

3. **Numerical Results** We demonstrate via simulations the superior performance of our proposed communication scheme over prior work in terms of normalized beamforming gain and pilot overhead under three stochastic mobility models. We show that the case of predictable mobility can be handled as well as the static case, and thus recovers our prior fundamental limits on initial beam alignment [74]. We also consider the cases where the AoA has large Gaussian angular variations or is subject to Bernoulli angular jumps, which we show are significantly more difficult to handle. Comparing our work against the algorithms of [75, 76, 80], we demonstrate our robust beamforming and efficient tracking of the AoA with minimum pilot overhead. In practical terms, and under stochastic mobility, this means that our algorithm achieves significantly higher average beamforming gains and reduced pilot overhead.

6.2 Problem Set-up

Consider a UAV to UAV communication set up with adaptive processing for a receiving UAV (RX) with a Uniform Planar Array equipped with $N \times M$ antennas and 3-D angular range.[1] A transmitting UAV (TX) has fixed beamforming acting as a single virtual antenna. We consider a low-power set-up where the both UAV use a single RF Chain. The RX combines the signal from the antenna elements to the RF chain by the directional beamforming vector $\mathbf{w_t} \in \mathbb{C}^{NM}$ at $t = 1, 2, \ldots, T$, where t represents a beamforming or sampling time slot. Without loss of generality, we assume normalized beamforming vectors such that, $\|\mathbf{w}_t\|^2 = 1$.

For an air-to-air scenario a transmitting UAV will likely be unobstructed and free of reflectors,

[1] Beamforming of the receiver can be done with reduced reliance on feedback, and hence is chosen here for its simplicity. We note that the proposed algorithm is also suitable for a 2-D set-up with a Uniform Linear Array and N antennas as discussed in Sect. 6.5.

where we may assume that communication is dominated by the line-of-sight path. Therefore, we use the stochastic multi-path model (see Ch.7 in [55]) with assumption of a single dominant path.

Assumption 7. *The small-scale channel can be described by an $NM \times 1$ complex vector:*

$$\mathbf{h} = \alpha_t \mathbf{a}(\Phi_t), \tag{6.1}$$

where $\alpha_t \in \mathbb{C}$ is the complex path gain, $\Phi_t = (\phi_{a,t}, \phi_{e,t})$ is the AoA in azimuth and elevation for $\phi_{a,t} \in [\theta_{min}, \theta_{max}]$ and $\phi_{e,t} \in [\theta_{min}, \theta_{max}]$,

$$\mathbf{a}(\Phi_t) := \sqrt{\frac{1}{NM}} \left[1, e^{j\frac{2\pi d}{\lambda}[\sin\phi_{a,t}\sin\phi_{e,t} + \cos\phi_{e,t}]}, e^{j\frac{2\pi d}{\lambda}[(N-1)\sin\phi_{a,t}\sin\phi_{e,t} + (M-1)\cos\phi_{e,t}]}\right] \tag{6.2}$$

is the array manifold created by the Angle-of-Arrival (AoA) with antenna spacing d.

We consider communications from a TX to the RX over one beamforming slot to be characterized by one of two possible phases: pilot training or data transmission. Let the current phase be denoted by $e_t \in \{P, D\}$. The continuous time received signal over beamforming slot t is

$$r_t(\tau) = \alpha_t \mathbf{a}(\Phi_t)\mathbf{x}(\tau) \tag{6.3}$$

where $\mathbf{x}(\tau)$ is the transmitted sequence $\mathbf{x}(\tau) = \sum_{n=1}^{Nc} \sqrt{P_T} x_n p_r(\tau - nTc)$, consisting of transmitted symbols x_n and a pulse shaping function $p_r(\tau)$ where $\int |p_r(\tau)|^2 d_\tau = 1$, for N_c modulation symbols with T_c symbol duration. A receive beamforming vector $\mathbf{w}_t$ is applied for the duration of the beamforming slot. The discrete time signal at the output of a matched filter for the pulse shaping function $p_r(\tau)$ is

$$y_t = \alpha_t \sqrt{P_T} \mathbf{w}_t^H \mathbf{a}(\Phi_t) x_t + \mathbf{w}_t^H \mathbf{n}_t. \tag{6.4}$$

where $\mathbf{n}_t \sim \mathcal{CN}(0_{[NM\times 1]}, \sigma^2 \mathbf{I})$ is the additive AWGN. We consider perfect knowledge of the operating SNR, defined as $\frac{P_T}{\sigma^2}$ which is the SNR that would be received with narrowest aligned beamforming.

Receive a pilot $e_t = P$

During the pilot training phase, i.e. $e_t = P$, the transmitted symbols are assumed to be known at the receiver. Thus, the discrete time detected pilot signal for a beamforming slot t can be expressed simply as

$$z_t(P) = \alpha_t \sqrt{P_T} \mathbf{w}_t^H \mathbf{a}(\Phi_t) + \mathbf{w}_t^H \mathbf{n}_t. \tag{6.5}$$

Recall $\|\mathbf{w}_t\|^2 = 1$, thus $\eta_t = \mathbf{w}_t^H \mathbf{n}_t \sim \mathcal{CN}(0, \sigma^2)$.

Receive data $e_t = D$

On the other hand, in the data transmission phase the transmitted data is unknown. We apply an additional processing step to the discrete time signal (6.4), where we calculate the received power (which will be used for the purpose of our tracking algorithm):

$$\begin{aligned} z_t(D) &= |y_t|^2 \\ &= |\alpha_t \sqrt{P_T} \mathbf{w}_t^H \mathbf{a}(\Phi_t) x_t + \mathbf{w}_t^H \mathbf{n}_t|^2. \end{aligned} \tag{6.6}$$

In the following sections we continue to describe the system model focusing on the active selection of beamforming vectors and formulate our algorithm in terms of the signal $z_t(e_t)$, while the specific communication protocol and pilot allocation is discussed in Sect. 6.4.

6.2.1 Mobility Model

We consider a UAV mobility model where the AoA trajectory changes according to an independent increment process consisting of predictable and unpredictable (random) elements. That is, the AoA Φ_t evolves as

$$\Phi_{t+1} = \Phi_t + V + \mathbf{r}_t \tag{6.7}$$

where the known vector V models predictable elements of mobility, for example an AoA position changing with constant speed. The zero mean random vector $\mathbf{r}_t \in \mathbb{R}^2$ models the unpredictable components such as a sudden jump.

6.2.2 Beamforming with a Codebook

At any given slot t, we are interested in selecting beam vectors for receive beamforming. In the pilot phase, probing various beams allows the RX to learn about and ultimately track the AoA. In data transmission phase, the main goal is to select a beam vector covering the TX in its angular range in order to receive and reliably detect a data sequence. We consider a stationary beamforming design policy as a causal (possibly random) mapping from past observations $\mathbf{z}_{1:t} = [z_1(e_1), \ldots, z_t(e_t)]$ and past beamforming $\mathbf{w}_{1:t}$ to the beamforming vector: $\mathbf{w}_{t+1} = \gamma(\mathbf{z}_{1:t}, \mathbf{w}_{1:t})$. Under Assumption 7, the quality of the established communication link depends on the estimate of channel state information $\hat{\mathbf{h}}_t$, which is determined by a current estimate $\hat{\Phi}_t$. In particular, each estimate provides beamforming $\mathbf{w}_t$ which results in normalized beamforming gain:

$$G_{BF} = \mathbb{E}\Big(\frac{|\mathbf{w}_t^H \alpha_t \mathbf{a}(\Phi_t)|^2}{|\alpha_t \mathbf{a}(\Phi_t)|^2}\Big). \tag{6.8}$$

In other words, the quality of the established communication link over a period of time $t = [1:T]$ strongly depends on a method to robustly and continuously detect and track the AoA Φ_t for $t = [1:T]$. To reduce complexity, it is common to limit $\mathbf{w}_t$ to a pre-designed beamforming codebook $\mathcal{W}^S$ with finite cardinality and a multi-level structure. We assume the codebook, $\mathcal{W}^S$, has S levels with k_l vectors in each level $l \in S$ that partition the angular search space into contiguous sectors with increasing resolution $k_l < k_{l+1}$ and finest resolution $k_S = \frac{1}{\delta_a} \times \frac{1}{\delta_e}$ in azimuth and elevation. Let $\tilde{\mathbf{w}}_t \in \{0,1\}^{\frac{1}{\delta_a} \times \frac{1}{\delta_e}}$ be a binary matrix representation of the angular space of $\mathbf{w}_t$. More specifically, the locations of 1's in $\tilde{\mathbf{w}}_t$ indicate angular regions covered by the beam $\mathbf{w}_t$ in a corresponding to an $\frac{1}{\delta_a} \times \frac{1}{\delta_e}$ angular grid. Beamforming vectors are assumed to be designed with the objective of near constant gain for intended directions (i.e. the non zero entries of $\tilde{\mathbf{w}}_t$) and almost zero

otherwise. One such structure is achieved by Hierarchical codebooks which are investigated for UAV communications in and in [80] for small angle variations.

6.3 Active and Sequential Beam Selection

We propose Alg. 7 which implements an active beamforming policy γ based on Bayesian posterior updates and predictions, and which achieves sequential refinement of uncertainty on the dynamic AoA Φ_t. Specifically, we implement $hiePM$ of [74] to actively select each $\mathbf{w}_t$ via posterior matching, and build on this algorithm to incorporate an update and prediction step for evolving the posterior dynamically. An overview of the proposed adaptive beamforming algorithm for mobile UAV is detailed in Alg. 7. Although the true AoA $\hat{\Phi}_t$ is continuous, we restrict the AoA point estimate $\hat{\Phi}_t = (\hat{\phi}_{a,t}, \hat{\phi}_{e,t})$ to the discrete set where $\hat{\phi}_{(a,t)} = \{\theta_1, \theta_2, \dots \theta_{1/\delta_a}\}$, and $\theta_i = \theta_{\text{min}} + (i - \frac{1}{2}) \times \delta_a \times (\theta_{\text{max}} - \theta_{\text{min}})$. $\hat{\phi}_{e,t}$ is discretized similarly. Let the probability vector over Φ_t with resolution (δ_a, δ_e) be defined as $\boldsymbol{\pi}(t|t) \in [0,1]^{\frac{1}{\delta_a} \times \frac{1}{\delta_e}}$, where each element is:

$$\pi_{i,j}(t|t) := \mathbb{P}(\Phi_t = (\theta_i, \theta_j) | \mathbf{z}_{1:t}),\ i = 1, ..., 1/\delta_a, j = 1, ..., 1/\delta_e \tag{6.9}$$

and the probability of Φ_t being in the angular range covered by a beamforming vector $\mathbf{w}_t$ (with angular span $\tilde{\mathbf{w}}_t$) is the sum of the posterior entries corresponding to the non-zero entries of $\tilde{\mathbf{w}}_t$:

$$\pi_{\tilde{\mathbf{w}}_t}(t|t) := \sum_{i,j} \tilde{\mathbf{w}}_t(i,j) \pi_{i,j}(t|t). \tag{6.10}$$

To dynamically evolve the posterior, upon receiving a new observation $z_t(e_t)$, $\boldsymbol{\pi}(t|t-1)$ is updated according to Bayes Rule [30] and followed by a prediction step incorporating the AoA dynamics:

$$\boldsymbol{\pi}(t+1|t) \leftarrow \boldsymbol{\pi}(t|t) \leftarrow z_t(e_t), \boldsymbol{\pi}(t|t-1). \tag{6.11}$$

A beamforming vector at either level l^* or $l^* + 1$ is selected for the next beamforming slot based on the accumulated belief around Φ_{t+1} as described by the prediction posterior probability $\boldsymbol{\pi}(t+1|t)$,

which is a sufficient statistic. In other words, $\mathbf{w}_{t+1}(\boldsymbol{\pi}(t+1|t))$ is chosen as the k_{t+1}^{th} codeword in level l_{t+1} covering $\tilde{\mathbf{w}}_{[l_{t+1},k_{t+1}]}$ where:

$$[l_{t+1}, k_{t+1}] = \underset{[l',k']}{\operatorname{argmin}} \left| \pi_{\tilde{\mathbf{w}}_{[l',k']}}(t+1|t) - \frac{1}{2} \right|. \tag{6.12}$$

To initialize the procedure of (6.11) we assume a uniform posterior $\boldsymbol{\pi}(1|0)$ at $t = 1$, i.e. no prior knowledge about the AoA is required. The first step in (6.11) is a Bayesian posterior update calculated as:

$$\pi_{i,j}(t|t) = \mathbb{P}(\Phi_t = (\theta_i, \theta_j)|\mathbf{z}_{1:t}) = \frac{f(z_t(e_t)|\Phi_t = (\theta_i, \theta_j), \mathbf{w}_t)\pi_{i,j}(t|t-1)}{\sum_{i'=1}^{1/\delta}\sum_{j'=1}^{1/\delta} f(z_t(e_t)|\Phi_t = (\theta_{i'}, \theta_{j'}), \mathbf{w}_t)\pi_{i',j'}(t|t-1)}. \tag{6.13}$$

where $f(z_t(e_t)|\Phi_t = (\theta_i, \theta_j), \mathbf{w}_t)$ is proportional to the probability of observing $z_t(e_t)$ conditioned on knowledge of $(\Phi_t, \mathbf{w}_t)$ and depends on the processing step at the receiver, i.e. either pilot (6.5) or data (6.6). Next we define $f(z_t(e_t)|\Phi_t = (\theta_i, \theta_j), \mathbf{w}_t)$ for each phase e_t.

Receiving a pilot $e_t = P$

In the pilot phase, conditioned on a point estimate and beam vector $(\Phi_t = (\theta_i, \theta_j), \mathbf{w}_t)$, the observation $z_t(P) \sim \mathcal{CN}(\mathbf{w}_t^H \mathbf{a}(\Phi_t), \sigma^2)$ by assuming $\alpha_t = 1$ and $P_T = 1$ (see Remark 9 below). Thus, the conditional probability is

$$f(z_t(P)|\Phi_t = (\theta_i, \theta_j), \mathbf{w}_t) = g\Big(z_t(P) - G_{i,j}\Big), \tag{6.14}$$

where $G_{i,j} = \mathbf{w}_t^H \mathbf{a}(\theta_i, \theta_j)$ is the gain conditioned on $(\Phi_t = (\theta_i, \theta_j), \mathbf{w}_t)$ and $g(x)$ is the circularly symmetric complex normal distribution with variance σ^2. In the posterior update of our algorithm, the Bayes update (6.13) is computed utilizing (6.14) for all t where $e_t = P$.

Remark 9. Our approach, and specifically the extensions detailed in [88], can handle stochastic and time varying complex gain through simultaneous estimation of α_t. However, in this chapter we

focus only on the performance in terms of recovering and tracking Φ_t by fixing the gain. Given knowledge of the operating SNR $\frac{P_T}{\sigma^2}$ we can assume $P_T = 1$ without loss of generality.

Receiving data $e_t = D$

In the data transmission phase of communication (6.14) does not apply since the RX does not have knowledge of the transmitted data. However, the received power measurement $z_t(D)$ can be used as a proxy for computing the Bayes Rule using the following lemma.

Lemma 4. Let each transmitted symbol $x_t \in \mathbb{C}$ have minimum energy $|x_t|^2 \geq 1$. Then, conditioned on a point estimate and beam vector $(\Phi_t = (\theta_i, \theta_j), \mathbf{w}_t)$, $z_t(D)$ follows a scaled non-central chi-squared probability distribution function $z_t(D) \sim \chi^2(k, \lambda_t)$ with $k = 2$ degrees of freedom and time-varying non-centrality parameter $\lambda_t = \frac{2|G_{i,j}|^2}{\sigma^2}$. The conditional probability is approximated as

$$f(z_t(D)|\Phi_t = (\theta_i, \theta_j), \mathbf{w}_t) = c_{\lambda_t}(z_t(D)) \tag{6.15}$$

where c_{λ_t} is the probability distribution function $\chi^2(2, \lambda_t)$ given as

$$c_{\lambda_t}(x) = \frac{1}{\sigma^2} e^{-(\frac{x}{\sigma^2} + \frac{\lambda_t}{2})} \sum_{k=0}^{\infty} \frac{(\frac{x\lambda_t}{2\sigma^2})^k}{(k!)^2},\ x \geq 0 \tag{6.16}$$

In the data transmission phase, applying a power only Bayesian update (6.13) using Lemma 4 will enable some learning of the AoA without a pilot. That is, the calculated power of a data signal $z_t(D)$ can be used to an extent for confirming (increasing probability of angles covered by $\tilde{\mathbf{w}}_t$) or rejecting (decreasing probability of angles covered by $\tilde{\mathbf{w}}_t$) the current use of the tracking beam $\mathbf{w}_t$. As a result, the duration of the transmission phase may be extended so long as a posterior continues to increase for the selected beam. Our proposed strategy for determining the tracking duration and thereby the pilot allocation is discussed in Sect. 6.4.

Remark 10. We note that our proposed approach has computational requirements from the selection policy γ (6.12), the Bayesian posterior update (6.13), the one-step prediction update, and the

pilot allocation. While the first steps of the proposed algorithm can be generalized as above, in order to incorporate mobility information, the one-step posterior update from $\boldsymbol{\pi}(t|t)$ to $\boldsymbol{\pi}(t+1|t)$ is formulated according to a particular movement model (6.7). Even so, the computation complexity of our proposed algorithm is dominated by the cost of the posterior update (6.13) at each beamforming slot t. The worst case cost is $O(\frac{1}{\delta_a} \times \frac{1}{\delta_e})$ if each element is updated individually. However, this can be reduced to $O(log(\frac{1}{\delta_a} \times \frac{1}{\delta_e}))$ by considering the geometric constraints on the hierarchical contiguous codebook elements [81].

6.4 Adaptive Pilot Allocation

Thus far we have discussed a procedure for sequentially selecting beamforming vectors $\mathbf{w}_{t+1}$ based on the accumulated belief about the AoA in the posterior vector $\boldsymbol{\pi}(t|t-1)$. Next, we discuss our proposed pilot allocation strategy in order to complement the communication scheme. We propose an adaptive communication scheme which allocates pilots based on the information reward of each phase, which we define to be a function of the mutual information between the channel state and the received signal, as well as the maximum achievable spectral efficiency. Fig. 6.1 is an overview of our pilot allocation approach. To reduce pilot overhead, the mutual information and spectral efficiency terms are continuously analyzed by the receiver. Furthermore, the active selection of beams and their width during both the pilot and data transmission phases enables quick re-alignment around angular regions with accumulated probability, and reduces the need for longer reset or pilot enabled channel re-estimation to recover alignment.

6.4.1 Information Reward

Let an action $e_t \in \{D, P\}$ of whether to trigger data D or pilot P transmission be determined by a weighted analysis of the expected information reward of each phase. We define the information reward to be a function of the mutual information between the channel state Φ_t and the received measurement $z_t(e_t)$, and of the maximum achievable spectral efficiency $S_t(e_t)$. That is, an action

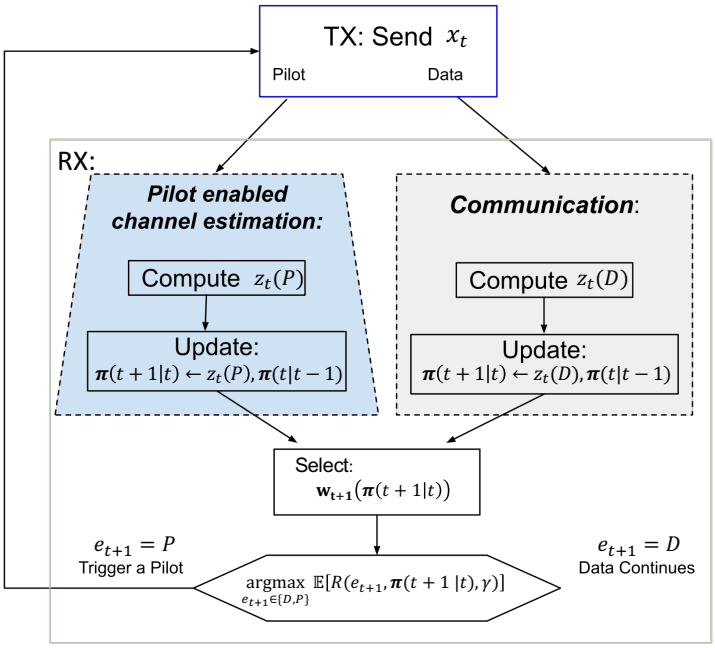

Figure 6.1: Overview of the proposed communication scheme. Adaptive pilot allocation is based on analysis of the mutual information and achievable spectral efficiency.

$e_t \in \{D, P\}$ is chosen at time t according to the following:

$$\begin{aligned} e_t &= \underset{e_t \in \{D,P\}}{\operatorname{argmax}} \, \mathbb{E}[R(e_t, \boldsymbol{\pi}(t|t-1), \gamma)] \\ &= \underset{e_t \in \{D,P\}}{\operatorname{argmax}} \, I(\Phi_t; z_t(e_t)|\mathbf{w}_t(\boldsymbol{\pi}(t|t-1))) + \gamma S_t(e_t) \end{aligned} \tag{6.17}$$

Before proceeding with the definitions of the mutual information and spectral efficiency terms, we note that the optimal choice in (6.17) is dictated by the key parameter γ. For $\gamma \geq \frac{I(X(\Phi_t,e_t);z_t(P)|\mathbf{w}_t) - I(X(\Phi_t,e_t);z_t(D)|\mathbf{w}_t)}{S_t(D)}$ data transmission is more heavily weighted than the potential learning under a pilot. Thus, γ imposes an exploration-exploitation trade-off by weighing the importance of communicating data, with reduced learning about Φ_t (exploitation with some exploration), against the importance of pilot enabled estimation (pure exploration). We will see that γ ultimately impacts critical performance measures such as the incurred pilot overhead, the received beamforming SNR, and the spectral efficiency.

6.4.2 Spectral Efficiency Terms

The maximum achievable spectral efficiency under a beamforming vector $\mathbf{w}_t$ covering a range of angles $\mathcal{D}_{l_t}^{k_t}$, as indicated in the binary vector representation $\tilde{\mathbf{w}}_t$, is given by

$$S_t(e_t) = \mathbb{E}\left[\log\left(1+\frac{\mid \mathbf{w}_t^H \mathbf{a}(\Phi) x_t \mid^2}{\sigma^2}\right)\mathbb{1}_{e_t=D}\right] \tag{6.18}$$

$$= \mathbb{P}\Phi_t \in \mathcal{D}_{l_t}^{k_t} \log\left(1+\frac{\mid G_l x_t \mid^2}{\sigma^2}\right)\mathbb{1}_{e_t=D}$$

$$= \boldsymbol{\pi}_{\tilde{\mathbf{w}}_t}(t|t-1)\log\left(1+\frac{|G_l|^2}{\sigma^2}\right)\mathbb{1}_{e_t=D}$$

where $|G_l|^2$ is the expected beamforming gain for a beam $\mathbf{w}_t$ in level $l_t = l$ under the following assumption of ideal beams.

Assumption 8. *The beam formed by the beamforming vector $\mathbf{w}_t \in \mathcal{W}^S$ covering a range of angles $\mathcal{D}_{l_t}^{k_t}$, as indicated in the binary vector representation $\tilde{\mathbf{w}}_t$, has constant beamforming power gain for any signal of AoA $\Phi \in D_{l_t}^{k_t}$ and rejects any signal outside of $D_{l_t}^{k_t}$, $i.e.$*

$$\mathbf{w}_t^H \mathbf{a}(\Phi) = \begin{cases} G_l, & \text{if } \Phi \in D_{l_t}^{k_t} \\ 0, & \text{if } \Phi \notin D_{l_t}^{k_t} \end{cases}. \tag{6.19}$$

6.4.3 Mutual Information Terms

Lemma 5. The mutual information term for the pilot phase $e_t = P$ of (6.17) is

$$I(\Phi_t; z_t(P)|\mathbf{w}_t) = -\int_{-\infty}^{\infty}\int_{-\infty}^{\infty} f(z_t(P)|\mathbf{w}_t)\log f(z_t(P)|\mathbf{w}_t) d_{\Re(z_t(P))} d_{\Im(z_t(P))} - \log(\pi e \sigma^2) \tag{6.20}$$

where

$$f(z_t(P)|\mathbf{w}_t) = \boldsymbol{\pi}_{\tilde{\mathbf{w}}_t}(t|t-1)\frac{1}{\pi\sigma^2}e^{-\frac{|z_t(P)-G_l|^2}{\sigma^2}} + (1-\boldsymbol{\pi}_{\tilde{\mathbf{w}}_t}(t|t-1))\frac{1}{\pi\sigma^2}e^{-\frac{|z_t(P)|^2}{\sigma^2}}. \tag{6.21}$$

The proof of Lemma 5 is given in the Appendix C, it follows from Assumption 8.

Lemma 6. The mutual information term for the data transmission phase $e_t = D$ of (6.17) is

$$I(\Phi_t; z_t(D)|\mathbf{w}_t) = -\int_{-\infty}^{\infty} f(z_t(D)|\mathbf{w}_t) \log f(z_t(D)|\mathbf{w}_t) d_{z_t(D)} - h(z_t(D)|\mathbf{w}_t, \Phi_t) \tag{6.22}$$

where

$$f(z_t(D)|\mathbf{w}_t) = \boldsymbol{\pi}_{\tilde{\mathbf{w}}_t}(t|t-1) \frac{1}{\sigma^2} e^{-(\frac{z_t - |G_l|^2}{\sigma^2})} \sum_{k=0}^{\infty} \frac{(\frac{z_t |G_l|^2}{\sigma^4})^k}{(k!)^2} + (1 - \boldsymbol{\pi}_{\tilde{\mathbf{w}}_t}(t|t-1)) \frac{1}{\sigma^2} e^{\frac{-z_t}{\sigma^2}} \tag{6.23}$$

and the conditional entropy is given by

$$\begin{aligned} h(z_t(D)|\mathbf{w}_t, X(\Phi_t, e_t)) = &- \boldsymbol{\pi}_{\tilde{\mathbf{w}}_t}(t|t-1) \int_{-\infty}^{\infty} \frac{1}{2} e^{-(\frac{z_t+\lambda}{2})} \sum_{i=0}^{\infty} \frac{(\frac{z_t \lambda}{4})^i}{(i!)^2} \log \frac{1}{2} e^{-(\frac{z_t+\lambda}{2})} \sum_{k=0}^{\infty} \frac{(\frac{z_t \lambda}{4})^k}{(k!)^2} d_{z_t} \\ &- (1 - \boldsymbol{\pi}_{\tilde{\mathbf{w}}_t}(t|t-1)) \int_{-\infty}^{\infty} \frac{1}{2} e^{\frac{-z_t}{2}} \log \frac{1}{2} e^{\frac{-z_t}{2}} dz_t. \end{aligned} \tag{6.24}$$

The proof of Lemma 6 is given in the Appendix C, it follows from Lemma 4 and Assumption 8.

Remark 11. The optimal choice of (6.17) depends on the mutual information terms and thus requires an additional computational cost per iteration of the proposed algorithm if computed in an online manner. This cost can be reduced by assuming perfect beams and by approximately calculating the mutual information terms offline. Under Assumption 8, the theoretical beamforming gains can be used to approximate the mutual information terms (5) and (6) offline for each level of the codebook $l \in S$ and for a range of input probabilities $q^* \in [0, 1]$ (n values chosen uniformly). As a result, an action (6.17) can be chosen by comparing the pre-calculated mutual information terms for a given level l_t and for a given input probability $q^* = \boldsymbol{\pi}_{\tilde{\mathbf{w}}_t}(t|t-1)$ (by interpolating) and thus save on the online computational complexity. The additional computational cost per iteration is $O(2\log(\log(n)) + 2)$ if the mutual information terms are computed offline.

Algorithm 7: Active beam tracking for mobile AoA

Input: target resolution (δ_a, δ_e), tracking quality parameter γ, codebook $\mathcal{W}^S$, T (total duration), Markov mobility model (6.7)

Output: Beam vector $\mathbf{w}_t \in \mathcal{W}$ and pilot allocation $e_t \in \{P, D\}$

Initialization: Set $\boldsymbol{\pi}(1|0)$ to be uniform, i.e. $\pi_{i,j}(t|t-1) = \delta_a \delta_e$

while $t \leq T$ **do**

Beam Selection: hierarchical posterior matching with variable width beams (6.12)

$$\mathbf{w}_t(\boldsymbol{\pi}(t|t-1)) \in \mathcal{W}^S$$

Allocate Pilot or Data slot based on the information reward (6.17)

$$e_t = \underset{e_t \in \{D,P\}}{\operatorname{argmax}} I(\Phi_t; z_t(e_t)|\mathbf{w}_t) + \gamma S_t\Big(e_t\Big|\mathbf{w}_t, \boldsymbol{\pi}(t|t-1)\Big)$$

if $e_t = P$ **then**

Receive and compute observation $z_t(P)$

Posterior update by Bayes' Rule (6.13)

$$\boldsymbol{\pi}(t|t) \leftarrow z_t(P), \boldsymbol{\pi}(t|t-1)$$

else

Receive and compute observation $z_t(D)$

Power only posterior update by Bayes' Rule (6.13)

$$\boldsymbol{\pi}(t|t) \leftarrow z_t(D), \boldsymbol{\pi}(t|t-1)$$

Posterior one-step prediction based on mobility model (6.7)

$$\boldsymbol{\pi}(t+1|t) \leftarrow \boldsymbol{\pi}(t|t)$$

6.5 Numerical Results

In this section, we analyze the proposed tracking scheme by considering a special case where we reduce the AoA point estimates to the 2-D angular domain $\hat{\Phi}_t = \hat{\phi}_t \in [\theta_{\text{min}}, \theta_{\text{max}}]$ and consider three examples of Markov mobility in the form (6.7). We utilize the hierarchical beamforming codebook of [46] where vectors in level $l \in S = log_2(1/\delta)$ have angular width $\|\tilde{\mathbf{w}}_t\|_0 = \frac{1/\delta}{2^l}$ that is half the size of the prior level. This is approximately achieved via a pseudo inverse approximation. The resulting beams are slightly imperfect with reduced gain in angles further from the center beam directions, however, these effects are fully accounted for in our numerical simulations.

To analyze the performance, we consider three movement models that fall into two broad categories: predictable and unpredictable mobility. These examples follow directly from Sect. 5.4 in chapter 5 please see Table 5.1 for a summary.

6.5.1 Simulation Scenario

We consider a simulation scenario where the RX is equipped with N=32 antennas in a uniform linear array. We utilize the hierarchical beamforming codebook of [46] where vectors in level $l \in S = log_2(1/\delta)$, for $\frac{1}{\delta} = 64$, have angular width $\|\tilde{\mathbf{w}}_t\|_0 = \frac{\Delta}{2^l}$ that is half the size of the prior level. This is approximately achieved via a pseudo inverse approximation. The resulting beams are slightly imperfect with reduced gain in angles further from the center beam directions, however, these effects are fully accounted for in our numerical simulations. The transmitted data symbols have a minimum energy $\|x_t\| \geq 1$, which we obtain by using a QPSK constellation [55]. We focus on relative comparisons to existing tracking strategies in terms of the performance measures of normalized beamforming gain and pilot overhead for a given SNR, although physical properties corresponding to the considered SNR values (like distance, cell size, and bandwidth) can be defined as in (Fig.6 in [74]). More specifically, we compare to the following prior works:

- The Extended Kalman Filtering algorithm of [76] selects beams based on tracking estimates of the state $\hat{\phi}_t$ with extended Kalman filter updates. The pilot allocation is determined by

a threshold on the mean squared error, i.e. $\sqrt{\mathbb{E}\left[|\phi_t - \hat{\phi}_t|^2\right]} \geq \frac{BW}{2}$ half beam width. When tracking is no longer valid, a reset is triggered and the exhaustive beams are used again in order to obtain another estimate.

- In the dynamic pilot insertion algorithm of [75], beams are selected based on predictions of AoA made using an estimated velocity. The pilot allocation is determined by a threshold on the normalized receive power $\left(\frac{\mathbb{E}[\|\mathbf{w}_t^H \mathbf{a}(\phi_t)\|^2]}{\mathbb{E}[\|\mathbf{w}_\tau^H \mathbf{a}(\phi_\tau)\|^2]} \geq P_{min}\right)$ where τ is the first transmission slot and $t > \tau$.

- The beam tracking strategy of [80] employs beams from a certain level of the hierarchical codebook $\mathbf{w}_t \in \mathcal{W}^S$ (we consider either narrow ($l = 6$) or wide ($l = 5$) beams). After an initial estimate of the AoA is obtained, subsequent recurring pilot phases consists of scanning only the neighboring local beams from the current estimate. The training frequency, i.e. tracking duration τ_{max} between pilot phases, is determined according to the channel coherence time.

The strategies we compare to utilize the pilot phase for acquiring an aligned estimate $\hat{\phi}_{T_E}$ (or re-estimation if tracking thresholds are not met) before switching to the transmission phase. In the absence of a better solution, and under the constraint of a single RF chain, we apply an exhaustive search over all candidate beams in order to obtain an estimate $\hat{\phi}$ for these algorithms. The duration of the exhaustive search T_E will depend on the beam width of the candidate beams; $T_E = \Delta$ for narrow beams and $T_E = 2^l$ for beams from any other level l of the codebook $\mathcal{W}^S$. The tracking thresholds $\sqrt{MSE}$ and P_{min}, and the tracking duration τ_{max} of the strategy [80] may be optimized for a given SNR or coherence time. In the following simulations we assume perfect exhaustive search estimates $\hat{\phi}_{T_E} = \phi_{T_E}$ and optimize the tracking parameters empirically as best as we can in order to compare performance.

6.5.2 Impact of the parameter γ

First, we discuss the impact of the parameter γ on the performance measures of pilot overhead $\sum_{t=1}^{T} \mathbb{1}_{e_t=P}$, average received beamforming gain $\mathbb{E}[G_{BF}]$ of (6.8), and spectral efficiency

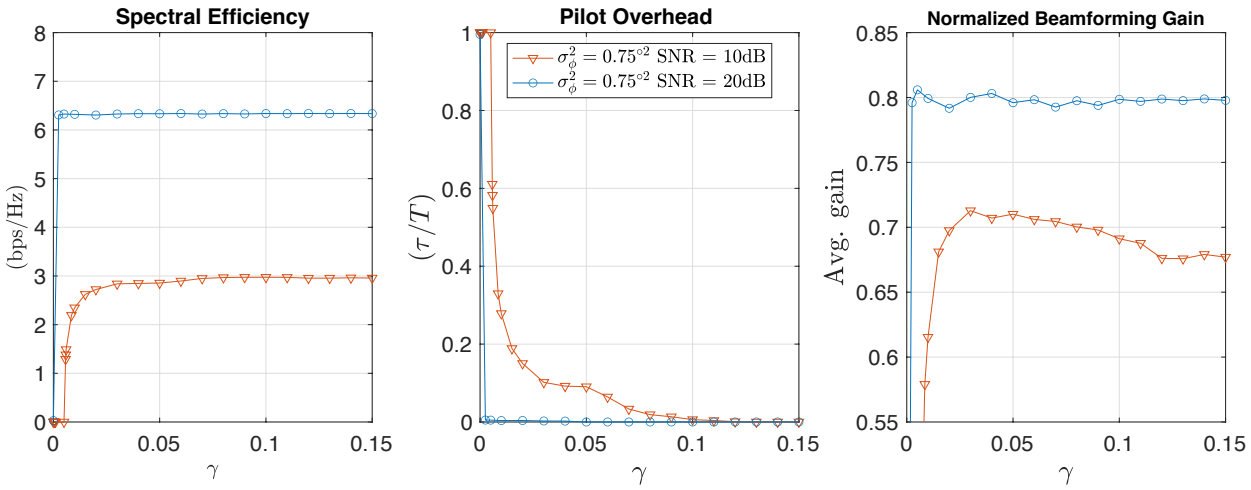

Figure 6.2: We investigate performance as a function of the choice of γ under the mobility model of Gaussian angular movements with variance ($\sigma_\phi^2 = 0.75^{\circ 2}$).

$\mathbb{E}\Big[S_t\Big(e_t\Big|\mathbf{w}_t, \boldsymbol{\pi}(t|t-1)\Big)\Big]$. The total time frame is set arbitrarily large, $T >> \frac{1}{\delta}$ at $T = 500$ beamforming slots. In Fig. 6.2 we plot the performance under the mobility model of Gaussian angular movements with variance $\left(\sigma_\phi^2 = 0.75^{\circ 2}\right)$ as a function of the parameter γ for SNR = $\frac{P}{\sigma^2} = 10$ dB, and SNR = $\frac{P}{\sigma^2} = 20$ dB. We see that selecting a large γ improves the spectral efficiency and reduces pilot overhead until these values saturate. This indicates that given high enough signal power, active and dynamic learning of the AoA in the data transmission phase is sufficient for maintaining alignment and results in high spectral efficiency even as the pilot overhead is reduced to 0 (in this example $\gamma > 0.1$). Alternatively, to maximize the average beamforming gain γ may be optimized for each SNR. In this example, for 20 dB SNR $\gamma^* = 0.005$, and for 10 dB SNR $\gamma^* = 0.03$.

6.5.3 Fixed Angular Movement

Next, we get a sense of performance of the proposed communication algorithm compared to existing approaches in terms of tracking quality by analyzing the achieved normalized beamforming gain (6.8) over time. In Fig. 6.3 we show an AoA trajectory example under the mobility model with predictable angular movement (5.14) with $\nu = 0.1$, i.e. increments $V = 0.1\delta$, at 10dB SNR. The normalized beamforming gains achieved are shown on the left, and corresponding AoA estimates and pilot allocation are shown on the right. For the proposed algorithm, the AoA estimate $\hat{\phi}_t$ is

defined as the main lobe pointing direction of the selected beam $\mathbf{w}_t$. In this example, all strategies are able to remain in the data transmission phase so long as the mobility is known or estimated correctly, i.e. fully predictable mobility. We notice that using wider beams only, rather than recurring narrow beams, in the Neighborhood search strategy of [80] results in slightly reduced maximum beamforming gain but achieves longer tracking duration, as expected. Slight dips in the beamforming gain are caused when the AoA lies near the edge of a selected beam or by using wider beams. In essence, Fig. 6.3 shows that under predictable mobility only, there is little difference in the performance by the various algorithms considered. Fig. 6.3 also highlights a strength of the proposed algorithm in obtaining an initial estimate of the AoA quickly and reliably, thereby initiating the transmission phase with tracking significantly more quickly than the compared to applying the exhaustive search for this initial alignment. As a result of this and subsequent short-duration pilot phases, the proposed algorithm also achieves the highest average beamforming gain.

6.5.4 Gaussian Angular Movement

Next, we analyze the more interesting cases of mobility with stochastic elements, starting with the scenario of Gaussian angular movements (5.17). In Fig. 6.4 we look a very high mobility case of incremental Gaussian movements with variance $\sigma_\phi^2 = 0.75^{\circ 2}$. We plot an example AoA trajectory along with the corresponding estimates and beamforming gains achieved over time by the algorithms considered. The algorithms of [76] and [75] have strict quality thresholds that trigger re-estimation when the random movement overcomes the predictable movement and the performance drops enough that the tracking is deemed invalid. Under the high mobility scenario considered in this example, these pilot phases are triggered frequently and a full scan over the potential beamforming vector pairs is costly resulting in a large amount of time spent in re-estimating the AoA (pilot phase) compared to tracking (in the data transmission phase)[2]. The strategy of frequently analyzing local neighboring beams [80], whether with narrow or wide beams, improves on the other strategies due

[2]Here we note that both the algorithms of [76] and [75] suggest reducing the overhead of the re-estimation phases according to current CSI estimates after initial alignment, however, no clear strategies for doing this are provided.

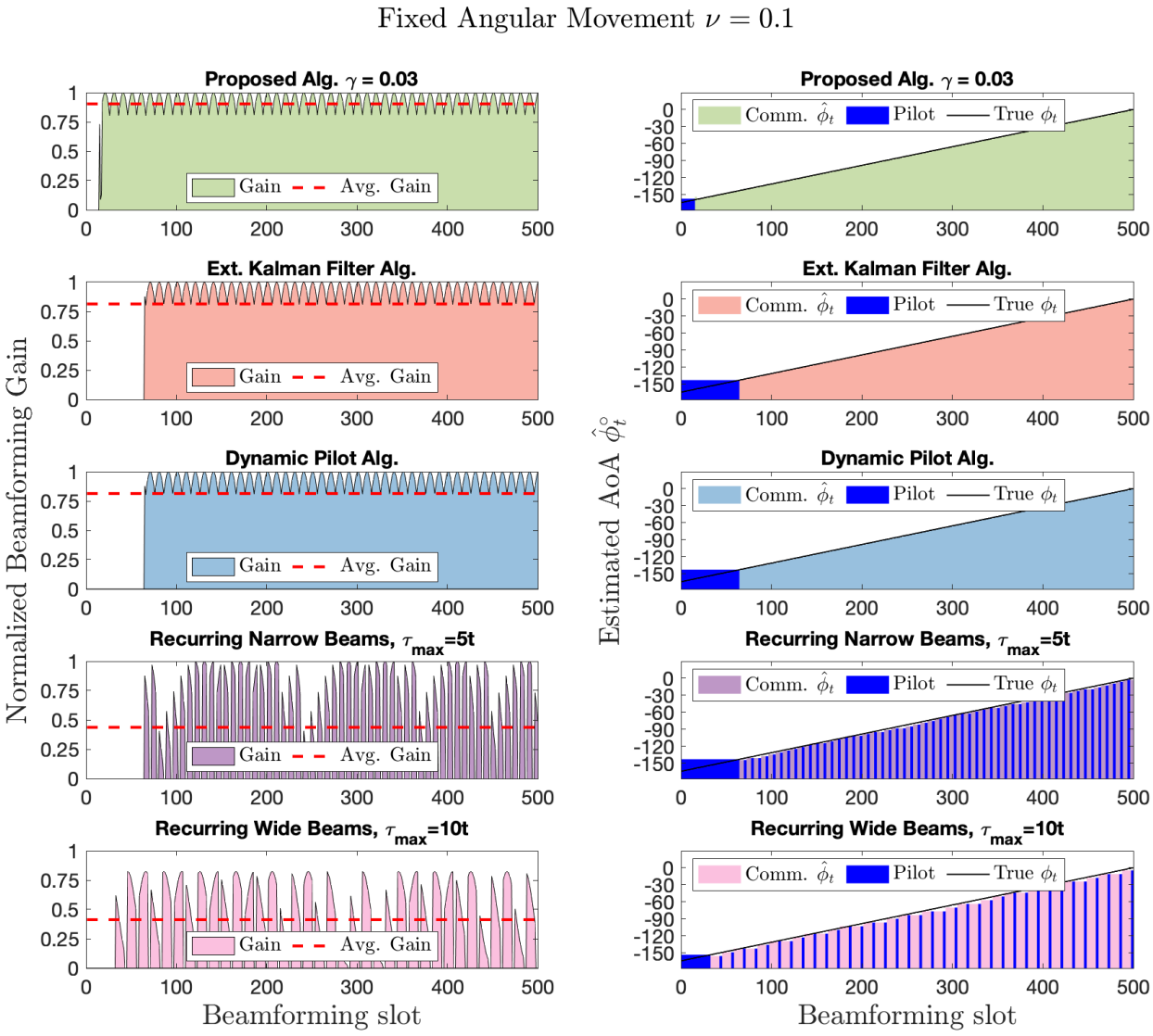

Figure 6.3: Normalized beamforming gain (6.8) at 10dB SNR for constant angular movement (5.14) with $\nu = 0.1$ at 10dB SNR. For the proposed algorithm $\gamma = 0.03$. On the right, the estimated AoA is compared to the true AoA and pilot allocation is shown.

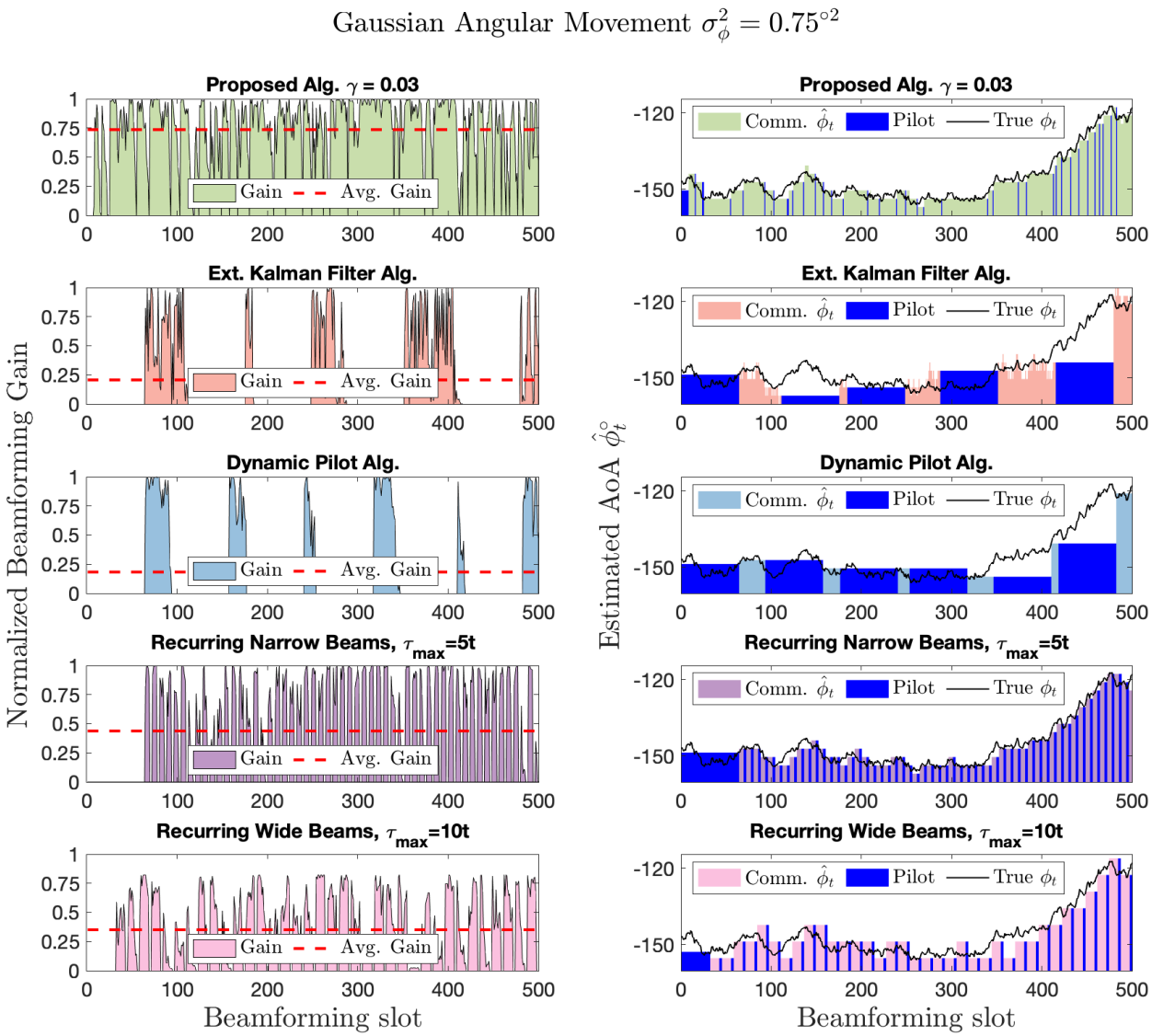

Figure 6.4: Normalized beamforming gain (6.8) at 10dB SNR for Gaussian Movement (5.17)with $\sigma_\phi^2 = 0.75^{\circ 2}$. For the proposed algorithm $\gamma = 0.03$. On the right, the estimated AoA is compared to the true AoA and pilot allocation is shown.

to the shorter pilot phases (scanning only neighboring beams). Our proposed algorithm recovers the benefit of high gains achieved by the tracking strategies of [76] and [75], as well as the benefit of lower overhead incurred by searching locally based on prior estimates [80] providing an overall more efficient strategy. Combined, our sequential beam selection and adaptive pilot allocation yield sustained larger gains overtime. Ultimately, our proposed algorithm enables efficient beam tracking for high mobility by incorporating mobility information into the sequential beam selection with variable width beams and into the pilot allocation strategy.

6.5.5 Bernoulli Angular Jumps

Lastly, we analyze the stochastic mobility model of occasional Bernoulli jumps (5.20). Such random jumps are very difficult to handle on two fronts. First, existing alignment schemes operate under the assumption quasi-static AoA at least for the duration of the initial alignment phase, and will struggle to obtain correct initial AoA estimates if a jumps occurs in this phase. Second, even if a robust AoA estimate is obtained successfully, the duration of data transmission phase (active tracking) will largely depend on the frequency of the jumps (the entropy of the mobility model), since each jump is likely to cause an outage that requires re-estimation of the AoA.[3] In Fig. 6.5 we plot an AoA trajectory and corresponding estimates and beamforming gain performance comparisons for each of the algorithms considered. As expected, under this unpredictable mobility the adaptive algorithms of [76] and [75] respond to sudden jumps by triggering the pilot phase for re-estimation of the AoA. We note that the pilot phase frequency and corresponding duration of the communication phases is correlated to the frequency and spread of jumps, where consecutive jumps can severely shorten the data transmission phase. A similar effect occurs for the recurring local search algorithm of [80], where consecutive jumps cause the algorithm under narrow beams be misaligned more severely[4]. The local search under wide beams is more robust to frequent

[3] We note that the Extended Kalman Filter updates of the algorithm of [76] are designed for state estimates of AoA under Gaussian noise, thus are not specifically designed for this mobility. Updates adapted for this mobility model are not immediately obvious to us, thus no such extensions are considered in this paper.

[4] Under unpredictable mobility with large jumps, these recurring or periodical algorithms would benefit from scanning a larger radius around the current CSI estimates, although though these extensions are not considered here.

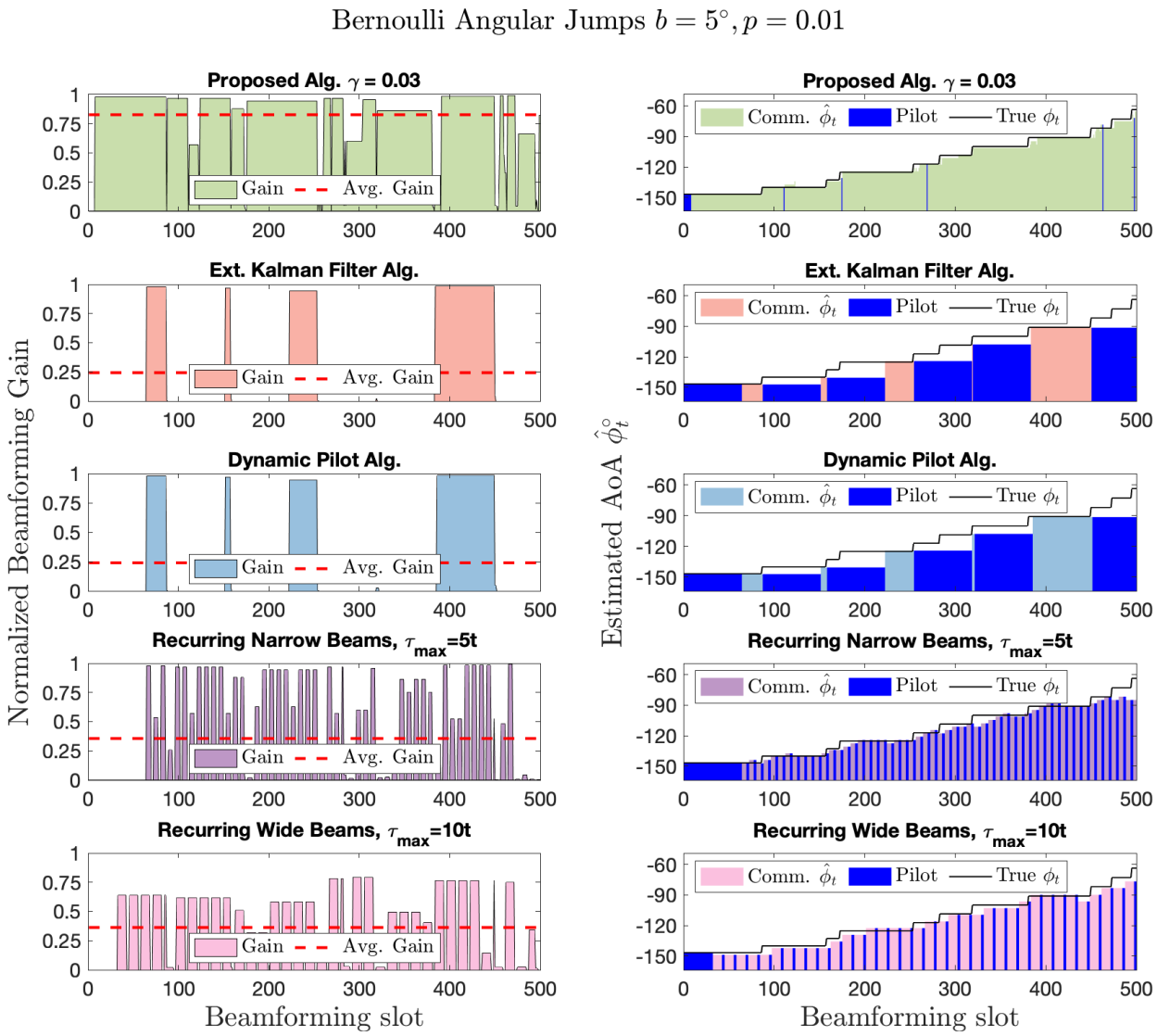

Figure 6.5: Normalized beamforming gain (6.8) at 10dB SNR for Bernoulli jumps (5.20) with jump size $b = 5^\circ$ and probability $p = 0.01$. For the proposed algorithm $\gamma = 0.03$. On the right, the estimated AoA is compared to the true AoA and pilot allocation is shown.

jumps, although estimates are less precise and the beamforming gain suffers. On the other hand, the proposed algorithm recovers quickly after a jump occurs due to the embedding of mobility information into dynamic evolution of the posterior and the active selection of beams with various widths.

6.6 Conclusion

We consider the problem of active and dynamical sequential tracking of the CSI for robust communications at mmWave frequencies and above. We are interested in tracking stochastic movements, which may be especially critical in systems of communication between mobile UAV. Existing beam tracking communication schemes implement approaches which require lengthy or too frequent re-estimation pilot phases in response to outages, and require long coherence times to maintain tracking quality. We continue our work of chapter 5 on active and dynamical beam tracking by introducing an information reward based adaptive pilot allocation. To allocate pilot slots adaptively, we continuously analyze the expected information reward of each (pilot and communication) phase via analysis of the mutual information and spectral efficiency terms. This adaptive allocation strategy is driven by a weighting parameter γ which imposes a special case of exploitation with some exploration vs. pure exploration, and can be chosen based on the performance measures of pilot overhead, average received SNR, and spectral efficiency. Although we provide a general formulation for our algorithm, which can be adapted to any stochastic mobility model, we study a selection of 2-D Markov mobility models in our numerical results. Our Numerical results show improved performance over existing strategies in terms of sustained beamforming gain, enabling tracking for movements with larger entropy.

Chapter 6, in full, is currently being prepared for submission for publication of the material. Nancy Ronquillo and Tara Javidi. The dissertation author was the primary investigator and author of this paper.

Appendix A

For Chapter 2

A.1 Proof of Lemma 1

Proof. Let $\mathbf{C} = \hat{\mathbf{W}}^{\mathsf{T}}\mathbf{A}_{1:N}$. We first note that $|Y_t - C(t)| \sim \mathcal{N}(0, \|\mathbf{A}_t\|_0\sigma^2)$, so we can write:

$$\begin{aligned}
\log \mathbb{P}[\mathbf{Y}_{1:N}|\mathbf{C}] &= \log \prod_{t=1}^{N} P[Y_t|C(t)] \\
&= \log \prod_{t=1}^{N} \frac{1}{\sqrt{2\pi\|\mathbf{A}_t\|_0\sigma^2}} e^{-\frac{1}{2\|\mathbf{A}_t\|_0\sigma^2}|y_t - C(t)|^2} \\
&= \sum_{t=1}^{N} -\frac{1}{2}\log\left(2\pi\sigma^2\right) - \frac{1}{2}\log\left(\|\mathbf{A}_t\|_0\right) - \frac{|y_t - C(t)|^2}{2\|\mathbf{A}_t\|_0\sigma^2} \\
&= -\frac{1}{2}\sum_{t=1}^{N} \log\left(2\pi\sigma^2\right) + \log\left(\|\mathbf{A}_t\|_0\right) + \frac{|y_t - C(t)|^2}{\|\mathbf{A}_t\|_0\sigma^2}.
\end{aligned}$$

The maximum liklihood estimate, $\hat{\mathbf{W}}$, of $\mathbf{W}$ is then given as:

$$\begin{aligned}
\hat{\mathbf{W}} &= \arg\max_{[\mathbf{C}\in\mathcal{C}]} \log \mathbb{P}[\mathbf{Y}_{1:N}|\mathbf{C}] \\
&= \arg\min_{[\mathbf{C}\in\mathcal{C}]} \frac{1}{2}\sum_{t=1}^{N} \frac{|y_t - C(t)|^2}{\|\mathbf{A}_t\|_0\sigma^2}.
\end{aligned}$$

□

A.2 Proof of Lemma 2

Applying Fano's inequality [44] to any non-adaptive search strategy that locates the target among $\frac{B}{\delta}$ locations with $P_e \leq \epsilon$, we have

$$\begin{aligned}
\log\left(\frac{B}{\delta}\right) &\overset{(a)}{\leq} \frac{1}{1-\epsilon}\sup_{X_{1:t}}\sum_{i=1}^{t} I(X_i, Y_i) + \frac{h(\epsilon)}{1-\epsilon} \\
&\overset{(b)}{\leq} \frac{1}{1-\epsilon}\sum_{i=1}^{t} C\left(q_i, q_i B\sigma^2\right) + \frac{h(\epsilon)}{1-\epsilon} \\
&\leq \frac{t}{1-\epsilon}\max_{q\in\mathbf{I}_{\frac{B}{\delta}}} C(q, qB\sigma^2) + \frac{h(\epsilon)}{1-\epsilon},
\end{aligned} \tag{A.1}$$

where (a) follows from the fact that X_i and N_i for $i = 1, 2, \ldots, n$ are independent over time and independent of past observations due to the non-adaptive nature of the search strategy. Since $X_i \sim \mathsf{Bern}(q_i)$ and $N_i \sim \mathcal{N}(0, q_i B\sigma^2)$, (b) follows from the fact that $I(X_i, Y_i) = C\left(q_i, q_i B\sigma^2\right)$. Rearranging the above equation, we have the assertion of the lemma.

A.3 Proof of Lemma 3

Before we provide the proof of Lemma 2, we define quantities required in the proof. For any $q \in \mathsf{I}_{\frac{B}{\delta}}$ and under any measurement vector $\mathbf{A}_t \in \mathcal{U}_{\frac{B}{\delta}}$ such that $\|\mathbf{A}_t\|_0 = \frac{qB}{\delta}$ we have the following

$$\begin{aligned}
&\left|\log \frac{\mathsf{P}(y|\mathbf{A}_t, \mathbf{W}(i) = 1)}{\mathsf{P}(y|\mathbf{A}_t, \mathbf{W}(j) = 1)}\right| \\
&= \begin{cases} 0 & \text{if } \mathbf{A}_t(i) = 1 \text{ and } \mathbf{A}_t(j) = 1, \\ 0 & \text{if } \mathbf{A}_t(i) \neq 1 \text{ and } \mathbf{A}_t(j) \neq 1, \\ \left|\frac{2y-1}{2qB\sigma^2}\right| & \text{Otherwise.} \end{cases}
\end{aligned} \tag{A.2}$$

Hence, we have

$$\begin{aligned}
&\max_{i,j \in [\frac{B}{\delta}]} \max_{\mathbf{A}_t \in \mathcal{U}_{\frac{B}{\delta}}} \int_{-\infty}^{\infty} \mathsf{P}(y|\mathbf{A}_t, \mathbf{W}(i) = 1) \times \\
&\qquad \times \left|\log \frac{\mathsf{P}(y|\mathbf{A}_t, \mathbf{W}(i) = 1)}{\mathsf{P}(y|\mathbf{A}_t, \mathbf{W}(j) = 1)}\right|^{1+\gamma} dy \\
&= \max_{q \in \mathsf{I}_{\frac{B}{\delta}}} \left\{ \int_{-\infty}^{\infty} \frac{e^{-\frac{y^2}{2qB\sigma^2}}}{\sqrt{2\pi qB\sigma^2}} \left|\frac{2y-1}{2qB\sigma^2}\right|^{1+\gamma} dy \right\}.
\end{aligned} \tag{A.3}$$

Therefore, there exists $\xi_{\frac{B}{\delta}} < \infty$ and $\gamma > 0$ such that

$$\begin{aligned}
&\max_{i,j \in [\frac{B}{\delta}]} \max_{\mathbf{A}_t \in \mathcal{U}_{\frac{B}{\delta}}} \int_{-\infty}^{\infty} \mathsf{P}(y|\mathbf{A}_t, \mathbf{W}(i) = 1) \times \\
&\qquad \times \left|\log \frac{\mathsf{P}(y|\mathbf{A}_t, \mathbf{W}(i) = 1)}{\mathsf{P}(y|\mathbf{A}_t, \mathbf{W}(j) = 1)}\right|^{1+\gamma} dy \leq \xi_{\frac{B}{\delta}}.
\end{aligned} \tag{A.4}$$

Define

$$\psi_{\frac{B}{\delta}}(a) := \max_{q \in \mathsf{I}_{\frac{B}{\delta}}} \left\{ \int_{-\infty}^{\infty} \frac{e^{-\frac{y^2}{2Bq\sigma^2}}}{\sqrt{2\pi qB\sigma^2}} \left[\frac{2y-1}{2qB\sigma^2}\right]_a dy \right\}, \tag{A.5}$$

and recall that $[g]_a = g$ if $g \geq a$ otherwise $[g]_a = 0$. The quantity a controls the maximum jump in the log-likelihood ratio of the Gaussian observations under all possible search sets determined by the values of $q \in \mathsf{I}_{\frac{B}{\delta}}$ and the quantity $\psi_{\frac{B}{\delta}}(a)$ controls the tail probability of log-likelihood ratios whose value is greater than a. Furthermore, we have $\psi_{\frac{B}{\delta}}(a)$ is non-increasing in a, and we have $\psi_{\frac{B}{\delta}}(a) \leq a^{-\gamma}\xi_{\frac{B}{\delta}}$. Therefore, the tail probability goes to 0, i.e, $\psi_{\frac{B}{\delta}}(a) \to 0$ as $a \to \infty$. Now we are ready to provide the proof for Stage I of our two stage strategy.

A.3.1 Stage I

Lemma 7. Under the fixed composition search strategy while searching over a search region of width B among $\frac{1}{\alpha}$ locations such that $\|\mathbf{A}'_t\|_0 \alpha = q^*$ for $n \geq 1$, the following holds true for all $n \geq 1$

$$\mathbb{E}\left[U(\boldsymbol{\rho}'_{t+1}) - U(\boldsymbol{\rho}'_t)|\mathcal{F}_t, \mathbf{A}'_t\right] \geq C\left(q^*, q^*B\sigma^2\right), \tag{A.6}$$

where define $U(\boldsymbol{\rho}'_t) := \sum_{i=1}^{\frac{1}{\alpha}} \boldsymbol{\rho}'_t(i) \log \frac{\boldsymbol{\rho}'_t(i)}{1-\boldsymbol{\rho}'_t(i)}$.

Proof. The proof follows closely the proof of inequality (9) in [89]. There are $\frac{1}{\alpha}$ locations of length αB and hence query vector $\|\mathbf{A}'_t\|_0 = \frac{1}{\alpha}$. At every time instant under the fixed composition strategy $K^* = \|\mathbf{A}_t\|_0 = \frac{q^*}{\alpha}$ number of locations are searched. i.e., a region of length q^*B is searched. Let $\mathcal{P}_{K^*}$ denote the collection of all partitions p of search locations 1 to $\frac{1}{\alpha}$ into sets $s_{0:t}$ and $S_{1:t}$ such that $|S_{1:t}| = K^*$. The probability of picking a partition $p \in \mathcal{P}_{K^*}$ is $\lambda_p = \binom{1/\alpha}{K^*}^{-1}$. For simplicity of exposition let $M = \frac{1}{\alpha}$. Also, we have $\sum_{p\in\mathcal{P}_{K^*}} \lambda_p \mathbb{1}_{\{i\in S_{0:t}\}} = \pi_0^* := \frac{M-K^*}{M}$, and $\sum_{p\in\mathcal{P}_{K^*}} \lambda_p \mathbb{1}_{\{i\in S_{1:t}\}} = \pi_1^* := \frac{K^*}{M}$.

Since a region of q^*B is searched at every time instant, the noise variance is fixed at $q^*B\sigma^2$.

Hence, let $\mathsf{P}_k = \mathsf{P}(Y|X=k, |S_{1:t}| = K^*) = \mathcal{N}(k, q^* B\sigma^2)$ for $k \in \{0,1\}$. Consider

$$\begin{aligned}
&\mathbb{E}\left[U(\boldsymbol{\rho}'_{t+1}) - U(\boldsymbol{\rho}'_t)|\mathcal{F}_t, \mathbf{A}_t\right] \\
&= \sum_{p\in\mathcal{P}_{K^*}} \lambda_p \sum_{i=1}^{M}\sum_{k=0}^{1} \boldsymbol{\rho}'_t(i)\mathbb{1}_{\{i\in S_{t:k}\}} \times \\
&\quad D\left(\mathsf{P}_k \middle\| \sum_{j\neq i}\sum_{l=1}^{1} \frac{\boldsymbol{\rho}'_t(j)}{1-\boldsymbol{\rho}'_t(i)} \mathbb{1}_{\{i\in S_{t:l}\}} \mathsf{P}_l\right)
\end{aligned}$$

$$\begin{aligned}
&= \sum_{i=1}^{M} \boldsymbol{\rho}'_t(i) \sum_{k=0}^{1} \pi_k^* \sum_{p\in\mathcal{P}_{K^*}} \frac{\lambda_p}{\pi_k^*} \mathbb{1}_{\{i\in S_{t:k}\}} \times \\
&\qquad D\left(\mathsf{P}_k \middle\| \sum_{j\neq i}\sum_{l=1}^{1} \frac{\boldsymbol{\rho}'_t(j)}{1-\boldsymbol{\rho}'_t(i)} \mathbb{1}_{\{i\in S_{t:l}\}} \mathsf{P}_l\right)
\end{aligned}$$

$$\begin{aligned}
&\overset{(a)}{\geq} \sum_{i=1}^{M} \boldsymbol{\rho}'_t(i) \sum_{k=0}^{1} \pi_k^* D\left(\mathsf{P}_k \middle\| \sum_{j\neq i}\sum_{l=1}^{1} \frac{\boldsymbol{\rho}'_t(j)}{1-\boldsymbol{\rho}'_t(i)} \times \right. \\
&\qquad \left. \times \sum_{p\in\mathcal{P}_{K^*}} \frac{\lambda_p}{\pi_k^*} \mathbb{1}_{\{i\in S_{t:k}\}} \mathbb{1}_{\{i\in S_{t:l}\}} \mathsf{P}_l\right) \\
&\overset{(b)}{=} \sum_{i=1}^{M} \boldsymbol{\rho}'_t(i) \left(\pi_1^* D\left(\mathsf{P}_1 \middle\| \frac{K^*-1}{M-1}\mathsf{P}_1 + \frac{M-K^*}{M-1} P_0\right)\right. \\
&\left. + \pi_0^* D\left(\mathsf{P}_0 \middle\| \frac{M-K^*-1}{M-1}\mathsf{P}_0 + \frac{K^*}{M-1} P_1\right)\right]
\end{aligned}$$

$$\begin{aligned}
&\geq \sum_{i=1}^{M} \boldsymbol{\rho}'_t(i) \left(\pi_1^* D\left(\mathsf{P}_1 \middle\| \frac{K^*}{M}\mathsf{P}_1 + \frac{M-K^*}{M} P_0\right)\right. \\
&\qquad \left. + \pi_0^* D\left(\mathsf{P}_0 \middle\| \frac{M-K^*}{M}\mathsf{P}_0 + \frac{K^*}{M} P_1\right)\right) \\
&\overset{(c)}{=} C\left(q^*, q^* B\sigma^2\right), \qquad \text{(A.7)}
\end{aligned}$$

where (a) follows from Jensen's inequality (b) follows from the definition of π_0^*, π_1^* and

$$\sum_{p\in\mathcal{P}_{K^*}} \lambda_p \mathbb{1}_{\{i\in S_{0:t}\}}\mathbb{1}_{\{j\in S_{1:t}\}}$$
$$= \sum_{p\in\mathcal{P}_{K^*}} \lambda_p \mathbb{1}_{\{i\in S_{1:t}\}}\mathbb{1}_{\{j\in S_{0:t}\}} = \frac{K^*(M-K^*)}{M(M-1)},$$

$$\sum_{p\in\mathcal{P}_{K^*}} \lambda_p \mathbb{1}_{\{i\in S_{0:t}\}}\mathbb{1}_{\{j\in S_{0:t}\}} = \frac{\pi_0^*(M-K^*-1)}{M-1},$$
$$\sum_{p\in\mathcal{P}_{K^*}} \lambda_p \mathbb{1}_{\{i\in S_{1:t}\}}\mathbb{1}_{\{j\in S_{1:t}\}} = \frac{\pi_1^*(K^*-1)}{M-1},$$

and (c) is the definition of non-adaptive BAWGN channel capacity with input distribution Bern(q^*) and noise variance $q^*B\sigma^2$. □

Lemma 8. Under the fixed composition search strategy while searching over a search region of width B among $\frac{1}{\alpha}$ locations such that $\|\mathbf{A}'_t\|_0\alpha = q^*$ for $t \geq 1$, the following holds true for the expected number of queries while searching with $\mathsf{P}_e \leq \frac{\epsilon}{2}$

$$\mathbb{E}_{\mathfrak{C}^1_\epsilon}[\tau^1] \leq \frac{\log\frac{1}{\alpha} + \log\frac{2}{\epsilon} + \log\log\frac{B}{\delta} + a_\eta}{C\left(q^*, q^*B\sigma^2\right) - \eta}. \tag{A.8}$$

Proof is similar to the proof of Lemma 10.

A.3.2 Stage II

Note that BAWGN capacity for all $q \in \mathsf{I}_{\frac{B}{\delta}}$ with capacity achieving input is

$$C\left(\frac{1}{2}, qB\sigma^2\right)$$
$$= D\left(\mathcal{N}(0,qB\sigma^2)\middle\|\frac{1}{2}\mathcal{N}(0,qB\sigma^2)+\frac{1}{2}\mathcal{N}(1,qB\sigma^2)\right)$$
$$= D\left(\mathcal{N}(1,qB\sigma^2)\middle\|\frac{1}{2}\mathcal{N}(0,qB\sigma^2)+\frac{1}{2}\mathcal{N}(1,qB\sigma^2)\right). \tag{A.9}$$

Hence, the following Lemma follows from Proposition 3 in [90].

Lemma 9. Under the sortPM search strategy while searching over a search region of width αB among $\frac{\alpha B}{\delta}$ locations, the following holds true for all $t \geq 1$

$$\mathbb{E}\left[U(\boldsymbol{\rho}''_{t+1}) - U(\boldsymbol{\rho}''_t)|\mathcal{F}_t, \mathbf{A}_t\right] \geq C\left(\frac{1}{2}, \frac{\alpha B \sigma^2}{2}\right), \tag{A.10}$$

where define $U(\boldsymbol{\rho}''_t) := \sum_{i=1}^{\frac{\alpha B}{\delta}} \boldsymbol{\rho}''_t(i) \log \frac{\boldsymbol{\rho}''_t(i)}{1-\boldsymbol{\rho}''_t(i)}$.

Lemma 10. Under the sortPM search strategy, the following holds true for the expected number of queries while searching over the search width αB among $\frac{\alpha B}{\delta}$ locations with $\mathsf{P}_e \leq \frac{\epsilon}{2}$

$$\mathbb{E}_{\mathfrak{C}^2_\epsilon}[\tau^2] \leq \frac{\log \frac{\alpha B}{\delta} + \log \frac{2}{\epsilon} + \log\log \frac{\alpha B}{\delta} + a_\eta}{C\left(\frac{1}{2}, \frac{\alpha B \sigma^2}{2}\right) - \eta}, \tag{A.11}$$

where a_η is the solution of the following equation

$$\eta = \frac{a}{a-3} \psi_{\frac{B}{\delta}}(a-3). \tag{A.12}$$

Proof. Fix some $a > 0$ to be chosen later. Let $M = \frac{\alpha B}{\delta}$. Let $\tilde{\rho}' = 1 - \frac{1}{1+\max\{\log M, \frac{2}{\epsilon}\}}$. Now, define $U'(\boldsymbol{\rho}''_0) = U(\boldsymbol{\rho}''_0) - \log \frac{\tilde{\rho}'}{1-\tilde{\rho}'}$ and define $U'(\boldsymbol{\rho}''_t)$ as follows: if $U'(\boldsymbol{\rho}''_t) < 0$, then

$$\begin{aligned} &U'(\boldsymbol{\rho}''_{t+1}) \\ &= \begin{cases} U(\boldsymbol{\rho}''_{t+1}) - U(\boldsymbol{\rho}''_n) + U'(\boldsymbol{\rho}''_t) \\ \text{if } U(\boldsymbol{\rho}''_{t+1}) - U(\boldsymbol{\rho}''_t) < a - U'(\boldsymbol{\rho}''_t), \\ a \\ \text{if } U(\boldsymbol{\rho}''_{t+1}) - U(\boldsymbol{\rho}''_t) \geq a - U'(\boldsymbol{\rho}''_t), \end{cases} \end{aligned} \tag{A.13}$$

and if $U'(\boldsymbol{\rho}''_t) \geq 0$, then

$$
\begin{aligned}
&U'(\boldsymbol{\rho}''_{t+1}) \\
&= \begin{cases} U(\boldsymbol{\rho}''_{t+1}) - U(\boldsymbol{\rho}''_t) + U'(\boldsymbol{\rho}''_t) \\ \text{if } U(\boldsymbol{\rho}''_{t+1}) - U(\boldsymbol{\rho}''_t) < a, \\ a + U'(\boldsymbol{\rho}''_t) \\ \text{if } U(\boldsymbol{\rho}''_{t+1}) - U(\boldsymbol{\rho}''_t) \geq a. \end{cases}
\end{aligned} \tag{A.14}
$$

By induction we can show that

$$
\log \frac{\tilde{\rho}'}{1-\tilde{\rho}'} \leq U(\boldsymbol{\rho}''_t) - U'(\boldsymbol{\rho}''_t). \tag{A.15}
$$

We have

$$
\begin{aligned}
&\mathbb{E}\left[U'(\boldsymbol{\rho}''_{t+1}) - U'(\boldsymbol{\rho}''_t)|\mathcal{F}_t\right] \\
&= \mathbb{E}\left[U(\boldsymbol{\rho}''_{t+1}) - U(\boldsymbol{\rho}''_t)|\mathcal{F}_t\right] \\
&+ \mathbb{E}\Big[\Big[-b - U(\boldsymbol{\rho}''_{t+1}) + U(\boldsymbol{\rho}''_t) \\
&\qquad\qquad -U'(\boldsymbol{\rho}''_t)\mathbb{1}_{\{U'(\boldsymbol{\rho}''_t)<0\}}\Big]^+ |\mathcal{F}_t\Big] \\
&\overset{(a)}{\geq} \mathbb{E}\left[U(\boldsymbol{\rho}''_{t+1}) - U(\boldsymbol{\rho}''_t)|\mathcal{F}_t\right] - \frac{a}{a-3}\psi_{\frac{B}{\delta}}(a-3) \\
&\overset{(b)}{\geq} C\left(\frac{1}{2}, \frac{\alpha B \sigma^2}{2}\right) - \frac{a}{a-3}\psi_{\frac{B}{\delta}}(a-3),
\end{aligned} \tag{A.16}
$$

where (a) follows from [3] equation (4.140) and (b) follows Lemma 9. Let $\tau' = \min\{t : U'(\boldsymbol{\rho}''_t) \geq 0\}$ and $\tau_{\frac{\epsilon}{\epsilon}} = \min\{t : U(\boldsymbol{\rho}''_t) \geq \log \frac{\tilde{\rho}}{1-\tilde{\rho}}\}$ where $\tilde{\rho} = 1 - \frac{2}{\epsilon}$. From equation (A.15) and since $\tilde{\rho}' > \tilde{\rho}$, we have

$$
\mathbb{E}_{\mathfrak{c}^2_\epsilon}[\tau_{\frac{\epsilon}{2}}] \leq \mathbb{E}_{\mathfrak{c}^2_\epsilon}|\tilde{\tau}'|. \tag{A.17}
$$

The sequence $\frac{U'(\boldsymbol{\rho}_t'')}{C\left(\frac{1}{2},\frac{\alpha B\sigma^2}{2}\right)-\frac{a}{a-3}\psi_{\frac{B}{\delta}}(a-3)}-t$ forms a submartingale with respect to filtration $\mathcal{F}_t$. Now by Doob's Stopping Theorem we have

$$\begin{aligned}&\frac{U'(\boldsymbol{\rho}_0'')}{C\left(\frac{1}{2},\frac{\alpha B\sigma^2}{2}\right)-\frac{a}{a-3}\psi_{\frac{B}{\delta}}(a-3)}\\&\leq\mathbb{E}\left[\frac{U'(\boldsymbol{\rho}_{\tilde{\tau}'}'')}{C\left(\frac{1}{2},\frac{\alpha B\sigma^2}{2}\right)-\frac{a}{a-3}\psi_{\frac{B}{\delta}}(a-3)}-\tilde{\tau}'\right].\end{aligned}\tag{A.18}$$

Hence, we have

$$\begin{aligned}\mathbb{E}_{\mathfrak{C}_\epsilon^2}[\tilde{\tau}']&\leq\frac{-U'(\boldsymbol{\rho}_0'')+\mathbb{E}[U'(\boldsymbol{\rho}_{\tilde{\tau}'}'')]}{C\left(\frac{1}{2},\frac{\alpha B\sigma^2}{2}\right)-\frac{a}{a-3}\psi_{\frac{B}{\delta}}(a-3)}\\&=\frac{-U(\boldsymbol{\rho}_0'')+\log\frac{\bar{\rho}'}{1-\bar{\rho}'}+\mathbb{E}[U'(\boldsymbol{\rho}_{\tilde{\tau}'}'')]}{C\left(\frac{1}{2},\frac{\alpha B\sigma^2}{2}\right)-\frac{a}{a-3}\psi_{\frac{B}{\delta}}(a-3)}\\&\overset{(a)}{\leq}\frac{\log\frac{\alpha B}{\delta}+\log\log\frac{\alpha B}{\delta}+\log\frac{2}{\epsilon}+\mathbb{E}[U'(\boldsymbol{\rho}_{\tilde{\tau}'}'')]}{C\left(\frac{1}{2},\frac{\alpha B\sigma^2}{2}\right)-\frac{a}{a-3}\psi_{\frac{B}{\delta}}(a-3)}\\&\overset{(b)}{\leq}\frac{\log\frac{\alpha B}{\delta}+\log\log\frac{\alpha B}{\delta}+\log\frac{2}{\epsilon}+a}{C\left(\frac{1}{2},\frac{\alpha B\sigma^2}{2}\right)-\frac{a}{a-3}\psi_{\frac{B}{\delta}}(a-3)},\end{aligned}\tag{A.19}$$

where (a) follows from the fact that $U(\boldsymbol{\rho}_0'')=-\log(\frac{B}{\delta}-1)$ and (b) follows from the fact that for all $t<\tau'$, $U'(\boldsymbol{\rho}_t'')<0$ and hence from equation (A.13) we have $U'(\boldsymbol{\rho}_{\tilde{\tau}'}'')<a$. Let $\eta>0$ such that $\eta\ll C\left(\frac{1}{2},\frac{\alpha B\sigma^2}{2}\right)$. Choose a to be the solution of the following

$$\eta=\frac{a}{a-3}\psi_{\frac{B}{\delta}}(a-3),\tag{A.20}$$

i.e., choose $a=a_\eta$. We have the assertion of the lemma by combining above equation with equations (A.17) and (A.19). Note that we control the maximum jump in the one-step evolution of average $U(\boldsymbol{\rho}_t'')$ by truncating the log likelihood ratio of the Gaussian observations under all possible search sets by the term a_η. However, truncating the log-likelihood results in a cutback in our capacity by an amount η, i.e., we obtain $C(\frac{1}{2},\frac{\alpha B\sigma^2}{2})-\eta$. □

A.4 Proof of Corollary 2

We make the following sub-optimal choices of a_η and $\alpha(\frac{B}{\delta})$ to obtain asymptotic bounds. Choose $a_\eta = \log\log\frac{B}{\delta}$ so that η goes to zero as $\frac{B}{\delta} \to \infty$, and choose $\alpha(\frac{B}{\delta}) = \frac{1}{\log\frac{B}{\delta}}$. Note that $\alpha(\frac{B}{\delta})$ goes to 0 slower than δ goes to 0. Combining this with Theorem 1 and using the fact $\lim_{\delta\to 0} C\left(\frac{1}{2}, \frac{1}{2}\alpha\left(\frac{B}{\delta}\right)B\sigma^2\right) = 1$, we have equation (2.27). Similarly, note that $\alpha(\frac{B}{\delta})$ goes to 0 slower than B goes to ∞. Using loose approximations $C(q^*, q^*B\sigma^2) \leq \frac{\log e}{B\sigma^2}$ and $C\left(\frac{1}{2}, \alpha(\frac{B}{\delta})B\sigma^2\right) \geq \frac{\log(\frac{B}{\delta})}{16B\sigma^2}\left(1 - \frac{\log(\frac{B}{\delta})}{16B\sigma^2}\right)$ with Theorem 1 we have equations (2.29–2.28).

Appendix B

For Chapter 3

B.1 Optimal Threshold for 1-bit measurement model

The complete 1-bit measurement model in Sect. 3.3.4 is written as

$$\begin{aligned} y_{t+1} &= \alpha\sqrt{P}\mathbf{w}_{t+1}^H\mathbf{a}(\phi) + \mathbf{w}_{t+1}^H\mathbf{n}_{t+1} \\ z_{t+1} &= \mathbb{1}(|y_{t+1}|^2 > v_t) \\ &= \mathbb{1}(\phi \in D_{l_t}^{k_t}) \oplus u_t(\phi), \;\; u_t(\phi) \sim \text{Bern}(p_t(\phi)). \end{aligned} \tag{B.1}$$

Lemma 11. The threshold v_t that minimizes the maximum flipping probability $p_t(\phi)$ for all ϕ is given by the solution of the following equation

$$\int_0^{v_t} \text{Rice}(x; PG, \sigma^2)\, dx = \int_{v_t}^{\infty} \text{Rice}(x; Pg, \sigma^2)\, dx, \tag{B.2}$$

where

$$\begin{aligned} G &:= \min_{\phi \in D_{l_t}^{k_t}} |\mathbf{w}^H(D_{l_t}^{k_t})\mathbf{a}(\phi)|^2 \\ g &:= \max_{\phi \in [\theta_{\min}, \theta_{\max}] \setminus D_{l_t}^{k_t}} |\mathbf{w}^H(D_{l_t}^{k_t})\mathbf{a}(\phi)|^2. \end{aligned} \tag{B.3}$$

Proof. Since $|y_t| \sim \text{Rice}(P|\mathbf{w}_t^H\mathbf{a}(\phi)|, \sigma^2)$, we can write the flipping probability $p_t(\phi)$ as:
if $\phi \in D_{l_t}^{k_t}$,

$$\begin{aligned} p_t(\phi) &= \int_0^{v_t} \text{Rice}(x; P|\mathbf{w}^H(D_{l_t}^{k_t})\mathbf{a}(\phi)|^2, \sigma^2)\, dx \\ &\le \int_0^{v_t} \text{Rice}(x; PG, \sigma^2)\, dx, \end{aligned} \tag{B.4}$$

and if $\phi \notin D_{l_t}^{k_t}$,

$$\begin{aligned} p_t(\phi) &= \int_{v_t}^{\infty} \text{Rice}(x; P|\mathbf{w}^H(D_{l_t}^{k_t})\mathbf{a}(\phi)|^2, \sigma^2)\, dx \\ &\le \int_{v_t}^{\infty} \text{Rice}(x; Pg, \sigma^2)\, dx, \end{aligned} \tag{B.5}$$

where the upper bound in (B.4) and (B.5) is reached by the minimizer and maximizer in (B.3), respectively. Since (B.4) is increasing in v_t and (B.5) is decreasing in v_t, setting them equal gives the minimax optimizer. □

B.2 Average Log-Likelihood and the Extrinsic Jensen-Shannon Divergence

Our analysis follows similarly to [9, 67] which analyzed a feedback coding scheme and an abstract adaptive target search algorithm, respectively. The analysis is based on the behavior of the posterior of the AoA

$$\pi_i(t) := \mathbb{P} * \phi = \theta_i | y_{1:t}, \mathbf{w}_{1:t} \quad \text{for } i = 1, 2, ..., \frac{1}{\delta}, \tag{B.6}$$

over time $t = 1, 2, ...$ Recall that the stopping time of $hiePM$ is given by

$$\tau_{\epsilon,\delta} = \min\{t : 1 - \max_i \pi_i(t) \leq \epsilon\}, \tag{B.7}$$

which is the first hitting time of the posterior to the ϵ corner of the probability simplex in $\mathbb{R}^{\frac{1}{\delta}}$.

Convex functionals on the probability simplex such as entropy, KL divergence, etc. have been shown to be useful for analyzing adaptive systems [9, 91–93] with the Bayes' rule dynamics on the posterior distribution. Particularly, the functional average log-likelihood [92] has shown its usefulness in analyzing the behaviour of the posterior in feedback coding systems [67], dynamic spectrum sensing [48], hypothesis testing [94], active learning [94], etc. Here, we review some useful concepts through the context of AoA estimation with sequential beamforming:

The average log-likelihood of the posterior $\boldsymbol{\pi}(t)$ is defined as

$$U(t) := \sum_{i=1}^{1/\delta} \pi_i(t) \log \frac{\pi_i(t)}{1 - \pi_i(t)}. \tag{B.8}$$

For any beamfomring strategy $\gamma : \boldsymbol{\pi}(t) \to \mathbf{w}_{t+1}$, $U(t)$ has the following useful properties

- $U(t)$ is a submartingale $w.r.t.$ $\boldsymbol{\pi}(t)$ with expected drift EJS:

$$\mathbb{E}[U(t+1) \mid \boldsymbol{\pi}(t)] = U(t) + EJS(\boldsymbol{\pi}(t), \gamma), \tag{B.9}$$

where EJS is the Extrinsic Jensen-Shannon divergence, defined as

$$EJS(\boldsymbol{\pi}(t),\gamma) = \sum_{i=1}^{1/\delta} \pi_i(t) D\left(P_{y_{t+1}|i,\gamma} \middle\| P_{y_{t+1}|\neq i,\gamma}\right), \tag{B.10}$$

with

$$P_{y_{t+1}|\theta_i,\gamma} := f(y_{t+1}|\phi=\theta_i, \mathbf{w}_{t+1} = \gamma(\boldsymbol{\pi}(t))), \tag{B.11}$$

and

$$P_{y_{t+1}|\neq i,\gamma} = \sum_{j\neq i} \frac{\pi_j(t)}{1-\pi_i(t)} P_{y_{t+1}|j,\gamma}. \tag{B.12}$$

- The initial value $U(0) = -\log(\frac{1}{\delta}-1)$ is related to the resolutuion $\frac{1}{\delta}$
- Level crossing of U is related to the error probability as $\pi_i(t) < 1-\epsilon \; \forall \; i \; \Rightarrow \; U(t) < \log\frac{1-\epsilon}{\epsilon}$.

Analyzing the random drift of $U(t)$ from time 0 with the initial value $U(0)$ up to the first crossing time $\nu := \min\{t : U(t) \geq \log\frac{1}{\epsilon}\}$ is closely related to the expected drift given by EJS. In particular, we can then establish an upper bound on the expected stopping time $\mathbb{E}[\tau_{\epsilon,\delta}]$ in terms of the predefined outage probability ϵ and resolution $1/\delta$. Specifically, we have the following theorem:

Fact 1 (Theorem 1 in [92])**.** *Define*

$$\tilde{\pi} := 1 - \frac{1}{1+\max\{n, \log(1/\epsilon)\}}. \tag{B.13}$$

For any feedback coding scheme γ, if

$$EJS(\boldsymbol{\pi}(t),\gamma) \geq R \quad \forall t \geq 0 \tag{B.14}$$

and

$$EJS(\boldsymbol{\pi}(t),\gamma) \geq \tilde{\pi}E \quad \forall t \geq 0 \textit{ s.t. } \max_i \pi_i(t) \geq \tilde{\pi}, \tag{B.15}$$

the expected decoding time associated with error probability ϵ is bounded by

$$E[\tau_{\delta,\epsilon}] \leq \frac{\log(1/\delta)}{R} + \frac{\log(1/\epsilon)}{E} + o(\log(\frac{1}{\delta\epsilon})), \tag{B.16}$$

where $o(\cdot)$ is such that $\frac{o(\log(\frac{1}{\delta\epsilon}))}{\log(\frac{1}{\delta\epsilon})} \to 0$ as $\delta \to 0$ or $\epsilon \to 0$.

On the other hand, in order to give a lower bound for the EJS divergence, it is useful to introduce the Jensen Shannon (JS) divergence [95], defined as

$$JS(\boldsymbol{\pi}(t), \gamma) := \sum_{i=1}^{1/\delta} \pi_i(t) D\left(P_{y_{t+1}|i,\gamma} \middle\| P_{y_{t+1}}\right), \tag{B.17}$$

where $P_{y_{t+1}} = f(y_{t+1}) = \sum_{i=1}^{1/\delta} P_{y_{t+1}|i,\gamma}$.

Fact 2 (Lemma 2 in [92])**.** *The EJS divergence is lower bounded by the Jensen Shannon (JS) divergence :*

$$EJS(\boldsymbol{\pi}(t), \gamma) \geq JS(\boldsymbol{\pi}(t), \gamma). \tag{B.18}$$

B.3 Variable-length analysis of hierarchical Posterior Matching

Here we provide the variable-length analysis of hierarchical Posterior Matching by using the EJS. Throughout this section, we will focus on the settings and assumptions in Theorem 3, where the beam pattern is perfect (Assumption 4) and 1-bit measurements are used. The corresponding EJS is written as

$$EJS(\boldsymbol{\pi}(t), \gamma_h) = \sum_{i=1}^{1/\delta} \pi_i(t) D\left(P_{\hat{y}_{t+1}|i,\gamma_h} \middle\| P_{\hat{y}_{t+1}|\neq i,\gamma_h}\right) \tag{B.19}$$

with the 1-bit measurement model

$$P_{\hat{y}_{t+1}|i,\gamma} := \text{Bern}(\hat{y}_{t+1} \oplus \mathbb{1}(\theta_i \in D_{l_t}^{k_t}); p[l_t]). \tag{B.20}$$

B.3.1 Proof of Theorem 3

Let γ_h be the $hiePM$ feedback coding scheme. By the same method in [67], the EJS can be lower bounded by

$$EJS(\boldsymbol{\pi}(t),\gamma_h) \geq I(1/3;p[l_{t+1}]),\ \forall\, t \tag{B.21}$$

$$EJS(\boldsymbol{\pi}(t),\gamma_h) \geq \tilde{\boldsymbol{\pi}} C_1(p[\log_2(1/\delta)]),\ \forall \max_i \boldsymbol{\pi}_i \geq \tilde{\boldsymbol{\pi}} \tag{B.22}$$

(for completeness, we include the proof of equation (B.21) and (B.22) in Lemma 12). By (B.21), (B.22) and Fact 1, we immediately have

$$\mathbb{E}[\tau_{\epsilon,\delta}] \leq \frac{\log(1/\delta)}{I(1/3;p[1])} + \frac{\log(1/\epsilon)}{C_1(p[\log_2(1/\delta)])} + o(\log(\frac{1}{\delta\epsilon})). \tag{B.23}$$

The gap from $I(1/3;p[1])$ to $I(1/3;p[l])$ is done similarly to [9]: we need to further show that $hiePM$ is able to zoom-in to higher level beamforming and effectively obtain less noisy measurements ($p\Big[\frac{K_0\lceil\log\log\frac{1}{\delta}\rceil}{\log 2}-1\Big] < p[1]$) for most of the time during initial access (Lemma 14). Indeed, let $E_t = \{l_{t+1} < \frac{K_0\lceil\log\log\frac{1}{\delta}\rceil}{\log 2} - 1\}$ be the event of using a lower level codeword, and let $F_n = \bigcup_{t=n}^{\infty} E_t$, by the total expectation theorem and the union bound we have

$$\begin{aligned}\mathbb{E}[\tau_{\epsilon,\delta}] &= \int_\Omega \tau_{\epsilon,\delta}\, d\mathbb{P} \leq \sum_{t=n}^{\infty}\int_{E_t} \tau_{\epsilon,\delta}\, d\mathbb{P} + \int_{F_n^C} \tau_{\epsilon,\delta}\, d\mathbb{P} \\ &= \sum_{t=n}^{\infty}\int_{E_t} \mathbb{E}[\tau_{\epsilon,\delta} \mid \boldsymbol{\pi}(t)]\, d\mathbb{P} + \int_{F_n^C} \mathbb{E}[\tau_{\epsilon,\delta} \mid \boldsymbol{\pi}(n)]\, d\mathbb{P}.\end{aligned} \tag{B.24}$$

By the time homogeneity of the Markov Chain $\boldsymbol{\pi}(t)$ together with Lemma 12, we can upper bound the two terms associated with the "good" event F_n^C and the "bad" but low probability event E_t in (B.24) as

$$\begin{aligned}&\int_{E_t} \mathbb{E}[\tau_{\epsilon,\delta} \mid \boldsymbol{\pi}(t)]\, d\mathbb{P} \leq \mathbb{P}E_t \times \\ &\quad\left(t + \frac{\log\frac{1}{\delta}}{I(1/3;p[1])} + \frac{\log\frac{1}{\epsilon}}{C_1(p[\log_2(1/\delta)])} + o(\log(\frac{1}{\delta\epsilon}))\right),\end{aligned} \tag{B.25}$$

and

$$\int_{F_n^C} \mathbb{E}[\tau_{\epsilon,\delta} \mid \boldsymbol{\pi}(n)]\, d\mathbb{P} \leq \\ n + \frac{\log\frac{1}{\delta}}{I(1/3; p[l'])} + \frac{\log\frac{1}{\epsilon}}{C_1(p[\log_2(1/\delta)])} + o(\log(\frac{1}{\delta\epsilon})), \tag{B.26}$$

where $l' := \frac{K_0\lceil \log\log\frac{1}{\delta}\rceil}{\log 2} - 1$. Plugging (B.25) and (B.26) back to (B.24) and further with Lemma 13 upper bounding $\mathbb{P}E_t$, we have

$$\mathbb{E}[\tau_{\epsilon,\delta}] \leq \frac{k_0 e^{-nE_0}}{1-e^{-E_0}} \left(n + \frac{\log\frac{1}{\delta}}{I(1/3; p[1])} + \frac{\log\frac{1}{\epsilon}}{C_1(p[\log_2(1/\delta)])} \right) \\ + n + \frac{\log\frac{1}{\delta}}{I(1/3; p[l'])} + \frac{\log\frac{1}{\epsilon}}{C_1(p[\log_2(1/\delta)])} + o(\log(\frac{1}{\delta\epsilon})) \tag{B.27}$$

for $n > \frac{(l'+1)\log 2}{K_0}$. Finally, letting $n = \lceil \log\log\frac{1}{\delta\epsilon}\rceil$ in equation (B.27) we conclude the assertion of the theorem.

B.3.2 Technical Lemmas

Lemma 12. Using the $hiePM$ beamforming strategy γ_h on codebook $\mathcal{W}^S$ with $S = \log_2(1/\delta)$, we have

$$EJS(\boldsymbol{\pi}(t), \gamma_h) \geq I(1/3; p[l_{t+1}]),\ \forall\, t \tag{B.28}$$

$$EJS(\boldsymbol{\pi}(t), \gamma_h) \geq \tilde{\boldsymbol{\pi}} C_1(p[\log_2(1/\delta)]),\ \forall \max_i \boldsymbol{\pi}_i \geq \tilde{\boldsymbol{\pi}} \tag{B.29}$$

Proof. We first prove equation (B.29). By the selection rule of $hiePM$, the last level beamforming $\mathbf{w}_t = \mathbf{w}(D_S^{k_t})$ is used whenever $\max_i \pi_i(t) \geq \tilde{\pi} > 1/2$. Therefore,

$$\begin{aligned} EJS(\boldsymbol{\pi}(t), \gamma_h) &= \sum_{i=1}^{1/\delta} \pi_i(t) D\left(P_{\hat{y}_{t+1}|i,\gamma_h} \middle\| P_{\hat{y}_{t+1}|\neq i,\gamma_h} \right) \\ &\geq \tilde{\pi} D\left(P_{\hat{y}_{t+1}|i,\gamma_h} \middle\| P_{\hat{y}_{t+1}|\neq i,\gamma_h} \right) \\ &= \tilde{\pi} D(\text{Bern}(1-p[S]) \| \text{Bern}(p[S])) \\ &= \tilde{\pi} C_1(p[\log_2(1/\delta)]). \end{aligned} \tag{B.30}$$

It remains to show equation (B.28). For notational simplicity, let

$$\rho \equiv \pi_{D_{l_{t+1}}^{k_{t+1}}}(t) := \sum_{\theta_i \in D_{l_{t+1}}^{k_{t+1}}} \pi_i(t) \tag{B.31}$$

and $B^0 \equiv \text{Bern}(p[l_{t+1}])$, $B^1 \equiv \text{Bern}(1-p[l_{t+1}])$. We separate the proof into two cases:

If $\rho > 2/3$, we know that $l_{t+1} = S$ by the selection rule of $hiePM$. Therefore, the set $D_{l_{t+1}}^{k_{t+1}}$ contains only 1 angle. Let $D_{l_{t+1}}^{k_{t+1}} = \{\theta^*\}$, we have

$$\begin{aligned}
&EJS(\boldsymbol{\pi}(t), \gamma_h) = \sum_{i=1}^{1/\delta} \pi_i(t) D\left(P_{\hat{y}_{t+1}|i,\gamma_h} \middle\| P_{\hat{y}_{t+1}|\neq i,\gamma_h}\right) \\
&= \rho D\Big(B^1 \Big\| B^0\Big) \\
&+ \sum_{i:\theta_i \neq \theta^*} \pi_i(t) D\left(B^0 \middle\| \frac{\rho}{1-\pi_i(t)} B^1 + \frac{1-\rho-\pi_i(t)}{1-\pi_i(t)} B^0\right) \\
&\overset{(a)}{\geq} D\left(B^0 \middle\| \frac{1}{2} B^1 + \frac{1}{2} B^0\right) \\
&= I(1/2; p[l_{t+1}]) \geq I(1/3; p[l_{t+1}]),
\end{aligned} \tag{B.32}$$

where (a) is by the fact that $D(B^1 \| B^0) = D(B^0 \| B^1)$ and that $D(B^0 \| \alpha B^1 + (1-\alpha) B^0)$ is increasing in α for $0 \leq \alpha \leq 1$, together with $\frac{\rho}{1-\pi_i(t)} > 2/3 > 1/2$.

For the other case where $\rho \leq 2/3$, again by the selection rule of $hiePM$, we have $1/3 \leq \rho \leq 2/3$. Now we can lower bound the EJS as

$$\begin{aligned}
EJS(\boldsymbol{\pi}(t), \gamma_h) &\overset{(a)}{\geq} JS(\boldsymbol{\pi}(t), \gamma_h) \\
&= \rho D\left(B^1 \middle\| \rho B^0 + (1-\rho) B^1\right) \\
&\quad + (1-\rho) D\left(B^0 \middle\| \rho B^0 + (1-\rho) B^1\right) \\
&= I(\rho; p[l_{t+1}]) \overset{(b)}{\geq} I(1/3; p[l_{t+1}])
\end{aligned} \tag{B.33}$$

where (a) is by Fact 2 and (b) is by the concavity of the mutual information w.r.t the input distribution, the symmetric of $I(\rho; p[l_{t+1}])$ around $\rho = 1/2$ for symmetric channels, and together with $1/$

$3 \leq \rho \leq 2/3$. This concludes the assertion. □

Lemma 13. Using the $hiePM$ beamforming strategy γ_h on codebook $\mathcal{W}^S$ with $S = \log_2(1/\delta)$, we have

$$\mathbb{P}E_t := \mathbb{P}l_{t+1} \leq l \leq k_0 e^{-E_0 t} \tag{B.34}$$

for all $t > \frac{\log(l+1)\log 2}{K_0}$, where $k_0 = e^{\frac{K_0(l+1)\log 2}{(2l\log 2+K_0)^2}}$, $E_0 = \frac{K_0^2}{2(2l\log 2+K_0)^2}$, and $K_0 > 0$ is a constant defined in Lemma 14.

Proof. Let $\boldsymbol{\pi}^{\{l\}}(t)$ and $U^{\{l\}}(t)$ be the nested posterior of level l and its averaged log-likelihood, defined in Appendix B.4, equations (B.38) and (B.39). Note that $U^{\{l\}}(t) \geq \log 2$ implies that $\max_q \pi_q^{\{l\}}(t) \geq 2/3$, and in turn implies that $l_{t+1} > l$ by the selection rule of $hiePM$. Therefore, it suffices to show that

$$\mathbb{P}U^{\{l\}}(t) < \log 2 \leq k_0 e^{-E_0 t} \quad \forall t > T_0. \tag{B.35}$$

We will show (B.35) using submartingale properties of $U^{\{l\}}(t)$ with Azuma's inequality [96]. Indeed, by Lemma 14 in Appendix B.4, $U^{\{l\}}(t) - K_0 t$ is a submartingale. Furthermore, we have bounded differences for this submartingale, $i.e.$

$$|U^{\{l\}}(t+1) - U^{\{l\}}(t) + K_0| \leq 2l\log 2 + K_0, \tag{B.36}$$

for all $t \geq 0$. Hence we have

$$\begin{aligned}
&\mathbb{P}(U^{\{l\}}(t) < \log 2) \\
&= \mathbb{P}\Big(U^{\{l\}}(t) - K_0 t - U^{\{l\}}(0) < (l+1)\log 2 - K_0 t\Big) \\
&\overset{(a)}{\leq} \exp\left(-\frac{((l+1)\log 2 - K_0 t)^2}{2t(2l\log 2 + K_0)^2}\right) \overset{(b)}{\leq} k_0 e^{-E_0 t}
\end{aligned} \tag{B.37}$$

for $t > \frac{\log(l+1)\log 2}{K_0}$, where (a) is by Azuma's inequality and (b) is by expanding the quadratic terms and rearrangements. □

B.4 Nested Posterior and its EJS

In this section, we introduce the nested posterior and its EJS lower bound (Lemma 14), which are used for proving Lemma 13. Let posterior $\pi_i(t)$ with $i = 1, 2, ..., 2^S$. We define a nested posterior $\boldsymbol{\pi}^{\{l\}}$ of level $l < S$ with length 2^l as

$$\pi_q^{\{l\}}(t) := \sum_{i \in \text{bin}(q)} \pi_i(t), \quad q = 1, 2, ..., 2^l, \tag{B.38}$$

where $\text{bin}(q) := \{(q-1)2^{S-l} + 1, ..., q2^{S-l}\}$. Further, we define the functional log-likelihood on $\boldsymbol{\pi}^{\{l\}}$ as

$$U^{\{l\}}(t) := \sum_{q=1}^{2^l} \pi_q^{\{l\}}(t) \log \frac{\pi_q^{\{l\}}(t)}{1 - \pi_q^{\{l\}}(t)}. \tag{B.39}$$

For any beamforming strategy $\gamma : \boldsymbol{\pi}^{\{S\}}(t) \to \mathbf{w}_{t+1}$ on the level S posterior, the level $l < S$ log-likelihood $U^{\{l\}}(t)$ is a submartingale $w.r.t.$ $\boldsymbol{\pi}(t)$. The expected drift can be written as

$$\begin{aligned} &\mathbb{E}[U^{\{l\}}(t+1) \mid \boldsymbol{\pi}(t)] \\ &\quad = U^{\{l\}}(t) + EJS(\boldsymbol{\pi}^{\{l\}}(t), \gamma; \boldsymbol{\pi}(t)), \end{aligned} \tag{B.40}$$

where

$$\begin{aligned} &EJS(\boldsymbol{\pi}^{\{l\}}(t), \gamma; \boldsymbol{\pi}(t)) \\ &\quad = \sum_{q=1}^{2^l} \pi_q^{\{l\}}(t) D\left(P_{y_{t+1}|q,\gamma} \middle\| P_{y_{t+1}|\neq q,\gamma}\right) \end{aligned} \tag{B.41}$$

with

$$\begin{aligned} P_{y_{t+1}|\in \text{bin}(q),\gamma} &:= \frac{1}{\sum_{i \in \text{bin}(q)} \pi_i(t)} \\ &\times \sum_{i \in \text{bin}(q)} \pi_i(t) f\Big(y_{t+1} \Big| \phi = \theta_i, \mathbf{w}_{t+1} = \gamma(\boldsymbol{\pi}(t))\Big) \end{aligned} \tag{B.42}$$

and

$$\begin{aligned} P_{y_{t+1}|\notin \text{bin}(q),\gamma} &:= \frac{1}{\sum_{i \notin \text{bin}(q)} \pi_i(t)} \\ &\times \sum_{i \notin \text{bin}(q)} \pi_i(t) f\Big(y_{t+1} \Big| \phi = \theta_i, \mathbf{w}_{t+1} = \gamma(\boldsymbol{\pi}(t))\Big). \end{aligned} \tag{B.43}$$

Lemma 14. With same assumptions as Theorem 3, using $hiePM$ with codebook $\mathcal{W}^S$ on $\boldsymbol{\pi}(t) \equiv \boldsymbol{\pi}^{\{S\}}(t)$, we have

$$\begin{aligned} &EJS(\boldsymbol{\pi}^{\{l\}}(t), \gamma_h; \boldsymbol{\pi}(t)) \geq K_0 := \min\Big\{ I\Big(\frac{1}{3}, p[1]\Big), \\ &\frac{2}{3} D\Big(\frac{1}{3}\text{Bern}(1-p[1]) + \frac{2}{3}\text{Bern}(p[1]) \Big\| \text{Bern}(p[1])\Big)\Big\} \end{aligned} \tag{B.44}$$

for all $t > 0$, for any $l < S$.

Proof. Given any $l < S$, if the selected codeword $\mathbf{w}(D_{l_{t+1}}^{k_{t+1}})$ is such that $l_{t+1} \leq l$, by Lemma 12 we conclude the results. If otherwise $l_{t+1} > l$, then for any $\theta_i \in D_{l_{t+1}}^{k_{t+1}}$, $i \in \text{bin}(q_t)$ for some q_t. For notational simplicity, let $\rho \equiv \pi_{D_{l_{t+1}}^{k_{t+1}}}(t) := \sum_{\theta_i \in D_{l_{t+1}}^{k_{t+1}}} \pi_i(t)$ and $B^0 \equiv \text{Bern}(p[l_{t+1}])$, $B^1 \equiv \text{Bern}(1-p[l_{t+1}])$. We have

$$\begin{aligned} &EJS(\boldsymbol{\pi}^{\{l\}}(t), \gamma; \boldsymbol{\pi}(t)) \\ &= \sum_{q=1}^{2^l} \pi_q^{\{l\}}(t) D\left(P_{\hat{y}_{t+1}|q,\gamma} \middle\| P_{\hat{y}_{t+1}|\neq q,\gamma}\right) \\ &\overset{(a)}{\geq} \frac{2}{3} D(\rho B^1 + (1-\rho)B^0 \| B^0) \overset{(b)}{\geq} \frac{2}{3} D(\frac{1}{3}B^1 + \frac{2}{3}B^0 \| B^0) \\ &\geq \frac{2}{3} D\Big(\frac{1}{3}\text{Bern}(1-p[1]) + \frac{2}{3}\text{Bern}(p[1]) \Big\| \text{Bern}(p[1])\Big)\Big\}. \end{aligned} \tag{B.45}$$

where (a) and (b) are by the selection rule of $hiePM$ that $\boldsymbol{\pi}_{q_t}^{\{l\}}(t) > 2/3$ whenever $l_t > l$ and that $1/3 \leq \rho \leq 2/3$. This concludes the assertion. □

Appendix C

For Chapter 6

C.1 Proof of Lemma 4

We assume $\alpha_t = 1$ and $P_T = 1$, and recall that $z_t(D) = |y_t|^2 = \Re(y_t)^2 + \Im(y_t)^2$. Furthermore, $\Re(y_t)^2 \sim \mathcal{N}(\Re(\mathbf{w}_t^H \mathbf{a}(\Phi_t)x_t), \frac{\sigma^2}{2})$ and $\Im \sim \mathcal{N}(\Im(\mathbf{w}_t^H \mathbf{a}(\Phi_t)x_t), \frac{\sigma^2}{2})$. Thus conditioned on a point estimate and beam vector $(\Phi_t = (\theta_i, \theta_j), \mathbf{w}_t)$, $z_t(D)$ is the sum of two Gaussian random variables squared, which by definition gives that $z_t(D) \sim \chi^2(k, \lambda_t)$ follows a non-central chi-squared probability distribution function scaled by the variance $\frac{\sigma^2}{2}$ with $k = 2$ degrees of freedom and time-varying non-centrality parameter

$$\begin{aligned} \lambda_t &= \frac{\Big(\Re(\mathbf{w}_t^H \mathbf{a}(\Phi_t)x_t)\Big)^2}{\sigma^2/2} + \frac{\Big(\Im(\mathbf{w}_t^H \mathbf{a}(\Phi_t)x_t)\Big)^2}{\sigma^2/2} \\ &= \frac{2|\mathbf{w}_t^H \mathbf{a}(\Phi_t)x_t|^2}{\sigma^2} \\ &\geq \frac{2|\mathbf{w}_t^H \mathbf{a}(\Phi_t)|^2}{\sigma^2} \end{aligned} \tag{C.1}$$

We approximate the conditional probability of $z_t(P)$ with the worst possible symbol energy $|x_t|^2 = 1$, i.e by setting $\lambda_t = \frac{2|\mathbf{w}_t^H \mathbf{a}(\Phi_t)|^2}{\sigma^2}$.

C.2 Proof of Lemma 5

Let $\alpha_t = 1$, and $P_T = 1$, thus recall the received measurement model $z_t(P)$ for the pilot phase is modeled as:

$$z_t(P) = \mathbf{w}_t^H \mathbf{a}(\Phi_t) + \mathbf{w}_t^H \mathbf{n}_t. \tag{C.2}$$

Under Assumption 8, for $e_t = P$ for a beam $\mathbf{w}_t$ in level $l_t = l$ the conditional probability density function of $z_t(P)$ is

$$\begin{aligned} f(z_t(P)|\mathbf{w}_t) &= \int_{-\infty}^{\infty} f(z_t(P)|\mathbf{w}_t, \Phi_t) d_{\Phi_t} \\ &= \mathbb{P}\Phi \in \mathcal{D}_{l_t}^{k_t} f(z_t(P)|\mathbf{w}_t, \Phi \in \mathcal{D}_{l_t}^{k_t}) + \mathbb{P}\Phi \notin \mathcal{D}_{l_t}^{k_t} f(z_t(P)|\mathbf{w}_t, \Phi \notin \mathcal{D}_{l_t}^{k_t}) \\ &= \boldsymbol{\pi}_{\tilde{\mathbf{w}}_t}(t|t-1)\mathcal{CN}(G_l, \sigma^2) + (1 - \boldsymbol{\pi}_{\tilde{\mathbf{w}}_t}(t|t-1))\mathcal{CN}(0, \sigma^2) \\ &= \boldsymbol{\pi}_{\tilde{\mathbf{w}}_t}(t|t-1)\frac{1}{\pi\sigma^2} e^{-\frac{|z_t(D)-G_l|^2}{\sigma^2}} + (1 - \boldsymbol{\pi}_{\tilde{\mathbf{w}}_t}(t|t-1))\frac{1}{\pi\sigma^2} e^{-\frac{|z_t(D)|^2}{\sigma^2}}. \end{aligned} \tag{C.3}$$

Additionally, for normalized beams $\|\mathbf{w}_t\|^2 = 1$ $\eta_t = \mathbf{w}_t^H \mathbf{n}_t \sim \mathcal{CN}(0, \sigma^2)$, which yields

$$\begin{aligned} h(\eta_t) &= h(\Re(\eta_t)) + h(\Im(\eta_t)) \\ &= \frac{1}{2}\log(2\pi e\frac{\sigma^2}{2}) + \frac{1}{2}\log(2\pi e\frac{\sigma^2}{2}) \\ &= \log(\pi e\sigma^2). \end{aligned} \tag{C.4}$$

The mutual information term for the pilot phase action $e_t = P$ of (6.17) is

$$\begin{aligned} I(\Phi_t; z_t(P)|\mathbf{w}_t) &= h(z_t(P)|\mathbf{w}_t) - h(z_t(P)|\mathbf{w}_t, \Phi_t) \\ &= h(z_t(P)|\mathbf{w}_t) - h(\eta_t) \\ &= h(z_t(P)|\mathbf{w}_t) - \log(\pi e\sigma^2) \\ &= -\int_{-\infty}^{\infty}\int_{-\infty}^{\infty} f(z_t(P)|\mathbf{w}_t)\log f(z_t(P)|\mathbf{w}_t) d_{\Re(z_t(P))} d_{\Im(z_t(P))} - \log(\pi e\sigma^2). \end{aligned} \tag{C.5}$$

C.3 Proof of Lemma 6

By Lemma 4 and under Assumption 8 $z_t(D) \sim \chi^2(k = 2, \lambda_t \geq \frac{2|\mathbf{w}_t^H \mathbf{a}(\Phi_t)|^2}{\sigma^2})$ scaled by the variance $\frac{\sigma^2}{2}$. Under the worst case assumption of $|x_t|^2 = 1$, i.e. by setting $\lambda_t = \frac{2|\mathbf{w}_t^H \mathbf{a}(\Phi_t)|^2}{\sigma^2}$, the

distribution of z_t conditioned on a beam $\mathbf{w}_t$ of level $l_t = 1$ is approximated as

$$\begin{aligned}
&f(z_t(D)|\mathbf{w}_t) \\
&= \int_{-\infty}^{\infty} f(z_t(D)|\mathbf{w}_t, \Phi_t) d_{\Phi_t} \\
&= \mathbb{P}\Phi_t \in \mathcal{D}_{l_t}^{k_t} f(z_t(D)|\mathbf{w}_t, \Phi_t \in \mathcal{D}_{l_t}^{k_t}) + \mathbb{P}\Phi_t \notin \mathcal{D}_{l_t}^{k_t} f(z_t(D)|\mathbf{w}_t, \Phi_t \notin \mathcal{D}_{l_t}^{k_t}) \\
&= \boldsymbol{\pi}_{\tilde{\mathbf{w}}_t}(t|t-1)\chi^2(2, \lambda_t = \frac{2|G_l|^2}{\sigma^2}) + (1 - \boldsymbol{\pi}_{\tilde{\mathbf{w}}_t}(t|t-1))\chi^2(2, \lambda_t = 0) \\
&= \boldsymbol{\pi}_{\tilde{\mathbf{w}}_t}(t|t-1)\frac{1}{\sigma^2} e^{-(\frac{z_t}{\sigma^2} + \frac{\lambda_t}{2})} \sum_{k=0}^{\infty} \frac{(\frac{z_t \lambda_t}{2\sigma^2})^k}{(k!)^2} + (1 - \boldsymbol{\pi}_{\tilde{\mathbf{w}}_t}(t|t-1))\frac{1}{\sigma^2} e^{\frac{-z_t}{\sigma^2}} \\
&= \boldsymbol{\pi}_{\tilde{\mathbf{w}}_t}(t|t-1)\frac{1}{\sigma^2} e^{-(\frac{z_t - |G_l|^2}{\sigma^2})} \sum_{k=0}^{\infty} \frac{(\frac{z_t |G_l|^2}{\sigma^4})^k}{(k!)^2} + (1 - \boldsymbol{\pi}_{\tilde{\mathbf{w}}_t}(t|t-1))\frac{1}{\sigma^2} e^{\frac{-z_t}{\sigma^2}}.
\end{aligned} \tag{C.6}$$

where we dropped (D) on $z_t(D)$ for clarity. Additionally, we have the conditional entropy

$$\begin{aligned}
&h(z_t(D)|\mathbf{w}_t, \Phi_t) \\
&= \mathbb{P}\Phi_t \in \mathcal{D}_{l_t}^{k_t} h(z_t(D)|\mathbf{w}_t, \Phi_t \in \mathcal{D}_{l_t}^{k_t}) + \mathbb{P}\Phi_t \notin \mathcal{D}_{l_t}^{k_t} h(z_t(D)|\mathbf{w}_t, \Phi_t \notin \mathcal{D}_{l_t}^{k_t}) \\
&= \boldsymbol{\pi}_{\tilde{\mathbf{w}}_t}(t|t-1) h(z_t|\Phi_t \in \mathcal{D}_{l_t}^{k_t}) + (1 - \boldsymbol{\pi}_{\tilde{\mathbf{w}}_t}(t|t-1)) h(|\eta_t|^2) \\
&= -\boldsymbol{\pi}_{\tilde{\mathbf{w}}_t}(t|t-1) \int_{-\infty}^{\infty} \chi^2(2, \frac{2|G_l|^2}{\sigma^2}) \log \chi^2(2, \frac{2|G_l|^2}{\sigma^2}) d_{z_t} \\
&\quad - (1 - \boldsymbol{\pi}_{\tilde{\mathbf{w}}_t}(t|t-1)) \int_{-\infty}^{\infty} \chi^2(2, 0) \log \chi^2(2, 0) dz_t \\
&= -\boldsymbol{\pi}_{\tilde{\mathbf{w}}_t}(t|t-1) \int_{-\infty}^{\infty} \frac{1}{\sigma^2} e^{-(\frac{z_t - |G_l|^2}{\sigma^2})} \sum_{k=0}^{\infty} \frac{(\frac{z_t |G_l|^2}{\sigma^4})^k}{(k!)^2} \log \frac{1}{\sigma^2} e^{-(\frac{z_t - |G_l|^2}{\sigma^2})} \sum_{k=0}^{\infty} \frac{(\frac{z_t |G_l|^2}{\sigma^4})^k}{(k!)^2} d_{z_t} \\
&\quad - (1 - \boldsymbol{\pi}_{\tilde{\mathbf{w}}_t}(t|t-1)) \int_{-\infty}^{\infty} \frac{1}{\sigma^2} e^{\frac{-z_t}{\sigma^2}} \log \frac{1}{\sigma^2} e^{\frac{-z_t}{\sigma^2}} dz_t.
\end{aligned} \tag{C.7}$$

where $\eta_t = \mathbf{w}_t^H \mathbf{N}_t \sim CN(0, \sigma^2)$ from our model (6.6). Thus, the mutual information term for an action $e_t = D$ of (6.17) is

$$\begin{aligned}
I(\Phi_t; z_t(D)|\mathbf{w}_t) &= h(z_t(D)|\mathbf{w}_t) - h(z_t(D)|\mathbf{w}_t, \Phi_t) \\
&= -\int_{-\infty}^{\infty} f(z_t(D)|\mathbf{w}_t) \log f(z_t(D)|\mathbf{w}_t) d_{z_t(D)} - h(z_t(D)|\mathbf{w}_t, \Phi_t)
\end{aligned} \tag{C.8}$$

Bibliography

[1] M. Horstein, "Sequential transmission using noiseless feedback," in *IEEE Transactions on Information Theory*, vol. 9, no. 3, July 1963, pp. 136–143. [Online]. Available: http://dx.doi.org/10.1109/TIT.1963.1057832

[2] M. V. Burnashev and K. Zigangirov, "An interval estimation problem for controlled observations," in *IEEE Information Theory Workshop (ITW)*, Sept. 2016.

[3] M. Naghshvar, "Active learning and hypothesis testing," *Ph.D. University of California San Diego*, 2013.

[4] A. Lalitha, "Belief refinement approaches to communication and inference problems," *UC San Diego. ProQuest ID: Lalitha ucsd 0033D 18723. Merritt ID: ark:/13030/m5xw9p46.*, 2019.

[5] S. Chiu, "Noisy binary search: Practical algorithms and applications," *UC San Diego. ProQuest ID: Chiu ucsd 0033D 18308. Merritt ID: ark:/13030/m5r260r1.*, 2019.

[6] Y. Kaspi, O. Shayevitz, and T. Javidi, "Searching with Measurement Dependent Noise," *IEEE Transactions on Information Theory*, vol. 64, no. 4, pp. 2690–2705, 2018.

[7] Y. Shabara, C. E. Koksal, and E. Ekici, "Linear Block Coding for Efficient Beam Discovery in Millimeter Wave Communication Networks," *arXiv preprint arXiv:1712.07161*, 2017. [Online]. Available: http://arxiv.org/abs/1712.07161

[8] T. Javidi and A. Goldsmith, "Dynamic joint source-channel coding with feedback," in *IEEE International Symposium on Information Theory*, 2013, pp. 16–20.

[9] S. E. Chiu and T. Javidi, "Sequential measurement-dependent noisy search," in *IEEE Information Theory Workshop*, 2016.

[10] G. R. Maccartney, J. Zhang, S. Nie, and T. S. Rappaport, "Path loss models for 5G millimeter wave propagation channels in urban microcells," *GLOBECOM - IEEE Global Telecommunications Conference*, pp. 3948–3953, 2013.

[11] T. S. Rappaport, Y. Xing, G. R. MacCartney, A. F. Molisch, E. Mellios, and J. Zhang, "Overview of Millimeter Wave Communications for Fifth-Generation (5G) Wireless Networks-With a Focus on Propagation Models," *IEEE Transactions on Antennas and Propagation*, vol. 65, no. 12, pp. 6213–6230, 2017.

[12] A. F. Molisch, V. V. Ratnam, S. Han, Z. Li, S. L. H. Nguyen, L. Li, and K. Haneda, "Hybrid Beamforming for Massive MIMO: A Survey," *IEEE Communications Magazine*, vol. 55, no. 9, pp. 134–141, 2017.

[13] M. Giordani, M. Mezzavilla, C. N. Barati, S. Rangan, and M. Zorzi, "Comparative analysis of initial access techniques in 5g mmwave cellular networks," in *Proceedings of the 2016 Annual Conference on Information Science and Systems (CISS)*, March 2016, pp. 268–273. [Online]. Available: http://dx.doi.org/10.1109/CISS.2016.7460513

[14] V. Va and R. W. Heath, "Performance analysis of beam sweeping in millimeter wave assuming noise and imperfect antenna patterns," in *IEEE 84th Vehicular Technology Conference*, vol. 63, September 2016. [Online]. Available: http://dx.doi.org/10.1109/VTCFall.2016.7881150

[15] E. Axell, G. Leus, E. G. Larsson, and H. V. Poor, "Spectrum sensing for cognitive radio : State-of-the-art and recent advances," *IEEE Signal Processing Magazine*, vol. 29, no. 3, pp. 101–116, 2012.

[16] ——, "Spectrum sensing for cognitive radio : State-of-the-art and recent advances," *IEEE Signal Processing Magazine*, vol. 29, no. 3, pp. 1053–5888, 05 2012. [Online]. Available: https://doi.org/10.1109/MSP.2012.2183771

[17] A. Sharma and C. Murthy, "Group testing-based spectrum hole search for cognitive radios," *IEEE Transactions on Vehicular Technology*, vol. 63, no. 8, pp. 3794–3805, October 2014. [Online]. Available: http://dx.doi.org/10.1109/TVT.2014.2305978

[18] J. Treichler, M. Davenport, and R. Baraniuk, "Application of compressive sensing to the design of wideband signal acquisition receivers," in *Proceedings of the 6th US/Australia Joint Work. Defense Applications of Signal Processing (DASP)*, September 2009, pp. 1–10. [Online]. Available: http://mdav.ece.gatech.edu/publications/tdb-dasp-2009.pdf

[19] M. E. Tipping, "Sparse bayesian learning and the relevance vector machine," *J. Mach. Learn. Res.*, vol. 1, p. 211–244, Sep. 2001. [Online]. Available: https://doi.org/10.1162/15324430152748236

[20] S. F. Cotter, B. D. Rao, Kjersti Engan, and K. Kreutz-Delgado, "Sparse solutions to linear inverse problems with multiple measurement vectors," *IEEE Transactions on Signal Processing*, vol. 53, no. 7, pp. 2477–2488, July 2005.

[21] D. Sundman, S. Chatterjee, and M. Skoglund, "Greedy pursuits for compressed sensing of jointly sparse signals," in *2011 19th European Signal Processing Conference*, Aug 2011, pp. 368–372.

[22] J. D. Blanchard, M. Cermak, D. Hanle, and Y. Jing, "Greedy algorithms for joint sparse recovery," *IEEE Transactions on Signal Processing*, vol. 62, no. 7, pp. 1694–1704, 2014.

[23] G. Hannak, A. Perelli, N. Goertz, G. Matz, and M. E. Davies, "Performance analysis of approximate message passing for distributed compressed sensing," *IEEE Journal of Selected Topics in Signal Processing*, vol. 12, no. 5, pp. 857–870, Oct 2018.

[24] A. Koochakzadeh, H. Qiao, and P. Pal, "On fundamental limits of joint sparse support recovery using certain correlation priors," *IEEE Transactions on Signal Processing*, vol. 66, no. 17, pp. 4612–4625, Sep. 2018.

[25] R. Kueng and P. Jung, "Robust nonnegative sparse recovery and the nullspace property of 0/1 measurements," *IEEE Transactions on Information Theory*, vol. 64, no. 2, pp. 689–703, 2018.

[26] R. S. Sutton and A. G. Barto, *Reinforcement Learning: An Introduction*. London, England: The MIT Press, 2018.

[27] Z. Quan, S.Cui, A. H. Sayed, and H. V. Poor, "Optimal multiband joint detection for spectrum sensing in cognitive radio networks," *IEEE Transactions Signal Process*, vol. 57, no. 3, March 2009.

[28] Y. Feng and X. Wang, "Adaptive multiband spectrum sensing," *IEEE Wireless Communications Letters*, vol. 1, no. 2, pp. 121–124, 2012.

[29] A. Tajer, R. Castro, and X. Wang, "Adaptive spectrum sensing for agile cognitive radios," in *IEEE Conference on Acoustics Speech and Signal Processing*, March 2010.

[30] T. M. Cover and J. A. Thomas, *Elements of Information Theory (Wiley Series in Telecommunications and Signal Processing)*. USA: Wiley-Interscience, 2006.

[31] O. Shayevitz and M. Feder, "Optimal feedback communication via posterior matching," *IEEE Transactions on Information Theory*, vol. 57, no. 3, pp. 1186–1222, 2011.

[32] J. Schalkwijk and T. Kailath, "A coding scheme for additive noise channels with feedback part i: No bandwidth constraint," in *IEEE Transactions on Information Theory*, vol. IT-12, April 1966, pp. 172–182.

[33] N. Bshouty, "Optimal algorithms for the coin weighing problem with a spring scale," in *Proceedings of the 22nd Conference on Learning Theory (COLT)*, June 2009, pp. 1–10. [Online]. Available: http://www.cs.mcgill.ca/~colt2009/papers/004.pdf

[34] S. C. Chang and E. Weldon, "Coding for t-user multiple-access channels," *IEEE Transactions on Information Theory*, vol. 25, no. 6, pp. 684–691, November 1979. [Online]. Available: http://dx.doi.org/10.1109/TIT.1979.1056109

[35] R. G. Gallager, *Information Theory and Reliable Communication*. John Wiley Sons, Inc., 1968.

[36] Y. Kaspi, O. Shayevitz, and T. Javidi, "Searching with measurement dependent noise," *IEEE Transactions on Information Theory*, vol. 64, no. 4, pp. 2690–2705, April 2018. [Online]. Available: http://dx.doi.org/10.1109/TIT.2017.2775614

[37] B. Jedynak, P. I. Frazier, and R. Sznitman, "Twenty questions with noise: Bayes optimal policies for entropy loss," *J. Appl. Probab.*, vol. 49, no. 1, pp. 114–136, 03 2012. [Online]. Available: https://doi.org/10.1239/jap/1331216837

[38] T. Tsiligkaridis, B. M. Sadler, and A. O. Hero, "Collaborative 20 questions for target localization," *IEEE Transactions on Information Theory*, vol. 60, no. 4, pp. 2233–2252, April 2014. [Online]. Available: http://dx.doi.org/10.1109/TIT.2014.2304455

[39] A. Lalitha, N. Ronquillo, and T. Javidi, "Measurement dependent noisy search: The gaussian case," in *Proceedings of the 2017 IEEE International Symposium on Information Theory (ISIT)*, June 2017, pp. 3090–3094. [Online]. Available: http://dx.doi.org/10.1109/ISIT.2017.8007098

[40] C. N. Barati, S. A. Hosseini, M. Mezzavilla, P. Amiri-Eliasi, S. Rangan, T. Korakis, S. S. Panwar, and M. Zorzi, "Directional initial access for millimeter wave cellular systems," in *Proceedings of the 49th Asilomar Conference on Signals, Systems and Computers*, Nov 2015, pp. 307–311. [Online]. Available: http://dx.doi.org/10.1109/ACSSC.2015.7421136

[41] O. Abari, H. Hassanieh, and D. Katabi, "Millimeter wave communications: From point-to-point links to agile network connections," in *Proceedings of the 15th ACM Workshop on Hot Topics in Networks*, November 2016, pp. 169–175. [Online]. Available: http://dx.doi.org/10.1145/3005745.3005766

[42] M. L. Malloy and R. D. Nowak, "Near-optimal adaptive compressed sensing," *IEEE Transactions on Information Theory*, vol. 60, no. 7, pp. 4001–4012, May 2014. [Online]. Available: http://dx.doi.org/10.1109/TIT.2014.2321552

[43] Y. Jin, Y. Kim, and B. Rao, "Limits on support recovery of sparse signals via multiple-access communication techniques," *IEEE Transactions on Information Theory*, vol. 57, no. 12, pp. 7877–7892, December 2011. [Online]. Available: http://dx.doi.org/10.1109/TIT.2011.2170116

[44] T. M. Cover and J. A. Thomas, *Elements of information theory*. John Wiley Sons, Inc., 2006.

[45] E. Nayebi and B. D. Rao, "Semi-blind channel estimation for multiuser massive MIMO systems," *IEEE Transactions on Signal Processing*, vol. 66, no. 2, pp. 540–553, 2017.

[46] A. Alkhateeb, O. E. Ayach, G. Leus, and R. W. Heath, "Channel Estimation and Hybrid Precoding for Millimeter Wave Cellular Systems," *IEEE Journal of Selected Topics in Signal Processing*, vol. 8, no. 5, pp. 831–846, 2014.

[47] M. Giordani, M. Mezzavilla, C. N. Barati, S. Rangan, and M. Zorzi, "Comparative analysis of initial access techniques in 5g mmwave cellular networks," in *Proceedings of the 2016 Annual Conference on Information Science and Systems (CISS)*, March 2016, pp. 268–273. [Online]. Available: http://dx.doi.org/10.1109/CISS.2016.7460513

[48] A. Lalitha, N. Ronquillo, and T. Javidi, "Improved target acquisition rates with feedback codes," *IEEE Journal of Selected Topics in Signal Processing*, vol. 12, no. 5, pp. 871–885, 2018.

[49] O. Abari, H. Hassanieh, M. Rodriguez, and D. Katabi, "Millimeter Wave Communications: From Point-to-Point Links to Agile Network Connections," in *Proceedings of the 15th ACM Workshop on Hot Topics in Networks - HotNets '16*, 2016, pp. 169–175. [Online]. Available: http://dl.acm.org/citation.cfm?doid=3005745.3005766

[50] X. Song, S. Haghighatshoar, and G. Caire, "Efficient beam alignment for mmWave single-carrier systems with hybrid MIMO transceivers," *IEEE Transactions on Wireless Communications*, 2019.

[51] Y. Ding, S. E. Chiu, and B. D. Rao, "Bayesian Channel Estimation Algorithms for Massive MIMO Systems with Hybrid Analog-Digital Processing and Low Resolution ADCs," *IEEE Journal on Selected Topics in Signal Processing*, vol. 12, no. 3, pp. 499–513, 2018.

[52] 3GPP, "NR - Multi-connectivity - Overall description (Stage 2)," *3GPP TS 37.340*, 2018.

[53] M. Naghshvar, T. Javidi, and K. Chaudhuri, "Bayesian Active Learning With Non-Persistent Noise," *IEEE Transactions on Information Theory*, vol. 61, no. 7, pp. 4080–4098, 2015. [Online]. Available: http://ieeexplore.ieee.org/lpdocs/epic03/wrapper.htm?arnumber=7105932

[54] W. Roh, J. Y. Seol, J. H. Park, B. Lee, J. Lee, Y. Kim, J. Cho, K. Cheun, and F. Aryanfar, "Millimeter-wave beamforming as an enabling technology for 5G cellular communications: Theoretical feasibility and prototype results," *IEEE Communications Magazine*, vol. 52, no. 2, pp. 106–113, 2014.

[55] D. Tse and P. Viswanath, *Fundamentals of Wireless Communication, Chapter 07: MIMO I : spatial multiplexing and channel modeling*. Cambridge University Press, 2005.

[56] S. Dasgupta, D. Hsu, and C. Monteleoni, "A general agnostic active learning algorithm," *Nips*, vol. 20, no. 2, pp. 353–360, 2007. [Online]. Available: http://dblp.uni-trier.de/db/conf/nips/nips2007.html{\#}DasguptaHM07

[57] J. Choi, J. Mo, S. Member, and R. W. H. Jr, "Near Maximum-Likelihood Detector and Channel Estimator for Uplink Multiuser Massive MIMO Systems With One-Bit ADCs," *IEEE Transactions on Communications*, vol. 64, no. 5, pp. 2005–2018, 2016.

[58] D. K. Ho and B. D. Rao, "Antithetic Dithered 1-bit Massive MIMO Architecture: Efficient Channel Estimation via Parameter Expansion and Pseudo Maximum Likelihood," *IEEE Transactions on Signal Processing*, 2019.

[59] T. S. Rappaport, *Wireless Communications: Principles and Practice*. NJ: Prentice-Hall, 2002.

[60] V. Va, J. Choi, and R. W. Heath, "The Impact of Beamwidth on Temporal Channel Variation in Vehicular Channels and Its Implications," *IEEE Transactions on Vehicular Technology*, vol. 66, no. 6, pp. 5014–5029, 2017.

[61] X. Lin, J. Li, R. Baldemair, J. T. Cheng, S. Parkvall, D. C. Larsson, H. Koorapaty, M. Frenne, S. Falahati, A. Grovlen, and K. Werner, "5g new radio: Unveiling the essentials of the next generation wireless access technology," *IEEE Communications Standards Magazine*, vol. 3, no. 3, pp. 30–37, 2019.

[62] T. S. Rappaport, Y. Xing, G. R. MacCartney, A. F. Molisch, E. Mellios, and J. Zhang, "Overview of millimeter wave communications for fifth-generation (5g) wireless networks—with a focus on propagation models," *IEEE Transactions on Antennas and Propagation*, vol. 65, no. 12, pp. 6213–6230, Dec 2017.

[63] S. Mukherjee, S. S. Das, A. Chatterjee, and S. Chatterjee, "Analytical calculation of rician k-factor for indoor wireless channel models," *IEEE Access*, vol. 5, pp. 19 194–19 212, 2017.

[64] G. K. Atia and V. Saligrama, "Boolean compressed sensing and noisy group testing," *IEEE Transactions on Information Theory*, vol. 58, no. 3, pp. 1880–1901, 2012.

[65] J. Scarlett, "Noisy adaptive group testing: Bounds and algorithms," *IEEE Transactions on Information Theory*, vol. 65, no. 6, pp. 3646–3661, 2019.

[66] T. Javidi, "Information acquisition and utilization problems," in *2013 IEEE Global Conference on Signal and Information Processing*, Dec 2013, pp. 209–212.

[67] S.-E. Chiu, A. Lalitha, and T. Javidi, "Bit-wise Sequential Coding with Feedback," in *IEEE International Symposium on Information Theory*, 2018.

[68] N. Ronquillo and T. Javidi, "Multiband noisy spectrum sensing with codebooks," in *2016 50th Asilomar Conference on Signals, Systems and Computers*, Nov 2016, pp. 1687–1691.

[69] P. Gerstoft, C. F. Mecklenbräuker, and A. Xenaki, "Multi snapshot sparse bayesian learning for doa estimation," *ArXiv*, vol. abs/1602.09120, 2016.

[70] N. Akdim, C. N. Manchón, M. Benjillali, and P. Duhamel, "Variational hierarchical posterior matching for mmwave wireless channels online learning," in *2020 IEEE 21st International Workshop on Signal Processing Advances in Wireless Communications (SPAWC)*, 2020, pp. 1–5.

[71] S. M. Kay, *Fundamentals of Statistical Signal Processing: Estimation Theory*. Upper Saddle River, NJ, USA: Prentice-Hall, Inc., 1993.

[72] X. Song, S. Haghighatshoar, and G. Caire, "A scalable and statistically robust beam alignment technique for millimeter-wave systems," *IEEE Transactions on Wireless Communications*, vol. 17, no. 7, pp. 4792–4805, July 2018.

[73] R. W. Heath, N. González-Prelcic, S. Rangan, W. Roh, and A. M. Sayeed, "An overview of signal processing techniques for millimeter wave mimo systems," *IEEE Journal of Selected Topics in Signal Processing*, vol. 10, no. 3, pp. 436–453, April 2016.

[74] S. Chiu, N. Ronquillo, and T. Javidi, "Active learning and csi acquisition for mmwave initial alignment," *arXiv preprint arXiv:1812.07722*, 2019. [Online]. Available: https://arxiv.org/abs/1812.07722

[75] Y. Huang, Q. Wu, T. Wang, G. Zhou, and R. Zhang, "3d beam tracking for cellular-connected uav," *IEEE Wireless Communications Letters*, vol. 9, no. 5, pp. 736–740, 2020.

[76] V. Va, H. Vikalo, and R. W. Heath, "Beam tracking for mobile millimeter wave communication systems," in *IEEE Global Conference on Signal and Information Processing*, 2016, pp. 743–747.

[77] J. Zhao, F. Gao, W. Jia, S. Zhang, S. Jin, and H. Lin, "Angle domain hybrid precoding and channel tracking for millimeter wave massive mimo systems," *IEEE Transactions on Wireless Communications*, vol. 16, no. 10, pp. 6868–6880, 2017.

[78] S. Shaham, M. Kokshoorn, M. Ding, Z. Lin, and M. Shirvanimoghaddam, "Extended kalman filter beam tracking for millimeter wave vehicular communications," in *IEEE International Conference on Communications Workshops*, 2020, pp. 1–6.

[79] Z. Xiao, P. Xia, and X. Xia, "Enabling uav cellular with millimeter-wave communication: potentials and approaches," *IEEE Communications Magazine*, vol. 54, no. 5, pp. 66–73, 2016.

[80] L. Yang and W. Zhang, "Beam tracking and optimization for uav communications," *IEEE Transactions on Wireless Communications*, vol. 18, no. 11, pp. 5367–5379, 2019.

[81] S. E. Chiu and T. Javidi, "Low complexity sequential search with size-dependent measurement noise," *arXiv*, May 2020.

[82] X. Gao, L. Dai, Y. Zhang, T. Xie, X. Dai, and Z. Wang, "Fast channel tracking for terahertz beamspace massive mimo systems," *IEEE Transactions on Vehicular Technology*, vol. 66, no. 7, pp. 5689–5696, 2017.

[83] D. Zhang, A. Li, M. Shirvanimoghaddam, P. Cheng, Y. Li, and B. Vucetic, "Codebook-based training beam sequence design for millimeter-wave tracking systems," *IEEE Transactions on Wireless Communications*, vol. 18, no. 11, pp. 5333–5349, 2019.

[84] L. Zhang, H. Zhao, S. Hou, Z. Zhao, H. Xu, X. Wu, Q. Wu, and R. Zhang, "A survey on 5g millimeter wave communications for uav-assisted wireless networks," *IEEE Access*, vol. 7, pp. 117 460–117 504, 2019.

[85] M. Mozaffari, W. Saad, M. Bennis, Y. Nam, and M. Debbah, "A tutorial on uavs for wireless networks: Applications, challenges, and open problems," *IEEE Communications Surveys Tutorials*, vol. 21, no. 3, pp. 2334–2360, 2019.

[86] S. Wang, J. Huang, and X. Zhang, "Demystifying millimeter-wave v2x: Towards robust and efficient directional connectivity under high mobility," in *Proceedings of the 26th Annual International Conference on Mobile Computing and Networking*, ser. MobiCom '20. New York, NY, USA: Association for Computing Machinery, 2020. [Online]. Available: https://doi.org/10.1145/3372224.3419208

[87] A. Zhou, X. Zhang, and H. Ma, "Beam-forecast: Facilitating mobile 60 ghz networks via model-driven beam steering," in *IEEE INFOCOM 2017 - IEEE Conference on Computer Communications*, 2017, pp. 1–9.

[88] N. Ronquillo, S. Chiu, and T. Javidi, "Sequential learning of csi for mmwave initial alignment," in *2019 53rd Asilomar Conference on Signals, Systems, and Computers*, 2019, pp. 1278–1283.

[89] M. Naghshvar and T. Javidi, "Optimal reliability over a DMC with feedback via deterministic sequential coding," in *Proceedings of the 2012 IEEE International Symposium on Information Theory and its Applications (ISITA)*, Oct 2012, pp. 51–55.

[90] ——, "Extrinsic Jensen–Shannon Divergence: Applications to Variable-Length Coding," in *IEEE Transactions on Information Theory*, July 2012, pp. 2191–2195. [Online]. Available: http://dx.doi.org/10.1109/ISIT.2012.6283840

[91] O. Shayevitz and M. Feder, "A Simple Proof for the Optimality of Randomized Posterior Matching," *IEEE Transactions on Information Theory*, vol. 62, no. 6, pp. 3410–3418, 2016.

[92] M. Naghshvar, T. Javidi, and M. Wigger, "Extrinsic Jensen-Shannon divergence: Applications to variable-length coding," *IEEE Transactions on Information Theory*, vol. 61, no. 4, pp. 2148–2164, 2015.

[93] C. T. Li and A. El Gamal, "An efficient feedback coding scheme with low error probability for discrete memoryless channels," *IEEE International Symposium on Information Theory - Proceedings*, vol. 61, no. 6, pp. 416–420, 2014.

[94] M. Naghshvar and T. Javidi, "Active sequential hypothesis testing," *Annals of Statistics*, vol. 41, no. 6, pp. 2703–2738, 2013.

[95] J. Lin, "Divergence Measures Based on the Shannon Entropy," *IEEE Transactions on Information Theory*, vol. 37, no. 1, pp. 145–151, 1991.

[96] F. Chung and L. Lu, "Concentration Inequalities and Martingale Inequalities: A Survey," *Internet Mathematics*, vol. 3, no. 1, pp. 79–127, 2006.